

**Synthesis, Characterization and Reactivity of Amine-phenolate Complexes Towards
the ROP of *rac*-Lactide and the Cycloaddition Reactions of Carbon Dioxide and
Epoxides**

by

© Dalal Alhashmialameer

A Thesis submitted to the School of Graduate Studies
in partial fulfillment of the requirements for the degree of

Doctor of Philosophy

Department of Chemistry

Memorial University of Newfoundland

May 2016

St. John's Newfoundland

ABSTRACT

Poly lactide (PLA) is an important polymer due to its mechanical properties, biodegradability, biocompatibility, and renewable nature. Two main pathways to produce poly lactide have been described in the literature: the polycondensation of lactic acid and the ring-opening polymerization (ROP) of lactide (LA). The latter is the most efficient route to produce high molecular weight polymers of low dispersity in the presence of a catalyst and/or an initiator. Furthermore, the transformation of CO₂ into cyclic carbonates is economical and uses a waste feedstock (*i.e.*, CO₂ emissions).

In this thesis, tetradentate amino-bis(phenolate) ligands were used to prepare catalysts for *rac*-lactide polymerization and the cycloaddition reactions of epoxides and CO₂. In these ligands, the substituents on the phenolate groups can be varied. Tetrametallic lithium and sodium complexes were synthesized and characterized; both of these metals are appealing for research in this area because of their low toxicity and cost. The complexes were fully characterized by elemental analysis, nuclear magnetic resonance spectroscopy, X-ray crystallography, and mass spectrometry.

The ROP reactions of *rac*-lactide using tetrametallic lithium and sodium complexes were studied in the melt and solution phase in the presence and absence of benzyl alcohol as co-initiator. All complexes were capable of ring-opening *rac*-lactide to produce poly lactide with and without benzyl alcohol. Data also showed that the complex containing the earth-abundant metal, sodium, gave excellent results. The isolated polymer was characterized by nuclear magnetic resonance spectroscopy, mass spectrometry, and gel permeation chromatography (GPC).

In addition, iron(III), cobalt(II), and cobalt(III) amino-bis(phenolate) complexes were synthesized and characterized. Their activity in the cycloaddition reaction of propylene oxide and various epoxides with CO₂ to yield cyclic carbonates was investigated. The effect of factors such as reaction conditions and the electronic and steric properties of the substituents on the phenolate rings was studied. The activation energy for the formation of cyclic propylene carbonate using iron(III) complexes was also determined to be close to previously reported values in the literature.

ACKNOWLEDGEMENTS

First, I would like to thank my supervisor Dr. Francesca Kerton for giving me the opportunity to join her research group and for her continuous guidance and support throughout my program. Thank you, Fran, for all of your insight and always being there to answer my questions. Special thanks to my supervisory committee members, Dr. Karen Hattenhauer and Dr. Chris Kozak, for providing valuable discussion and suggestions throughout the course of my studies.

I am also thankful to everyone in C-CART for their knowledge and advice on the many instruments I used (*e.g.*, NMR and MALDI-TOF MS); thank you to Linda Winsor, Dr. Celine Schneider, Julie Collins, and Dr. Louise Dawe.

I would like to thank all members of the Green Chemistry and Catalysis group—especially Katalin, Ali, and Hart—for many helpful discussions and encouragement. I would also like to thank NSERC, Memorial University, RDC-NL (Research & Development Corporation of Newfoundland and Labrador), and CFI (Canada Foundation for Innovation) for operating and instrument grants to my supervisor. Furthermore, special thanks to the Saudi Arabian Cultural Bureau in Canada and Taif University (Saudi Arabia) for financial support.

Finally, I want to express my gratitude to my family members—my parents, sisters, and brothers. I am also very grateful to my sister Amal and my friend Manal for their support and encouragement to follow my dreams throughout my educational career. Last, but not least, thanks to Allah (God). Without his mercy, it would not have been possible for me to achieve all that I have.

Table of Contents

ABSTRACT	i
ACKNOWLEDGEMENTS	iii
Table of Contents	iv
List of Tables	ix
List of Schemes	x
List of Figures	xii
List of Abbreviations and Symbols	xxi
List of Appendices	xxvi
Chapter 1	1-115
1.1 Introduction	1
1.2 Ring-opening polymerization of lactide	2
1.2.1 Catalysts for the polymerization of lactide	8
1.2.2 Ligands and single-site initiators used in the ROP of cyclic esters	11
1.2.2.1 Amino-bis(phenolate) ligands and their applications	12
1.2.2.1.1 Complexes for polymerization of cyclic esters	13
1.2.2.1.2 Complexes for the polymerization of alkenes	17
1.2.2.2 Chemistry of lithium and sodium	23
1.2.2.3 Lithium and sodium catalysts, especially phenolates, for the ROP of lactides	24

1.3 Reactions of epoxides catalyzed by transition metal complexes	53
1.3.1 Epoxides	55
1.3.2 Polymerization of epoxides	56
1.3.2.1 Cationic polymerization	57
1.3.2.2 Anionic and coordination insertion polymerization	58
1.3.3 Stereochemistry of epoxides	60
1.4 Synthesis of polycarbonate and cyclic carbonates by reaction of CO ₂ and epoxides	63
1.4.1 Homogenous catalyst systems for coupling and polymerizing CO ₂ and epoxides	67
1.4.1.1 A brief history of iron and its chemistry.....	69
1.4.1.2 Iron catalysts for polycarbonate and cyclic carbonate formation.....	70
1.4.1.3 A brief history of cobalt and its chemistry	84
1.4.1.4 Cobalt catalysts for polycarbonate and cyclic carbonate formation.....	86
1.5 Objectives.....	107
1.6 References.....	109

Chapter 2 Ring-opening polymerization of *rac*-lactide mediated by tetrametallic lithium and sodium diamino-bis(phenolate) complexes 117-180

2.1 Introduction.....	117
2.2 Results and discussion	120
2.2.1 Synthesis and characterization of ligands, lithium and sodium complexes.....	120

2.2.2	Crystal structure determination	123
2.2.3	Solution-state NMR spectroscopy	129
2.2.4	Polymerization of <i>rac</i> -lactide	138
2.2.4.1	Solvent free polymerization.....	138
2.2.4.2	Polymerizations in solution	141
2.2.4.3	NMR spectroscopy of polymers in bulk and solvent polymerization ...	151
2.2.4.4	Mass spectrometry of polymers.....	156
2.1.1	Proposed Mechanism	159
2.3	Conclusions.....	166
2.4	Experimental	167
2.4.1	General experimental conditions.....	167
2.4.2	Instrumentation.....	168
2.4.3	X-ray crystallography.....	170
2.4.4	Polymerization procedures	171
2.4.5	Synthesis and characterization	172
2.5	References.....	177

Chapter 3 Iron amino-bis(phenolate) complexes for the formation of organic carbonates from CO₂ and oxiranes 181-211

3.1	Introduction.....	181
3.2	Results and discussion	182
3.2.1	Synthesis and characterization of iron complexes	182
3.2.2	Crystal structure determination	183

3.2.3	UV-visible spectroscopic and magnetic data	188
3.2.4	Cyclization of propylene oxide with carbon dioxide	191
3.2.5	Kinetic measurements	198
3.3	Conclusions	201
3.4	Experimental	201
3.4.1	General experimental conditions	201
3.4.2	Instrumentation	201
3.4.3	<i>In situ</i> monitoring of the cycloaddition reaction by IR spectroscopy	202
3.4.4	Synthesis and characterization of ligands and catalysts	203
3.4.5	Spectroscopic data for carbonate products	206
3.5	References	208

Chapter 4 Synthesis and reactivity of cobalt amino-bis(phenolate) complexes

	211-233
4.1	Introduction	211
4.1.1	Dinuclear complexes	211
4.2	Results and discussion	216
4.2.1	Synthesis and characterization of dinuclear cobalt complexes	216
4.2.2	Synthesis and characterization of cobalt(III) acetate complex	216
4.2.3	Characterization of cobalt complexes	219
4.2.3.1	MALDI-TOF mass spectrometry	219
4.2.4	UV-visible spectroscopic and magnetic data	223
4.2.5	Proton NMR spectroscopy	225

4.2.6	Cyclization of propylene oxide with carbon dioxide	227
4.3	Conclusions.....	228
4.4	Experimental	229
4.4.1	General experimental conditions.....	229
4.4.2	Synthesis and characterization of catalysts	229
4.5	References.....	232
Chapter 5	Conclusions.....	233-236
5.1	Summary	233
Appendix A:	NMR spectra.....	236
Appendix B:	MALDI-TOF mass spectra.....	272

List of Tables

Table 1.1. Substrates and their products for carbon dioxide utilization.....	54
Table 2.1. Crystallographic data and structure refinement for 2.4 and 2.7	126
Table 2.2. Selected bond lengths (Å) and angles (°) for 2.4 and 2.7	127
Table 2.3. Polymerization of <i>rac</i> -lactide using 2.4 , 2.5 , 2.6 and 2.7 in the presence and absence of BnOH in the melt phase.....	140
Table 2.4. Polymerization of <i>rac</i> -lactide using 2.4 , 2.5 , 2.6 and 2.7 in the presence and absence of BnOH.....	142
Table 3.1. Crystallographic data and structure refinement for 3.1 and 3.2	186
Table 3.2. Selected bond lengths (Å) and angles (°) for 3.1 and 3.2	187
Table 3.3. Cycloaddition reactions of propylene oxide and carbon dioxide catalyzed by iron(III) complexes 3.1–3.5	193
Table 3.4. Catalytic cyclization of carbon dioxide and epoxides using 3.1	197
Table 4.1. Cycloaddition reactions of propylene oxide and carbon dioxide catalyzed by dicobalt(II) and cobalt(III) complexes 4.5–4.7	228

List of Schemes

Scheme 1.1. Petroleum route to lactic acid.	3
Scheme 1.2. The life cycle of polylactide (PLA) produced from corn.	4
Scheme 1.3. Synthesis of polylactide by direct condensation reaction and/or catalytic ring-opening polymerization (ROP).	6
Scheme 1.4. General coordination-insertion mechanism for lactide ROP.	7
Scheme 1.5. Polymerization of lactides initiated by Sn(Oct) ₂ /ROH system.	10
Scheme 1.6. Synthesis of hexalithium complexes for ROP of lactide.	26
Scheme 1.7. Synthesis of octalithium and tetralithium clusters.	27
Scheme 1.8. Synthesis of mono- and dilithium complexes.	28
Scheme 1.9. Amino-bis(phenolate) tetralithium complexes for the ROP of lactide.	29
Scheme 1.10. Synthesis of di- and tetralithium and sodium complexes.	32
Scheme 1.11. Synthesis of sodium and potassium complexes by Shen <i>et al.</i>	35
Scheme 1.12. Preparation of hexa- and disodium complexes.	39
Scheme 1.13. Dinuclear lithium, -sodium, and -potassium complexes.	42
Scheme 1.14. Synthesis of lithium complexes 1.35a–1.35e	45
Scheme 1.15. Synthesis of alkali metal derivatives.	46
Scheme 1.16. Synthesis of sodium and potassium complexes.	48
Scheme 1.17. Hexalithium complexes used by Sobota <i>et al.</i> for ROP of L-lactide.	50
Scheme 1.18. Di-lithium, -sodium, and -potassium complexes bearing iminophenolate ligands.	52

Scheme 1.19. Cationic mechanism of ring-opening polymerization of epoxide.	58
Scheme 1.20. Polymerization of propylene oxide by anionic and coordination mechanisms.....	60
Scheme 1.21. Regioisomers of polyether.....	62
Scheme 1.22. Ring opening of propylene oxide.....	62
Scheme 1.23. Tacticity of polyether.....	62
Scheme 1.24. General reaction of common epoxides and CO ₂ , producing cyclic carbonate and/or polycarbonate. PO = propylene oxide, CHO = cyclohexene oxide, and SO = styrene oxide.	63
Scheme 1.25. Industrial process for the production of BPA-PC.....	65
Scheme 1.26. Asahi Kasei's new non-phosgene polycarbonate process.	66
Scheme 1.27. Possible reaction routes for metal-catalyzed coupling reaction of CO ₂ and epoxides.	68
Scheme 1.28. Monometallic-ionic Fe(II) and (III) complexes used by Döring <i>et al.</i>	76
Scheme 2.1. Synthesis of amino-bis(phenol) ligands.....	120
Scheme 2.2. Synthesis of lithium and sodium complexes.....	123
Scheme 3.1. Proligands used with iron(III) in this study.	182
Scheme 3.2. Synthesis of iron(III) complexes.....	183
Scheme 4.1. Dinuclear catalytic mechanisms for CO ₂ /epoxide copolymerization. A. Dinuclear pathway with simultaneous activation of epoxide and CO ₂ . B. Dinuclear pathway with complexes containing –OR groups.	212
Scheme 4.2. Synthesis of dinuclear Co(II) amino-bis(phenolate) complexes.....	216
Scheme 4.3. Synthesis of Co(III) acetate complex (4.7).....	218

List of Figures

Figure 1.1. Chemical structure of initiators used in ROP of lactide (tin(II) octoate, zinc(II) lactate, aluminum(III) isopropoxide).	9
Figure 1.2. The general structure of the aminobisphenolate ligands. The groups R and R' are different phenol substituents and D is any alkyl chain containing the side chain donor atom.....	12
Figure 1.3. Synthesis of chloro-bis(phenolate)diamine complexes of lanthanides.....	14
Figure 1.4. Synthesis of divalent ytterbium and samarium bis(phenolate) compounds. ..	15
Figure 1.5. Synthesis of amino bis-(phenolate) lanthanide aryloxides.	16
Figure 1.6. Dinuclear amino bis-(phenolate) lanthanide aryloxides (top) and alkoxides (bottom).....	17
Figure 1.7. Zirconium complexes of amino-bis(phenolate) ligands.	18
Figure 1.8. Zirconium dibenzyl complexes of amino-bis(phenolate) ligands.	19
Figure 1.9. [ONXO]-Type Zr and Hf amino-bis(phenolate) complexes.	20
Figure 1.10. Dibenzylamino-bis(phenolate) Ti(IV) complexes.	20
Figure 1.11. Zirconium amino-bis(phenolate) complexes used in ethylene/1-hexene copolymerization studies.	21
Figure 1.12. Vanadium(IV) amino-bis(phenolate) complexes.	22
Figure 1.13. <i>Cis</i> and <i>trans</i> oxo configurations with a <i>trans</i> -phenoxy configuration of vanadyl complex.	23
Figure 1.14. Monoanionic amino-bis(phenolate) dinuclear lithium complexes.	30
Figure 1.15. Ligand precursors and sodium complexes based on TMEDA, PMDETA and	

Me ₆ TREN.	34
Figure 1.16. Lithium and sodium complexes based on BHT ligands.	36
Figure 1.17. Structures of tetralithium and potassium complexes by Kozak and coworkers.	38
Figure 1.18. Synthesis of tetralithium compounds.	41
Figure 1.19. Representation of mono- and dilithium complexes used by Sarazin <i>et al.</i> ...	44
Figure 1.20. Direct epoxidation of propylene oxide.	56
Figure 1.21. A) The addition reaction of oxiranes with Grignard reagents. B) The ring-expansion carbonylation of epoxides.	56
Figure 1.22. Double metal cyanide (DMC) catalyst used by Darensbourg and coworkers.	71
Figure 1.23. Dinuclear Fe(III/III) complex with reduced Robson-type ligand.	72
Figure 1.24. Mononuclear Fe(II) system designed by Rieger and coworkers.	73
Figure 1.25. Monomeric and dimeric Fe(III) triphenolate complexes used by Kleij <i>et al.</i>	74
Figure 1.26. Fe(IV) and (III) complexes reported by Nozaki and coworkers.	78
Figure 1.27. Fe(II) complexes reported by Wang <i>et al.</i>	79
Figure 1.28. Dinuclear Fe(III)-based thioether-triphenolate complexes for synthesis of CPC from CO ₂ and propylene oxide.	80
Figure 1.29. Dinuclear Fe(III) complexes bearing thioether-triphenolate ligands for synthesis of CPC from CO ₂ and propylene oxide.	82
Figure 1.30. Structure of Fe(III)X[O ₂ NN'] complex used for the copolymerization of CO ₂ and CHO/VCHO.	83

Figure 1.31. Cobalt salen complexes used by Coates <i>et al.</i>	87
Figure 1.32. Cobalt salen complexes used by Lu and coworkers.	88
Figure 1.33. Salen cobalt(III)X used by Brandenburg's group.....	89
Figure 1.34. Cobalt salen complexes with cationic 'arms'.	90
Figure 1.35. The highly active bifunctional catalysts designed by Lee and coworkers....	91
Figure 1.36. Asymmetric bifunctional (salen)CoX complexes used by Lu <i>et al.</i>	93
Figure 1.37. Bifunctional chiral catalysts used by Jing <i>et al.</i>	94
Figure 1.38. Tetradentate Schiff base cobalt complex designed by Niu <i>et al.</i>	95
Figure 1.39. Cobalt/Schiff base complexes used in the coupling of PO/CO ₂	96
Figure 1.40. (Salen)Co(III)-2,4-dinitrophenoxide catalyst for the synthesis of poly- (indene carbonate).....	97
Figure 1.41. Cobalt acetate complexes of reduced Robson ligand.	98
Figure 1.42. Salen cobalt(III)X used by Lu's group.	99
Figure 1.43. Schematic structure of Co(II) and Co(III) complexes used by Kerton and coworkers.....	100
Figure 1.44. Multichiral salen cobalt(III) complex for coupling reaction of CO ₂ and racemic terminal epoxides.	101
Figure 1.45. Bifunctional cobalt(III) catalyst reported by Darensbourg and coworkers.	102
Figure 1.46. Highly active porphyrin cobalt complexes for CO ₂ /PO copolymerization.	104
Figure 1.47. Configurations of quaternary onium-modified catalysts.	106
Figure 2.1. Dimeric Li ₂ [O ₂ N ₂] ^{BuBu} complex (2.1) and single unit of Li ₂ [O ₂ NN'] ^{BuBu} complex (2.2).	118
Figure 2.2. Compounds 1.8a–1.8c reported by Chen and coworkers. 2.3 reported by	

O'Hara while 1.28a used by Kozak <i>et al.</i>	119
Figure 2.3. ^1H NMR spectrum (300 MHz, 298 K, CDCl_3) of [L1]H₂	121
Figure 2.4. MALDI-TOF mass spectrum of [L1]H₂	122
Figure 2.5. Experimental (top) and calculated (bottom) isotopic distribution pattern for [L1]H₂	122
Figure 2.6. Molecular structure (ORTEP) and partial numbering scheme for 2.4 . Ellipsoids are shown at the 50% probability level (H-atoms omitted for clarity).	125
Figure 2.7. Molecular structure (ORTEP) and partial numbering scheme for 2.7 . Ellipsoids are shown at the 50% probability level (H-atoms omitted for clarity).	129
Figure 2.8. [a] Schematic representation of 2.7 . [b] Representation of the five-coordinate environment of Na(1).....	129
Figure 2.9. ^1H NMR spectrum (300 MHz, 298 K, C_6D_6) of 2.4	130
Figure 2.10. VT ^1H NMR spectra (500 MHz, $\text{C}_5\text{D}_5\text{N}$) of 2.4	131
Figure 2.11. ^1H NMR spectra (500 MHz, 298 K, C_6D_6 and $\text{C}_5\text{D}_5\text{N}$) of 2.4	132
Figure 2.12. VT ^7Li NMR spectra (116.6 MHz, $\text{C}_5\text{D}_5\text{N}$) of 2.4 ($\omega_{1/2}$ values were calculated from the line fitting program in MestReNova NMR processing software).	133
Figure 2.13. ^7Li NMR spectrum (116.6 MHz, 298 K, C_6D_6) of 2.4	134
Figure 2.14. ^1H NMR spectrum (300 MHz, 298 K, C_6D_6) of 2.7	135
Figure 2.15. VT ^1H NMR spectra (500 MHz, $\text{C}_5\text{D}_5\text{N}$) of 2.7	136
Figure 2.16. ^1H NMR spectrum (500 MHz, 308 K, $\text{C}_5\text{D}_5\text{N}$) of 2.7 . (Labels as shown in inset).....	137
Figure 2.17. Conversion (%) vs. time for the ROP of LA initiated by 2.6 under the conditions in Table 2.3, entry 9.	139

Figure 2.18. Conversion (%) vs. time for the ROP of LA initiated by 2.6 [conditions: 2.95 mmol LA, 250 LA :1 Li :0 BnOH, 25 °C]. ● CH ₂ Cl ₂ (5 mL), ■ Toluene (30 mL), ▼ THF (20 mL).....	143
Figure 2.19. First-order plot of LA consumption initiated by 2.6 [conditions: 2.95 mmol LA, 250 LA :1 Li :0 BnOH, 25 °C]. ● CH ₂ Cl ₂ (5 mL, $y = 0.0397x - 0.0594$, $R^2 = 0.9933$), ■ Toluene (30 mL, $0.0506x - 0.0448$, $R^2 = 0.96$), ▼ THF (20 mL $y = 0.0255x + 0.1097$, $R^2 = 0.9742$).	144
Figure 2.20. Conversion (%) vs. time for the ROP of LA initiated by 2.6 under the conditions in Table 2.4, entries 13, 15 and 17. ● CH ₂ Cl ₂ , ■ Toluene, ▼ THF.	144
Figure 2.21. First-order plot of LA consumption initiated by 2.6 according to the conditions in Table 2.4, entries 13 and 15. ● CH ₂ Cl ₂ ($y = 0.0256x + 0.1897$, $R^2 = 0.9894$), ■ Toluene ($y = 0.0884x + 0.3487$, $R^2 = 0.9593$).	145
Figure 2.22. Conversion (%) vs. time for the ROP of LA initiated by 2.4 , 2.5 , 2.6 and 2.7 in CH ₂ Cl ₂ (5 mL) [conditions: 2.95 mmol LA, 250 LA :1 M :0 BnOH, 25 °C]. ● 2.4 , ▼ 2.5 , ■ 2.6 , ◆ 2.7	145
Figure 2.23. First-order plot of LA consumption initiated by 2.4 and 2.6 in CH ₂ Cl ₂ (5 mL) [conditions: 2.95 mmol LA, 250 LA :1 Li :0 BnOH, 25 °C]. ● 2.4 ($y = 0.0358x + 0.0123$, $R^2 = 0.9954$), ■ 2.6 ($y = 0.0395x - 0.0471$, $R^2 = 0.9951$).	146
Figure 2.24. Conversion (%) vs. time for the ROP of LA initiated by 2.4 , 2.5 , 2.6 and 2.7 in CH ₂ Cl ₂ under the conditions in Table 2.4, entries 2, 8, 13 and 19. ● 2.4 , ▼ 2.5 , ■ 2.6 , ◆ 2.7	146
Figure 2.25. First-order plot of LA consumption initiated by 2.4 and 2.6 in CH ₂ Cl ₂ under	

the conditions in Table 2.4, entries 2 and 13. ● 2.4 ($y = 0.0114x + 0.0834$, $R^2 = 0.96$), ■ 2.6 ($y = 0.0257x + 0.2068$, $R^2 = 0.9983$).	147
Figure 2.26. Plot of PLA M_n and dispersity (M_w/M_n) as a function of <i>rac</i> -lactide conversion under the conditions in Table 2.4, entries 13. Line shown to indicate the linear trend and proportional increases in M_n as conversion increases.	147
Figure 2.27. Conversion (%) vs. time for the ROP of LA initiated by 2.4 in CH_2Cl_2 under the conditions in Table 2.4, entries 2, 3 and 5. ● 1 eq. BnOH , ▼ 2 eq. BnOH , ■ 4 eq. BnOH .	148
Figure 2.28. First-order plot of LA consumption initiated by 2.4 with different quantities of BnOH [conditions: CH_2Cl_2 (5 mL), 2.95 mmol LA, 250 LA :1 Li :n BnOH, 25 °C]. ● 1 eq. BnOH ($y = 0.0507x + 0.3033$, $R^2 = 0.9858$), ▼ 2 eq. BnOH ($y = 0.0259x + 0.2026$, $R^2 = 0.9944$), ■ 4 eq. BnOH ($y = 0.0812x + 0.2446$, $R^2 = 0.9963$).	148
Figure 2.29. ^1H NMR spectrum in CDCl_3 of PLA obtained under the conditions in Table 2.4, entry 12, similar spectra also obtained for entries 13, 18 and 19.	153
Figure 2.30. ^1H NMR spectrum in CDCl_3 of PLA obtained under the conditions in Table 2.4, entry 3, similar spectrum obtained for entry 5.	154
Figure 2.31. $^1\text{H}\{^1\text{H}\}$ NMR spectrum (500 MHz, CDCl_3) of the methine region of PLA produced under the conditions in Table 2.4, entry 7, similar results were obtained for entries 8, 12 and 13.	155
Figure 2.32. ^{13}C NMR spectrum (500 MHz, CDCl_3) of the methine region of PLA produced under the conditions in Table 2.4 , entry 7, similar results were obtained for entries 8, 12 and 13.	155

Figure 2.33. Representative region of the MALDI-TOF mass spectrum (reflectron mode) of PLA formed using 2.6 under the following conditions: CH ₂ Cl ₂ (5 mL), 2.95 mmol LA, 250 LA :1 Li :0 BnOH, 25 °C (similar spectra obtained for PLA from other reactions using no BnOH).	157
Figure 2.34. Representative region of the MALDI-TOF mass spectrum (reflectron mode) of PLA formed using 2.4 under the following conditions: CH ₂ Cl ₂ (5 mL), 2.95 mmol LA, 250 LA :1 Li :2 BnOH, 25 °C.....	158
Figure 2.35. Proposed mechanism of the ROP of <i>rac</i> -LA in the absence of BnOH initiated by lithium and sodium diamino-bis(phenolate) complexes (THF omitted for clarity, coordination sphere of the metals will be completed by either LA or THF).....	161
Figure 2.36. ⁷ Li NMR spectrum (116.6 MHz, C ₆ D ₆) of 2.4	162
Figure 2.37. Proposed mechanism of the ROP of <i>rac</i> -LA in the presence of BnOH initiated by sodium diamino-bis(phenolate) complexes (THF omitted for clarity, coordination sphere of the metals will be completed by either LA or THF).....	163
Figure 2.38. Monitoring of stoichiometric (M:BnOH:LA, 1:1 and 1:1:1) model reactions by ¹ H NMR spectroscopy in dichloromethane- <i>d</i> ₂ at 298 K (500 MHz).	164
Figure 2.39. Monitoring of stoichiometric (M:BnOH:LA, 1:2 and 1:2:1) model reactions by ¹ H NMR spectroscopy in dichloromethane- <i>d</i> ₂ at 298 K (500 MHz).	165
Figure 2.40. Monitoring of stoichiometric (M:BnOH:LA, 1:4 and 1:4:1) model reactions by ¹ H NMR spectroscopy in dichloromethane- <i>d</i> ₂ at 298 K (500 MHz).	166
Figure 3.1. Molecular structure (ORTEP) and partial numbering scheme for 3.1 . Ellipsoids are shown at the 50% probability level (H-atoms omitted for clarity).	185
Figure 3.2. Molecular structure (ORTEP) and partial numbering scheme for 3.2 .	

Ellipsoids are shown at the 50% probability level (H-atoms omitted for clarity).	185
Figure 3.3. Electronic absorption spectrum of 3.1 in dichloromethane.	189
Figure 3.4. Electronic absorption spectrum of 3.2 in dichloromethane.	189
Figure 3.5. Electronic absorption spectrum of 3.3 in dichloromethane.	190
Figure 3.6. Electronic absorption spectrum of 3.4 in dichloromethane.	190
Figure 3.7. Electronic absorption spectrum of 3.5 in dichloromethane.	191
Figure 3.8. Three-dimensional stack plots of IR spectra using 3.1 at 20 bar, 100 °C and [Fe]:[PO]:[Cocat] 1:4000:4.	198
Figure 3.9. Initial rates profile at various temperature based on the absorbance of the $\nu(\text{C}=\text{O})$ of the cyclic propylene carbonate (CPC). All measurements performed on the same reaction mixture and therefore different $t = 0$ for each temperature. • At 50 °C ($y = 0.0001066 x + 0.04121$, $R^2 = 0.9838$), ▼ At 60 °C ($y = 0.0004866 x + 0.01444$, $R^2 = 0.9987$), ■ At 70 °C ($y = 0.001141 x - 0.05657$, $R^2 = 0.9971$), ◆ At 80 °C ($y = 0.002372 x - 0.2107$, $R^2 = 0.988$).	200
Figure 3.10. Arrhenius plot for the formation of PC. Straight line: $y = -11840x + 27.25$, $R^2 = 0.9713$	200
Figure 4.1. β -Diiminate zinc acetate complexes used for the alternating copolymerization of CHO and CO ₂	213
Figure 4.2. Dinuclear cobalt(III) salen complexes.	214
Figure 4.3. Dinuclear macrocyclic cobalt catalyst.	215
Figure 4.4. MALDI-TOF mass spectrum of Co ₂ Cl ₂ [L1] (4.5).	219
Figure 4.5. Experimental (top) and calculated (bottom) isotopic distribution pattern for 4.5	220

Figure 4.6. MALDI-TOF mass spectrum of $\text{Co}_2\text{Cl}_2[\text{L2}]$ (4.6).....	221
Figure 4.7. Experimental (top) and calculated (bottom) isotopic distribution pattern for 4.6	221
Figure 4.8. MALDI-TOF mass spectrum of $\text{CoOAc}[\text{L1}]$ (4.7).....	222
Figure 4.9. Experimental (top) and calculated (bottom) isotopic distribution pattern for 4.7	223
Figure 4.10. Electronic absorption spectrum of $\text{Co}_2\text{Cl}_2[\text{L1}]$ (4.5) in dichloromethane. .	224
Figure 4.11. Electronic absorption spectrum of $\text{Co}_2\text{Cl}_2[\text{L2}]$ (4.6) in dichloromethane. .	225
Figure 4.12. Electronic absorption spectrum of $\text{CoOAc}[\text{L1}]$ (4.7) in dichloromethane. .	225
Figure 4.13. ^1H NMR spectrum (300 MHz, 298 K, CDCl_3) of 4.7	226

List of Abbreviations and Symbols

R: alkyl moiety

Å: Angstrom (10^{-10} m)

OR: alkoxide

BnOH: benzyl alcohol

BPA: bisphenol A

br: broad

BuLi: butyllithium

μ_B : bohr magneton

PPNCl: bis(triphenylphosphoranylidene)iminium chloride

PPN₃: bis(triphenylphosphoranylidene)iminium azide

salan: N,N'-bis(phenolato)-1,2-diaminoethane

salen: N,N'-bis(salicylaldehydo)ethylenediamine)

CHC: cyclohexene carbonate

CHO: cyclohexene oxide

Cl⁻: chloride ion

cm: centimetre (10^{-2} m)

CPC: cyclic propylene carbonate

calcd: calculated

Cat.: catalyst

δ : chemical shift

J: coupling constant

C_5D_5N : deuterated pyridine
 C_6D_6 : deuterated benzene
 CD_2Cl_2 : deuterated dichloromethane
 $CDCl_3$: deuterated chloroform
 D_2O : deuterium oxide
BDI: β -diketiminat
($^\circ$): degree
d: doublet
dd: doublet of doublets
Da: Dalton
 D : dispersity index
DHBA: 2,5-dihydroxybenzoic acid
DMAP: (4-dimethylamino)pyridine
EDBP: 2,2'-ethylidene-bis(4,6-di-tert-butylphenol)
VCHO: 1,2-epoxy-4-vinylcyclohexane
ECH: epichlorohydrin
F: goodness of fit
GPC: gel permeation chromatography
 T_g : glass transition temperature
g: gram
h: hour
Hz: Hertz
 K_i : initiation rate

i: isotactic

in situ: in the reaction mixture

IR: infrared spectroscopy

ⁱPr: isopropyl

kJ: Kilojoules

kg: Kilogram

K: Kelvin

LA: lactide

L-LA: L-lactide

LMCT: ligand to metal charge transfer

MALDI-TOF: matrix assisted laser desorption/ionization time-of-flight

MS: mass spectrometry

m/z: mass-to-charge ratio

λ_{\max} : maximum wavelength (nm)

Me: methyl

N-MeIm: 1-methylimidazole

MHz: megahertz (10^6 Hz)

min: minute

mL: millilitre (10^{-3} L)

mmol: millimole (10^{-3} mol)

μ L: microlitre (10^{-6} L)

MMAO: modified methylaluminoxane

M: molar (mol L^{-1})

m: multiplet (in NMR)

nm: nanometre (10^{-9} m)

M_n : number average molecular weight

NMR: nuclear magnetic resonance

cis: on the same side

trans: on the other side

et al.: and others

ORTEP: Oak Ridge thermal-ellipsoid plot program

Oct: Octoate

PO: propylene oxide

PPC: poly(propylene carbonate)

PCHO: poly(cyclohexene oxide)

PLA: poly(lactic acid) or polylactide

PCL: polycaprolactone

P_m : probability of meso enchainment

ppm: parts per million

P_r : probability of racemic enchainment

Ph: phenyl

PE: poly(ethene)

PGSE: Pulse-gradient spin-echo

K_p : propagation rate

q: quartet (NMR)

rac: racemic

RT: room temperature

ROP: ring-opening polymerization

K_{tr} : reversible transfer reactions

NaH: sodium hydride

s: singlet (in NMR)

SO: styrene oxide

T: temperature (°C)

t: triplet (in NMR)

^tAm: tertiary amyl

O^tBu: tert-butoxide

TBAB: tetrabutylammonium bromide

^tBu: tertiary-butyl

THF: tetrahydrofuran

TOF: turnover frequency

TON: turnover number

TPB: tris(pyrazolyl)borate

PCy₃: tricyclohexylphosphine

UV–Vis: ultraviolet-visible

vs.: versus

VT: variable temperature

M_w : weight average molecular weight

List of Appendices

Figure A. 1. ^1H NMR spectrum (300 MHz, 298 K, CDCl_3) of [L1] H_2	236
Figure A. 2. ^{13}C NMR spectrum (75.4 MHz, 298 K, C_6D_6) of [L1] H_2	237
Figure A. 3. ^1H NMR spectrum (300 MHz, 298 K, CDCl_3) of [L2] H_2	238
Figure A. 4. ^{13}C NMR spectrum (75.4 MHz, 298 K, CDCl_3) of [L2] H_2	239
Figure A. 5. ^1H NMR spectrum (300 MHz, 298 K, CDCl_3) of [L3] H_2	240
Figure A. 6. ^{13}C NMR spectrum (75.4 MHz, 298 K, CDCl_3) of [L3] H_2	241
Figure A. 7. ^1H NMR spectrum (300 MHz, 298 K, CDCl_3) of [L4] H_2	241
Figure A. 8. ^{13}C NMR spectrum (75.4 MHz, 298 K, CDCl_3) of [L4] H_2	243
Figure A. 9. ^1H NMR spectrum (300 MHz, 298 K, C_6D_6) of 2.4	244
Figure A. 10. ^{13}C NMR spectrum (75.4 MHz, 298 K, C_6D_6) of 2.4	245
Figure A. 11. ^1H NMR spectrum (500 MHz, 298 K, $\text{C}_5\text{D}_5\text{N}$) of 2.4	246
Figure A. 12. ^{13}C NMR spectrum (75.4 MHz, 298 K, $\text{C}_5\text{D}_5\text{N}$) of 2.4	247
Figure A. 13. ^{13}C NMR spectrum (75.4 MHz, 298 K, CDCl_3) of 2.4	248
Figure A. 14. ^1H NMR spectrum (300 MHz, 298 K, C_6D_6) of 2.5	249
Figure A. 15. ^{13}C NMR spectrum (75.4 MHz, 298 K, $\text{C}_5\text{D}_5\text{N}$) of 2.5	250
Figure A. 16. ^{13}C NMR spectrum (75.4 MHz, 298 K, CDCl_3) of 2.5	251
Figure A. 17. ^1H NMR spectrum (300 MHz, 298 K, C_6D_6) of 2.6	252
Figure A. 18. ^{13}C NMR spectrum (75.4 MHz, 298 K, C_6D_6) of 2.6	253
Figure A. 19. ^1H NMR spectrum (300 MHz, 298 K, C_6D_6) of 2.7	254
Figure A. 20. ^{13}C NMR spectrum (75.4 MHz, 298 K, CDCl_3) of 2.7	255
Figure A. 21. ^1H NMR spectrum (300 MHz, 298 K, CDCl_3) of 4-methyl-1,3-dioxolan-2-	

one (Table 3.4, entry 1).....	256
Figure A. 22. ^{13}C NMR spectrum (75.4 MHz, 298 K, CDCl_3) of 4-methyl-1,3-dioxolan-2-one (Table 3.4, entry 1).....	257
Figure A. 23. ^1H NMR spectrum (300 MHz, 298 K, CDCl_3) of 4-chloromethyl-1,3-dioxolan-2-one (Table 3.4, entry 2).....	258
Figure A. 24. ^{13}C NMR spectrum (75.4 MHz, 298 K, CDCl_3) of 4-chloromethyl-1,3-dioxolan-2-one (Table 3.4, entry 2).....	259
Figure A. 25. ^1H NMR spectrum (300 MHz, 298 K, CDCl_3) of 4-hydroxymethyl-1,3-dioxolan-2-one (Table 3.4, entry 3).....	260
Figure A. 26. ^{13}C NMR spectrum (75.4 MHz, 298 K, CDCl_3) of 4-hydroxymethyl-1,3-dioxolan-2-one (Table 3.4, entry 3).....	261
Figure A. 27. ^1H NMR spectrum (300 MHz, 298 K, CDCl_3) of 4-allyloxymethyl-1,3-dioxolan-2-one (Table 3.4, entry 4).....	262
Figure A. 28. ^{13}C NMR spectrum (75.4 MHz, 298 K, CDCl_3) of 4-allyloxymethyl -1,3-dioxolan-2-one (Table 3.4, entry 4).....	263
Figure A. 29. ^1H NMR spectrum (300 MHz, 298 K, CDCl_3) of 4-phenoxyethyl-1,3-dioxolan-2-one (Table 3.4, entry 5).....	264
Figure A. 30. ^{13}C NMR spectrum (75.4 MHz, 298 K, CDCl_3) of 4-phenoxyethyl-1,3-dioxolan-2-one (Table 3.4, entry 5).....	265
Figure A. 31. ^1H NMR spectrum (300 MHz, 298 K, CDCl_3) of 4-phenyl-1,3-dioxolan-2-one (Table 3.4, entry 6).....	266
Figure A. 32. ^{13}C NMR spectrum (75.4 MHz, 298 K, CDCl_3) of 4-phenyl-1,3-dioxolan-2-one (Table 3.4, entry 6).....	267

Figure A. 33. ^1H NMR spectrum (300 MHz, 298 K, CDCl_3) of <i>cis</i> -1,2-cyclohexene carbonate (Table 3.4, entry 7).	268
Figure A. 34. ^{13}C NMR spectrum (75.4 MHz, 298 K, CDCl_3) of <i>cis</i> -1,2-cyclohexene carbonate (Table 3.4, entry 7).	269
Figure A. 35. ^1H NMR spectrum (300 MHz, 298 K, CDCl_3) of 4-methyl-1,3-dioxolan-2-one (Table 4.1, entry 5).	270
Figure A. 36. ^1H NMR spectrum (300 MHz, 298 K, CDCl_3) of 4-methyl-1,3-dioxolan-2-one (Table 4.1, entry 6).	271
Figure B. 1. MALDI-TOF mass spectrum of $[\text{L1}]\text{H}_2$.	272
Figure B. 2. Experimental (top) and calculated (bottom) isotopic distribution pattern for $[\text{L1}]\text{H}_2$.	272
Figure B. 3. MALDI-TOF mass spectrum of $[\text{L2}]\text{H}_2$.	273
Figure B. 4. Experimental (top) and calculated (bottom) isotopic distribution pattern for $[\text{L2}]\text{H}_2$.	273
Figure B. 5. MALDI-TOF mass spectrum of $[\text{L3}]\text{H}_2$.	274
Figure B. 6. Experimental (top) and calculated (bottom) isotopic distribution pattern for $[\text{L3}]\text{H}_2$.	274
Figure B. 7. MALDI-TOF mass spectrum of $[\text{L4}]\text{H}_2$.	275
Figure B. 8. Experimental (top) and calculated (bottom) isotopic distribution pattern for $[\text{L4}]\text{H}_2$.	275
Figure B. 9. MALDI-TOF mass spectrum of 2.4 .	276
Figure B. 10. Experimental (top) and calculated (bottom) isotopic distribution pattern for 2.4 .	276

Figure B. 11. MALDI-TOF mass spectrum of 2.5	277
Figure B. 12. Experimental (top) and calculated (bottom) isotopic distribution pattern for 2.5	277
Figure B. 13. MALDI-TOF mass spectrum of 2.6	278
Figure B. 14. Experimental (top) and calculated (bottom) isotopic distribution pattern for 2.6	278
Figure B. 15. MALDI-TOF mass spectrum of 2.7	279
Figure B. 16. Experimental (top) and calculated (bottom) isotopic distribution pattern for 2.7 . Na[L2] (left) and Na ₂ [L2] (Right).....	279
Figure B. 17. MALDI-TOF mass spectrum of 3.1	280
Figure B. 18. Experimental (top) and calculated (bottom) isotopic distribution pattern for 3.1 with K.....	280
Figure B. 19. MALDI-TOF mass spectrum of 3.2	281
Figure B. 20. Experimental (top) and calculated (bottom) isotopic distribution pattern for 3.2 with K.....	281
Figure B. 21. MALDI-TOF mass spectrum of 3.3	282
Figure B. 22. Experimental (top) and calculated (bottom) isotopic distribution pattern for 3.3	282
Figure B. 23. Experimental (top) and calculated (bottom) isotopic distribution pattern for 3.3 with K.	283
Figure B. 24. MALDI-TOF mass spectrum of 3.4	284
Figure B. 25. Experimental (top) and calculated (bottom) isotopic distribution pattern for 3.4	284

Figure B. 26. MALDI-TOF mass spectrum of 3.5	285
Figure B. 27. Experimental (top) and calculated (bottom) isotopic distribution pattern for 3.5	285

Chapter 1

1.1 Introduction

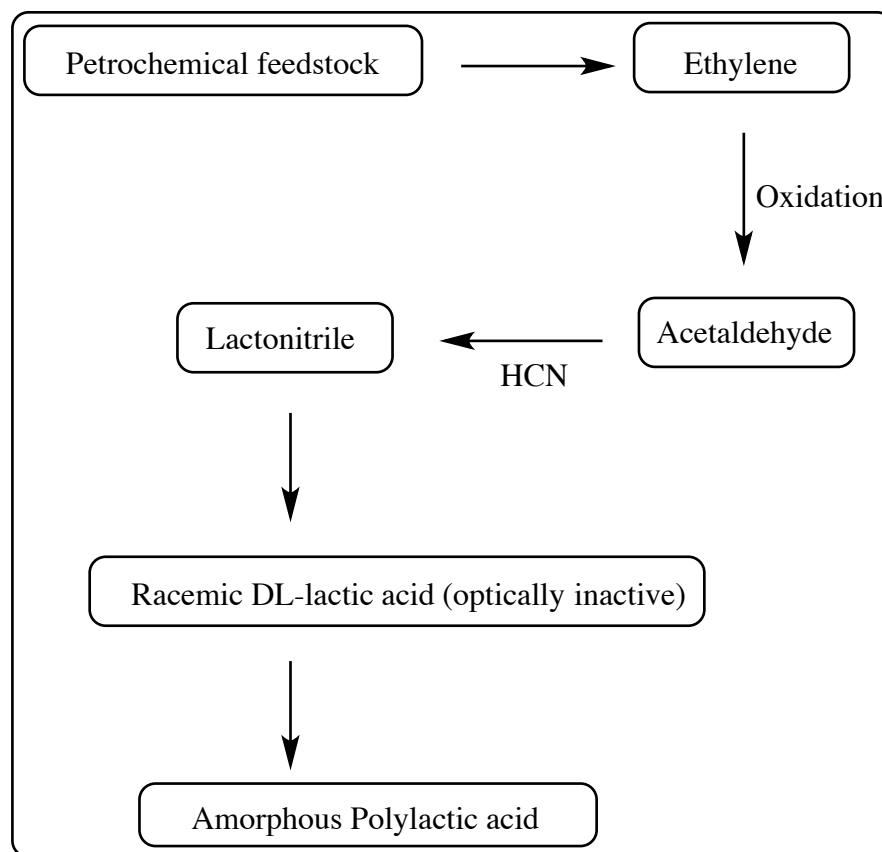
Nowadays a large number of polymers introduced into the daily life of humans are derived from fossil fuels. However, with the benefit of these fossil fuel based polymeric goods come concerns regarding the depletion of these non-renewable resources and environmental problems associated with their waste disposal. As a result there has been a heightened awareness towards the importance of alternative and, more importantly, renewable carbon-based sources as raw materials.¹⁻⁴ In light of this, biodegradable and biocompatible polymers such as polyesters and polycarbonates (PC) whose monomers can be sources from renewable feedstocks offer an alternative making them of particular interest in the field of polymer chemistry.^{2,4} The most common method used to produce these polymers is ring-opening polymerization (ROP) initiated by metal complexes.^{5,6}

For the polyester, polylactide (PLA), the lactide monomer is the cyclic dimer of lactic acid which can be obtained by fermentation of glucose.^{2,4} Over the past few years, much concern has been raised with respect to the rising levels of CO₂ released into our environment and its contribution to the Greenhouse Effect as a result of combustion of hydrocarbon based resources. However, viewing this from an alternate point of view, this CO₂ could also be considered as a source for the preparation of polycarbonates (PC).^{4,7,8}

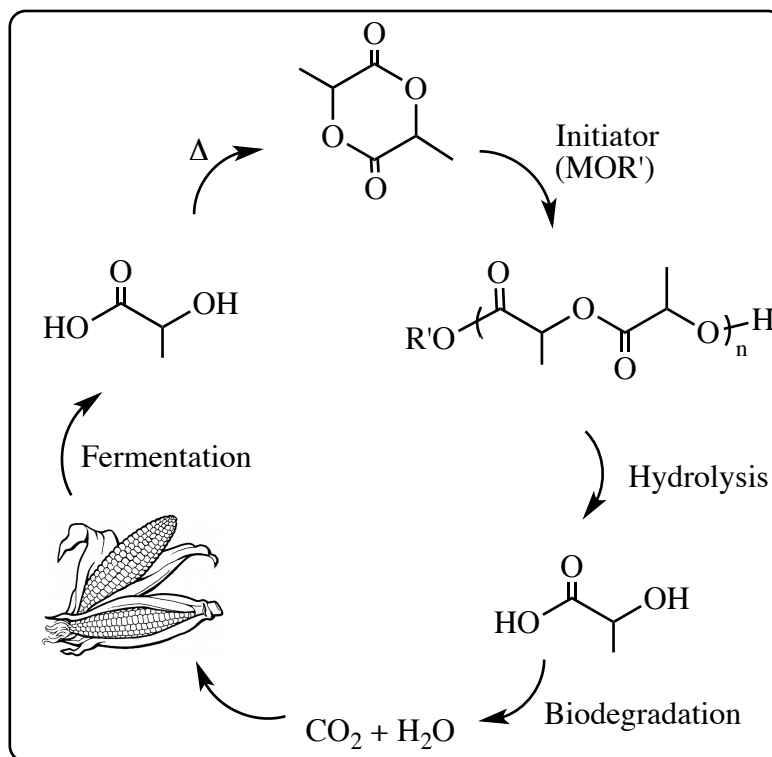
1.2 Ring-opening polymerization of lactide

In recent years, considerable efforts have been directed towards the design of bio-based and degradable polymers with particular interest focused on linear aliphatic polyesters such as polylactide (PLA) and polycaprolactone (PCL).^{3,9,10} Commercially, as a result of being biodegradable, biocompatible, and its renewable nature, PLA has received a significant amount of interest as a packing material and in the pharmaceutical and biomedical fields.^{5,11-20} The lactic acid monomer used in the production of polylactide was first synthesized from a petrochemical source to yield an optically inactive racemic mixture of the L- and D- enantiomers (**Scheme 1.1**). However, with the recognition of the need for more economic and renewable carbon resources coupled with increasing concerns about the depletion of fossil fuels, the petrochemical route of monomer production lost prevalence around 1990.¹¹ An alternative route, the bacterial-fermentation of molasses or corn starch using an optimized strain of *Lactobacillus* is regarded as a renewable way of making lactic acid (**Scheme 1.2**).^{12,21}

The biopolymer PLA was first obtained by Carothers in 1932 as a low molecular weight product by heating lactic acid in a vacuum.¹¹ However, the production of high molecular weight polymer was patented by DuPont. Today, Cargill Dow LLC operates the world's largest PLA operation, manufacturing PLA from corn on a 140,000 ton per year industrial scale.^{22,23} The first commercialized PLA produced by Cargill Dow LLC was synthesized from renewable resources under the trade name NatureWorks.²⁴



Scheme 1.1. Petroleum route to lactic acid.¹¹

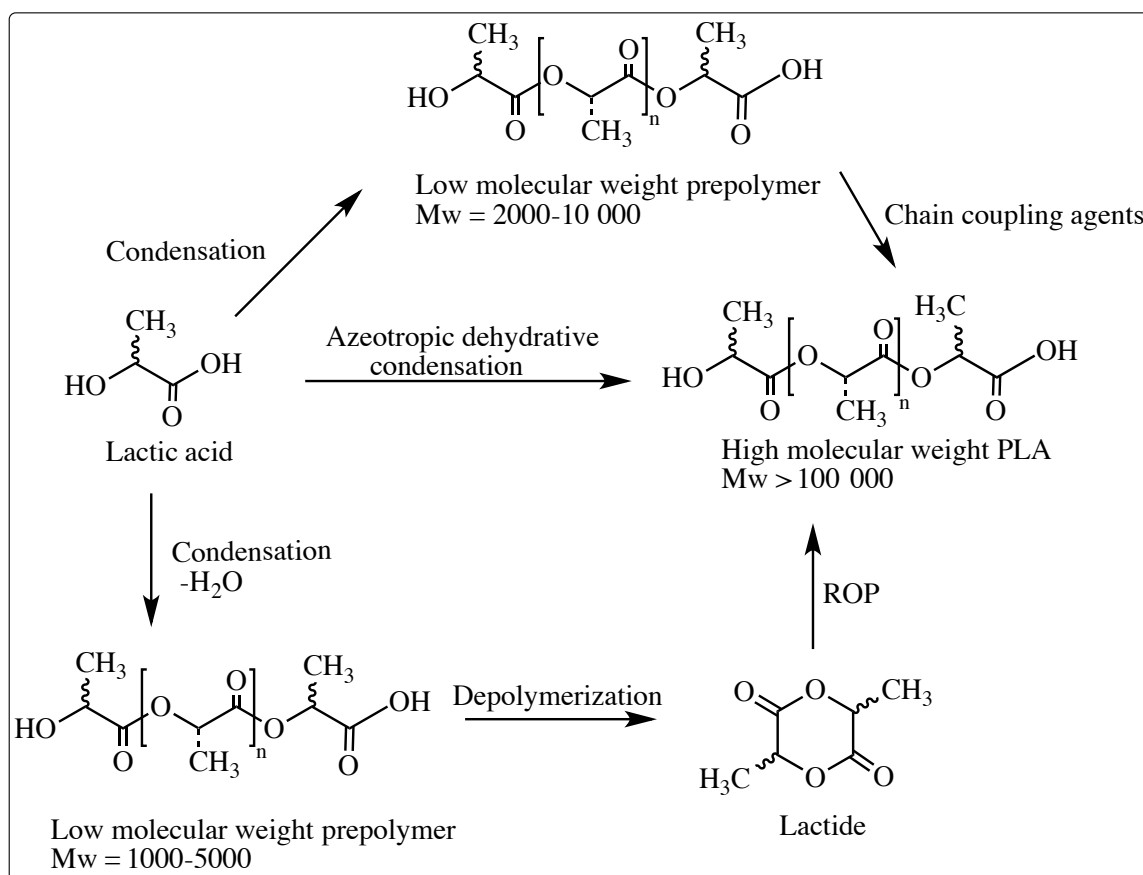


Scheme 1.2. The life cycle of polylactide (PLA) produced from corn.^{12,21}

The unique physical properties of PLA such as its resistance to moisture and grease in addition to its high tensile strength make it a viable alternative to more traditional polymers like polystyrene and polyethylene terephthalate, which are typically used to make containers, including bottles.^{5,14,18} Commercial PLA can be synthesized in one of two ways; either by way of a condensation reaction or a catalytic ring-opening polymerization. As seen in **Scheme 1.3**, in the polycondensation route, PLA with a high molecular weight can be produced by a direct condensation reaction in the presence of solvents and under high vacuum. Alternatively, it can be produced by the depolymerization of low molecular weight PLA to yield lactide and the subsequent ROP of lactide to produce PLA with controlled molecular weights.^{11,13,22} The direct condensation process used by Carothers is still used by Mitsui Chemicals and starts with a continuous

condensation reaction of aqueous lactic acid to produce low molecular weight PLA prepolymer. The resulting polymer can be used as a low molecular weight polymer or coupled with isocyanates, epoxides or peroxide to produce higher molecular weight polymers. Although it is possible to obtain PLA by polycondensation routes, the difficulty of removing water produced in the condensation reaction, the high temperatures and long reaction times limits its widespread use.¹¹ As a means to high molecular weight PLA, Mitsui Chemicals patented an azeotropic distillation process, used until 2008. This method used a high-boiling solvent such as diphenyl ether and a catalyst. Water is continuously removed by Soxhlet extraction through molecular sieves.^{13,22,24}

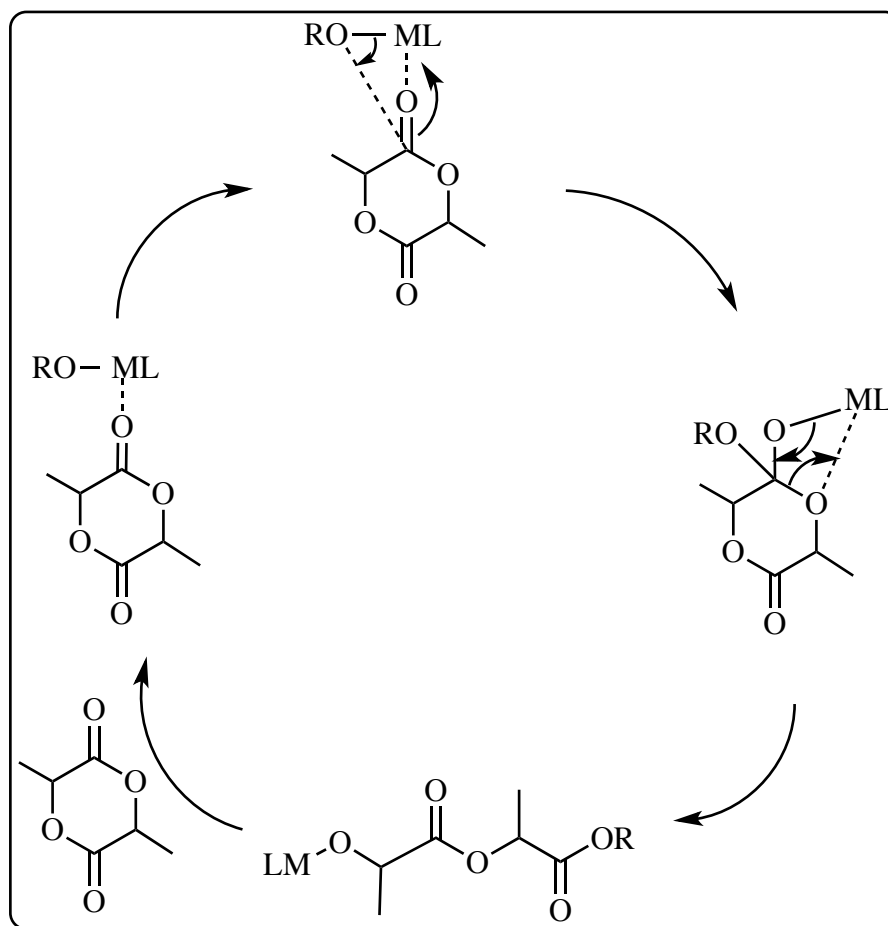
The direct ring-opening polymerization (ROP) of the cyclic lactide dimer has been the most common method of PLA synthesis since the 1970s.^{5,6} Perhaps this is due to the fact that by conducting the ROP in the presence of catalysts and/or initiators, it is possible to create a “living polymerization” which allows a high degree of control over polymer growth resulting in the desired high molecular weight and low dispersity polymers.^{20,24} Ultimately, “living polymerization” is defined as a chain polymerization without irreversible transfer and termination reactions and allows control of polymer features such as chain length. To successfully control ROP, the rate of chain initiation of the first monomer unit should be faster than the rate of chain propagation ($k_i \gg k_p$). In addition, in order to obtain polymers with narrow molar weight distributions, reversible transfer reactions must proceed faster than propagation ($k_{tr} \gg k_p$).²⁵



Scheme 1.3. Synthesis of polylactide by direct condensation reaction and/or catalytic ring-opening polymerization (ROP).^{4,6}

The thermodynamic driving force for the polymerization is the relief of ring strain, which enables the entropy to be overcome.^{12,24} The generally accepted and commonly postulated mechanism for ROP is the coordination insertion mechanism (**Scheme 1.4**), which provides lower energy costs, higher atom efficiency (catalytic initiators being used), and allows for the synthesis of higher molecular weight polymers when compared to molecular weights of polymers produced using a polycondensation route. The catalytic cycle starts when the metal alkoxide catalyst, which may originate from the ligand within the same complex or from the addition of a co-initiator such as an aliphatic alcohol, coordinates to and activates the lactide (LA) monomer by attack of the

alkoxide bond at the carbonyl carbon of lactide. Acyl bond cleavage then results in ring-opening of lactide and generation of a novel metal alkoxide species, which can reinitiate the cycle. Termination then occurs by hydrolysis of the propagating chain.¹² The production of PLA through ROP has been successfully carried out in solution, melt, and suspension phases using a variety of metal catalysts. Several factors influence the selection of the metal catalyst including its Lewis acidity, cost, toxicity, and the high abundance of the desired metal initiator.²⁶



Scheme 1.4. General coordination-insertion mechanism for lactide ROP.¹²

Although, the commercial production of PLA has been dominated by ROP, the process is not without its synthetic challenges. One difficulty of the process is that it is plagued by undesirable side reactions during polymerization, particularly at elevated temperature.^{25,27} Transesterification reactions⁵ may be either intermolecular, resulting in high molecular weight polymers, or intramolecular, resulting in macrocyclic polymers; thus polymers with a range of molecular weights and broad dispersity are produced.^{4,24, 26-}
²⁸ Generally, transesterification reactions are influenced by factors such as temperature, reaction time, type of initiator, and nature of the monomer. However, it has been established that these side reactions can be avoided by using metal complexes bearing bulky ligands, which lead to more controlled polymerization. A second drawback of ROP is the presence of catalyst residue and unwanted residual monomer in the synthesized polymers. This can lead to the production of high molecular weight PLA which requires complicated purification and isolation processes making its manufacture costly and thereby limiting its application for commodity materials.^{4,21}

1.2.1 Catalysts for the polymerization of lactide

As a result of the synthetic challenges presented by the production of PLA, one focus for improvement has been on the design of the catalysts used in the reaction. The most common initiator for coordination-insertion polymerization is a metal alkoxide with a covalent bond between the metal and oxygen atoms. The most frequently used coordination initiators and catalysts are $[\text{Al}(\text{O}i\text{Pr})_3]$, zinc(II) lactate $[\text{Zn}(\text{Lact})_2]$ and tin(II) bis(2-ethylhexanoate), also known as $[\text{Sn}(\text{Oct})_2]$ (tin(II) octoate) (**Figure 1.1**).^{3,6,13,22,29-31}

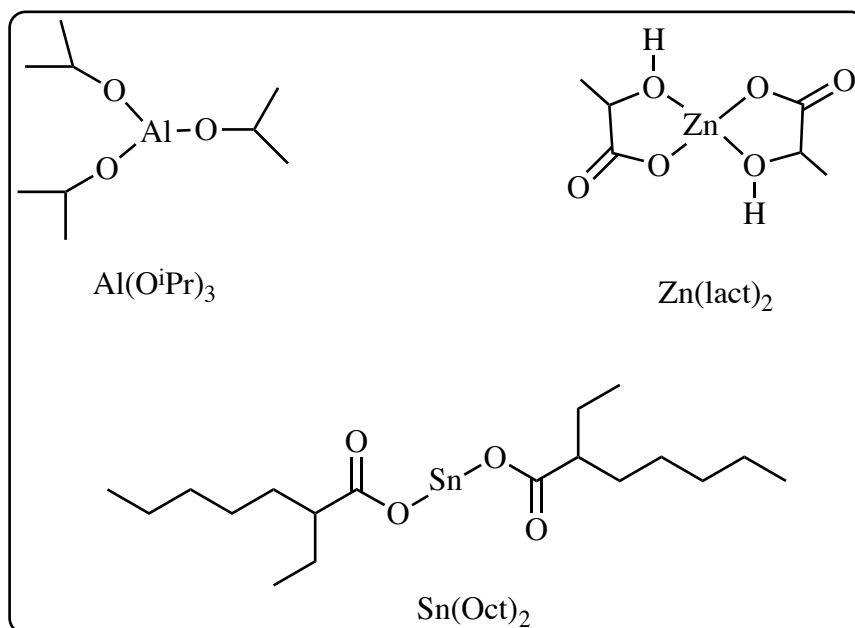
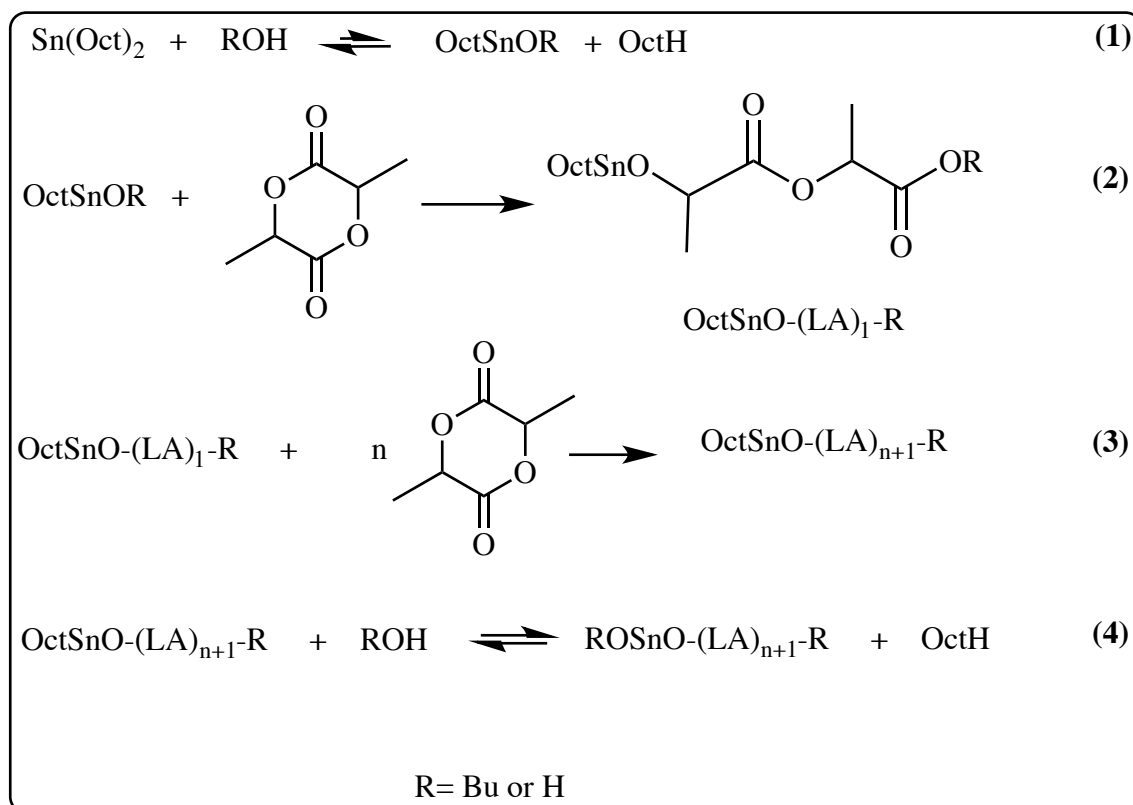


Figure 1.1. Chemical structure of initiators used in ROP of lactide (tin(II) octoate, zinc(II) lactate, aluminum(III) isopropoxide).^{3,6,13,22,29-31}

Industrially, the most widely used catalyst to initiate ROP of lactide (LA) via a coordination-insertion mechanism is tin octoate ($\text{Sn}(\text{Oct})_2$). This catalyst is preferred for bulk polymerization to produce high molecular weight polymers for several reasons: its solubility in molten lactide, high catalytic activity with a conversion greater than 90%, and the low rate of racemization of the polymer. Typical conditions for polymerization to reach 95% conversion are 180–210 °C, a catalyst concentration of 100–1000 ppm, and a reaction time of 2–5 h. To accelerate the reaction and control the molecular weight, 1-octanol has been used as a hydroxyl-containing initiator.²² The mechanism has been elucidated by Polish researchers, as shown in **Scheme 1.5**.^{13,32,33} The first step is the establishment of equilibrium if a protic compound ROH (such as water or alcohol) is present in the polymerization mixture. The second step is initiation involving the ROP of lactide (LA) by tin(II) alkoxide groups, followed by propagation or continuous insertions

of monomer. The final step is hydrolysis and termination of polylactide chains with –OH groups.¹³ Although widely used, these polymerizations using Sn(Oct)₂ suffer from a need for elevated temperatures or long reaction times and problems with toxicity should not go unrecognized. Moreover, the resulting polymers have uncontrolled molecular weights and broad molecular weight distributions, which can be attributed to the presence of transesterification side reactions and multiple nuclearities in the catalyst structure.^{6, 34, 35}



Scheme 1.5. Polymerization of lactides initiated by Sn(Oct)₂/ROH system.¹³

1.2.2 Ligands and single-site initiators used in the ROP of cyclic esters

Multidentate ligands with N-donor atoms were among the earliest used to prepare metal catalysts for ROP of LA. It is worth noting the impact of the work of Coates, in which β -diketiminate (BDI)-supported catalysts, and Chisholm, in which tris(pyrazolyl)borate (TPB) complexes were used as initiators in the polymerization of lactide.^{36,37}

Many other ligand frameworks have been employed to make catalysts for ROP of LA, including ligands with N- and O-donor atoms, such as amino-bis(phenolates). These have become an important ligand class in this field due to their ability to coordinate to a wide range of metal centres and to form sterically bulky complexes that enhance the formation of PLA with controlled molecular weights. Additionally, the toxicity issues encountered as a result of incorporation of toxic metals such as tin in the polymer chains limits application of these catalysts. As a result, main group metals including magnesium,^{23,38-41} calcium,^{23,42,43} barium,⁴⁴ and aluminum⁴⁵⁻⁴⁸ with these ligands have been studied. In particular, alkali metal complexes of lithium and sodium bearing bulky ligands have shown promise in the ROP of cyclic esters in general as presented in section 1.2.2.3, with few side reactions, and is relevant to the work described in this thesis. Both metals tend to form aggregated species in solution and in the crystalline state, depending on the steric properties of the ligand or solvent used, thereby decreasing the occurrence of side reactions while affording control over polymer formulations and microstructures. These complexes are attractive in this field because of their stability, low cost, and low toxicity.

1.2.2.1 Amino-bis(phenolate) ligands and their applications

For polymerization of LA and other cyclic esters, controlling the activity and selectivity of the metal species depends on the variability of the electronic and steric properties of the ligand.⁴⁹ Amino-bis(phenolates) are multidentate ligands with N and O donor atoms which surround the metal in a cavity or cup-shaped structure (**Figure 1.2**). These ligands can be electronically or sterically modified by either substitution of the *ortho* and *para* substituents (R) on the aromatic ring or the substituents on the amine unit.⁵⁰ Amine-bis(phenolate) ligands can be effective in producing an active metal centre, and they are often bulky enough to prevent side reactions.

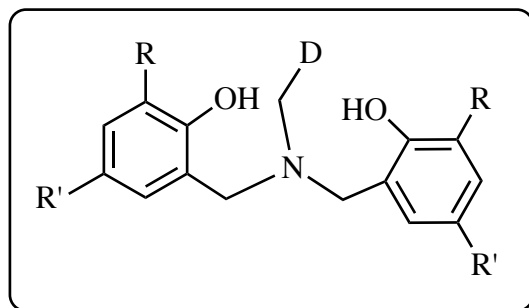


Figure 1.2. The general structure of the aminobisphenolate ligands. The groups R and R' are different phenol substituents and D is any alkyl chain containing the side chain donor atom.⁵⁰

The first method for the synthesis of tetradentate tripodal amino-bis(phenols) was introduced by Hinshaw and coworkers in 1989.⁵¹ Their synthesis was based on the reductive amination of salicylaldehyde in the presence of sodium cyanoborohydride as a reducing agent. Since this time, several methods to prepare these ligands have been reported, with the most common one based on the single-step Mannich condensation reaction. This method involves the combination of readily available starting materials

including amines, formaldehyde, and substituted phenols in stoichiometric amounts. Although dioxane⁵² and ether⁵³⁻⁵⁵ have been reported as solvents for this reaction, low yields of the desired product were obtained. Kerton and coworkers used water as the reaction medium in a more environmentally friendly route to the preparation of amino-phenol ligands with higher yield and better reproducibility.^{56,57}

The complexation of a wide range of metals with amino-bis(phenolates) was demonstrated in the late 1980s, yielding group 4, 5, 6, and 7 metal complexes.⁵⁰ Moreover, the role of amino-bis(phenolate) ligands in stabilizing the active catalytic species under different reaction conditions, including polymerization of cyclic esters, alkene polymerization, and oxidation reactions has been clearly demonstrated in the past 20 years.⁵⁰ The following section is not intended to give a comprehensive review of all transition metal amino-bis(phenolate) complexes reported but to describe references that are relevant to the research presented in this thesis.

1.2.2.1.1 Complexes for polymerization of cyclic esters

A number of complexes supported by amino-bis(phenolate) ligands have been shown to be active in the polymerization of lactide and ϵ -caprolactone. Complexes of Li and Na used in this area are presented in section 1.2.2.3. The majority of the research carried out in the late 90s and 2000s was based on the lanthanide series. For example, lanthanide amino-bis(phenolate) complexes with the formula $[M(O_2NN^R)Cl(THF)]$ (where M = Y, Yb, Ho, Gd, Sm, and Pr) were efficient initiators for the controlled ROP of ϵ -caprolactone (**Figure 1.3**).²⁶ The size of the metal centre can result in significant changes in the reactivity of the complex and molecular weights achieved. The Yb catalyst

species was the least catalytically active and yielded the lowest molecular weight polymer; however, the polymer had the narrowest dispersity.

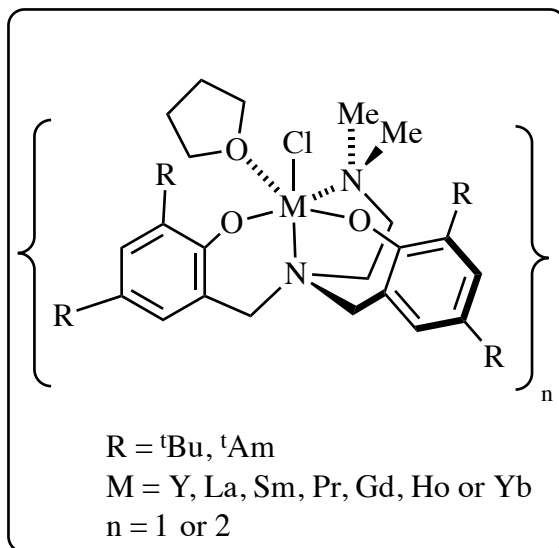


Figure 1.3. Synthesis of chloro-bis(phenolate)diamine complexes of lanthanides.²⁶

A number of novel divalent lanthanide bis(phenolate) complexes have been evaluated as catalysts for the ROP of ϵ -caprolactone and L-lactide cyclic esters (**Figure 1.4**).⁵⁸ Two main conclusions were noted from this study: 1) dinuclear M(II) compounds have similar activity to their monomeric counterparts, and 2) samarium-based catalysts polymerized ϵ -caprolactone and L-lactide more rapidly than their ytterbium analogues, indicating that larger lanthanide metal catalysts were more active for ROP than those containing smaller lanthanide ions.

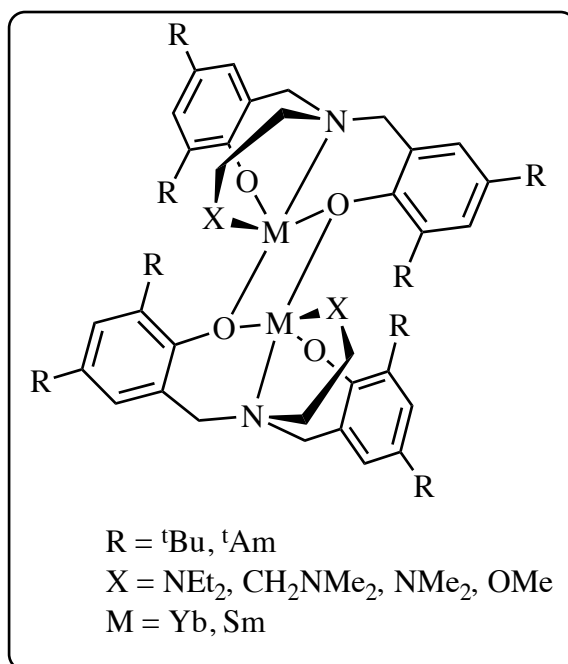


Figure 1.4. Synthesis of divalent ytterbium and samarium bis(phenolate) compounds.⁵⁸

Yao and coworkers reported a series of neutral amine-bridged lanthanide aryloxo bis(phenolate) complexes of the form $[\text{M}(\text{O}_2\text{NN}^t\text{Bu})(\text{OAr})(\text{THF})]$ (where $M = \text{Nd}, \text{Sm}, \text{Yb}$), which successfully initiated the ROP of L-lactide (**Figure 1.5**).⁵⁹ All complexes produced polymers with high molecular weights and relatively narrow molecular weight distributions ($\mathcal{D} = 1.10\text{--}1.59$). The activity of the complexes was affected by the temperature, with higher temperature giving faster polymerization. The ionic radii of the lanthanide metals also had a significant effect on catalytic activity, where activity decreased in the order $\text{Nd} > \text{Sm} > \text{Yb}$. The same study showed that the structure of the aryloxo groups themselves had no obvious effect on the catalytic activity.

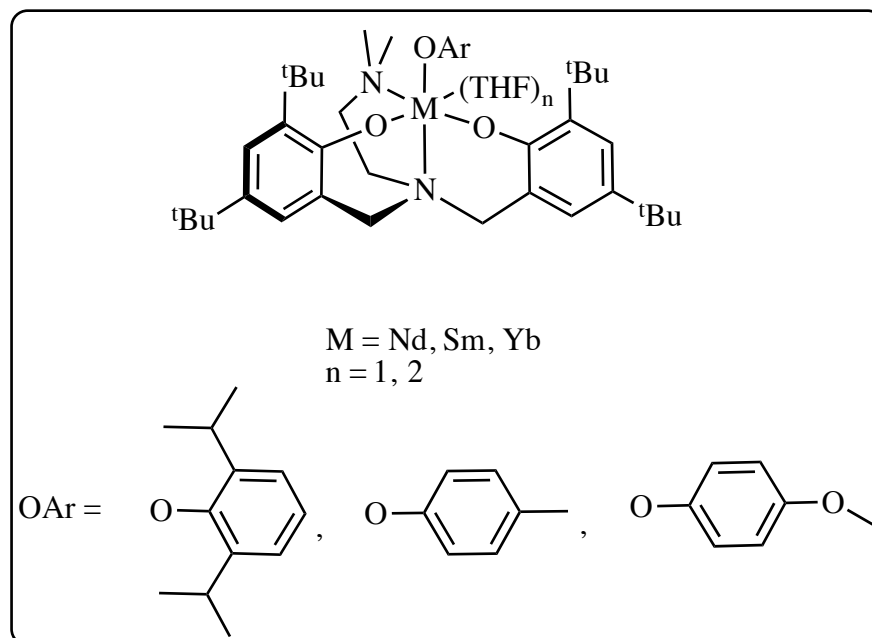


Figure 1.5. Synthesis of amino bis-(phenolate) lanthanide aryloxides.⁵⁹

In 2014, dinuclear lanthanide aryloxides and alkoxides supported by an amino-bridged bis(phenolate) ligand were found to be efficient initiators for the ROP of *rac*-lactide at room temperature (**Figure 1.6**).⁶⁰ The resulting polymers were highly heterotactic (P_r values of up to 0.99) with high molecular weights and narrow molecular weight distributions. Similarly, lanthanides of larger ionic radii proved to be more active for the ROP of *rac*-lactide than those of smaller ionic radii as the observed activity trend in decreasing order is Nd > Sm > Yb \approx Y. Moreover, alkoxide complexes demonstrated higher activities and greater control than aryloxides with the same metal centre.

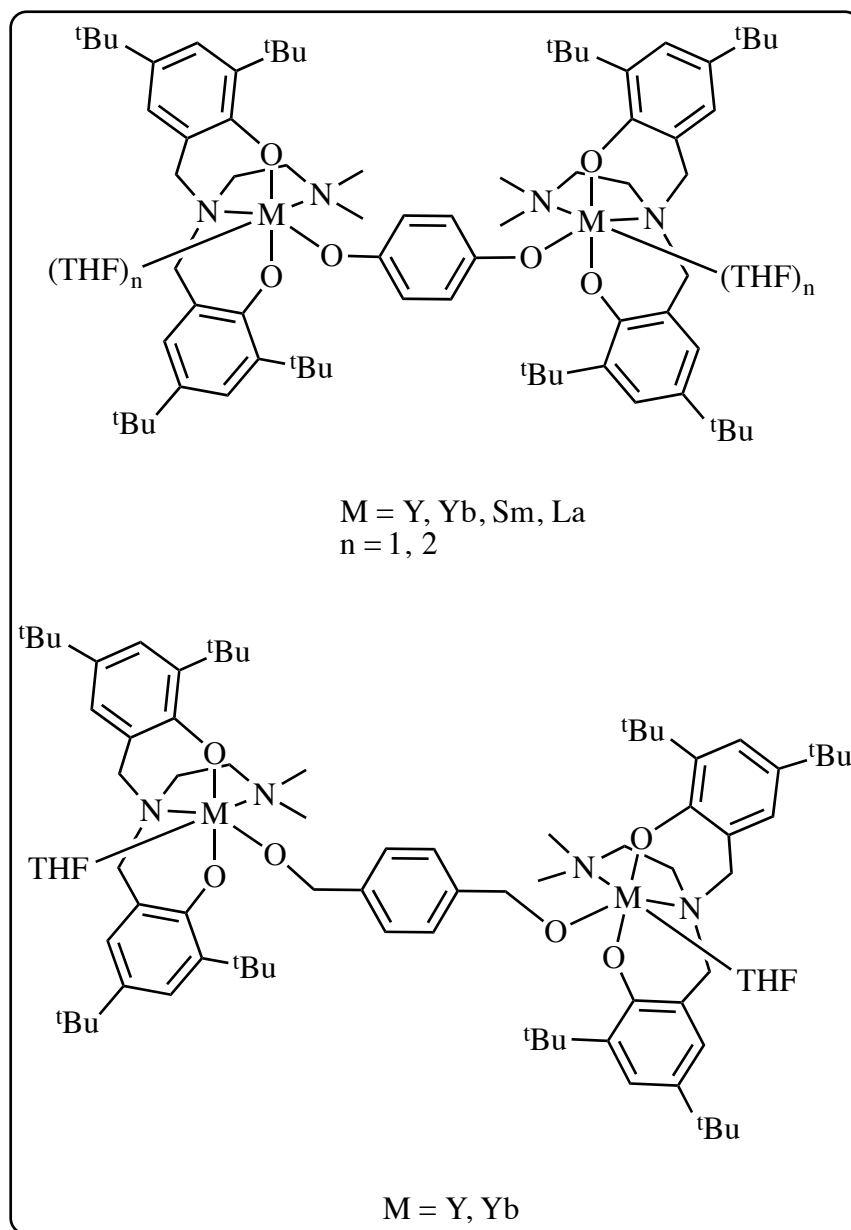


Figure 1.6. Dinuclear amino bis(phenolate) lanthanide aryloxides (top) and alkoxides (bottom).⁶⁰

1.2.2.1.2 Complexes for the polymerization of alkenes

Amino-bis(phenolate) complexes based on Group 4 transition metals have been extensively studied by Kol *et al.* as catalysts for olefin polymerization.⁶¹ As seen in **Figure 1.7**, amino-bis(phenolate) zirconium complexes were first used bearing a

dimethylamine donor side-arm. This side-arm donor proved to be necessary for high activity towards 1-hexene polymerization and to produce a high molecular weight polymer. The high activity was attributed to the presence of a tetradentate ligand around the metal centre and the *cis* positions of the active benzyl groups.

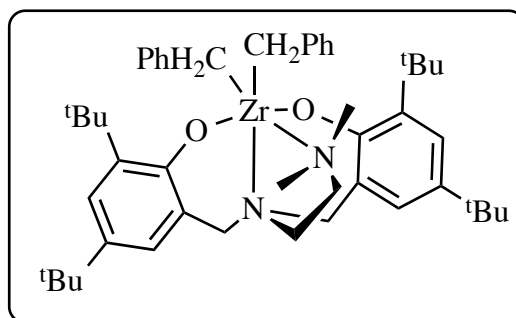


Figure 1.7. Zirconium complexes of amino-bis(phenolate) ligands.⁶¹

Further advances in ligand design were made by Kol and coworkers, who introduced a different side-arm donor (**Figure 1.8**).⁶² Bulky substituents on the N-donor, such as diethylamine, reduced the reactivity dramatically and led to oligomers, whereas a pyridine donor group led to a moderately active polymerization catalyst. In addition, the incorporation of a dimethylamino group into the ligand did not form any polymer, resulting in a rapidly deactivated catalyst.

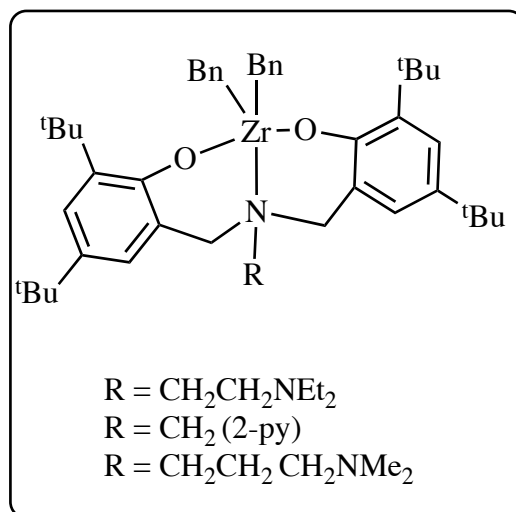


Figure 1.8. Zirconium dibenzyl complexes of amino-bis(phenolate) ligands.⁶²

In 2002, the same group investigated the activity of zirconium and hafnium dibenzyl complexes of amino-bis(phenolate) ligands, where X was a heteroatom donor located on a pendant arm (**Figure 1.9**).⁶³ All complexes exhibited remarkable activities in the polymerization of 1-hexene, yielding high molecular weight polymers. The activity of zirconium complexes varied as a function of the side-arm donor in the following order from most active to least active: OMe > NMe₂ > SMe. However, the activity of hafnium complexes decreased in the order SMe > OMe > NMe₂.

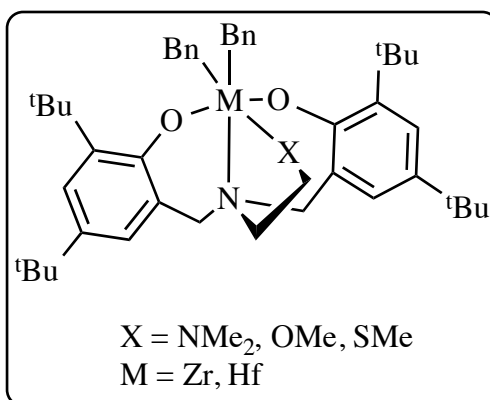


Figure 1.9. [ONXO]-Type Zr and Hf amino-bis(phenolate) complexes.⁶³

The effect of phenolate substituent variation was also explored by Kol and coworkers,⁶⁴ who investigated the activity of titanium complexes for the polymerization of 1-hexene. The complexes contained either a dimethylamino or methoxy group as the pendant donor, and the substituents on the phenolate rings were either electron-donating alkyl groups of varying bulkiness or electron-withdrawing chloro groups (**Figure 1.10**). The most active titanium catalyst carried a dimethylamino side-arm donor and chloro groups in the *ortho* and *para* positions of the phenolate rings. Within only 1 h at room temperature, the polymer reached a very high molecular weight (>4,000,000 g mol⁻¹).

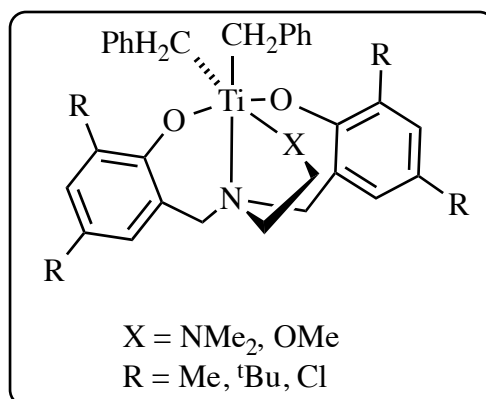


Figure 1.10. Dibenzylamino-bis(phenolate) Ti(IV) complexes.⁶⁴

Waymouth and coworkers found that the type of side-arm donor and substituents in the phenolate part of the ligand had a powerful effect on catalyst activity.⁶⁵ They investigated the activity of zirconium complexes on ethylene/1-hexene copolymerization when activated with modified methylaluminoxane (MMAO) (**Figure 1.11**). The authors found that the complex bearing methyl substituents had a lower activity than the complexes with *tert*-butyl and phenyl substituents. The polymerization was also sensitive to the pendant donor, with activity increased by several factors upon substitution of a methoxy side-arm donor with a dimethylamino group.

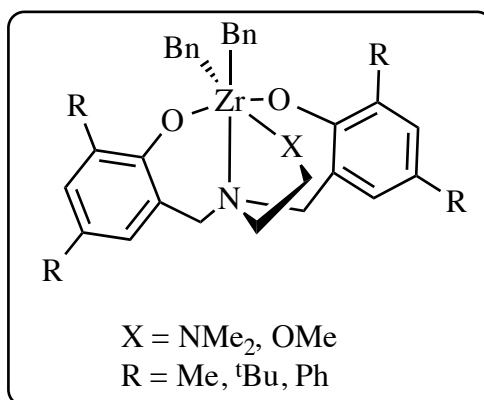


Figure 1.11. Zirconium amino-bis(phenolate) complexes used in ethylene/1-hexene copolymerization studies.⁶⁵

The current research is not limited to Group 4 metals, Lorber and coworkers described the synthesis of new amino-bis(phenolate) complexes of vanadium(II) to vanadium(V).⁶⁶ The complexes catalyzed ethylene polymerization in the presence of 10 equivalents of EtAlCl₂ as a cocatalyst under 1 atm of ethylene at 20 °C in toluene. The highest activity was reported for the V(IV) complex [V(ONNO)(OPrⁱ)₂] (**Figure 1.12**) resulting in a polymer with a molecular weight of 338,000 g mol⁻¹ and dispersity of 2.

However, the V(II) complex gave poor yields of polyethylene, suggesting that the low oxidation state of vanadium gives rise to inactive or less active catalysts.

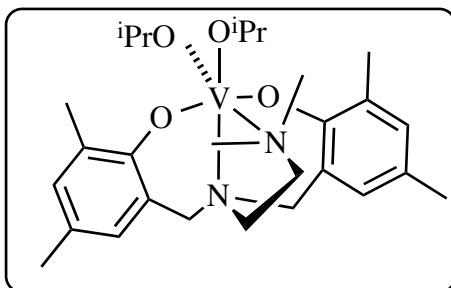


Figure 1.12. Vanadium(IV) amino-bis(phenolate) complexes.⁶⁶

In 2011, Lorber and coworkers extended their catalyst studies to the *cis* and *trans* isomers of the vanadyl complex [VO(ONNO)(OPr¹)] in the presence of other cocatalysts, including dimethylaluminium chloride (DMAC), methylaluminoxane (MAO), and trimethylaluminium (TMA); all with or without the re-activator trichloroethylacetate (ETA).⁶⁷ Both configurations (**Figure 1.13**) were found to effectively initiate the polymerization of ethylene using DMAC as the superior cocatalyst in the presence of ETA. They observed that the role of the side-arm donor is mainly to increase the thermal stability of the complex while the reactions are performed at high temperature (60–80 °C).

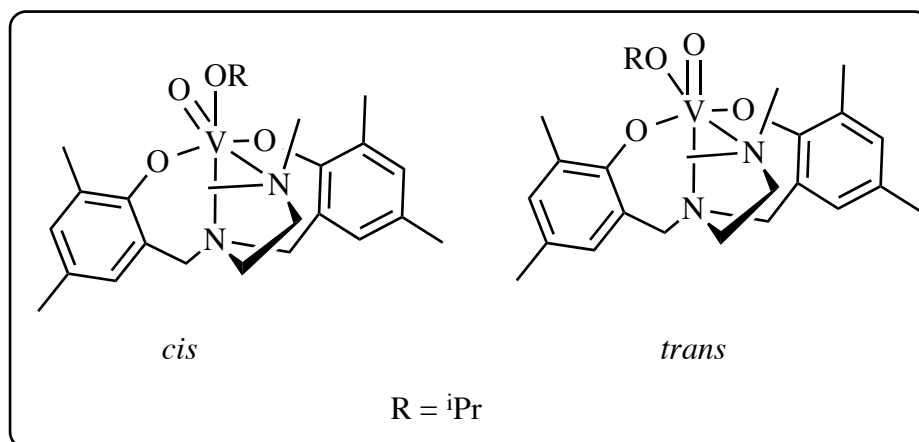


Figure 1.13. *Cis* and *trans* oxo configurations with a *trans*-phenoxy configuration of vanadyl complex.⁶⁷

In the area of catalyst development, significant efforts have been made to replace tin catalyst systems with low-toxicity metals such as lithium and sodium. Therefore, it is vital to gain further insight into their reactivity in order to design improved catalyst systems. The following section will provide the background chemistry of lithium and sodium and a literature overview of lithium and sodium complexes of phenolate and related ligands that are employed as catalysts for the polymerization of lactides.

1.2.2.2 Chemistry of lithium and sodium

Lithium is a moderately abundant element occurring at 65 ppm in the Earth's crust. Johan Arfvedson discovered the element in 1817 upon analyzing a sample of petalite and finding that it contained "silica, alumina and an alkali."²¹ A year later, the pure metal was isolated independently by William Brande and Humphrey Davy. Its name is derived from the Greek word *lithos*, meaning "stone." Lithium reacts easily with water; because it has a low first ionization energy, so it is oxidized to Li^+ in H_2O . Lithium only occurs in nature within compounds including silicates in igneous rocks, in a number of clay minerals, and generally as chloride in brines.⁶⁸

Lithium is a member of the most electropositive group (Group 1) in the periodic table. Its chemistry is dictated by an oxidation state of +1 (M^+), and the nature of its binding in Li(I) complexes is predominantly electrostatic.⁶⁹ In the pharmaceutical, dye, and pigment industries, lithium compounds replace transition or lanthanide metal ions because they are non-toxic, inexpensive, and soluble in aqueous media. Lithium carbonates (Li_2CO_3) are used to strengthen glass or ceramic materials.²¹

Sodium (Na) is a soft alkali metal whose atomic symbol originates from the Latin word *natrium*. This word comes from "natron", used by Egyptians to preserve bodies. It has an atomic weight of $22.989 \text{ g mol}^{-1}$; its melting and boiling points are $97.81 \text{ }^\circ\text{C}$ and $892.9 \text{ }^\circ\text{C}$, respectively, and it has a specific gravity of 0.971 g cm^{-3} at $20 \text{ }^\circ\text{C}$. As a Group 1 element, sodium exists in the +1 oxidation state. Similar to lithium, it reacts violently with water to form the hydroxide, and it also oxidizes rapidly in air; therefore, sodium should be handled carefully. The metal is usually prepared by electrolysis of the fused sodium chloride (the Downs Process) and is used in sodium arc lamps for street lighting. Its alloy with potassium is used as a heat-transfer liquid, for example, in certain nuclear reactors.⁷⁰

1.2.2.3 Lithium and sodium catalysts, especially phenolates, for the ROP of lactides

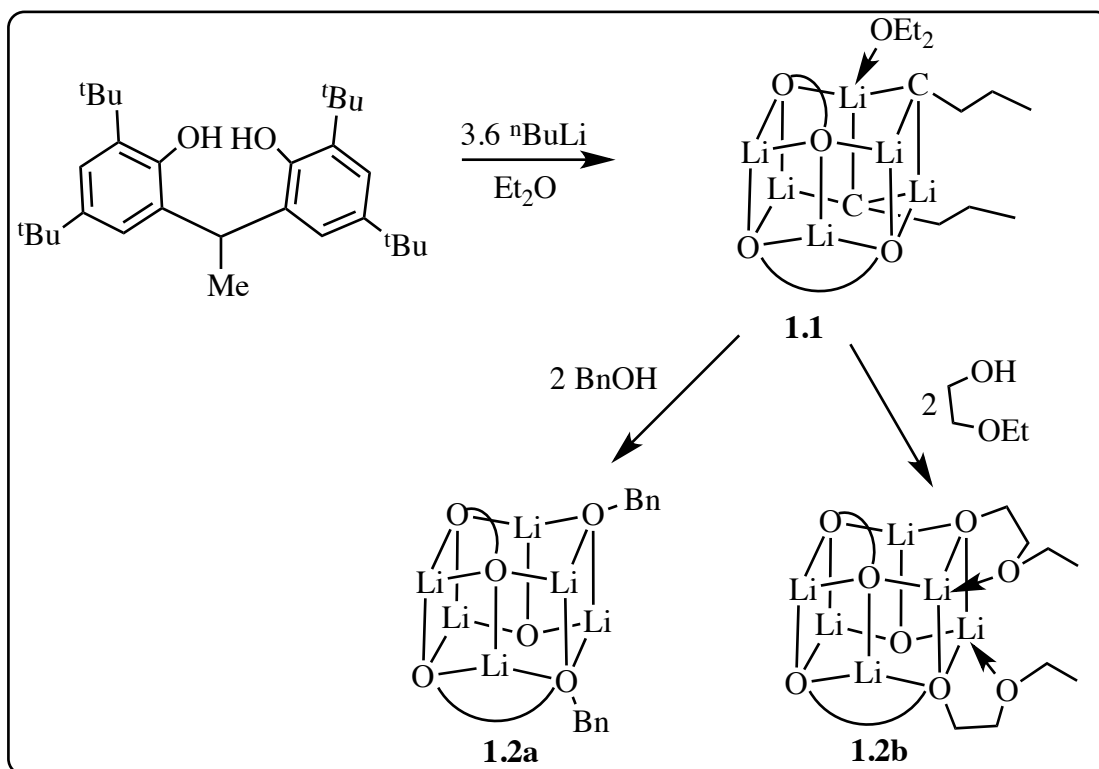
Simple metal alkoxide complexes such as lithium *tert*-butoxide (LiO^tBu) were described by Kasperczyk and coworkers. These complexes effectively initiated the polymerization of lactide to afford polymer with an M_n of $40,000 \text{ g mol}^{-1}$.⁷¹⁻⁷³ Later, the authors reported the formation of stereocontrolled heteroatactic polymers at low temperatures ($0 \text{ }^\circ\text{C}$) as a result of the inhibition of transesterification side reactions.⁷²

However, broad molecular weight distributions reported by Kreiseraunders were due to the presence of macrocycles formed via back-biting reactions that led to intramolecular transesterification.⁷³ An initiator for the ROP of lactide based on lithium chloride was found to be both effective and biocompatible in the presence of ethylene glycol and methyl α -D-glucopyranoside as co-initiators. However, the polymer produced after 10 h had broad dispersity ($D > 2.2$).⁷⁴

Butyllithium (BuLi) was shown to be catalytically active in the ROP of lactide in THF at 20 °C.⁷⁵ Polymers were generally of high molecular weight (M_n values ranged from 7,000–45,000 g mol⁻¹) with broad dispersity values. The uncontrolled polymerization behavior exhibited by these initiators was attributed to their highly basic nature, which led to side reactions that resulted in polymers with very broad molecular weight distributions.

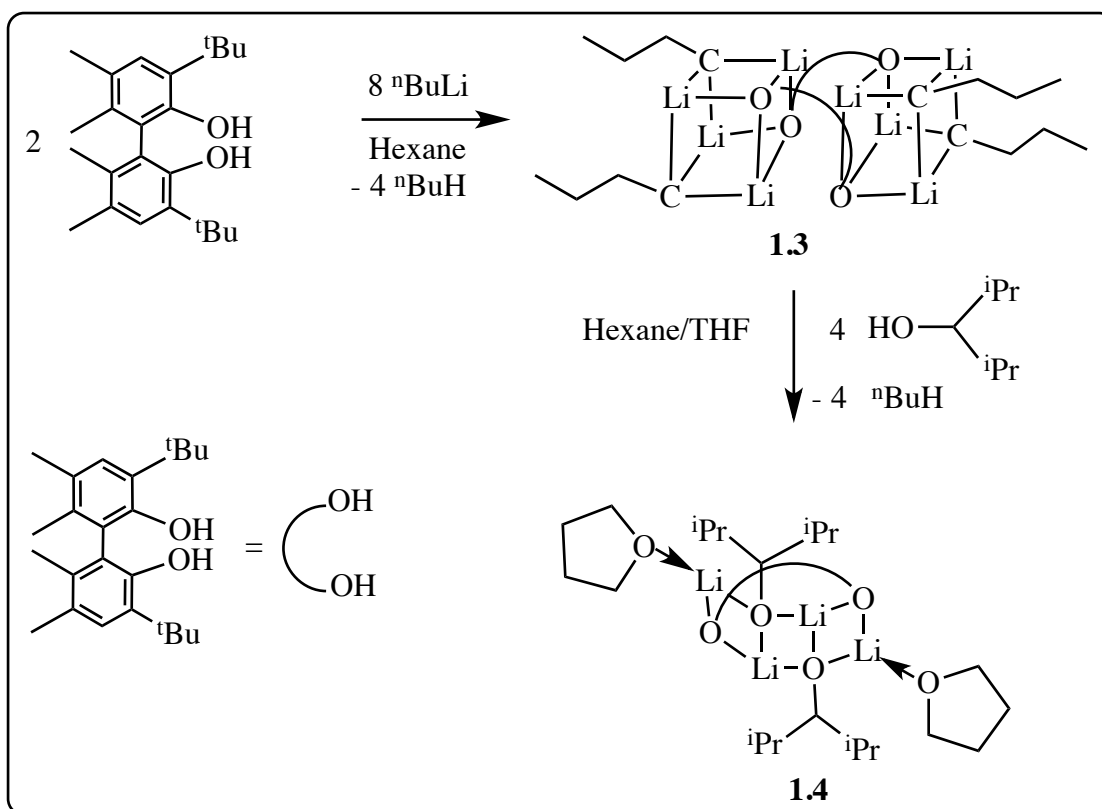
In order to suppress the formation of unwanted products from side reactions, bulky ligand-supported, metal-based catalyst systems have been designed. They also offer the advantage of producing polymers with well-controlled molecular weights and low dispersities. The first example of a lithium bisphenoxide aggregate for this purpose was described by Lin and coworkers.⁷⁶ The bulky ligand precursor [2,2-ethylidene-bis(4,6-di-*tert*-butylphenol)] (EDBP-H₂) was incorporated into the complex by the reaction of EDBP-H₂ and ⁿBuLi in diethyl ether (Et₂O), as shown in **Scheme 1.6**. Lithium alkoxide complexes **1.2a** and **1.2b** were prepared from **1.1** by the addition of 2 equivalents of benzyl alcohol (BnOH) and 2 equivalents of 2-ethoxyethanol, respectively. Both complexes were highly active initiators for the ROP of L-lactide in CH₂Cl₂ at 25 °C, with reactions reaching completion within 1 h. However, when the reaction was conducted at 0

°C, the PLA obtained after 6 h had a narrower molecular weight distribution ($D = 1.11$) than that obtained at room temperature ($D = 1.43$).



Scheme 1.6. Synthesis of hexalithium complexes for ROP of lactide.⁷⁶

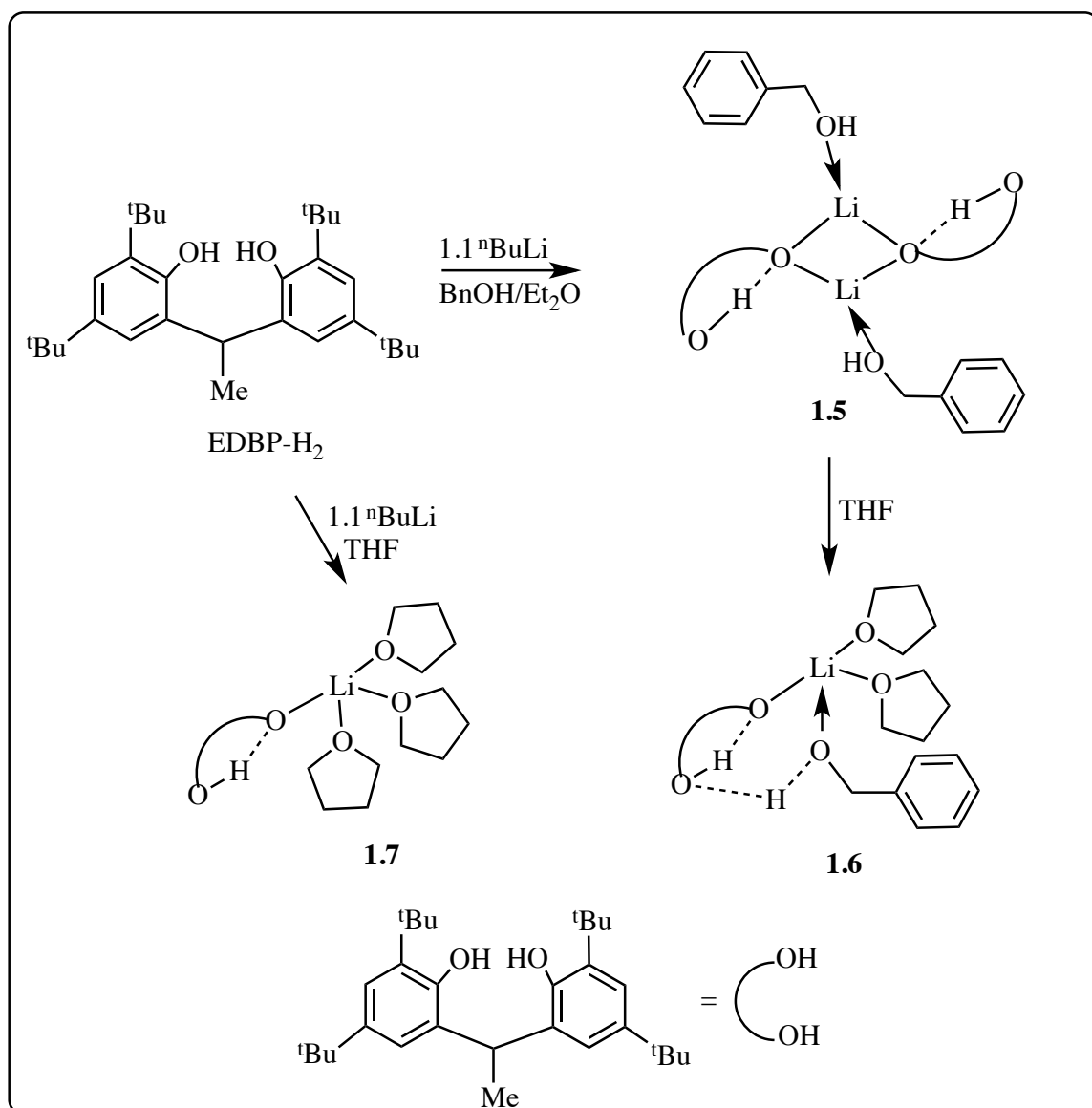
Following a similar synthetic route, Chisholm and coworkers reported the preparation of an octalithium cluster (**1.3**) by adding eight equivalents of $n\text{BuLi}$ in hexane to a bis(phenol), as illustrated in **Scheme 1.7**.⁷⁷ A tetralithium complex (**1.4**) was subsequently prepared by the addition of 2,4-dimethyl-3-pentanol in THF. The octalithium species **1.3** was an efficient catalyst for the ROP of lactide within 1 h at ambient temperature, producing atactic PLA due to transesterification.



Scheme 1.7. Synthesis of octalithium and tetralithium clusters.⁷⁷

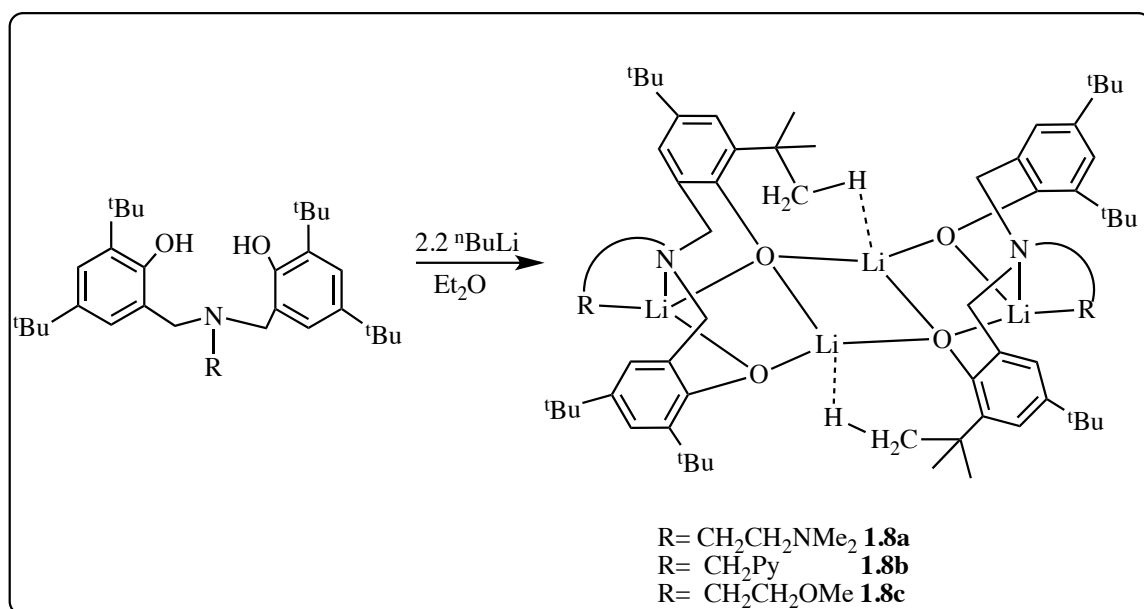
As part of continued efforts by Lin and coworkers to use the EDBP- H_2 ligand, the dilithium complex (**1.5**) was obtained by the addition of a mixture of BnOH , $n\text{BuLi}$, and EDBP- H_2 in diethyl ether (**Scheme 1.8**).⁷⁸ The addition of a coordinating solvent such as THF at ambient temperature afforded a monometallic lithium complex (**1.6**). A related lithium species (**1.7**) was also isolated in the absence of BnOH . The data showed that dinuclear lithium complex (**1.5**) efficiently initiated the ROP of L-lactide in CH_2Cl_2 in a controlled fashion. Complex **1.5** was more active than **1.6**, and the former was able to produce PLA at 0 and 25 °C. The low activity of **1.6** was attributed to the coordinating nature of THF, which competes with the monomer for binding and hinders insertion of

the lactide. The controlled behavior of the polymerization was apparent by the linear relationship between the molecular weights M_n of the polymer and the molecular weight distributions. Both mono- and dinuclear lithium species were more active compared to the previous hexalithium clusters.



Scheme 1.8. Synthesis of mono- and dilithium complexes.⁷⁸

Tetralithium complexes supported by multidentate amino-bis(phenolate) ligands (**1.8a-1.8c**, **Scheme 1.9**) in boat-like structures were reported by Chen and coworkers.⁷⁹ Using these complexes in the absence of benzyl alcohol, poor conversions (41%) and poor dispersity values ($D = 1.26-1.55$) were observed when ROP reactions of L-lactide were conducted at 26.5 °C in CH_2Cl_2 within 30 min. The addition of benzyl alcohol as a co-initiator accelerated the reaction to a time of 20 min, along with achieving high conversions (above 93%) and maintaining a controlled polymerization. All dispersities reported were low (1.08–1.18), suggesting that the polymerization behaves in a controlled and living manner. The polymers produced have moderate molecular weights ranging from 5,000 to 20,000 g mol^{-1} . The mechanism of ring-opening is thought to occur by insertion of a benzyl oxide group into the carbonyl carbon of lactide.



Scheme 1.9. Amino-bis(phenolate) tetralithium complexes for the ROP of lactide.⁷⁹

Chen and coworkers also tested lithium complexes bearing mono-anionic amino-bis(phenolate) ligands (**1.9a-c**, **Figure 1.14**) as initiators for ROP of L-lactide in the presence of benzyl alcohol at 26.5 °C.⁸⁰ The reactions were conducted in various solvents, such as CH₂Cl₂, THF, and toluene. Similar to their previous results, the best-controlled process was observed in CH₂Cl₂, which was also a living polymerization. High catalytic activities and immortal polymerization was achieved with complex **1.9c**, bearing amine functionalities.

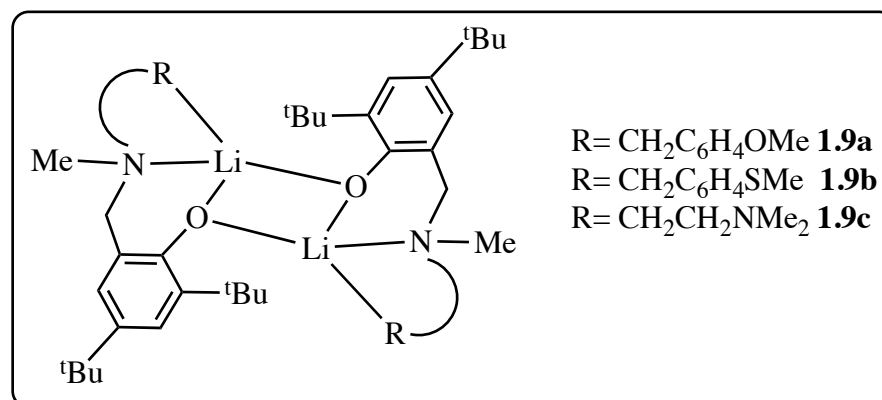
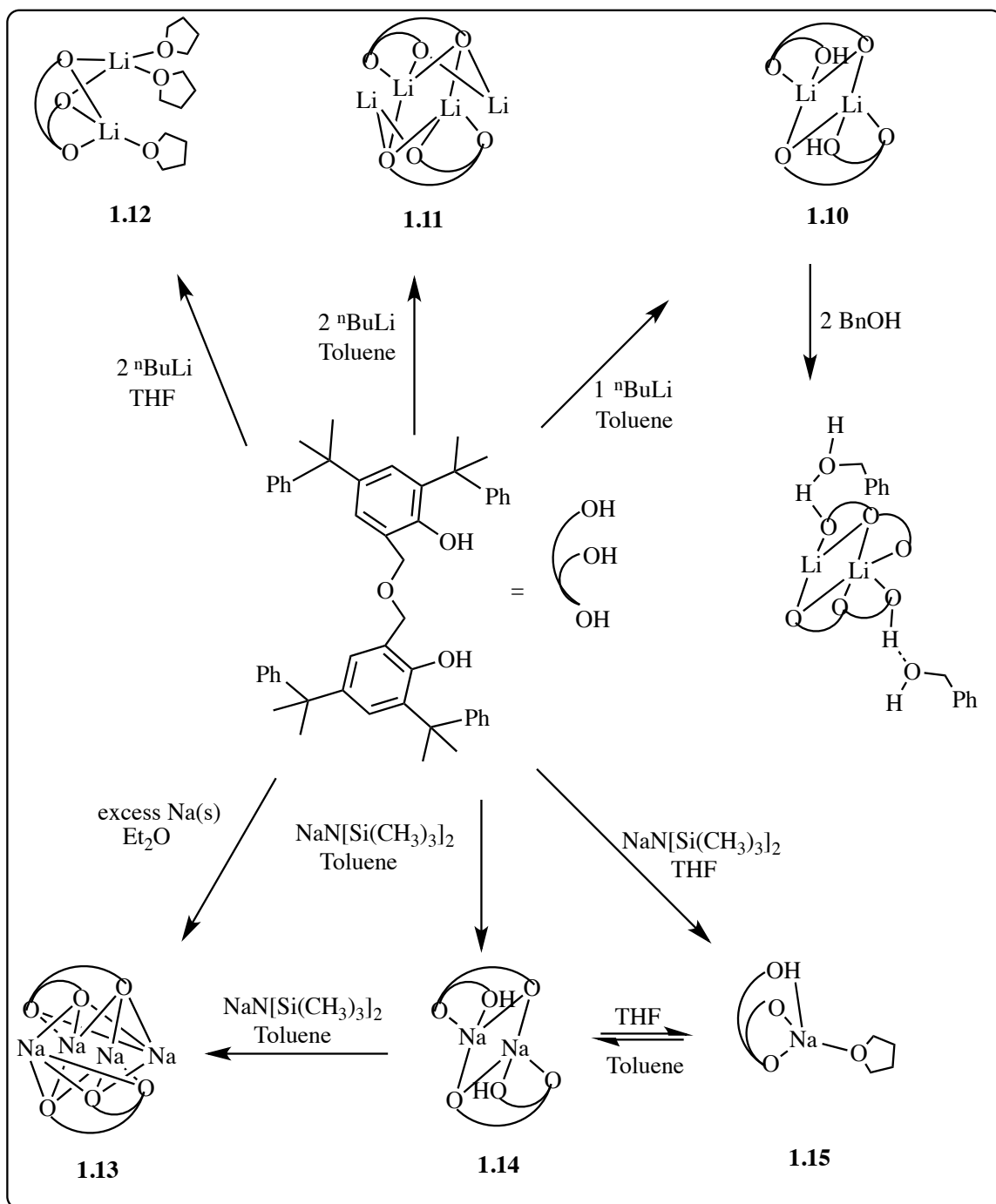


Figure 1.14. Monoanionic amino-bis(phenolate) dinuclear lithium complexes.⁸⁰

Lin and colleagues described a series of well-characterized lithium and sodium complexes bearing OOO-tridentate bis(phenolate)-ether ligands.⁸¹ Various di- and tetra-lithium and sodium complexes were synthesized in solvents such as THF, toluene, diethyl ether, and BnOH (**Scheme 1.10**). Most of these catalysts were active towards the ROP of L-lactide in CH₂Cl₂ with BnOH as a co-initiator. The PLA produced had low dispersity values ($D = 1.04\text{--}1.30$), which indicated a controlled polymerization. In addition, under a wide range of monomer:initiator ratios, the tetrasodium complex **1.13** demonstrated the

highest catalytic activity with the reaction completed in less than 10 min at 0 °C, affording PLA with controlled molecular weights and narrow dispersity values. Moreover, the polymerization reaction rate was faster for the tetranuclear lithium and sodium species (**1.11** and **1.13**, respectively) compared to the dinuclear complexes (**1.10** and **1.14**). Furthermore, the polymerization itself was immortal and the reaction proceeded more quickly upon the addition of 2 equivalents of BnOH, evidenced by the reduced M_n values for the polymer in comparison to those observed with 1 equivalent of BnOH.



Scheme 1.10. Synthesis of di- and tetralithium and sodium complexes.⁸¹

New sodium aryloxide complexes stabilized by the polyamine ligands *N,N,N',N'*-tetramethylethylenediamine (TMEDA), *N,N,N',N'',N''*-pentamethyldiethylenetriamine

(PMDETA), and [tris(2-dimethylaminoethyl)amine] (Me₆TREN) were reported by the groups of Davidson and García-Vivó (**Figure 1.15**).⁸² The complexes were prepared by the addition of phenol to a toluene solution of NaN(SiMe₃)₂ and the appropriate Lewis base in stoichiometric amounts. The complexes were shown to be active as initiators for the ROP of *rac*-lactide in CH₂Cl₂ solution at room temperature in both the absence and presence of BnOH. High dispersities (ranging from 2.6–1.5) and higher *M_n* values than predicted were observed in the absence of BnOH, suggesting the occurrence of transesterification during the polymerization process. Complex **1.18**, based on the Me₆TREN supporting ligand, was more active than those based on TMEDA and PMDETA ligands, with nearly complete conversions in a short time (99% after 5 min). In contrast, the presence of BnOH resulted in a more controlled and faster reaction (completion within only 5 min). The polymers exhibited low dispersity and *M_n* values in agreement with the expected theoretical values for isotactic polymer.

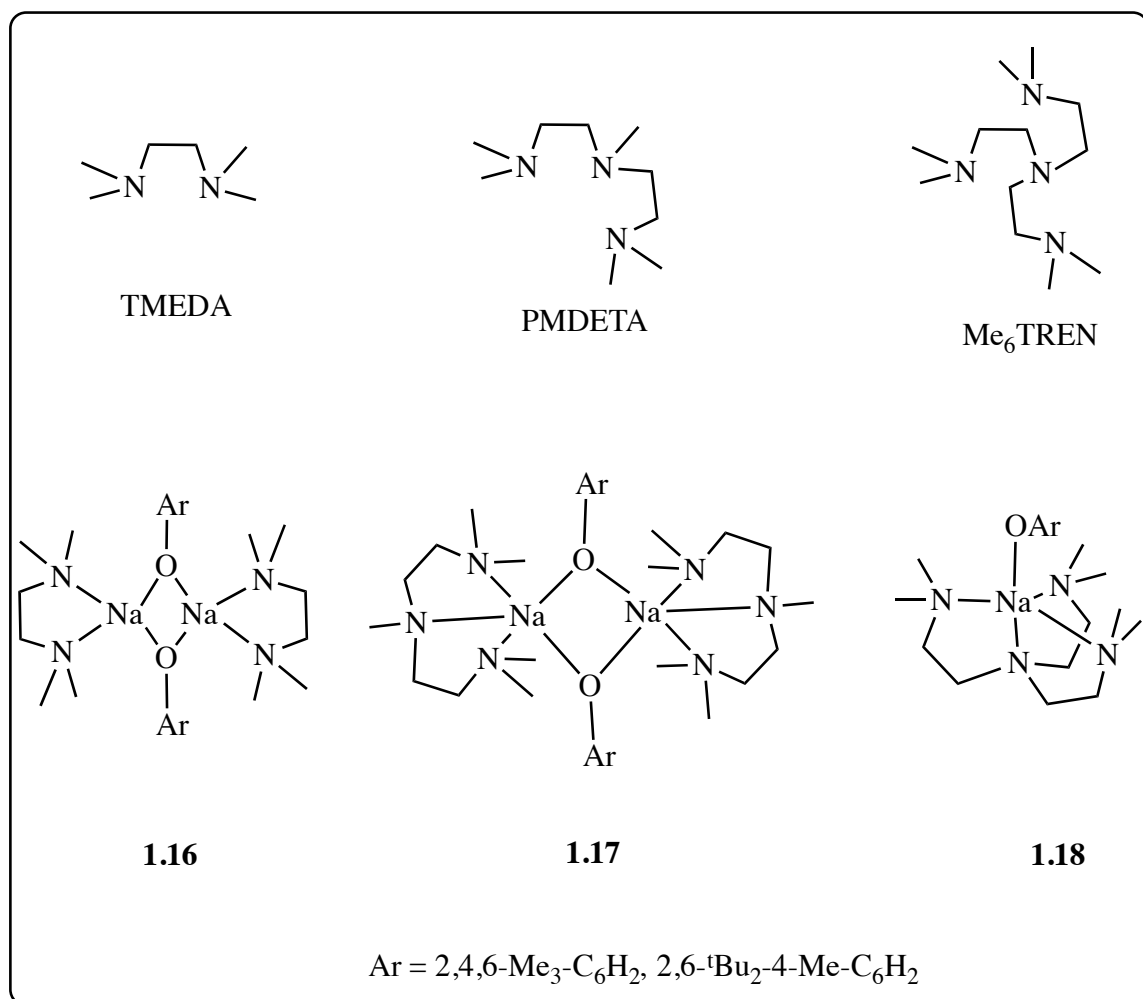
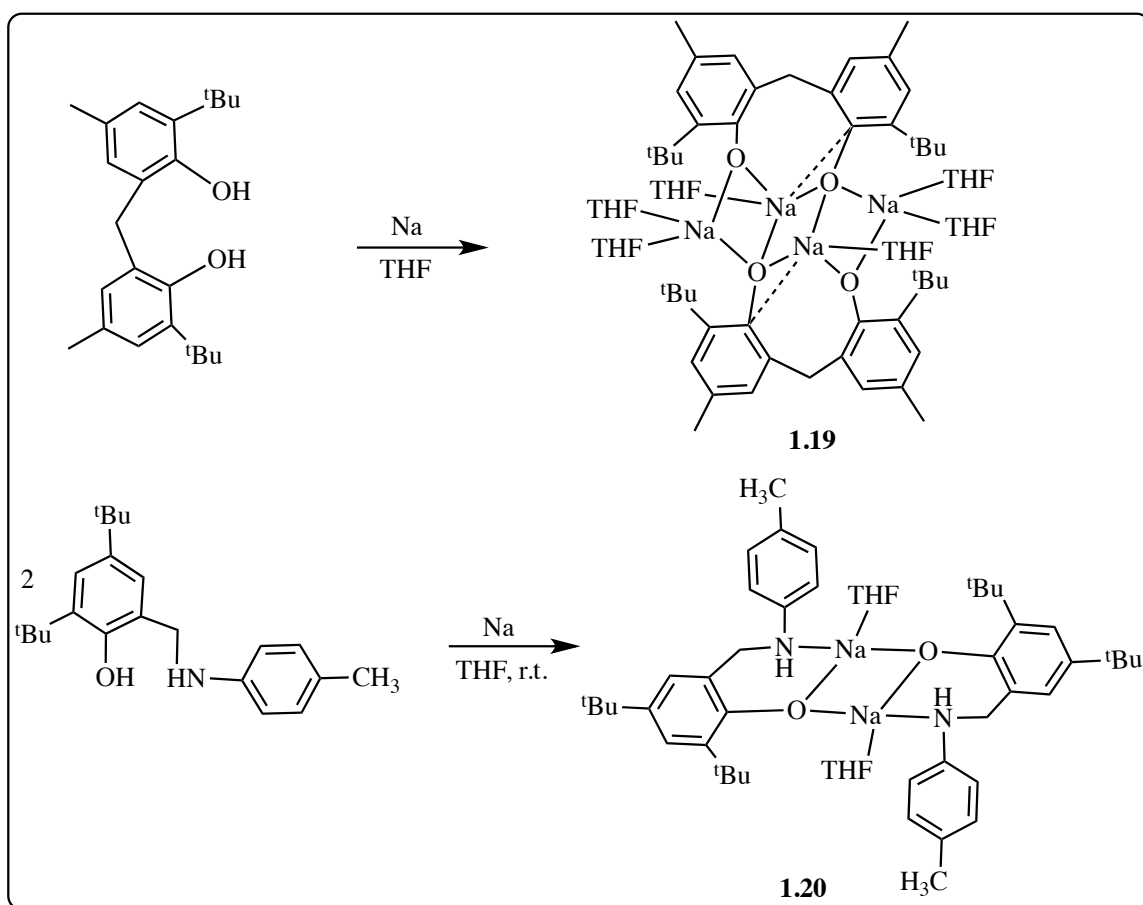


Figure 1.15. Ligand precursors and sodium complexes based on TMEDA, PMDETA and Me₆TREN.⁸²

Shen and coworkers synthesized four-coordinate tetrasodium and disodium complexes supported by amino-bis(phenolate) ligands (**1.19** and **1.20**, **Scheme 1.11**) to catalyze the polymerization of L-lactide.⁸³ Polymerization reactions were carried out in toluene at 70 °C in the absence of alcohol. Tetrasodium complex **1.19** was a more efficient initiator than **1.20**, yielding PLA within 5 min and achieving almost complete conversion (96%). The less active disodium complex was able to polymerize L-lactide after 2 h with 90% conversion. In addition, experimental results provided some evidence

for controlled polymerization using complex **1.20**, in the form of a linear relationship between M_n and the monomer-to-initiator ratio ($[M]/[I]$). However, polymers with broad molecular weight distributions were obtained from the polymerization systems ($D = 1.39$ – 1.60). Interestingly, the addition of propyl alcohol did not affect either the reaction rates or the molecular weight distributions.



Scheme 1.11. Synthesis of sodium and potassium complexes by Shen *et al.*⁸³

In 2012, Miller and coworkers synthesized lithium and sodium complexes based on the 2,6-di-*tert*-butyl-4-methylphenol (BHT) ligand (**Figure 1.16**) and studied the controlled ROP of L-lactide in the presence of BnOH in toluene at room temperature.⁴²

They observed that a trisodium complex (**1.22**) was the superior catalyst, reaching a conversion of 99% within only 3 min. For complexes **1.21** and **1.22**, polymerization control is evidenced by the linear relationship between M_n and the conversion percentage, which is consistent with the low dispersity. Broader D values (1.49) were obtained by increasing the catalyst concentration and using unpurified lactic acid. They also conducted the polymerization using calcium and magnesium catalysts; the polymerization rates descended in the order $\text{Na} \geq \text{Li} > \text{Ca} \geq \text{Mg}$.

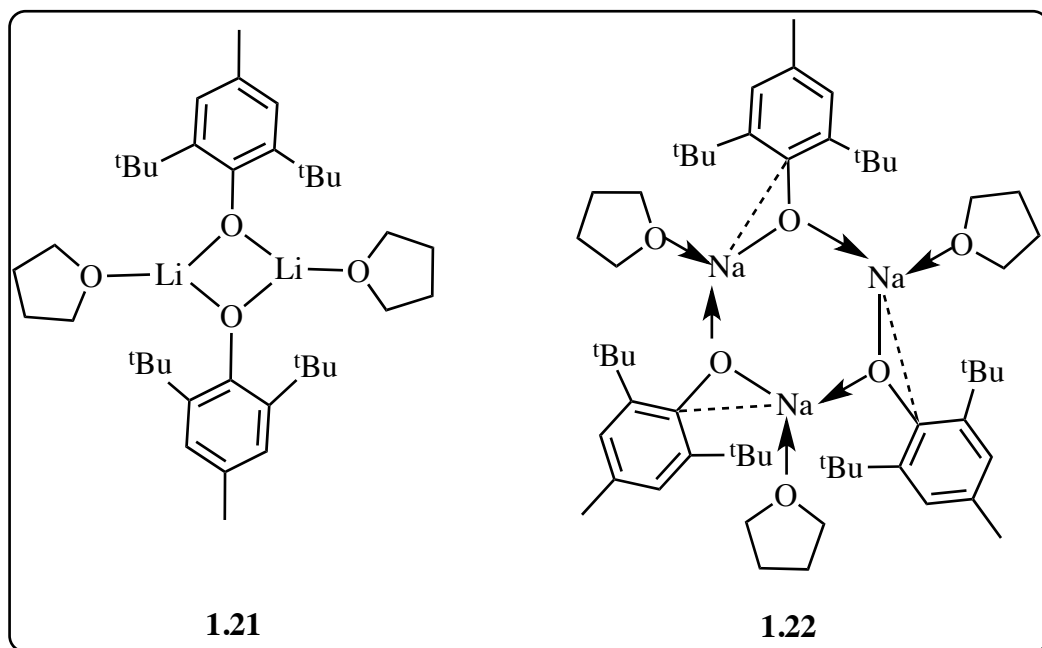


Figure 1.16. Lithium and sodium complexes based on BHT ligands.⁴²

Lithium, sodium, and potassium amino-bis(phenolate) complexes incorporating a benzylamine backbone were reported by Kozak and coworkers to be active for the ROP of *rac*-lactide at room temperature (**Figure 1.17**).⁸⁴ After only 15 min, the complexes produced polymers in an uncontrolled manner in the absence of BnOH; higher molecular

weights than expected and high D were observed (1.82-4.33), suggesting the occurrence of intermolecular transesterification reactions. Benzyl alcohol was shown to be important in controlling polymerization reactions by yielding PLAs with low molecular weights and intermediate dispersity values. Furthermore, Kozak and coworkers noted that the highest polymerization rates were observed with complex **1.24**, a potassium species, both in the absence and presence of BnOH. Although the polymerization was poorly controlled, almost complete conversion was achieved (98%). They attributed the high activity of this complex to the larger ionic radius of potassium compared to other metals.

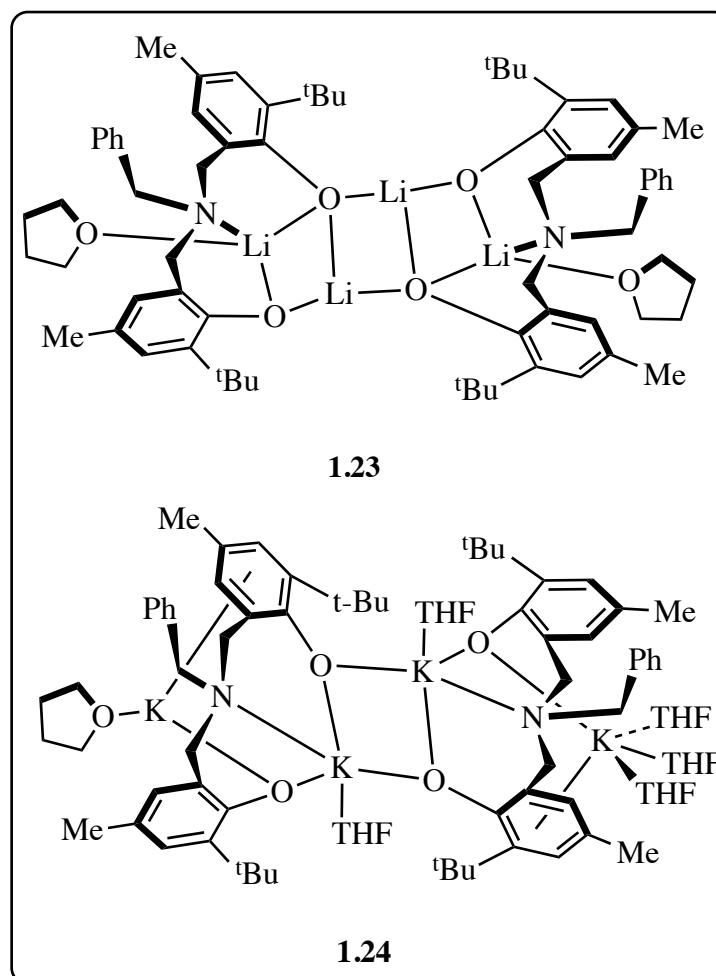
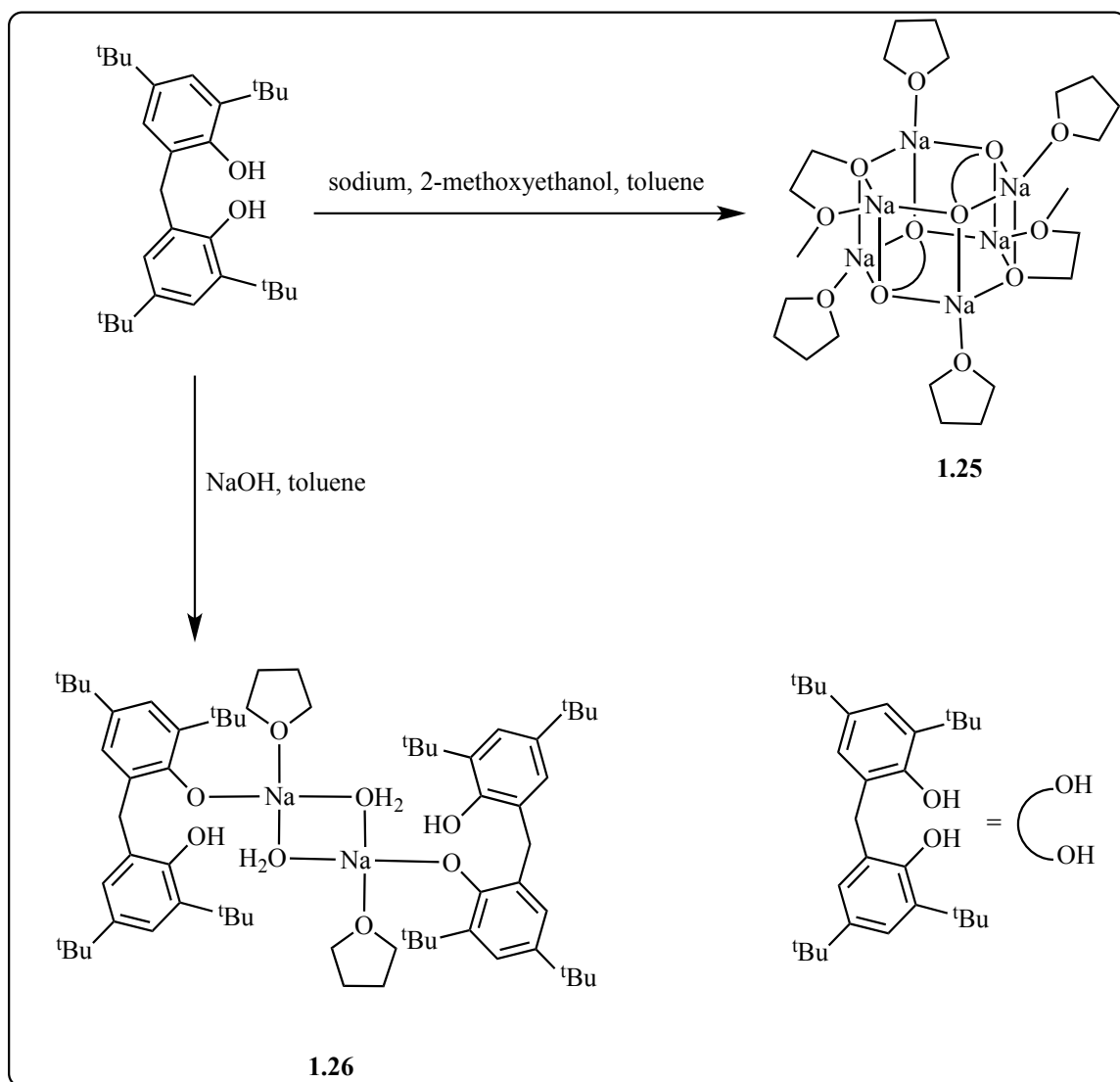


Figure 1.17. Structures of tetralithium and potassium complexes by Kozak and coworkers.⁸⁴

Zhao and colleagues investigated the activity of hexa- and disodium complexes supported by bis(phenol) ligands to polymerize L-lactide in the absence of a co-initiator (**Scheme 1.12**).⁸⁵ The complexes efficiently initiated the ROP of L-lactide in toluene at both 0 and 25 °C. Notably faster reaction rates and high \bar{D} (1.48) were observed at room temperature; the reaction was complete within 30 min. At 0 °C, a linear relationship was found to exist between M_n and the monomer-to-initiator ratio ($[M]_0/[I]_0$), indicating a controlled polymerization. However, they reported that the hexasodium species (**1.25**) demonstrated higher ROP activities than the disodium aggregates (**1.26**).



Scheme 1.12. Preparation of hexa- and disodium complexes.⁸⁵

In 2013, several tetralithium complexes based on tetradentate amino-bis(phenolate) ligands exhibited high catalytic activity for the polymerization of *rac*-lactide in toluene solutions (**Figure 1.18**).⁸⁶ Lithium-7 NMR spectroscopy was conducted for two of these complexes in both non-coordinating solvent (*e.g.*, benzene-*d*₆) and coordinating solvent (*e.g.*, pyridine-*d*₅). Consistent with the solid state structure, two symmetric ⁷Li environments were observed for four-coordinate Li centres. Investigating

the effect of varying the functional group on the phenolate moieties in terms of activity (**1.27a** vs. **1.27b**) revealed very little difference. Kinetic studies indicated a first-order dependence on monomer concentration at 26 and 40 °C for **1.27a** and at 26, 40, and 60 °C when initiated by **1.27a**. Increasing the temperatures to 60 and 80 °C for **1.27a** and 80 °C for **1.27b** resulted in a second-order dependence. However, none of the catalysts were effective in controlling the polymerization; dispersities were high, and molecular weights were higher than expected from monomer conversion, indicating the occurrence of transesterification reactions. Unfortunately, the addition of 1 equivalent of BnOH did not accelerate the reaction rates, nor did it aid in controlling the polymerization. Therefore, the authors suggested that the complexes initiated the polymerization via monomer insertion into the metal-phenoxide bond. The best-controlled polymerization occurred by adding 2 equivalents of BnOH to the sterically bulkier **1.28a** and **1.28b**. Although narrow D were observed, M_n values differed significantly from theoretical values.

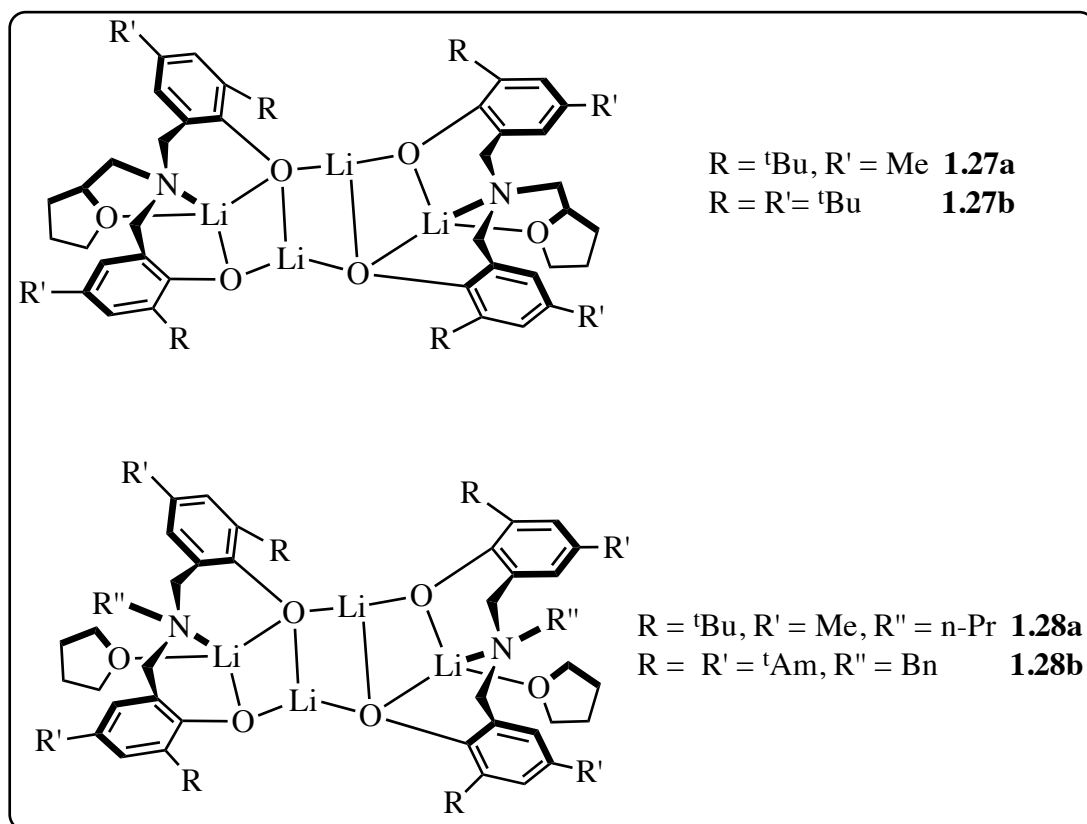
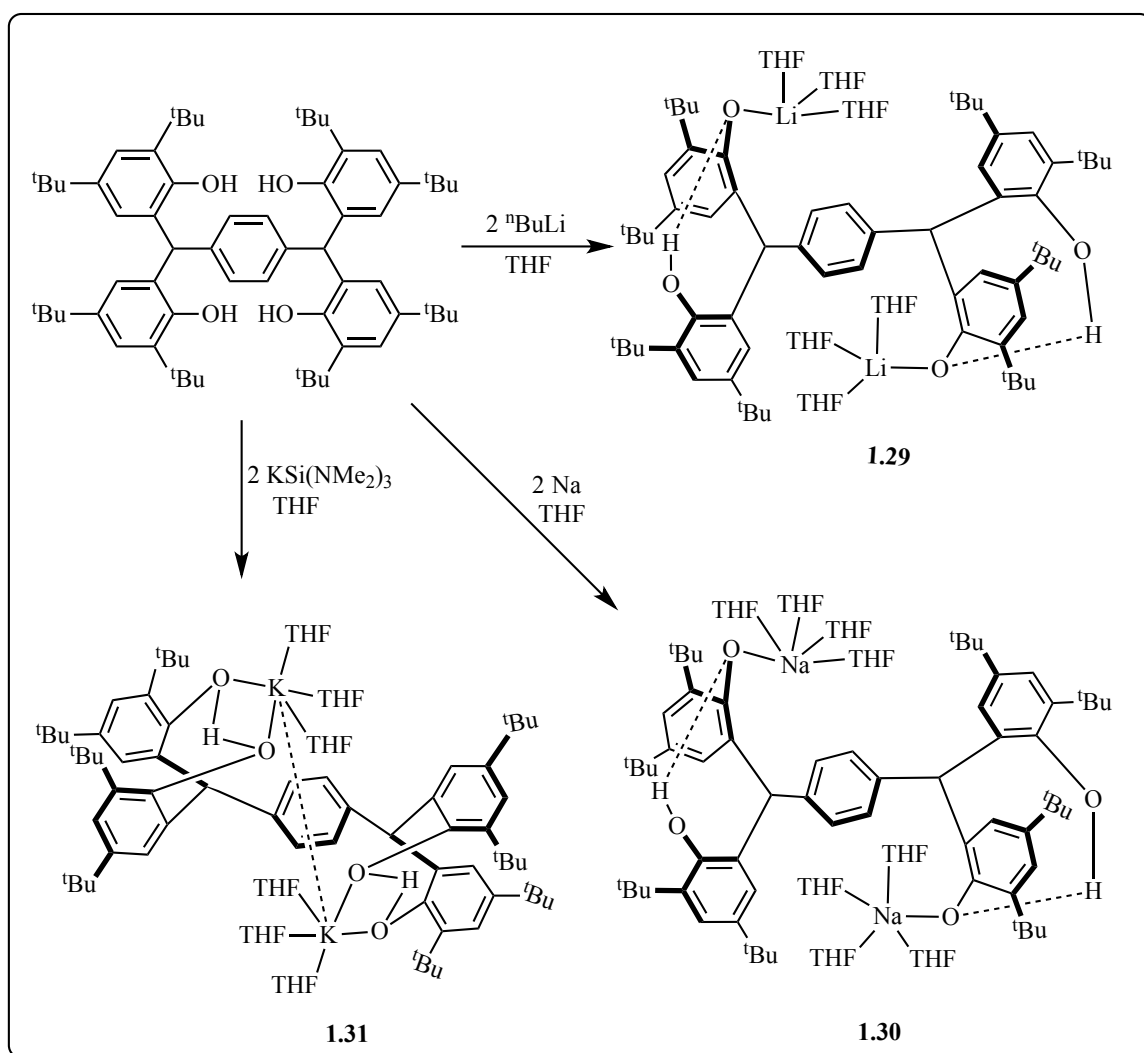


Figure 1.18. Synthesis of tetralithium compounds.⁸⁶

Wu and coworkers reported the catalytic activities of dinuclear lithium, sodium, and potassium supported by bulky tetraphenolates towards the ROP of L-lactide in CH₂Cl₂ solution at room temperature (**Scheme 1.13**).⁸⁷ In the polymerization reactions without BnOH, the sodium and potassium complexes proved to be more efficient catalysts than the lithium complex; the reaction was complete in 5 and 2 min for the sodium and potassium complexes, respectively. The polymers obtained had high *D* and unpredictable molecular weights. However, upon introducing BnOH as a co-initiator, the *D* of the polymers became narrower, especially for those produced with **1.31** (*D* = 1.05–1.24). The observed molecular weights were in good agreement with the calculated values. All complexes gave rise to a linear correlation between the molecular weights of

polymers (M_n) and the ratio $[LA]_0/[BnOH]_0$, indicative of living polymerizations. Polymerization reaction rates in the absence and presence of BnOH occurred in the order $K > Na > Li$. The high activities of sodium and potassium compared to lithium were attributed to their larger sizes, which increased the ability of lactide to coordinate to the metal.



Scheme 1.13. Dinuclear lithium, -sodium, and -potassium complexes.⁸⁷

Sarazin and coworkers used a series of lithium and potassium aminoether phenolate complexes to successfully polymerize L-lactide in CH_2Cl_2 at 30 °C in the presence of BnOH (**Figure 1.19**).⁸⁸ Among all the catalysts investigated, **1.34** demonstrated both high activity and living polymerization characteristics. Evidence of living and immortal polymerization was confirmed by the relationship between M_n and conversion%, narrow dispersities (1.05–1.3), and a satisfactory agreement between observed and theoretical molecular weights. In addition, first-order dependence on monomer concentration was confirmed for **1.34** by the perfectly linear relationship between the $\ln([\text{L-LA}]_0/[\text{L-LA}]_t)$ plot and the reaction time. The authors found that **1.32** and **1.33** gave high reaction rates with nearly complete monomer conversion in 2 h; however, the reactions afforded PLAs with broad molecular weight distributions ($D = 1.76\text{--}1.87$). The addition of 2 and 4 equivalents of BnOH to the reaction resulted in a drop in M_n , which is characteristic of a well-behaved, immortal ROP. The more highly controlled living polymerizations of **1.34** were attributed to its electron rich and sterically-congested structure in comparison to the less stabilizing structures of **1.32** and **1.33**. Stoichiometric reactions monitored by ^1H NMR spectroscopy suggested that the reaction proceeded by the activated monomer mechanism.

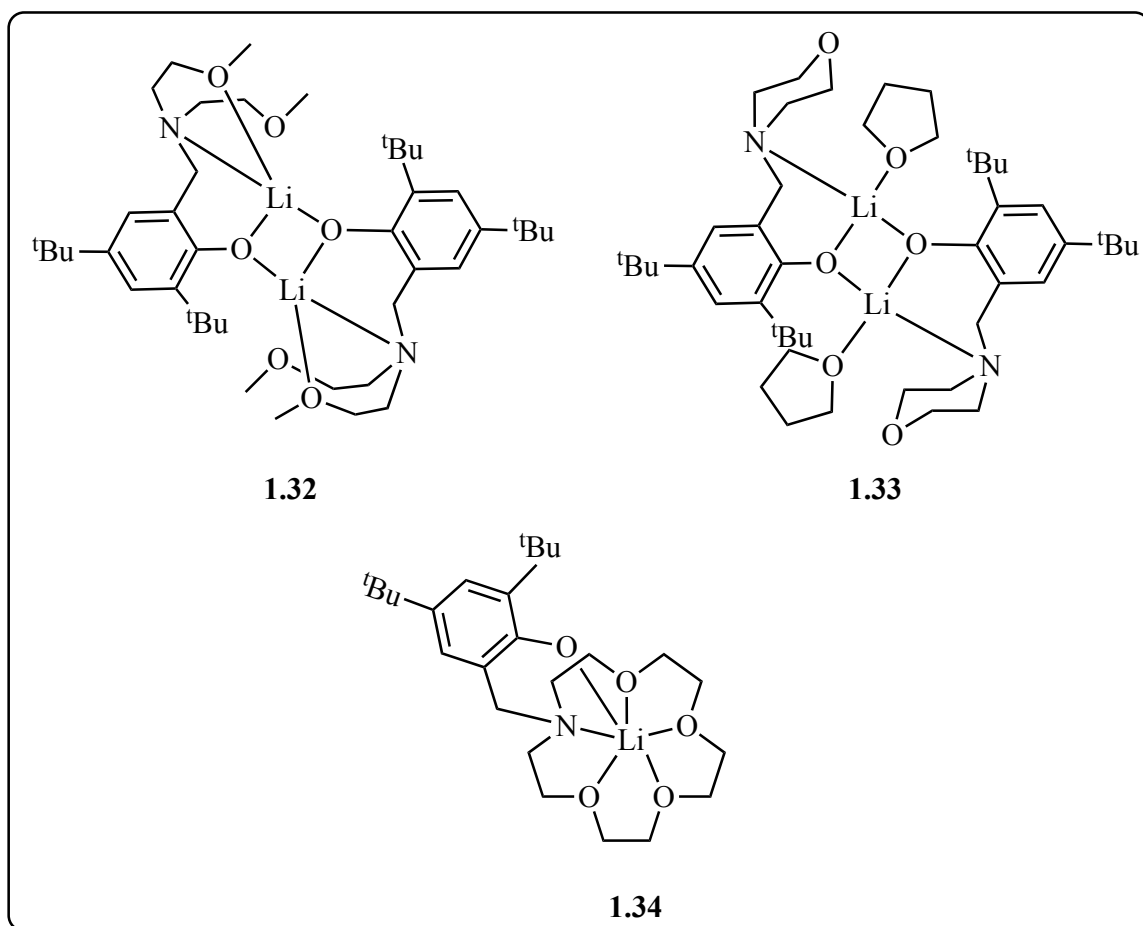
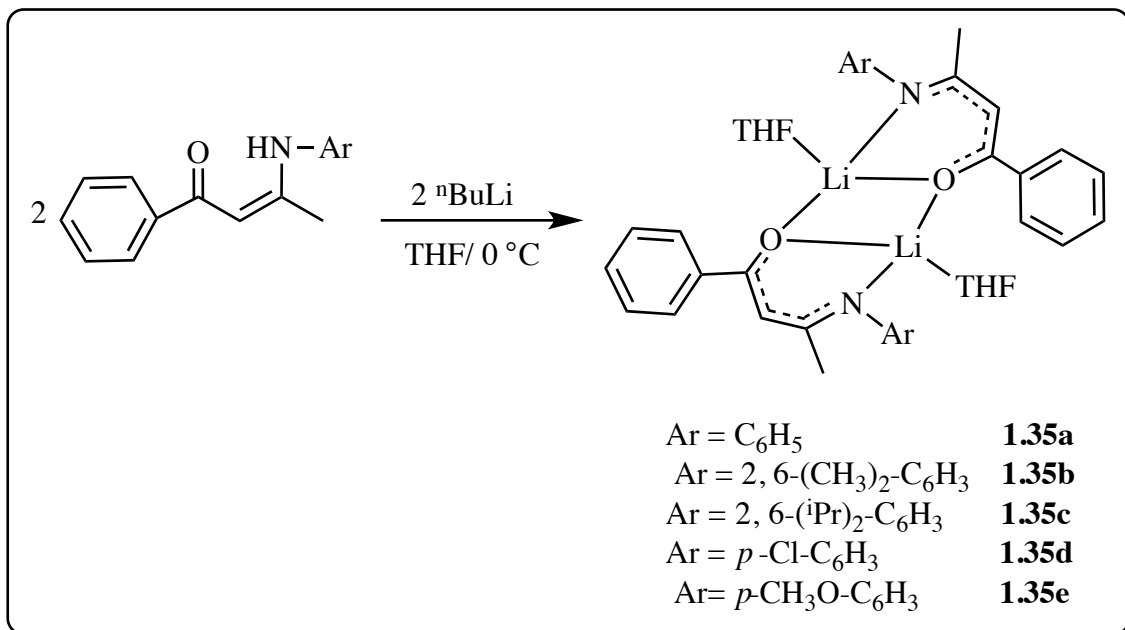


Figure 1.19. Representation of mono- and dilithium complexes used by Sarazin *et al.*⁸⁸

Yao and coworkers designed several lithium β -ketoiminate complexes and tested their activity towards the ROP of L-lactide in THF at 20 °C (**Scheme 1.14**).⁸⁹ The complexes were synthesized by the reaction of 2 equivalents of ⁿBuLi with 2 equivalents of β -ketoiminate ligands in a mixture of THF and hexane at 0 °C. All lithium complexes effectively initiated the ROP of L-lactide to yield PLAs with relatively narrow molecular weight distributions ($D = 1.42\text{--}1.87$) and higher molecular weights than expected. Specifically, complex **1.35e** had the highest reactivity (in THF instead of toluene). The reaction time affected the yield of the resulting polymers in that longer times increased

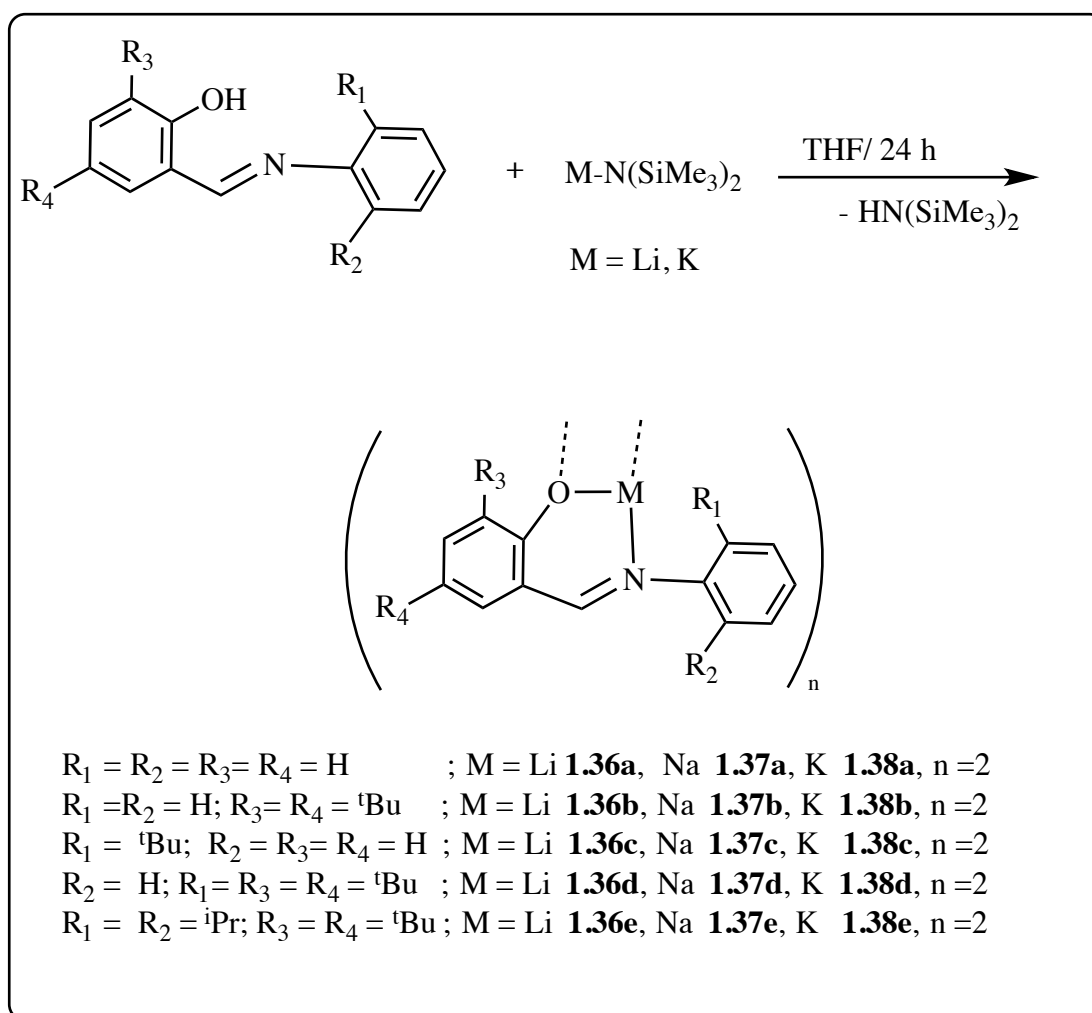
the yield compared to short reaction times.



Scheme 1.14. Synthesis of lithium complexes **1.35a–1.35e**.⁸⁹

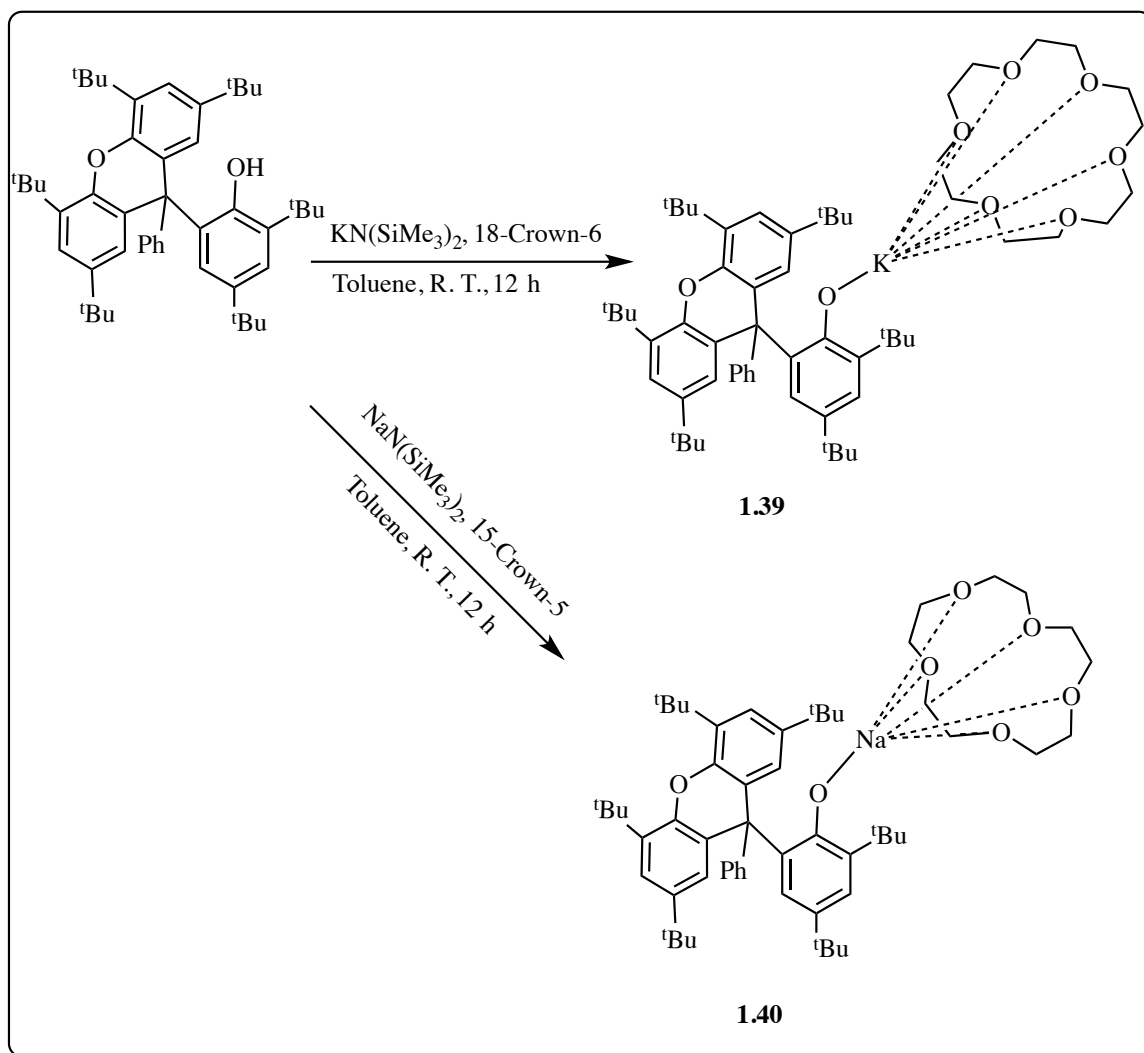
A series of lithium, sodium, and potassium complexes with phenol-imine ligands were explored for their potential use as initiators in the ROP of *rac*-lactide with 1 equivalent of BnOH at 25 °C in CH₂Cl₂ (**Scheme 1.15**).⁹⁰ The identity of the metal centre had a strong influence on the activity, but the nature of the ligand substituents did not. The sodium and potassium complexes were extremely active catalysts, reaching 100% conversion in less than 1 min, while lithium complexes required longer reaction times (more than 30 min) to obtain high conversions. The polymers produced had molecular weights lower than predicted values, confirming the occurrence of transesterification reactions. The addition of excess BnOH effected more controlled polymerizations having immortal characteristics, similar molecular weights to those predicted, and narrow

dispersity (1.25–1.54). Interestingly, the high activity and controlled behavior were maintained when the amount of lactide was increased with respect to the metal complex. Moreover, the substituents of the phenyl ring had a clear effect on the tacticities of the polymer chain, where complexes **1.36a**, **1.37a**, and **1.38a** (having no substituents on the phenoxo ring) afforded more stereoregular polymers ($P_r = 0.71$ – 0.75). An activated monomer mechanism was proposed for the reaction involving BnOH after monitoring the reactions with ^1H NMR spectroscopy.



Scheme 1.15. Synthesis of alkali metal derivatives(---- linkage to other half of molecule).⁹⁰

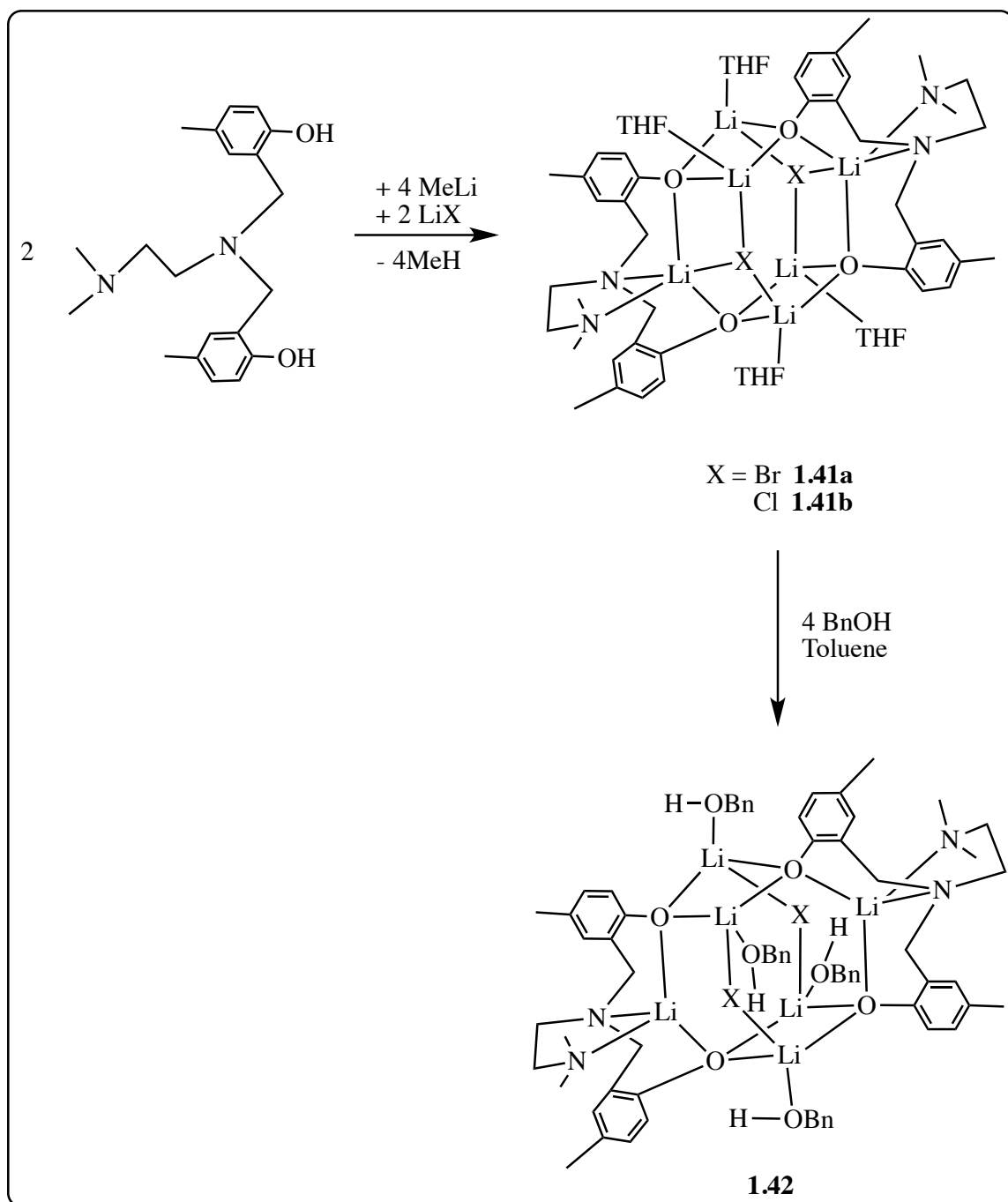
Recently, Wu and coworkers demonstrated the effect of embedding an active sodium and potassium phenoxide into 18-crown-6 and 15-crown-5 as auxiliary ligands to influence the stereocontrol of the polymerization (**Scheme 1.16**, complexes **1.39** and **1.40**).⁹¹ The complexes were highly active for the ROP of *rac*-lactide in THF at -60 °C, producing isotactic PLA with the highest reported iso-selectivity P_m value to date (as high as 0.86). However, the molecular weights were lower than expected as a result of a cyclization side reaction. Interestingly, the addition of 1 equivalent of BnOH did not suppress the formation of the side product because the crowding around the metal centres hindered BnOH coordination to the K/Na atom. With increasing amounts of BnOH, 5–10 equivalents, PLA with more controlled D (1.03–1.1) was produced while maintaining high iso-selectivities. It was also observed that the reaction was temperature dependent, as the activity of these complexes was reduced when the temperature was increased to -30 °C. The low activity was attributed to the rapid oscillations of the crown ether, which clog the entrance to the half cavity and inhibit the transport of lactide and BnOH. Moreover, these complexes achieved the highest recorded iso-selectivities due to the strong interaction between the incoming lactide and the active end of polylactide in the presence of the bulky crown ether.



Scheme 1.16. Synthesis of sodium and potassium complexes.⁹¹

Sobota *et al.* also examined the ROP of L-lactide initiated by hexametallic lithium complexes supported by dianionic amino-bis(phenolate) ligands (**Scheme 1.17**).⁹² Complexes **1.41a** and **1.41b** catalyzed the polymerization in conjunction with 1 equivalent of BnOH in CH₂Cl₂ at room temperature. Complete conversions (>98 %) were achieved within a 3 h period to yield isotactic polymers possessing low molecular weights and low *D* (1.05–1.4). The authors reported that the lower-than-expected molecular weights were a result of chain-shortening transesterification reactions. First-order

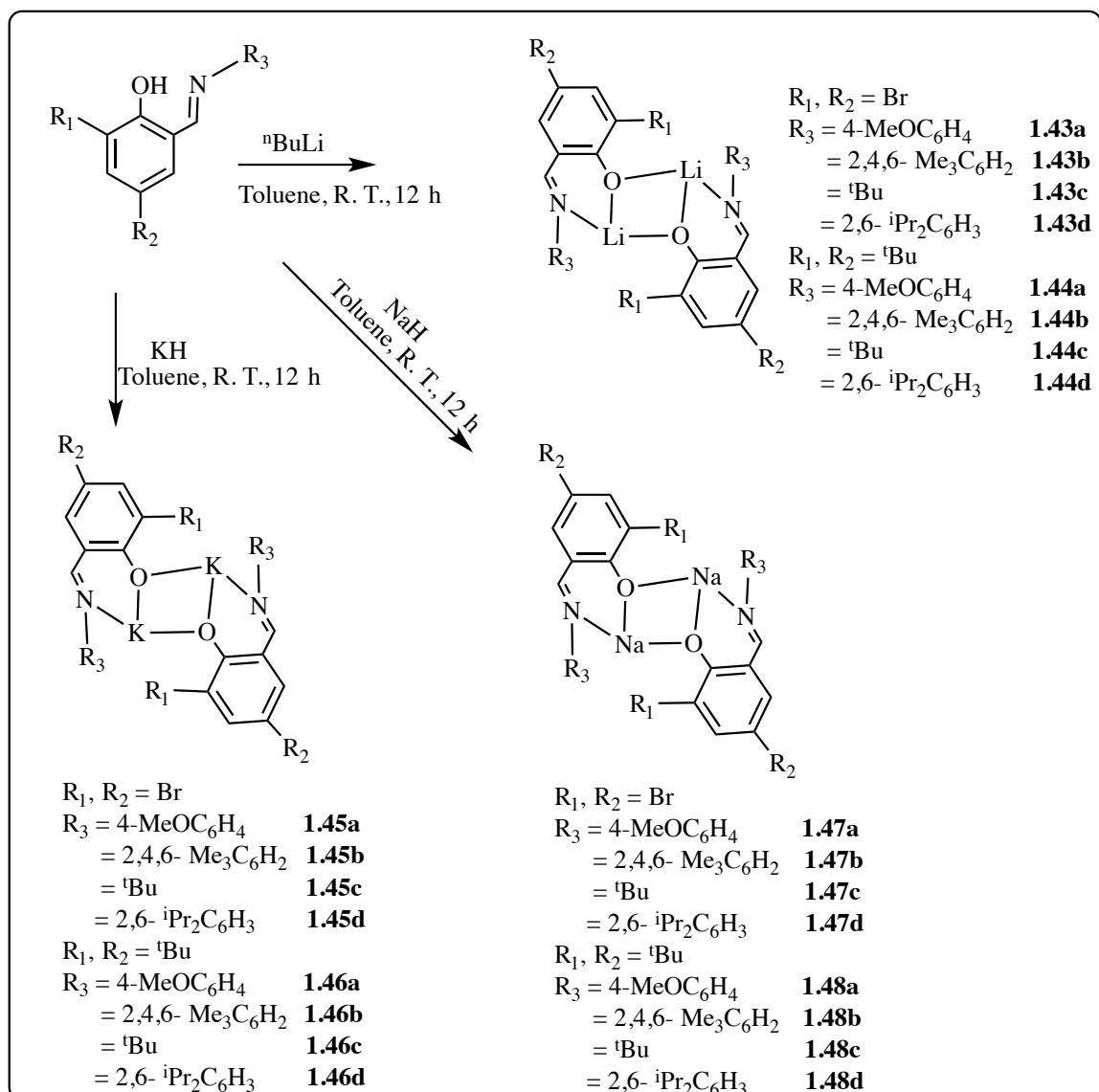
dependence on monomer concentration was obtained from the plots of $\ln[\text{monomer}]$ versus reaction time. Substitution of THF molecules by the addition of 4 equivalents of BnOH to **1.41a** and **1.41b** yielded complex **1.42**. Unfortunately, **1.42** was inactive towards the ROP of L-lactide due to the stronger Lewis basicity of BnOH than THF, which inhibited BnOH substitution and the coordination of incoming lactide.



Scheme 1.17. Hexalithium complexes used by Sobota *et al.* for ROP of L-lactide.⁹²

Lithium, sodium, and potassium complexes bearing iminophenolate ligands were reported to exhibit high catalytic activity towards ROP of L-lactide and *rac*-lactide under

bulk polymerization conditions at 140 °C (**Scheme 1.18**).⁹³ The reactivity of these complexes descended in the order Na > K > Li; thus, sodium complexes necessitated shorter reaction times to afford heteroatactic PLA with varying molecular weights. Introducing electron-withdrawing groups in the phenyl moieties, such as in complexes **1.47a–1.47d**, enhanced the reaction rate compared to those containing ^tBu moieties (**1.48a–1.48d**). This effect is attributed to the increase in Lewis acidity of the metal centre, leading to an improvement in the coordination ability of lactide. Benzyl alcohol was found to speed up the reactions in a controlled manner to yield polymers with *D* of 1.16 to 1.26, as evidenced by a continuous increase in M_n and a rise in the $[M]_0/[C]_0$ ratio.



Scheme 1.18. Di-lithium, -sodium, and -potassium complexes bearing iminophenolate ligands.⁹³

In summary, a wide range of lithium and sodium complexes have been reported as efficient catalysts for ROP of lactide. The nuclearity of the complexes influenced the observed activities, where tetrametallic lithium and sodium complexes were often more active than their dimetallic analogues. Only a few highly active catalysts afford polymer with narrow dispersity and controlled molecular weight. Consequently, the presence of

BnOH is essential to increasing the reaction rate, resulting in more controlled polymerization and dispersities closer to unity. To date, the best catalyst systems for ROP of lactide in the presence of BnOH include monolithium complexes (**1.9a-c**) reported by Chen *et al.*^{79,80} and multinuclear complexes of sodium by the Lin⁸¹ (**1.13**) and Miller⁴² (**1.22**) groups.

1.3 Reactions of epoxides catalyzed by transition metal complexes

The accumulation of carbon dioxide (CO₂) and other greenhouse gases in the atmosphere is believed to be responsible for climate change. This problem is the result of human activities that use carbon-based fossil fuels to produce energy, including industrial processes.⁹⁴ Since 1800, the amount of CO₂ in the Earth's atmosphere has increased by 90 ppm (480 billion tons); however, from 2002–2010 alone, it has increased by more than 2.25 ppm (12 billion tons).^{95,96} Thus, industrial and academic studies are focused on reducing levels of CO₂ emissions by the utilization of alternative greener technologies based on atom efficiency, reduced energy costs, and environmental considerations.

The utilization of CO₂ in the preparation of useful chemicals with significant commercial value has become an important endeavor because CO₂ is cheap, non-toxic, and abundant.⁹⁷⁻¹⁰⁴ Highly reactive substrates such as hydrogen, alcohols, acetals, amines, epoxides, oxetanes, and carbon–carbon unsaturated compounds allow the thermodynamic stability of CO₂ to be overcome in the presence of metal compounds acting as catalysts.^{95-98,105} An overview of the types of organic chemicals produced by the utilization of CO₂ are given in **Table 1.1**.⁹⁵ Among these chemicals, urea is produced in the greatest amount (about 100 million tons per year) for use as chemical fertilizer, urea resins, and animal

feed additive. In 2010, the International Fertilizer Industry Association (IFA) announced that 157 million tons of urea were produced, while other chemicals are produced in smaller amounts (*e.g.*, methanol production amounted to 4000 million tons).⁹⁵

Table 1.1. Substrates and their products for carbon dioxide utilization.⁹⁵

	Substrates	Products
1. Oxygen-containing compounds	Epoxides	Cyclic carbonates Alternating polycarbonates Aromatic polycarbonates
	Alcohols	Acyclic carbonate
2. Nitrogen-containing compounds	Ammonia, amines	Ureas Carbamic acid esters Polyurethane
	Aziridines	Oxazolidinones
	3. Carbon-carbon unsaturated compounds	Aromatic compounds
Alkynes		Carboxylic acid esters
Alkenes		Lactones
Dienes		
4. Others	Hydrogen	Formic acid
		Methanol

1.3.1 Epoxides

It is important to consider how the reagent that will be reacted with CO₂ is obtained or prepared. In this thesis, the reaction of epoxides with CO₂ is studied. Epoxides are also known as oxiranes and are a type of ether. They are easily prepared by oxidation of the corresponding alkenes. For example, the crucial feedstock propylene oxide can be produced by metal-catalyzed epoxidation, where molecular oxygen, a catalytic system of palladium(II) acetate and a peroxo-heteropoly compound are reacted in methanol (**Figure 1.20**).^{106,107} Epoxides are highly reactive towards a large number of nucleophiles, electrophiles, acids, and bases due to their ring strain, which creates a high thermodynamic driving force—usually greater than 20 kcal/mol.¹⁰⁸ This reactivity is coupled with an inherent polarity, as epoxides contain partially positively charged carbon atoms and a Lewis-basic oxygen atom in a three-membered ring.¹⁰⁹ Epoxides have been applied industrially directly or as precursors to surfactants, plasticizers, adhesives, coatings, and raw materials for the manufacture of urethane elastomers and foams. They are also used as starting materials in many organic syntheses to produce a variety of bulk chemicals such as ethylene glycol and epoxy resins; epoxides are useful in this context because they can be ring-opened with a broad range of nucleophiles with high stereoselectivity and regioselectivity.¹¹⁰ A notable example is the addition of oxiranes with Grignard reagents to form new C–C bonds by opening the three-membered ring to give an alcohol upon hydrolysis (**Figure 1.21-A**).¹¹¹ In addition, compounds such as β -lactones are highly attractive targets in organic chemistry. For example, they can be used as monomers to produce poly(3-hydroxyalkanoate)s, which are naturally occurring biodegradable polyesters. β -Lactone is produced by the ring-expansion carbonylation of

epoxides in the presence of a catalyst (**Figure 1.21-B**).¹¹²

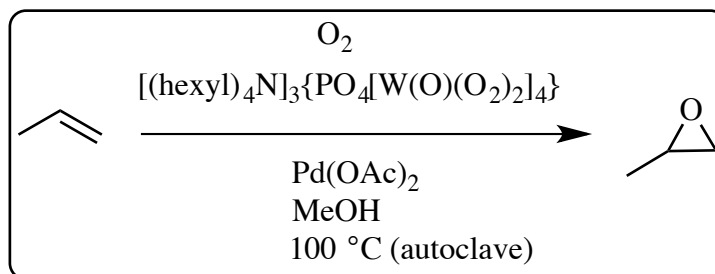


Figure 1.20. Direct epoxidation of propylene oxide.¹⁰⁶

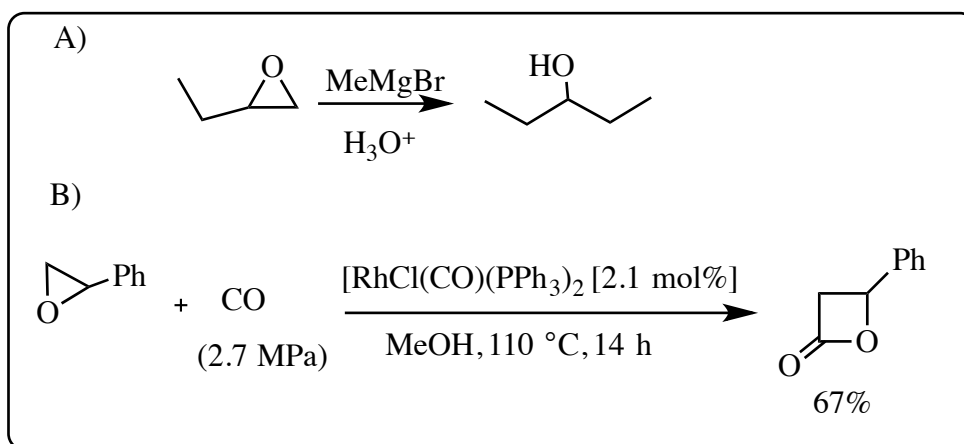


Figure 1.21. A) The addition reaction of oxiranes with Grignard reagents. B) The ring-expansion carbonylation of epoxides.¹¹³

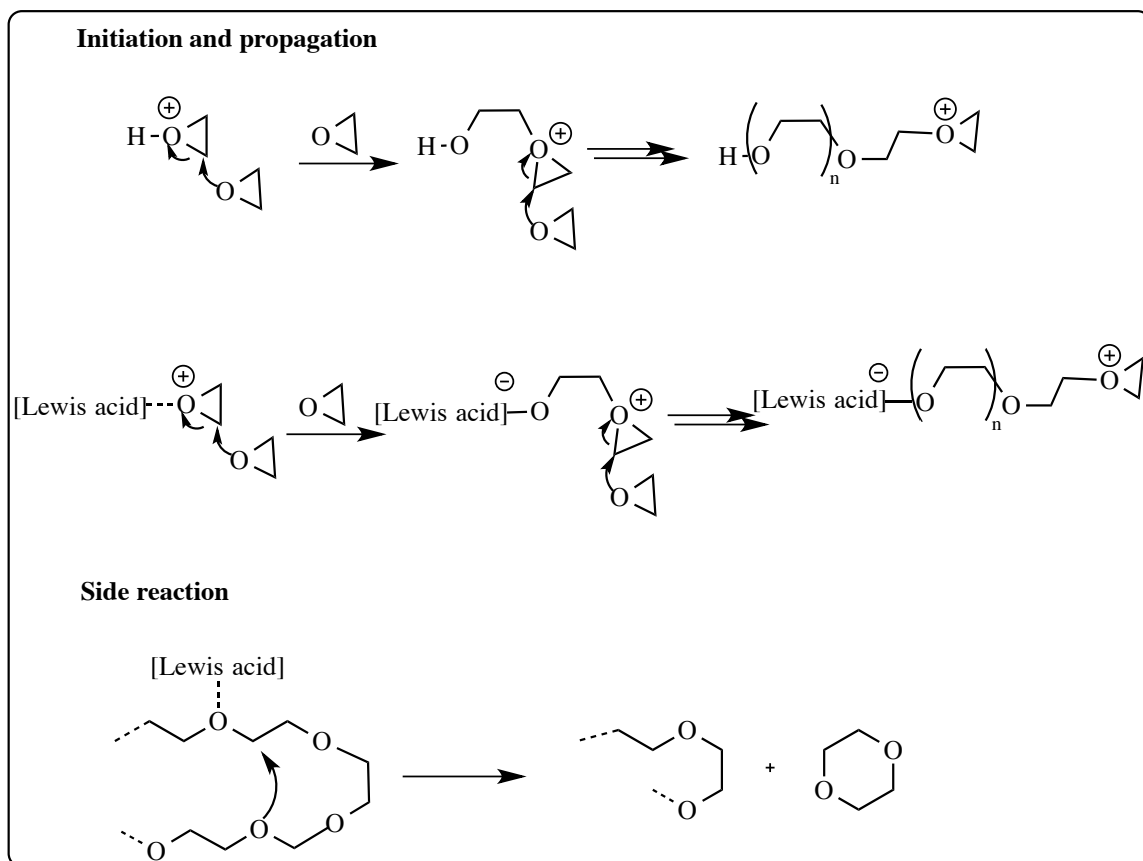
1.3.2 Polymerization of epoxides

The production of oligo(ethylene oxide) was reported in 1863 by Wurtz and Staudinger *et al.*¹¹³ followed by the first successful polymerization of propylene oxide in 1927 by Levene and Walti.¹¹⁴ Since then, ethylene oxide (EO) and propylene oxide (PO) have become two of the most important products in the synthetic chemical industry.^{111, 115} Over five million tons of PO are now produced per year, and almost two-thirds the amount of this monomer is converted into polyethers. Epoxides are produced on a large scale by the oxidation of C–C double bonds with oxygen or peroxides in the presence of

silver or through the halohydrin process.^{111,115} Depending on the type of initiator, the ROP of epoxides can proceed through several different reaction mechanisms: anionic, cationic or coordination-insertion. The coordination-insertion mechanism has been widely used and is promoted by a Lewis acid, which can coordinate to the oxygen atom of the epoxide.¹¹⁶

1.3.2.1 Cationic polymerization

In cationic polymerization, Lewis acid and protic acid catalysts activate the epoxide by protonation of the epoxide oxygen, resulting in the formation of a positively charged species (**Scheme 1.19**). The initiation reaction involves ring opening of a protonated epoxide by nucleophilic attack of a second monomer to form a tertiary oxonium ion. The propagation step includes subsequent attacks by additional monomers. For example, a Lewis acid can induce cationic polymerization by ring-opening the activated epoxide in the initiation step to give a tertiary oxonium ion. Upon initiation, the activated epoxide carbon at the chain end reacts with a free epoxide to propagate a polymer chain. However, products of side reactions, such as 1,4-dioxane derivatives, complicate the reaction; these unwanted products arise by intramolecular nucleophilic attack of an ether oxygen in the main chain at the methylene carbon adjacent to the oxonium ion (**Scheme 1.19**). In addition, the regioselectivity in cationic polymerization of terminal epoxides is not so high due to ring opening occurring equally at both methylene-oxygen and methine-oxygen bonds. Therefore, controlling the polymer properties (including molecular weight, tacticity, and regioregularity) by cationic polymerization is difficult.¹⁰⁹



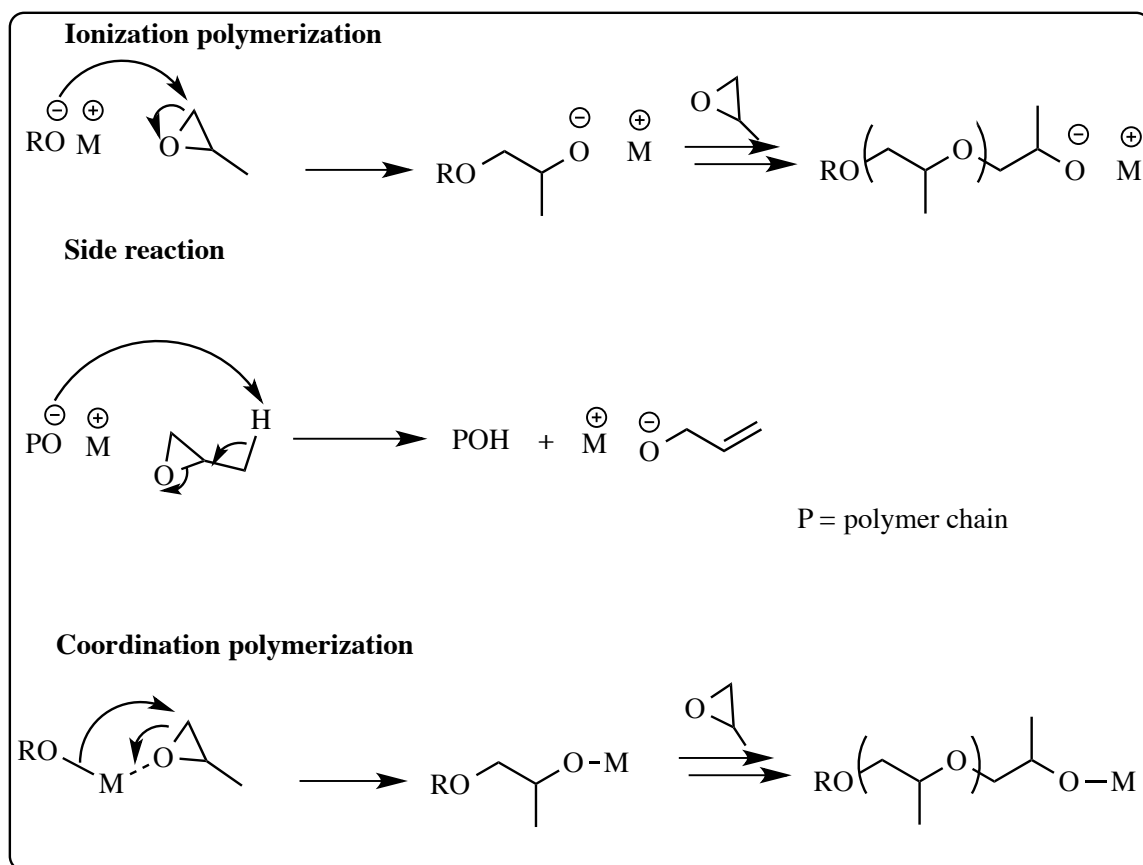
Scheme 1.19. Cationic mechanism of ring-opening polymerization of epoxide.¹⁰⁹

1.3.2.2 Anionic and coordination insertion polymerization

In (coordination) anionic polymerization, epoxides are typically polymerized with metal alkoxides as initiators. The mechanism for propylene oxide coordination polymerization is illustrated in **Scheme 1.20**. The monomer inserts itself into the metal-alkoxide bond once a Lewis acidic metal centre coordinates to the monomer molecule through the oxygen atom. Coordination of the monomer increases the nucleophilicity of the metal alkoxide initiator, rendering the methylene-oxygen bond of the monomer (a less hindered carbon atom) more susceptible to nucleophilic attack. Therefore, ring

opening of the epoxide occurs via nucleophilic attack of an alkoxide on the (activated) epoxide at the less sterically hindered β -carbon atom to generate another metal alkoxide, which is the propagating species. Finally, the reaction is terminated by hydrolysis of the propagating chain.⁷ The nature of the metal-alkoxide bond determines the reaction mechanism: the alkoxide can act as a coordination catalyst, having a covalent bond between the metal atom and the oxygen atom to promote the coordination insertion mechanism; or it can form an ionic bond to initiate anionic polymerization.

In the anionic polymerization of PO, alkali metal alkoxides can abstract a proton from the methyl group of PO because of their high basicity (**Scheme 1.20**). This chain transfer reaction results in the significant formation of oligomers with a terminal allyl group as an initiating group. As mentioned previously, the ring opening generally takes place at a less hindered methylene–oxygen bond; as a result, there is no configurational change at the original stereogenic centre, and highly controlled regioregularity of the resulting polymer is observed. Less basic metal alkoxides, such as zinc and aluminum alkoxides, are also effective for the production of high molecular weight polymers.¹⁰⁹



Scheme 1.20. Polymerization of propylene oxide by anionic and coordination mechanisms.¹⁰⁹

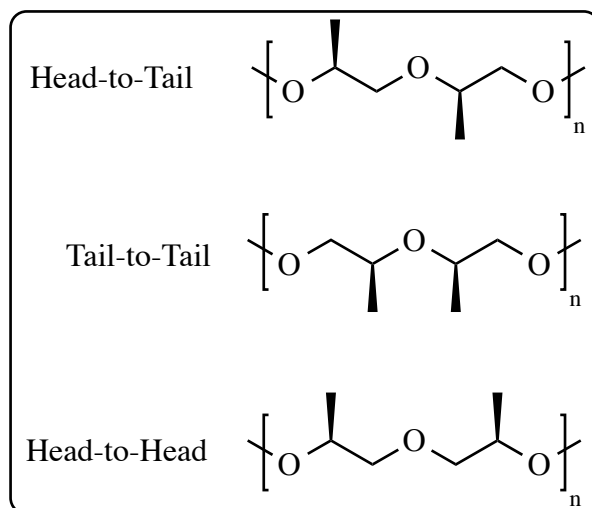
1.3.3 Stereochemistry of epoxides

Stereochemistry introduced by asymmetric epoxides has a large influence on the physical and mechanical properties of the polymer, such as the melting temperature, mechanical strength, and crystallinity.¹¹⁷ Ring opening of epoxides can occur via C–O bond cleavage; the symmetry of the epoxide (symmetrical or unsymmetrical) governs the regio- and stereoisomerism of the polymerization, which can be controlled.¹⁰⁹

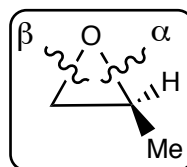
For unsymmetrical epoxides like PO, there are three possible regioisomers of two repetitive constitutional units (**Scheme 1.21**).¹¹⁸ Bond cleavage can occur at either the

methine-oxygen bond (α) or the methylene-oxygen bond (β) (**Scheme 1.22**).¹¹⁹ Head-to-tail ether linkages are produced by successive epoxide ring opening at either the methylene or methine C–O bond. Head-to-head or tail-to-tail linkages result from alternating ring opening at the methylene C–O bond of one epoxide and the methine C–O bond of the following epoxide.¹²⁰ These different isomers can be identified by ¹³C NMR spectroscopy, as reported by Goriot *et al.*¹²¹

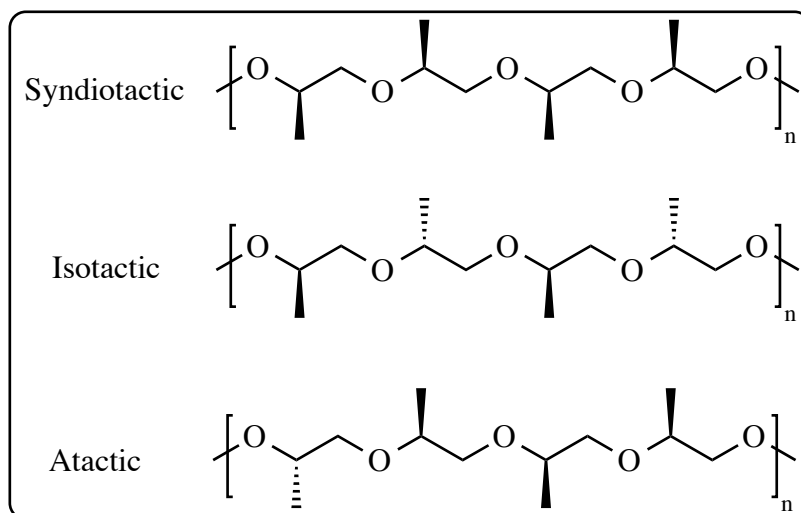
Stereoregularity refers to the arrangement of atoms in the repeating units along the chain (**Scheme 1.23**). Propylene oxide exists in both the *R*- and *S*- configurations and the regularity of the structure can be described in terms of tacticity. If the absolute optical configurations are identical, the polymer is isotactic, and if they are opposite, the polymer is syndiotactic. When the optical configurations are completely random, an atactic polymer is obtained. Stereochemical regulation is achieved through either polymer chain end control, in which the growing chain induces selective incorporation of a monomer, or enantiomorphic site control, where enantioselective incorporation is induced by ligands around the metal centre.¹¹⁷



Scheme 1.21. Regioisomers of polyether.¹¹⁸



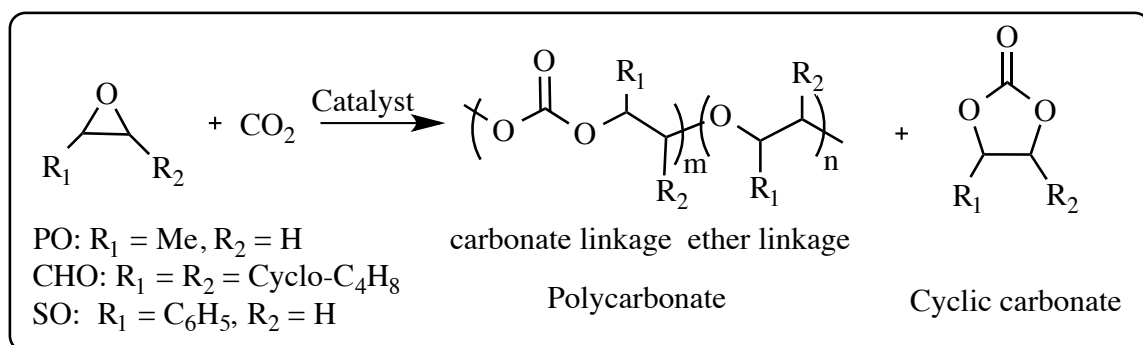
Scheme 1.22. Ring opening of propylene oxide.¹¹⁹



Scheme 1.23. Tacticity of polyether.¹¹⁸

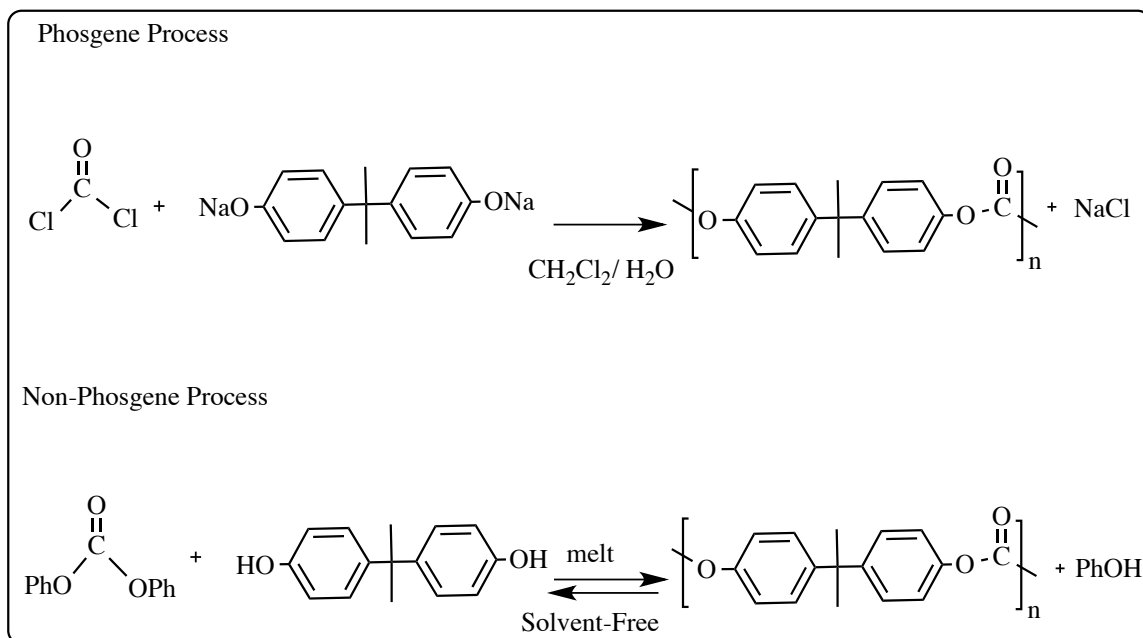
1.4 Synthesis of polycarbonate and cyclic carbonates by reaction of CO₂ and epoxides

The transformation of CO₂ and epoxides into valuable polycarbonates and/or cyclic carbonates is an important process, as shown in **Scheme 1.24**.¹²² I.G. Farbenindustrie was the first to report the synthesis of cyclic carbonates by the direct coupling of oxiranes with carbon dioxide.²⁴ The reaction was catalyzed by sodium hydroxide on activated charcoal, but yields were low because the catalyst was short lived. Many different types of catalysts have since been developed to accelerate this reaction, including amines, onium salts, metal oxides, metal halides, and several transition metal complexes.¹²³ Poly(bisphenol A carbonate) (BPA-PC) was first synthesized in the late 1950s as an alternative to polyethylene terephthalate (PET).¹²⁴ Polycarbonates have several attractive properties, including strength, lightness, high transparency, and heat resistance; therefore, they are widely used in many industrial applications, such as electronic devices, packaging materials, engineering thermoplastics, and resins. In 2008, about 3.2 million tons of BPA-PC was produced worldwide, marketed by Bayer as Makrolon[®] and Lexan[®], and Innovative Plastics by SABIC.¹²⁵



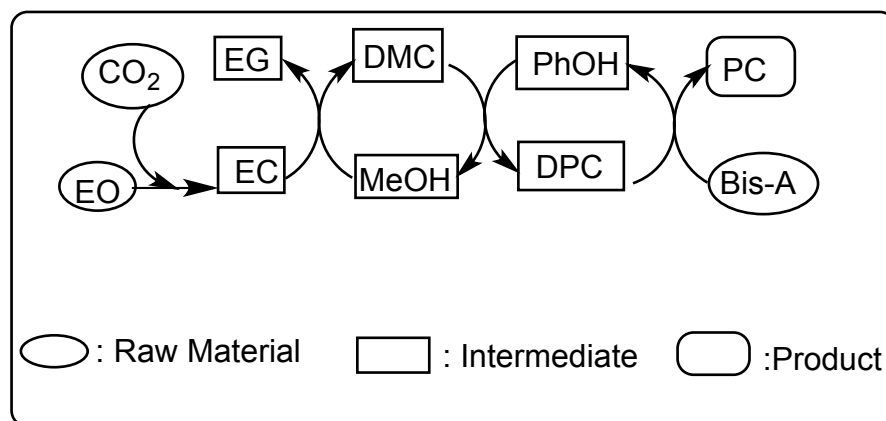
Scheme 1.24. General reaction of common epoxides and CO₂, producing cyclic carbonate and/or polycarbonate. PO = propylene oxide, CHO = cyclohexene oxide, and SO = styrene oxide.¹²³

As seen in **Scheme 1.25**, high molecular weight BPA-PC is produced through two industrial routes.¹²⁵⁻¹²⁷ One process is heterogeneous and involves the interfacial reaction of phosgene, dissolved in dichloromethane (CH_2Cl_2), and the sodium salt of bisphenol-A, dissolved in water. However, this process is far from green: it requires the use of hazardous CH_2Cl_2 and highly toxic phosgene (a well-known chemical weapon); large amounts of sodium chloride are generated; and a large amount of water is used in the washing and purification steps to remove contaminants from the obtained polymer.^{125, 127} The non-phosgene route is a melt-phase transesterification between diphenyl carbonate (DPC) and bisphenol-A. Although the monomer DPC is safer than phosgene, the reaction has disadvantages of its own, namely producing low-molecular weight PC and requiring high temperatures to remove the byproduct phenol. In both processes, BPA-PC itself is linked to endocrine disruption and reproductive ailments through human exposure to the BPA that can leach from the polymer.^{125,127-130} Nowadays, under the Chemical Weapons Convention, the production and use of phosgene has been banned in 185 countries worldwide.



Scheme 1.25. Industrial process for the production of BPA-PC.¹²⁵

Asahi Kasei's researchers and engineers introduced a novel non-phosgene process for producing high-quality polycarbonates, in which ethylene oxide (EO), its byproduct CO₂, and bisphenol-A are used as starting materials.^{125,127} This process, depicted in **Scheme 1.26**, is free of phosgene, DCM, and water. There are several other advantages to this method: reduced CO₂ emissions using CO₂ as a starting material, which is produced as a byproduct from the oxidation of ethylene with oxygen; all intermediates, such as ethylene carbonate (EC), dimethyl carbonate (DMC), and methanol are completely used or recycled as raw materials; and purification and separation of the polymer are unnecessary.^{125,127}



Scheme 1.26. Asahi Kasei's new non-phosgene polycarbonate process.¹²⁷

Another greener pathway to polycarbonate synthesis is given in **Scheme 1.24**: the direct fixation of CO₂. Cyclic carbonates, which serve as aprotic solvents, electrolytes in lithium ion batteries, and starting materials for polycarbonates can also be produced in this way.¹³¹ Reaction selectivity towards either polycarbonate or cyclic carbonate products can be controlled by altering reaction conditions such as temperature, CO₂ pressure, and cocatalyst loading. For example, cyclic carbonates can be obtained by carrying out the reaction at an elevated temperature.⁷ Compared to conventional methods of polycarbonate synthesis, this approach has several advantages: the monomers are less toxic than phosgene; CO₂ is cheap, abundant, and non-toxic; and the PC produced has more controlled molecular weights. On the other hand, the physical properties of the polymer cannot be improved to match commercially available BPA-PC. In addition, the lack of ring strain and low reactivity of larger cyclic ethers suppresses copolymerization with CO₂ and limits the types of co-reacting monomers available.

The first successful green approach was demonstrated by Inoue *et al.*¹³² in the late 1960s. They investigated the catalytic copolymerization of CO₂ with a heterogeneous

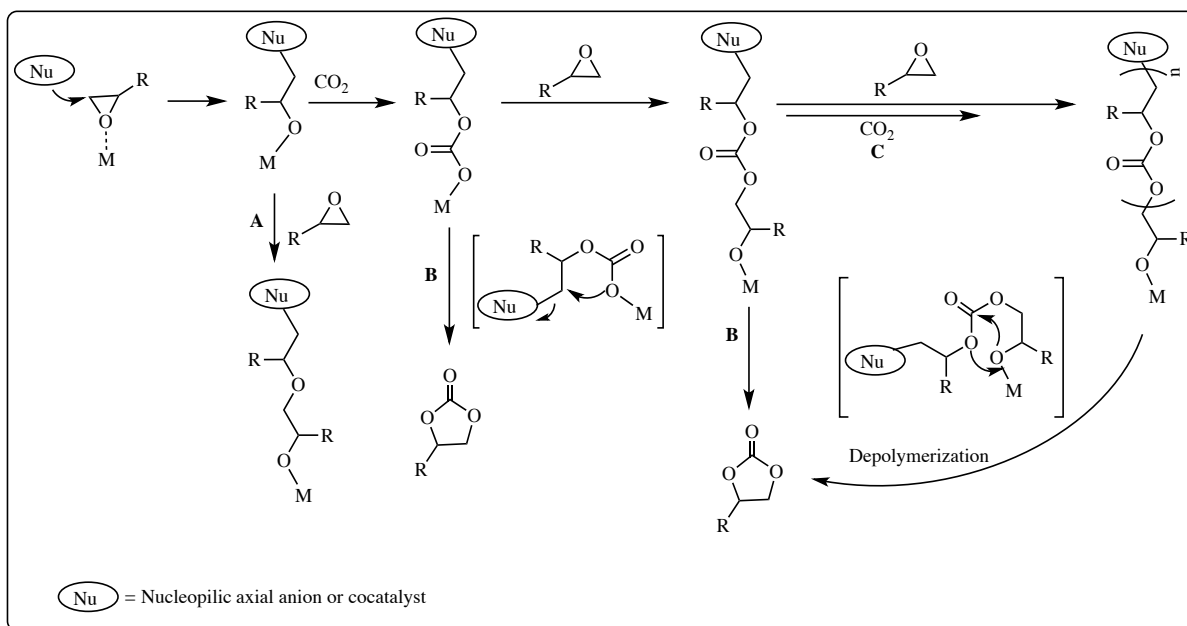
catalyst composed of a mixture of diethyl zinc and H₂O. The copolymerization of propylene oxide and CO₂ yielded aliphatic polycarbonates with a TOF of 0.12 h⁻¹ at 20–50 bar CO₂ and 80 °C in the presence of a metal alkoxide species. However, these reactions suffered from several drawbacks: high catalyst loading, elevated CO₂ pressure, long reaction times, high ether content in the produced polymer and unpredictable molecular weights. In addition, controlling the physical properties of the polymers was difficult; as such, several homogenous catalysts have been developed to provide higher activity and selectivity for this process.

1.4.1 Homogenous catalyst systems for coupling and polymerizing CO₂ and epoxides

Various Lewis acidic metal halides are known to couple CO₂ and epoxides, forming cyclic carbonate and/or poly(ether-*co*-carbonate). Salen-metal complexes are one of the most popular groups of homogenous catalysts for epoxide/CO₂ ring-opening copolymerizations in that they are easy to synthesize, their steric and electronic properties are easily tunable by modification of the ligand, and they operate as catalysts under mild temperatures and pressures.¹³³

The coupling reaction of CO₂ and epoxides is proposed to occur via a coordination-insertion mechanism. Three different types of products can be obtained from this reaction including cyclic carbonate, polycarbonate, and polyether (**Scheme 1.27**). One pathway proceeds by the formation of a metal-bound alkoxide, where the metal complex initiates the ring opening of the epoxide by coordination of the monomer to the metal centres, followed by attack of a methine carbon by the nucleophilic group

(nucleophilic axial/leaving group or added cocatalyst *e.g.*, chloride ion). This can lead to the formation of polyether linkages by consecutive epoxide ring opening and insertion into the M–O bond (Route A). The other pathway is formation of a metal-bound carboxylate by insertion of CO₂ into a metal-alkoxide bond. Cyclic carbonate is formed in the event of back-biting (Route B), or polycarbonate is formed by consecutive alternating insertions of epoxide and CO₂ (Route C).



Scheme 1.27. Possible reaction routes for metal-catalyzed coupling reaction of CO₂ and epoxides.¹²³

Tremendous effort has been devoted to the design of efficient catalysts for this transformation under mild reaction conditions,¹³¹ especially for Zn, Al, Cr, and Co complexes supported by sterically demanding ligands such as phenoxides, salens, porphyrins, and diketiminates. In order to address potential toxicity issues associated with some of these metals, iron based complexes have become more widely studied in the past

decade. They are not only lower in toxicity but are cheap and abundant. Therefore, it is important to understand the basics of iron chemistry in order to put their work in context.

As Fe and Co complexes are studied in this PhD research; what follows is a literature review of their use in this field and brief overview of the chemistry of these metals.

1.4.1.1 A brief history of iron and its chemistry

The name “iron” (symbol: Fe) originates from the Latin word *ferrum*. The atomic weight of Fe is 55.847 g mol⁻¹; its specific gravity is 7.874 g cm⁻³; its melting point is 1535 °C; and its boiling point is 2750 °C. Iron is considered to be the second most abundant metal after aluminum in the Earth’s crust.^{134,135} In nature, iron is one of 94 naturally occurring elements. It is extracted from its ores; the most common ore minerals are magnetite (Fe₃O₄), hematite (Fe₂O₃), goethite (FeO(OH)), limonite (FeO(OH)·n(H₂O)) and siderite (FeCO₃). Iron exists in four naturally occurring stable isotopes: ⁵⁴Fe (5.82% abundance), ⁵⁶Fe (91.66% abundance), ⁵⁷Fe (2.19% abundance), and ⁵⁸Fe (0.335% abundance). The ground state electron configuration of Fe is [Ar] 3d⁶4s².¹³⁶ The most common oxidation states of Fe are +2 and +3, and rarer oxidation states are +1, +4, +5, +6, 0, -1, and -2. Compounds of Fe(III) are the most stable; therefore, in air, Fe(II) compounds easily oxidize to their Fe(III) analogues. Furthermore, Fe(III) preferentially binds to hard Lewis bases because it is a harder Lewis acid than Fe(II). Fe(II) (electron configuration: [Ar] 3d⁶) has a common coordination number of six with an octahedral ligand sphere. Fe(III), with a configuration of [Ar] 3d⁵, can coordinate three to eight ligands and often exhibits octahedral coordination geometry. Fe(0) can adopt trigonal bipyramidal and octahedral geometries by coordination to five or six

ligands, respectively, while Fe(-2) is most often tetrahedrally coordinated. Low-oxidation state iron can form more reactive complexes than their Fe(II) and Fe(III) counterparts; therefore, they are favored in organometallic chemistry, particularly for iron-catalyzed reactions. For example, iron carbonyl complexes having an Fe(0) centre are of special interest due to their high stability.¹³⁴

Iron is also an essential element in nearly all biological systems.¹³⁷ It is involved in the transport of oxygen within heme-containing proteins such as hemoglobin and myoglobin. These proteins consist of an Fe(II) ion bound to a porphyrin ring, where Fe is situated at the centre of a square pyramidal environment, and the axial position is occupied by a histidine group from a protein chain. Oxygen can be transported through this complex in the blood by binding with an available coordination site at the Fe centre.

1.4.1.2 Iron catalysts for polycarbonate and cyclic carbonate formation

In the context of green chemistry, inexpensive and environmentally friendly iron catalysts are desirable and ecological choices for the synthesis of polycarbonates. Many promising results in the conversion of CO₂/epoxides were achieved using catalysts that meet these criteria. In view of this, a brief historical description of CO₂/epoxide copolymerization with iron complexes follows.

Double metal cyanides (DMC) based on heterometallic derivatives of Zn(II) and Fe(II) containing bridging cyanide ligands (e.g., [Zn₃[Fe(CN)₆]₂]) were reported as viable heterogeneous catalysts for the copolymerization of CO₂/epoxides.¹³⁸ Catalysts were prepared by reacting a transition metal cyanide complex with a metal salt in aqueous media. Water was completely removed to enhance the activity of the catalyst. The

copolymerization reactions were performed at temperatures between 0 and 150 °C; however, the CO₂ pressure required was 50–60 bar. In 2001, the research group of Darensbourg *et al.*^{139,140} investigated the homogenous analogues. They incorporated iodide as an initiator into a tetrahedrally coordinated Zn centre with two bridging cyanide ligands and stable anionic iron cyanide moieties for epoxide binding/activation (**1.49**, **Figure 1.22**). The complexes were thermally stable at 80 °C and capable of producing both polycarbonates and cyclic carbonates after 24 h; however, the complexes are less active for the copolymerization reactions than the heterogeneous catalysts under the same conditions.

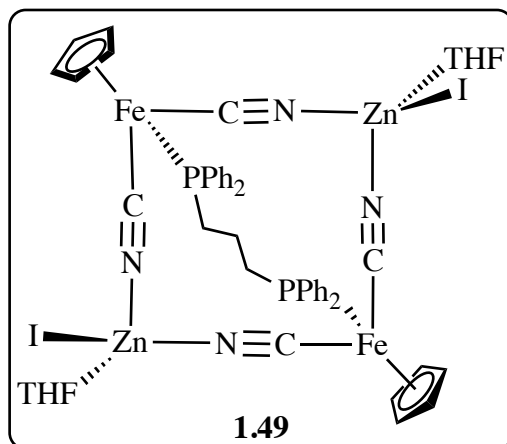


Figure 1.22. Double metal cyanide (DMC) catalyst used by Darensbourg and coworkers.^{139,140}

Williams and coworkers made a considerable impact in this area of study with the development of a highly active dinuclear Fe(III/III) catalyst (**1.50**) with a reduced Robson-type ligand structure (**Figure 1.23**) for the production of either cyclic carbonate or polycarbonate in the coupling of CHO/CO₂.¹⁴¹ The complex achieved a TOF of 107 h⁻¹ at 80 °C and 10 bar CO₂ with a [Fe]/[CHO] ratio of 1:1000. The copolymer had 99%

carbonate linkages, an M_n of 17200 g mol⁻¹, and a narrow dispersity (1.03). However, this system converted PO into only CPC with a TOF around 25 h⁻¹ in the presence of 1 equivalent of PPNCl per Fe centre, with no formation of the copolymer. The high activity of **1.50** was attributed to the dinuclear active site and the macrocyclic ligand coordination environment, allowing the halide ion to initiate the ring opening of CHO to generate an Fe–OR species. The oxyanion generated from ring opening then attacks CO₂ to form an iron-carbonate intermediate; this step is followed by propagation, or sequential repetition of ring opening and insertion reactions.

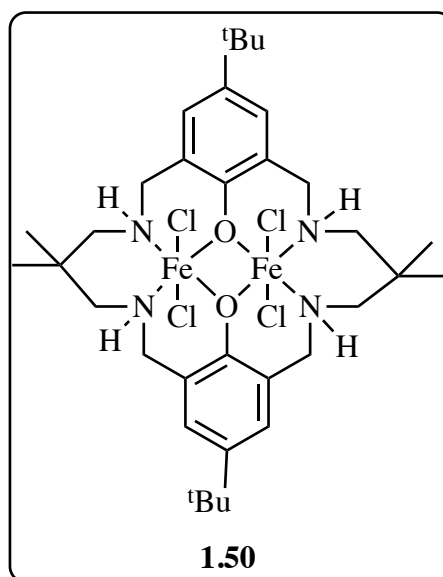


Figure 1.23. Dinuclear Fe(III/III) complex with reduced Robson-type ligand.¹⁴¹

In 2011, a mononuclear Fe(II) system based on a diamine-diquinolyl ligand (**1.51**), depicted in **Figure 1.24**, was reported to be active in the production of CPC without the addition of a cocatalyst.¹⁴² The complex exhibited high activity after 2 h at elevated temperature (100 °C) and 15 bar CO₂ with a conversion of 80%. However, **1.52** (the diimine-diquinolyl analogue) was unable to produce CPC without the addition of

TBAB as a cocatalyst, giving a conversion of up to 82% within 2 h. The high activity of **1.51** was suggested to be due to the dissociation of chloride ligand from iron, thereby allowing PO to coordinate to the cationic iron centre. The free chloride anion is then able to attack the less hindered side of the epoxide and ring-open PO. The proposed mechanism was backed up by the X-ray crystal structure of **1.51**, which reveals an extremely long, and thus labile, Fe–Cl bond. The reaction was monitored *in situ* by IR spectroscopy, and an increase in the intensity of the CPC absorption at 1791 cm^{-1} was observed during the course of the reaction. Kinetic studies indicated a second-order dependence on the catalyst concentration, and the activity of the cyclization reaction of propylene oxide with CO_2 had an activation energy of 100.5 kJ mol^{-1} .

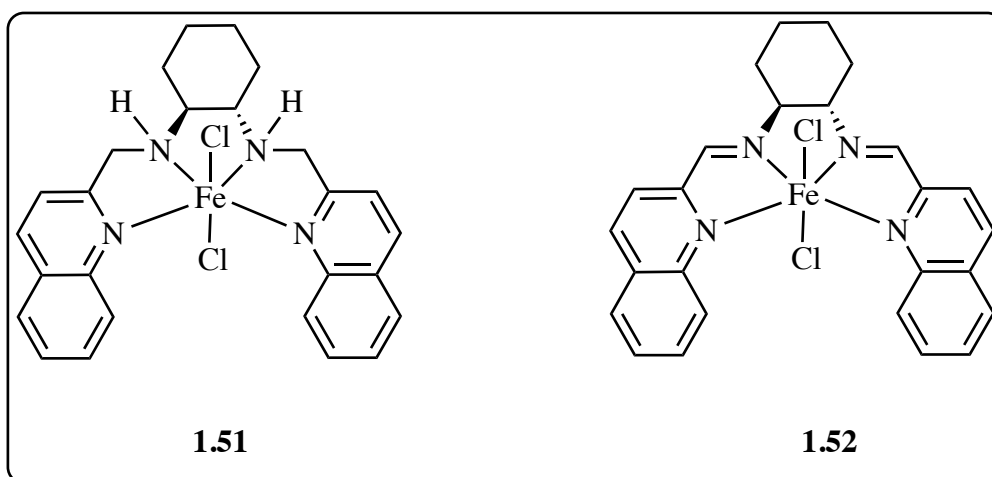


Figure 1.24. Mononuclear Fe(II) system designed by Rieger and coworkers.¹⁴²

The catalytic activity of monomeric and dimeric Fe(III) triphenolate complexes bearing different substituents in the phenoxide moiety (^tBu, Ph, H, and Me) (**Figure 1.25**) was investigated by Kleij *et al.* for the coupling of CO_2 and oxiranes.¹⁴³ The complexes

were synthesized by the reaction of iron(III) chloride and the sodium salt of the ligand; the formation of a dimetallic or monometallic species was dependent on the substituent in the *ortho*-position of the phenolate rings. The monometallic complexes (**1.53a** and **1.53b**) were more active than the dimetallic complexes (**1.54a** and **1.54b**) in forming cyclic carbonates after 18 h at room temperature and 10 bar CO₂. In addition, changing the reaction conditions by using higher temperature and a coordinating solvent had a significant effect on catalyst behavior. For example, adding a coordinating solvent such as methylethylketone (MEK) can disrupt the less-active dimetallic structure to form a monomeric MEK adduct, enhancing the activity.

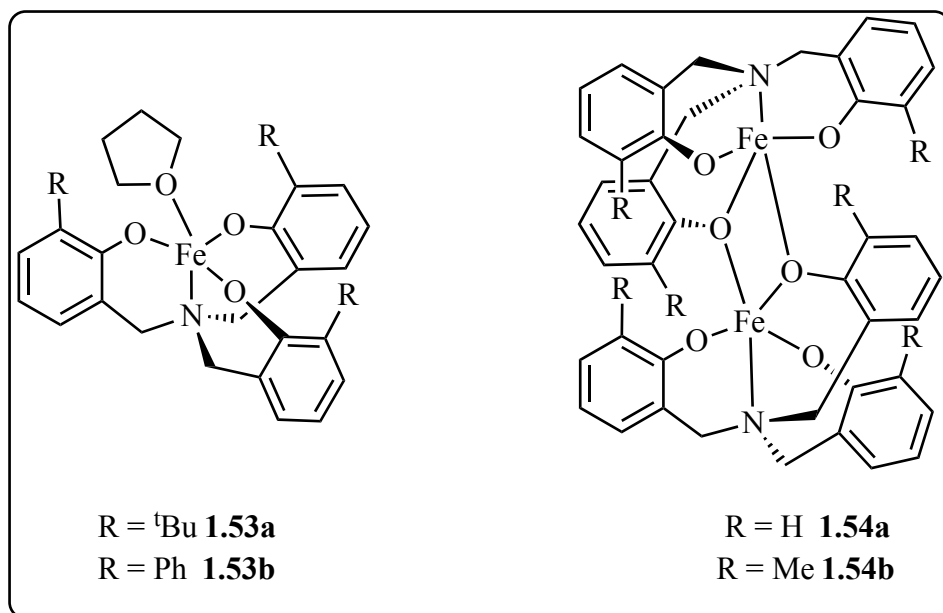


Figure 1.25. Monomeric and dimeric Fe(III) triphenolate complexes used by Kleij *et al.*¹⁴³

In 2013, a new, challenging ring opening reaction of CHO using the previously described Fe(III) triphenolate complexes was reported (**Figure 1.25**).¹⁴⁴ The complexes demonstrated excellent catalytic efficiency and selectivity towards either cyclic or

polymeric products in combination with a cocatalyst, such as TBAX or PPNX (where X = F, Cl, Br, and I). The reactions were carried out at 85 °C under supercritical carbon dioxide (*scCO*₂) (80 bar) for 3 h. The selectivity was highly dependent on the cocatalyst ratio; for example, higher nucleophile:metal ratios corresponded to selective formation of cyclic carbonate, and lower ratios produced polycarbonate. Moreover, the formation of cyclic carbonate was enhanced by the presence of a nucleophile with strong leaving ability, such as I⁻ and Br⁻, whereas weak leaving ability increased the formation of polycarbonates. Notably, the most efficient catalyst was **1.54b**, which achieved a TOF of 187 h⁻¹ with PPNCl as a cocatalyst to yield polycyclohexene carbonate (PCHC) with no ether linkages.

A new family of ionic monometallic Fe(II)- and Fe(III)-based N₂O₂ catalysts was investigated for the coupling of PO/CO₂.¹⁴⁵ Fe(II) complex **1.55** was synthesized according to **Scheme 1.28** by the reaction of Fe(OAc)₂ with an N₂O₂-based ligand in DMF and pyridine. The complex was then oxidized by iodine under mild conditions to afford **1.56**. Fe(III) complexes produced CPC in high yield (99%) with a TOF of 165 h⁻¹ at 80 °C and 50 bar CO₂ in a short reaction time (3 h), without the addition of cocatalyst. In contrast, Fe(II) complexes with TBAB as a cocatalyst produced CPC in 37% yield in 20 h, with a TOF of 9.3 h⁻¹. The high activity of the Fe(III) catalysts was attributed to three features: the high Lewis acidity of the metal centre, the presence of two pyridine molecules in the complex structure, which can act as cocatalysts and the ionic character of the complex, in which the iodide anion interacts with the epoxides.

weight, $M_n = 29,000 \text{ g mol}^{-1}$. In addition, it was also noted that the loading of cocatalyst, the temperature, and the CO_2 pressure affects the catalytic activity. For example, increasing the cocatalyst loading from 0.5 equivalents to 0.76 and 1 equivalent reduced the catalytic activity from 1004 h^{-1} to 525 h^{-1} and 19 h^{-1} , respectively. Furthermore, they discovered that other iron-corrole complexes (**1.58a–1.58b**) could also produce polypropylene carbonate (PPC) with different catalytic activities. Monomeric complex **1.58a** with chloride demonstrated lower catalytic activity than **1.57a** ($\text{TOF} = 701 \text{ h}^{-1}$), while complex **1.58b** showed higher catalytic activity than **1.57a** ($\text{TOF} = 1209 \text{ h}^{-1}$); however, complex **1.57b** gave only cyclic carbonate. Under similar conditions, the complexes were also observed to copolymerize CHO/ CO_2 to yield PCHC with high carbonate linkages ($>90\%$), where the highest catalytic activity ($\text{TOF} = 109 \text{ h}^{-1}$) was detected for **1.57b** in 3 h. Moreover, the study also focused on the coupling of GPE (glycidyl phenyl ether)/ CO_2 using **1.57a**, which provided highly crystalline copolymers because of the isotactic poly(GPE) units, with a TOF of 401 h^{-1} .

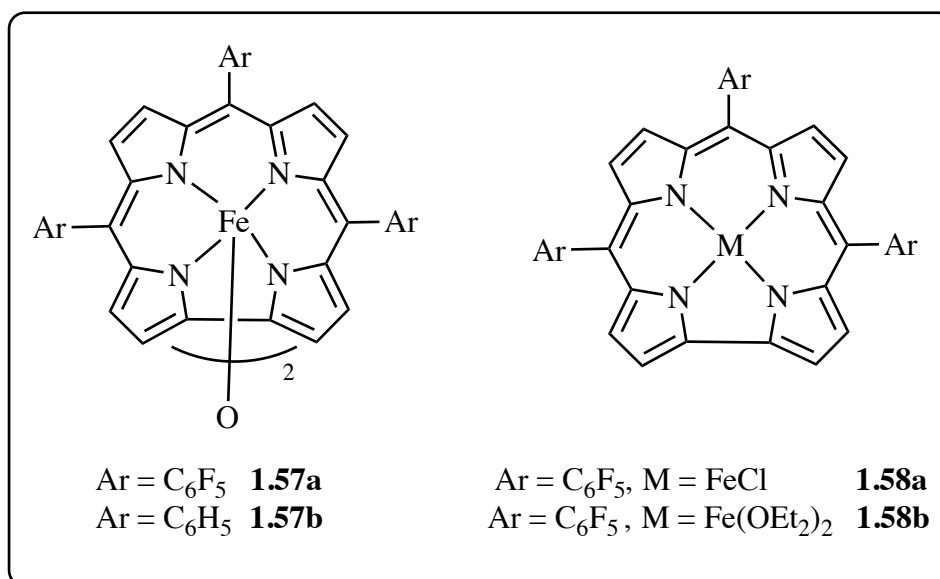


Figure 1.26. Fe(IV) and (III) complexes reported by Nozaki and coworkers.¹⁴⁶

Wang *et al.*¹⁴⁷ introduced novel Fe(II) complexes that could catalyze the cycloaddition of CO₂ and propylene oxide in combination with TBAB to generate the corresponding CPC under neat conditions at 40 bar CO₂ (**Figure 1.27**). The temperature was an important parameter in these reactions with high temperatures (130 °C) leading to the highest catalytic activities for **1.59** and **1.60** with the addition of TBAB. For example, 95% conversion of PO was achieved by **1.60** with a TOF of 238 h⁻¹ in 4 h at 100 °C; however, once the temperature increased to 130 °C, 100% conversion was achieved with a TOF of 250 h⁻¹. Lower temperatures (70 °C) did not yield CPC. The authors attributed the high activity of these complexes at high temperatures to the improved solubility of the catalyst in the reaction mixture and the decomposition of quaternary ammonium salts (Bu₄NBr) to tributylamine (Bu₃N). These compounds can form a carbamate salt with CO₂ (Bu₃N⁺-CO₂⁻), which is beneficial for the activation of carbon dioxide. Furthermore, under the optimized reaction conditions of 100 °C, 40 bar CO₂, and 4 h, the catalysts

displayed high catalytic activities in the cycloaddition of cyclohexene oxide (CHO) and epiochlorohydrin (ECH) with CO₂ to afford the corresponding cyclic carbonates in the presence of TBAB. For the conversion of ECH, the catalysts achieved TOFs of 215 and 243 h⁻¹ for **1.59** and **1.60**, respectively. However, they showed decreased ability to convert CHO due to its larger ring strain.

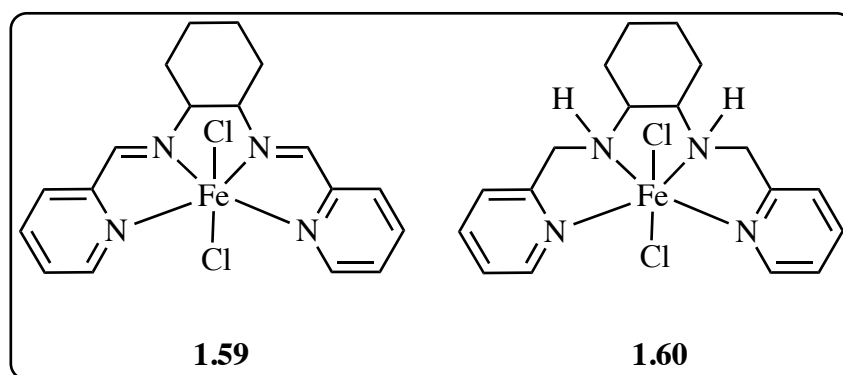


Figure 1.27. Fe(II) complexes reported by Wang *et al.*¹⁴⁷

Recently, dinuclear Fe(III)-based thioether-triphenolate complexes have shown high activity towards the production of CPC from the coupling of CO₂ and propylene oxide in solvent free conditions (**Figure 1.28**).¹⁴⁸ Complex **1.61** afforded complete conversion of PO within 6 h with a TOF of 66 h⁻¹ under the following reaction conditions: 60 °C, 20 bar CO₂, and 0.5 mol% cocatalyst loading. Decreasing the reaction time to 3 h led to a drop in PO conversion (to 68%) and an increase in the TOF (to 90 h⁻¹). In addition, the catalytic performance was sensitive to the amount of cocatalyst used. For example, doubling the cocatalyst loading from 0.05 to 0.1 mol% increased the catalytic activity from 111 to 130 h⁻¹ and increased the conversion from 67 to 78%. On the other hand, the efficiency of the catalysis was compromised by halving

the loading from 0.05 to 0.025 mol%, reducing the activity from 111 h⁻¹ to 38 h⁻¹. The temperature also influenced the catalytic performance: performing the reaction at higher temperature (100 °C) afforded cyclic carbonate with a high TOF value (580 h⁻¹) and a conversion of 87% after 6 h. The high activity of **1.61** was attributed to the presence of soft sulfur donor atoms, which weakly coordinate to the hard Lewis-acidic Fe(III) centre. As a consequence, the epoxide can coordinate to the metal centre, followed by attack of the nucleophile and formation of the cyclic carbonate.

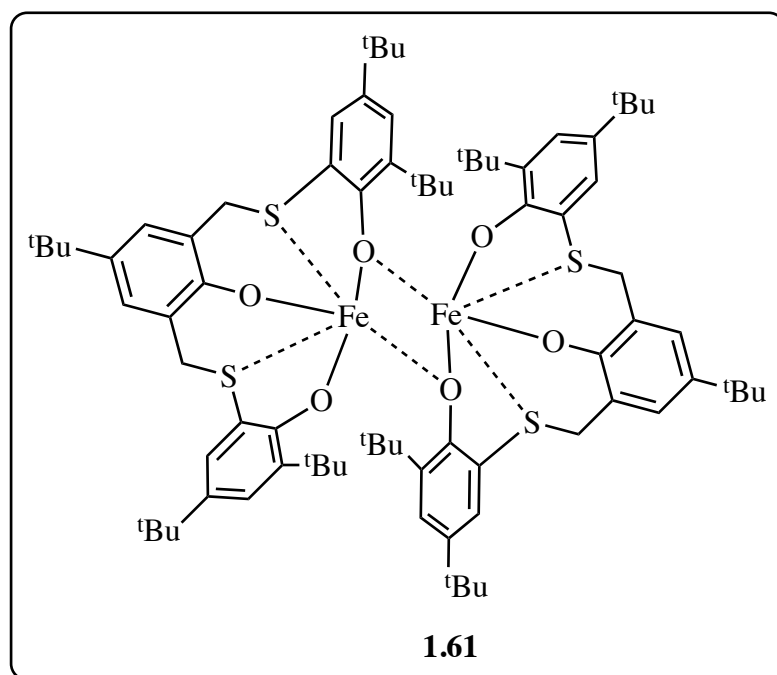


Figure 1.28. Dinuclear Fe(III)-based thioether-triphenolate complexes for synthesis of CPC from CO₂ and propylene oxide.¹⁴⁸

As part of continuing efforts to develop more efficient dinuclear Fe(III)-based thioether-triphenolate complexes for the cyclization reaction of CO₂ and propylene oxide, the Rieger group investigated the effect of varying the substituents of the aromatic ring on

the catalytic activity (**Figure 1.29**).¹⁴⁹ By reducing the reaction time to 1 h under reaction conditions of 140 °C, 20 bar CO₂, and 0.05 mol% TBAB, the order of reactivity was **1.62b** > **1.62a** > **1.62c** (TOF 2420 > 2300 > 1900 h⁻¹). This result confirms that less sterically hindered groups allow for more accessible coordination sites for the epoxide than the restricted access imposed by bulkier groups. The authors observed that increasing the cocatalyst molar ratio to 0.25 mol% increased the catalytic activity to a conversion of 95% and gave an impressive TOF of 3800 h⁻¹. Complex **1.62b** was also highly active for the transformation of a wide range of epoxides into cyclic carbonates. For example, glycerol carbonate was produced with 96% conversion and a TOF of 3830 h⁻¹, while the formation of cyclohexene carbonate proceeded with a conversion of 63%. Unfortunately, no solid-state structures have been reported for these complexes so their actual geometry and bond distances are not known.

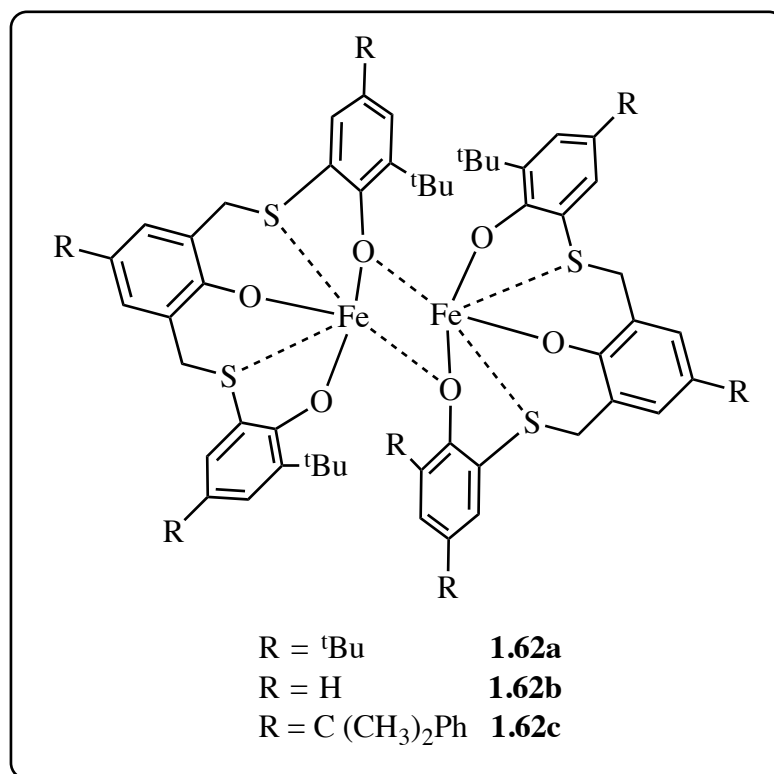


Figure 1.29. Dinuclear Fe(III) complexes bearing thioether-triphenolate ligands for synthesis of CPC from CO₂ and propylene oxide.¹⁴⁹

Pescarmona and coworkers used Fe(III) pyridylamino-bis(phenolate) complexes FeX[O₂NN'] (where X = Cl, Br) to promote the coupling reaction between cyclohexene oxide and CO₂ (**Figure 1.30**).¹⁵⁰ All catalytic tests were carried out under solvent-free conditions at 60 °C in *sc*CO₂ within 18 h. Complexes **1.63a** and **1.63b** acted as bifunctional catalysts to produce either cyclic carbonates (CHC) or polycyclohexene carbonates (PCHC), in which the halide nucleophile attacks the coordinated epoxide. Complex **1.63a** demonstrated higher activity and selectivity towards polycarbonates compared to **1.63b**, which favored the formation of cyclic carbonates. The high selectivity of **1.63a** was suspected to be due to the poor leaving ability of Cl⁻ compared to that of Br⁻; the high activity was attributed to the high degree of steric repulsion between

the larger-radius bromide and the incoming epoxide substrate when approaching the iron centre. The copolymer had a low M_n of 1418 g mol^{-1} and a very narrow dispersity of 1.2. The authors also explored the effect of different external organic halides (such as NBu_4Br and NBu_4Cl) as cocatalysts in the reaction. However, their presence did not improve the efficiency of the catalytic system. Reaction temperature also influenced the tendency to form either cyclic carbonate or polycyclohexene carbonate. It was observed that by increasing the temperature to $85 \text{ }^\circ\text{C}$ the selectivity of **1.63a** towards cyclic carbonates was enhanced with a conversion ranging from 60 to 99%. In addition, complete selectivity towards poly(vinylcyclohexene carbonate) was achieved using **1.63a** via the coupling reaction of 1,2-epoxy-4-vinylcyclohexane (VCHO). Polycarbonate produced using PPNCl as a cocatalyst had a higher content of carbonate linkages (>99%) compared to polycarbonate produced with NBu_4Cl , which contained approximately 86% carbonate linkages and 14% ether linkages.

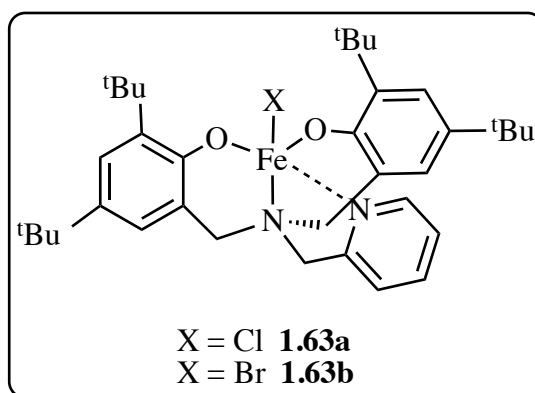


Figure 1.30. Structure of $\text{Fe(III)X}[\text{O}_2\text{NN}']$ complex used for the copolymerization of CO_2 and CHO/VCHO .¹⁵⁰

In summary, the results demonstrated that, in respect to other catalytic systems, the highest catalytic activity and selectivity in the cycloaddition of CO₂ with propylene oxide was observed with dinuclear Fe(III)-based thioether-triphenolate complexes in the presence of TBAB (**1.62a–1.62c**).¹⁴⁹ The presence of soft donors such as sulfur atoms in the ligand skeleton enhanced catalytic activity and strengthened coordination of the incoming epoxide. In addition, the results also showed that PPC was efficiently formed with the highest reported activity (TOF = 1004 h⁻¹) using Fe(IV) and (III) complexes based on corrole ligands in combination with PPNCI (**1.57a** and **1.58b**).¹⁴⁶

High activity and selectivity for copolymer formation at a very low catalyst loading and/or low CO₂ pressure have also been reported using cobalt complexes based salen ligands. Therefore, the following section will provide a brief overview of the chemistry and a literature review of its use in this field. Cobalt phenolate compounds are prepared and used in these reactions as part of this thesis research and are presented in Chapter 4 of this thesis.

1.4.1.3 A brief history of cobalt and its chemistry

Cobalt is a first-row transition metal with an atomic weight of 58.993 g mol⁻¹, a specific density of 8.9 g cm⁻³, a melting point of 1495 °C, and a boiling point of 2927 °C. In nature, cobalt does not exist as a free metal but is found in association with nickel and arsenic.¹⁵¹ Cobalt is extracted from different mineral ores. However, smaltite (CoAs₂), cobaltite (CoAsS), and linnaeite (Co₃S₄) are the most important commercial sources of cobalt.^{152,153} In 1735, the Swedish chemist Brandt separated cobalt as a metal (cobalt rex) while studying a dark blue ore obtained from a local copper mine. However, cobalt

originating from ores had been used for many centuries as a major coloring agent for glass and ceramics. For example, blue glazed pottery and Portland vases had been found in Egyptian tombs, and the British Museum confirms that blue cobalt was widely used in the past.^{152,154} The term “cobalt,” originating from the German name *Kobalt*, meaning “goblin” or “ill-natured fairy,” refers to ores which were not readily reduced by normal procedures and instead emitted toxic arsenical fumes.¹⁵⁴

Cobalt occurs in nature as one stable isotope, ⁵⁹Co, and 12 radioactive isotopes ranging in mass from 54 to 64 amu.¹⁵² The ground state electron configuration of cobalt is [Ar] 3d⁷4s², and its oxidation states range between -1 to +5, where the most common oxidation states are +2 and +3. The +3 oxidation state is unstable in simple compounds but can be stabilized by coordination to ligands or chelators, especially those having nitrogen donor atoms. The +2 oxidation state, which occurs in simple cobalt salts, has been widely used with a variety of ligands.^{151,153} Cobalt in low oxidation states (-1, 0, +1) is comparatively rare and is usually found in organometallic complexes containing C-donor ligands. However, cobalt in the +1 oxidation state exists in vitamin B12, which contains five-coordinate Co(I) in a square pyramidal N5 coordination environment. Higher oxidation states for cobalt (+4, +5) can be stabilized in the presence of fluorine or oxygen atoms, but these states are rare.^{151,153}

Cobalt(II) complexes typically have tetrahedral or octahedral geometries, while trigonal bipyramidal and square pyramidal coordination environments are less common. Numerous studies of Co(II) indicate that tetrahedral structures dominate in comparison to other transition metals. This is because of small differences in the crystal field stabilization energy between octahedral and tetrahedral structures for a high-spin d⁷

electron configuration.⁸ In addition, the polarizability of the ligand plays a critical role in determining the geometry of the complex. For example, ligands with soft donor atoms such as P, S, As, and aromatic N usually give tetrahedral complexes, while ligands with O and amine N donor atoms form octahedral complexes.¹⁵³

1.4.1.4 Cobalt catalysts for polycarbonate and cyclic carbonate formation

Salen-metal complexes are one of the most popular groups of homogenous catalysts for epoxide/CO₂ ring-opening copolymerizations as they offer several advantages including: easy synthetic preparation, the easy tuning of steric and electronic properties by modification of the ligand, and the use as catalysts in copolymerization reactions under mild temperatures and pressures.¹³³

The most active and selective metal salen complexes are Cr(III) and Co(III) species.⁸ However, in the case of propylene oxide/CO₂ copolymerization both selectivity and activity are increased for copolymer formation. In fact, the excellent selectivity for copolymer formation at a very low catalyst loading and/or low CO₂ pressure with a wide range of substrates, including epoxides bearing functional groups, gives salen Co(III) complexes numerous advantages over many other homogenous catalysts in the coupling of CO₂ and epoxides to produce polycarbonates.⁷

Coates *et al.*¹⁵⁵ reported the first application of salen cobalt(III) complexes with a nucleophilic counterion in the production of PPC. The reaction proceeded with 99% selectivity and a TOF of 17–81 h⁻¹ at ambient temperature in solvent free conditions (**Figure 1.31**). However, this catalyst system required high CO₂ pressure (up to 55 bar) because there was a complete loss of catalyst activity at low CO₂ pressure and/or elevated

temperature.

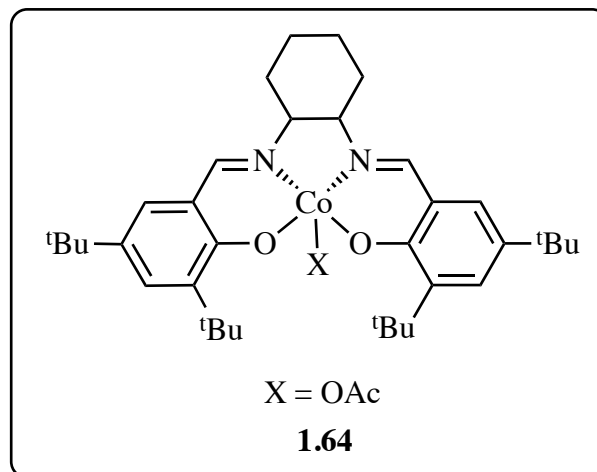


Figure 1.31. Cobalt salen complexes used by Coates *et al.*¹⁵⁵

In 2004, inspired by the novel work of Coates' group, Lu and coworkers designed a binary catalyst based on salen Co(III)X and a nucleophilic cocatalyst (**Figure 1.32**).¹⁵⁶ The presence of a tetrabutyl ammonium salt (Bu₄NY, Y = Br, Cl, OAc) as a cocatalyst plays an important role in enhancing the catalytic activity, even at low CO₂ pressures and/or elevated temperatures (80 °C). The product selectivity was affected by modifications in the axial group X of the salen Co(III)X and the anion of quaternary ammonium salts. For example, the selectivity towards PPC was significantly improved by using a cobalt complex (**1.65c**, X = 2,4-dinitrophenoxy, DNP) and quaternary ammonium salt, whose anion had low leaving ability (Y = Cl).

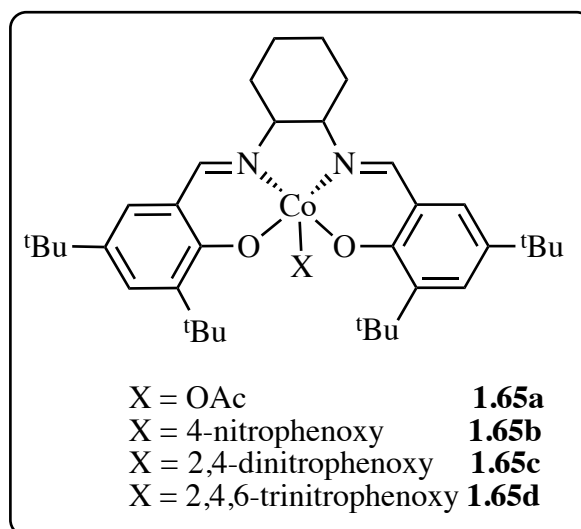


Figure 1.32. Cobalt salen complexes used by Lu and coworkers.¹⁵⁶

A two component system of salen cobalt(III)X complexes with a nucleophilic Lewis base as a cocatalyst was able to produce the corresponding cyclic carbonates from internal and terminal epoxides.¹⁵⁷ The initial study of the production of cyclic carbonates with a binary catalyst was reported in 2004. High production of cyclic carbonates was achieved using complex **1.66c**, which consists of chloride as an anion and two equivalents of 4-dimethyl-amino-pyridine (DMAP), at 100 °C under 22 bar CO₂ pressure (**Figure 1.33**). A subsequent study by the Berkessel group has investigated the activity of the same complex at atmospheric pressure for the production of CPC with substitution of the cocatalyst with bis(triphenylphosphine)iminium halide (PPNY, Y= F, Cl) and the halide group of the complex (**Figure 1.33**).¹⁵⁸ It was found that **1.66b** can produce CPC in 40% yield with 83% *ee* at -20 °C.

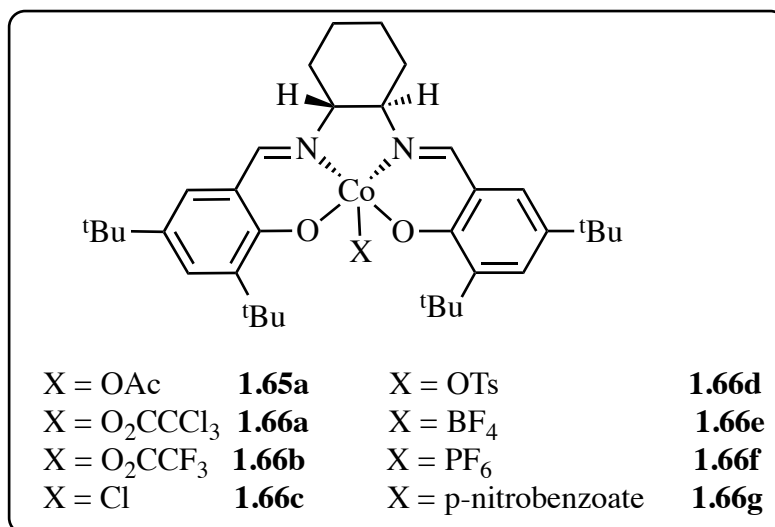


Figure 1.33. Salen cobalt(III)X used by Brandenburg's group.^{157, 158}

In 2007, a bifunctional catalyst system was introduced, where a Lewis acidic metal centre Co(III) and a nucleophilic cocatalyst were incorporated into a single complex. This merging led to a major increase in the catalytic activity (**Figure 1.34**).¹⁵⁹ Complex **1.67**, bearing quaternary ammonium salts at the 5-position of the phenyl ring in the salen ligand, showed excellent activity in the production of polycarbonates at high temperature (90 °C) and a high epoxide:catalyst ratio (25000:1). The TOF reached up to 3500 h⁻¹ with 90% selectivity toward PPC, and a high molecular weight copolymer of 53,000 g mol⁻¹ was produced. However, complex **1.68c**, with four quaternary ammonium cations and a methyl group at the 3-position of the phenyl ring, was more active. The TOF was greater than 20000 h⁻¹ at 1:25000 catalyst loading, 80 °C, and 20 bar, which is significantly greater than those achieved in binary systems.¹⁶⁰ The PPC produced had a molecular weight of 285,000 g mol⁻¹ with 99% selectivity. Interestingly, salen complexes **1.68a–1.68c** could be recovered after the copolymerization process by filtering the reaction mixture through a pad of silica gel without loss in activity.

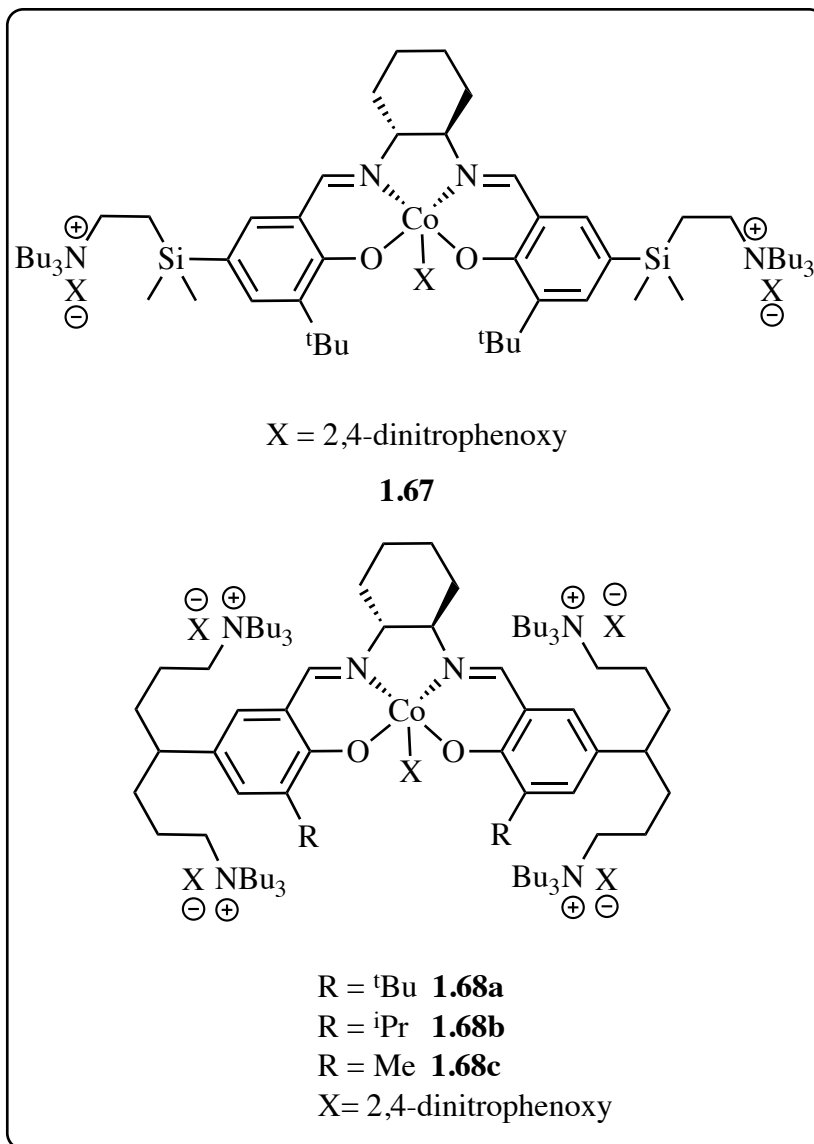


Figure 1.34. Cobalt salen complexes with cationic ‘arms’.¹⁵⁹

To date, complex **1.68c** is the most active bifunctional system in the production of PPC at high temperatures and low catalyst loading.¹⁶⁰ The substitution of a methyl group in the *ortho* position of the phenyl ring resulted in a higher activity than with substitution of a bulky *tert*-butyl group. The higher activity is attributed to the formation of an unusual

binding mode where the imino nitrogens do not coordinate to the metal centre in the salen pocket, but the X anions of the quaternary ammonium salt coordinate to the cobalt centre with a negative charge (**Figure 1.35**). As mentioned earlier, an important feature of these catalysts is that they can be separated from the polymer by filtration of the polymer solution through silica gel and then the catalysts can be recovered from the silica and they still retain their activity.

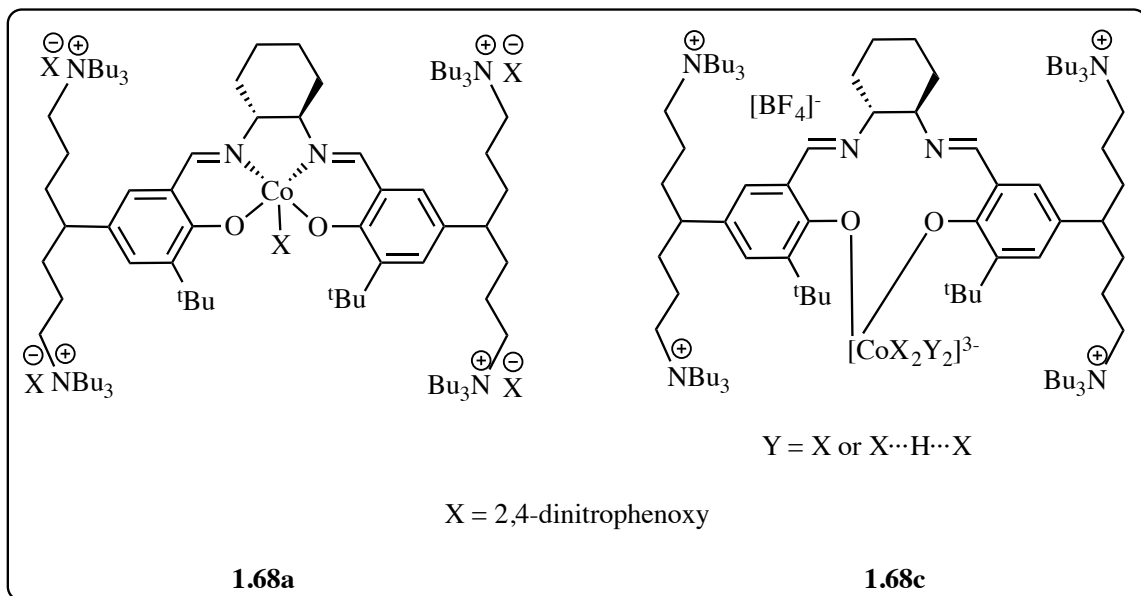


Figure 1.35. The highly active bifunctional catalysts designed by Lee and coworkers.¹⁶⁰

The high activity of these catalysts for the production of polycarbonates was attributed to several factors, including low catalyst loading, suppression of cyclic carbonate formation, and stabilization of the active Co(III) metal centre.¹²³

The improved activity of single component catalysts has led to the design of many successful catalysts. In 2009, a highly active Co(III)X complex bearing a bulky amine or quaternary ammonium salt at the 3-position of one phenyl ring was reported for the

copolymerization of CO₂ and propylene oxide to produce PPC (**Figure 1.36**).¹⁶¹ The nucleophilicity of the axial anion of cobalt(III) complexes has been shown to have a significant effect on copolymerization reactions. Complex **1.69a**, with acetate as the coordinating anion, produced the copolymer at ambient temperature just under 1 bar CO₂, with a TOF of up to 265 h⁻¹ and greater than 99% selectivity. Moreover, the catalyst system could operate at temperatures as high as 100 °C and reached a TOF of 10880 h⁻¹ under a pressure of 25 bar. However, complex **1.70**, bearing a quaternary ammonium salt, was less active in the production of PPC, with a TOF of 3900 h⁻¹ and 95% selectivity at 90 °C. In addition, both systems were shown to be highly effective for the production of polycyclohexene carbonate, with TOFs of 3079 h⁻¹ and 6105 h⁻¹ at 90 °C and 120 °C, respectively.

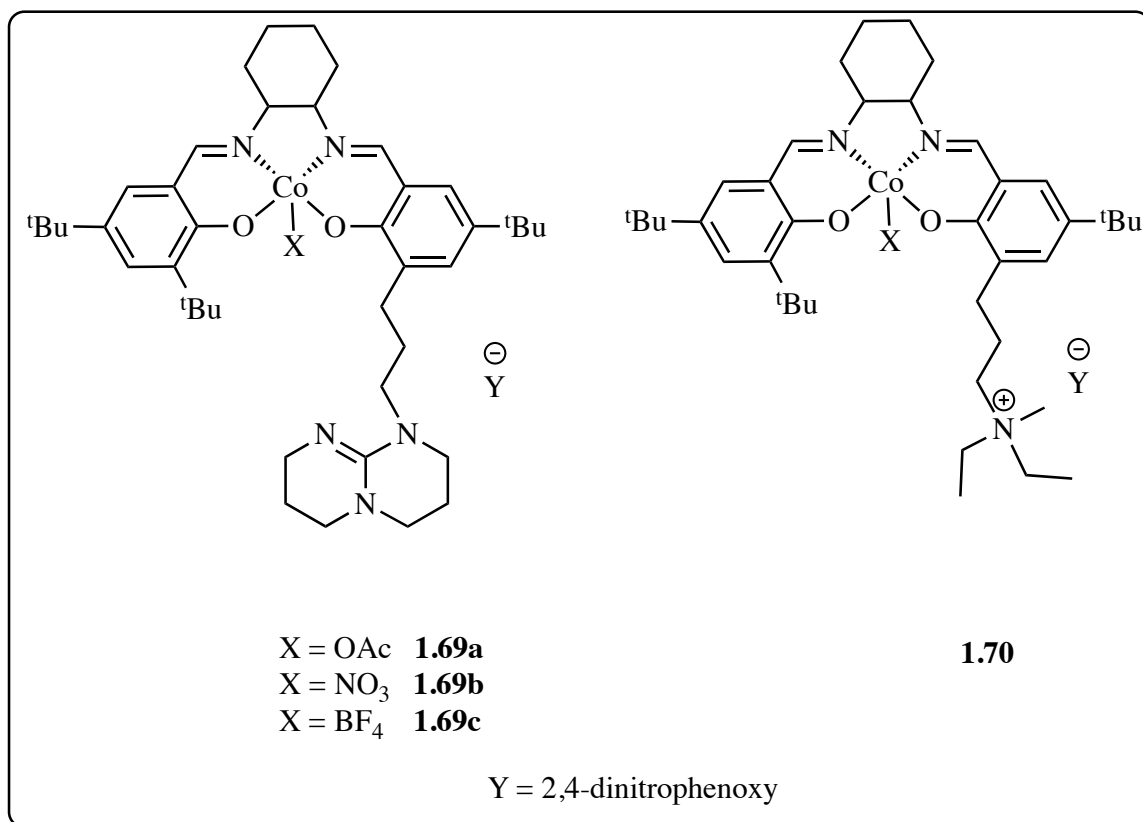


Figure 1.36. Asymmetric bifunctional (salen)CoX complexes used by Lu *et al.*¹⁶¹

Bifunctional chiral catalysts of salen Co(III)X and quaternary ammonium or phosphonium salts showed excellent activity and moderate enantioselectivity depending on the identity of the axial anion in the Co(III) complexes and the anion of the onium salts (**Figure 1.37**).¹⁶² For example, complex **1.71** ($X = \text{OAc}$ and $Z = \text{Cl}^-$) catalyzed the cycloaddition of carbon dioxide and propylene oxide to yield chiral cyclic carbonates in reasonable to high yields. The reaction rate was enhanced with catalyst **1.72** when the quaternary onium group was in the 3-position. The catalysts could also be reused five times without significant reductions in yield and enantioselectivity.

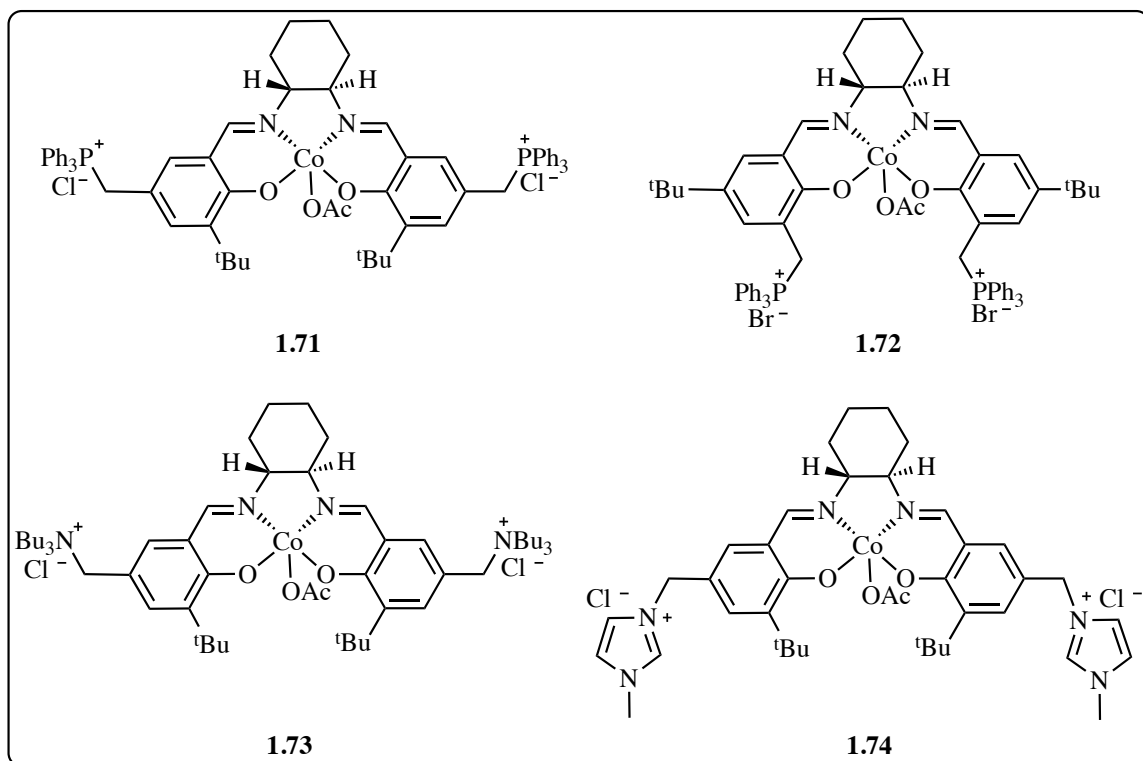


Figure 1.37. Bifunctional chiral catalysts used by Jing *et al.*¹⁶²

Niu *et al.*¹⁶³ designed tetradentate Schiff-base cobalt complexes with two Lewis base units as phenolate para substituents in order to stabilize the active salen Co(III) complex against decomposition to salen Co(II) (**1.75**, **Figure 1.38**). The catalyst efficiently copolymerized CO₂ and PO at 15 bar CO₂ and 25 °C in 1,2-dimethoxyethane (DME). A TOF of 116 h⁻¹ was reached after 10 h with PPC selectivity >99%, $M_n = 33\ 200\ \text{g mol}^{-1}$, and $D = 1.12$. However, the polymer yield was low (58%) and a small amount of CPC byproduct was obtained. The catalyst exhibited high thermal stability at 60 °C, with higher activity (TOF = 673 h⁻¹) after 1 h, suppression of CPC formation, and $M_n = 12,500\ \text{g mol}^{-1}$. Moreover, the high selectivity of PPC vs PC at 25 °C was maintained with increasing reaction time up to 50 h, and the molecular weight reached 110,200 g mol⁻¹ with no CPC formation.

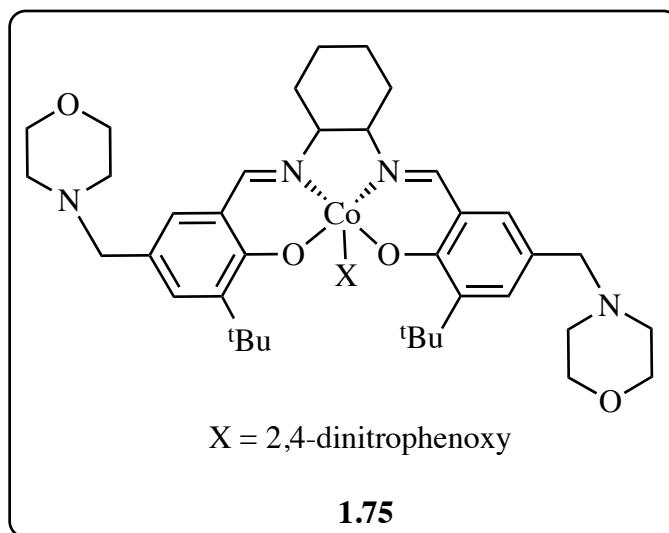


Figure 1.38. Tetradentate Schiff base cobalt complex designed by Niu *et al.*¹⁶³

In 2011, a series of cobalt Schiff base complexes were tested in the coupling reaction of PO/CO₂ in conjunction with PPNCI as cocatalyst (**Figure 1.39**).¹⁶⁴ The selectivity towards CPC or PPC formation was controlled by variation of the X group, the molar ratio of the catalyst to cocatalyst, the temperature, and the CO₂ pressure. High activity (TOF = 290 h⁻¹) and selectivity towards the copolymer (98%) were obtained with complex **1.76a** (X = OOCF₃). The copolymer contained 95% head-to-tail linkages and had a molecular weight of 72,500 g mol⁻¹. The results also showed that increased reaction time led to increased selectivity for polymer formation because the production of CPC occurred at an early stage of the reaction.

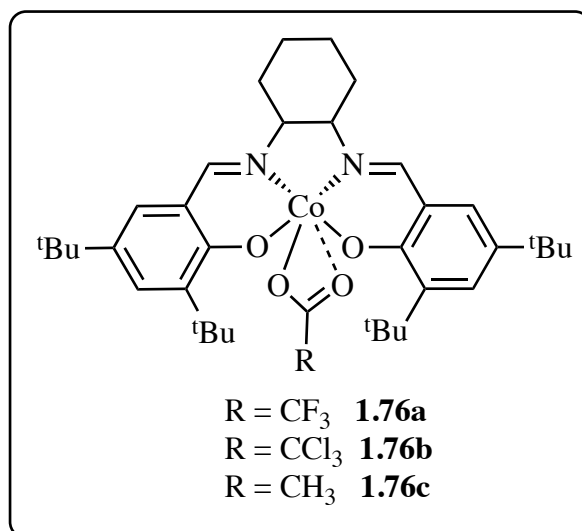


Figure 1.39. Cobalt/Schiff base complexes used in the coupling of PO/CO₂.¹⁶⁴

The first successful attempt to synthesize poly(indene carbonate) using the traditional binary (salen)Co(III)X/cocatalyst system (**1.65c**) was accomplished by Darensbourg and coworkers (**Figure 1.40**).¹⁶⁵ Selectivity towards polycarbonate only occurred at low temperature (0 °C) in dichloromethane (CH₂Cl₂), while indene carbonate was produced at higher temperatures, such as 25 °C and 60 °C. The polymers have molecular weights of up to 7100 g mol⁻¹, with the highest reported glass transition temperatures for polycarbonates (up to 134 °C) resulting from CO₂/epoxide coupling. Polymerizations were well controlled, with $D \leq 1.3$, low TOFs (1.7 h⁻¹), and 59% selectivity towards poly(indene carbonate) using PPNY (Y = 2,4-dinitrophenoxide) as a cocatalyst.

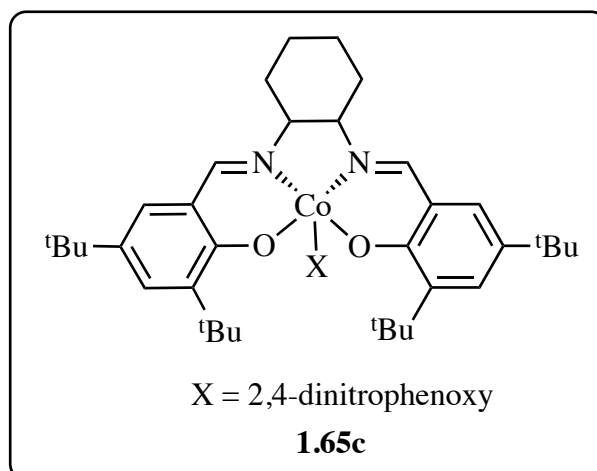


Figure 1.40. (Salen)Co(III)-2,4-dinitrophenoxide catalyst for the synthesis of poly-(indene carbonate).¹⁶⁵

A significant development occurred in 2012 when the Williams group reported a series of dinuclear cobalt(II,II), cobalt(II,III), and trinuclear cobalt (II,II,II) complexes coordinated by a novel “reduced Robson’s type” macrocyclic ligand (**Figure 1.41**).¹⁶⁶ The main advantage was their high activity for the copolymerization of CO₂ and cyclohexene oxide at only 1 atm CO₂. At 100 °C, complex **1.77** and **1.79**, with TOF = 200 and 250 h⁻¹, respectively, are more effective than **1.78**. The higher activity of these complexes at low pressure was attributed to the macrocyclic ligand environment and dinuclear structure. In contrast, the low activity of trinuclear cobalt complex **1.78** was attributed to the inactivity of the external metal towards the coupling of CHO/CO₂.

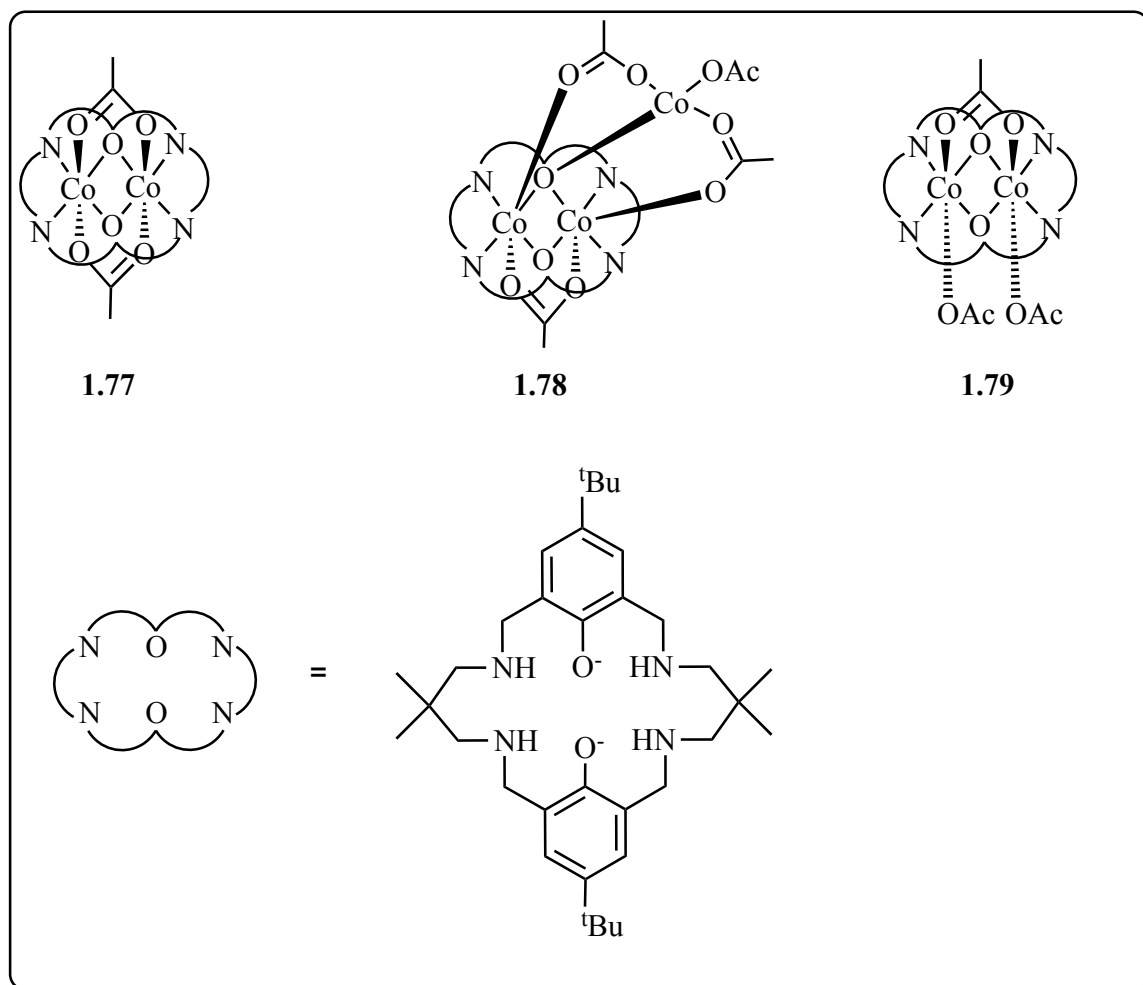


Figure 1.41. Cobalt acetate complexes of reduced Robson ligand.¹⁶⁶

Salen Co(III) complexes have been used for the ring opening of *meso*-CHO with CO₂ in the presence of PPNC1 (**Figure 1.42**).¹⁶⁷ The introduction of a chiral agent such as (*S*)-PO or (*S*)-2-methyltetrahydrofuran significantly improved the enantioselectivity. The PPC obtained was highly isotactic and was semi-crystalline, with a melting point of 216 °C and a decomposition temperature of 310 °C. Catalyst **1.80d**, bearing one bulky adamantyl group and one ^tBu group on the aromatic rings, was a more effective enantioselective catalyst in the presence of toluene at RT. Furthermore, when the reaction

temperature was decreased from 25 to -25 °C, the reaction rate decreased, but no cyclic carbonate byproduct was formed, and the polymers had >99% carbonate linkages.

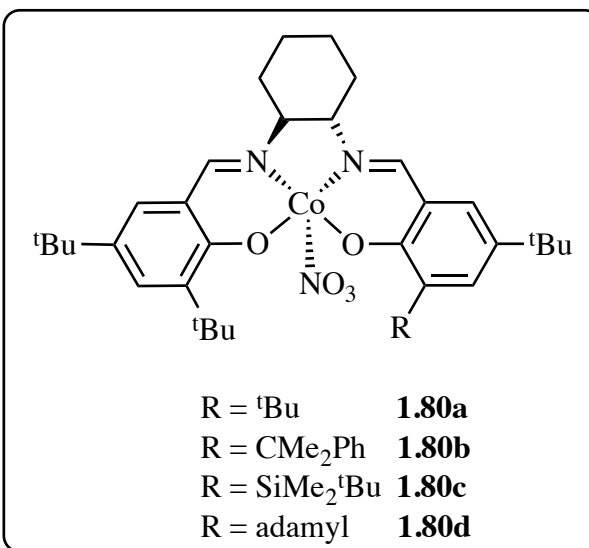


Figure 1.42. Salen cobalt(III)X used by Lu's group.¹⁶⁷

The Kerton group synthesized a series of cobalt(II)/(III) complexes based on tripodal amino-bis(phenolate) ligands (**Figure 1.43**).¹⁶⁸ The complexes showed promising activities for the cycloaddition of CO₂ with propylene oxide to form CPC at room temperature under solvent-free conditions. The oxidation state of the metal was found to play an essential role in the catalytic performance. For example, in the absence of cocatalyst, cobalt(II) complexes were unable to produce PPC, whereas cobalt(III) complexes catalyzed CO₂ and propylene oxide addition without a cocatalyst. Various cocatalysts were used to enhance the reactivity; however, tetrabutyl ammonium bromide (TBAB) was found to be the superior cocatalyst.

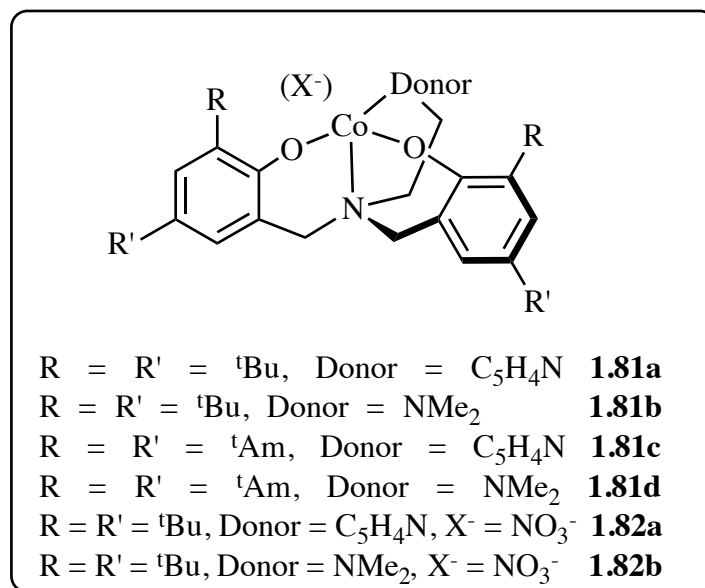


Figure 1.43. Schematic structure of Co(II) and Co(III) complexes used by Kerton and coworkers.¹⁶⁸

A multichiral cobalt(III) complex has shown high activity towards the asymmetric coupling reaction of CO_2 and racemic terminal epoxides in the presence of an ammonium salt (**Figure 1.44**).¹⁶⁹ The enantioselectivity for the cyclic carbonate product reached up to 97.1% *ee*. The product selectivity and enantioselectivity were affected by the variation of cocatalyst and its relative loading. For example, a nucleophilic cocatalyst with strong leaving ability and/or excess cocatalyst loading selectively produced cyclic carbonate. In addition, the use of an ammonium salt with an anion of poor leaving ability and a bulky cation improved the enantioselectivity. For example, an organic ammonium salt with a 2,4-dinitrophenoxide anion gave the best enantioselectivity, while an iodide anion, which has better leaving ability, gave the lowest.

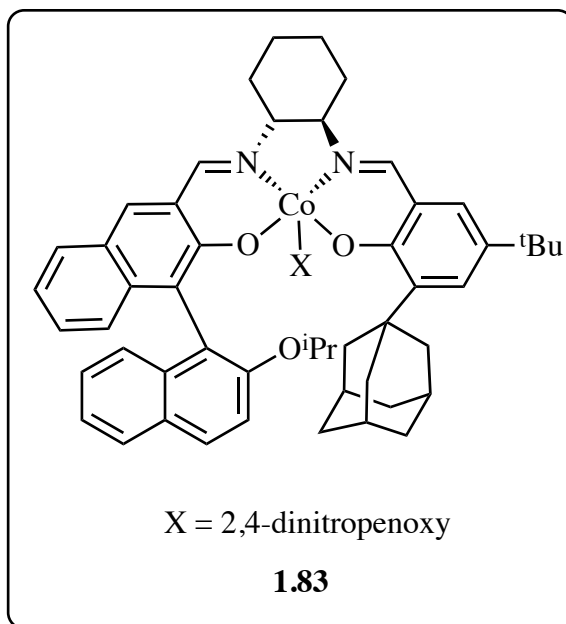


Figure 1.44. Multichiral salen cobalt(III) complex for coupling reaction of CO₂ and *racemic* terminal epoxides.¹⁶⁹

In an ongoing effort to improve the activity of cobalt catalysts for the synthesis of poly(indene carbonate), Darensbourg and coworkers investigated bifunctional cobalt(III) catalysts with appended quaternary ammonium salts for the polymerization of CO₂ and indene oxide (**1.70** and **1.84**, **Figure 1.45**).¹⁷⁰ Compared to the previous traditional catalyst/cocatalyst system (**1.65c**), these catalysts displayed higher activity and selectivity for the formation of poly(indene carbonate) using PPNY (Y = 2,4-dinitrophenoxide) as a cocatalyst at 0 °C in dichloromethane (CH₂Cl₂). The catalysts were twice as active as the earlier catalyst/cocatalyst system, with TOF values of 4.7 and 4.0 h⁻¹ for **1.70** and **1.84**, respectively. Moreover, the complexes could also produce polycarbonates at 25 °C while maintaining good reaction control (*D* < 1.2). Complex **1.70** and **1.84** demonstrated >99% and 93% selectivity, respectively. Changing the reaction solvent from dichloromethane to toluene using **1.84** increased activity and selectivity, providing polymers with *M_n* values

complexes having less sterically hindered groups (**1.85a**) displayed the best reactivity (94.9% yield) and PPC selectivity (>99%) under 15 bar CO₂ at 25 °C for 72 h. Substitution at the *meso*-position of the porphyrin with an electron withdrawing substituent (**1.85c**) resulted exclusively in cyclic carbonate product. The temperature also has a significant role in determining the selectivity. For example, increasing the temperature from 0 to 25 °C increases selectivity towards PPC. However, a further increase in temperature caused a decrease in PPC selectivity and polymer molecular weight, and also resulted in a broader molecular weight distribution.

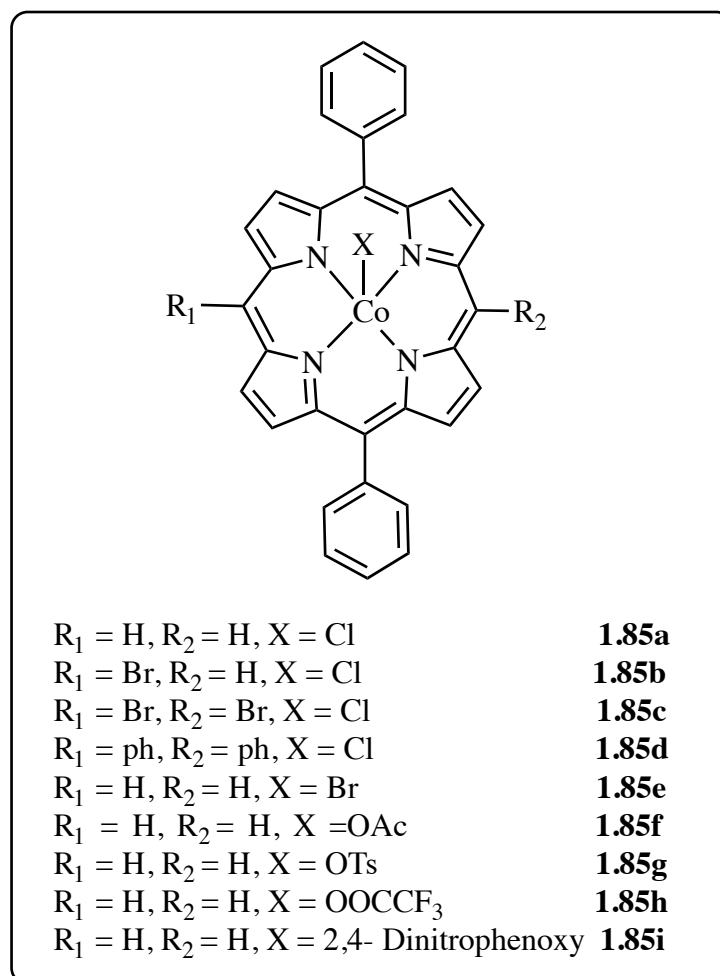


Figure 1.46. Highly active porphyrin cobalt complexes for CO_2/PO copolymerization.¹⁷¹

Recently, Darensbourg and coworkers introduced a binary catalyst system composed of a Co(III)–salen complex (**1.65c**) in conjunction with PPNY (Y = 2,4-dinitrophenoxide) for the coupling of 1,3-cyclohexadiene oxide (CHDO) or 1,4-CHDO and CO_2 at 40 °C under solvent-free conditions (**Figure 1.32**).¹⁷² Complex **1.65c** was more active in catalyzing the reaction of CO_2 with 1,3-CHDO compared to 1,4-CHDO, with TOFs of 30 to 70 h^{-1} . The lower activity of 1,4-CHDO was attributed to the symmetrical nature of the double bond. By increasing the reaction times, TOFs decreased

from 66.5 to 33.5 h⁻¹, but higher conversions and molecular weights were observed. At room temperature, similar activity was obtained, but the molecular weight of the copolymer increased ($M_n = 24,600 \text{ g mol}^{-1}$).

Quaternary onium-modulated salenCoXY (X = Cl, Br, NO₃; Y = phenoxy, benzene-1,4-bisoxo, benzene-1,3,5-trisoxo) catalysts have been found to be capable of producing both PPC and CPC at 20 bar CO₂ and 25 °C (**Figure 1.47**).¹⁷³ The selectivity towards the polymer was significantly affected by the axial anion X, the counter anion Y, and the quaternary onium group. The investigators found that catalysts with quaternary phosphonium groups are better for polymerization than those with quaternary ammonium groups. Therefore, among all complexes explored, complex (**1.86Ca**) proved to be the best initiator, affording a copolymer with 90% selectivity, an M_n of 10872 g mol⁻¹, and a dispersity of 1.26. The authors also studied the effect of different axial phenoxy anions on the copolymerization. For example, complex **1.89Ec** demonstrated excellent polymer selectivity (94%), while **1.88Ec** gave good polymer selectivity (85%). However, only cyclic carbonate was observed with **1.87Ec**. The detailed kinetic data under various temperatures showed that PPC was more readily produced than CPC because the activation energy for the polymerization was only 18.0 kJ mol⁻¹, compared to 67.7 kJ mol⁻¹ to produce CPC. However, these values are low compared to the activation energies calculated by Darensbourg *et al.* for chromium(III) salen complex in which 67.6 kJ mol⁻¹ and 100.5 kJ mol⁻¹ were observed for PPC and CPC, respectively.¹⁷⁴

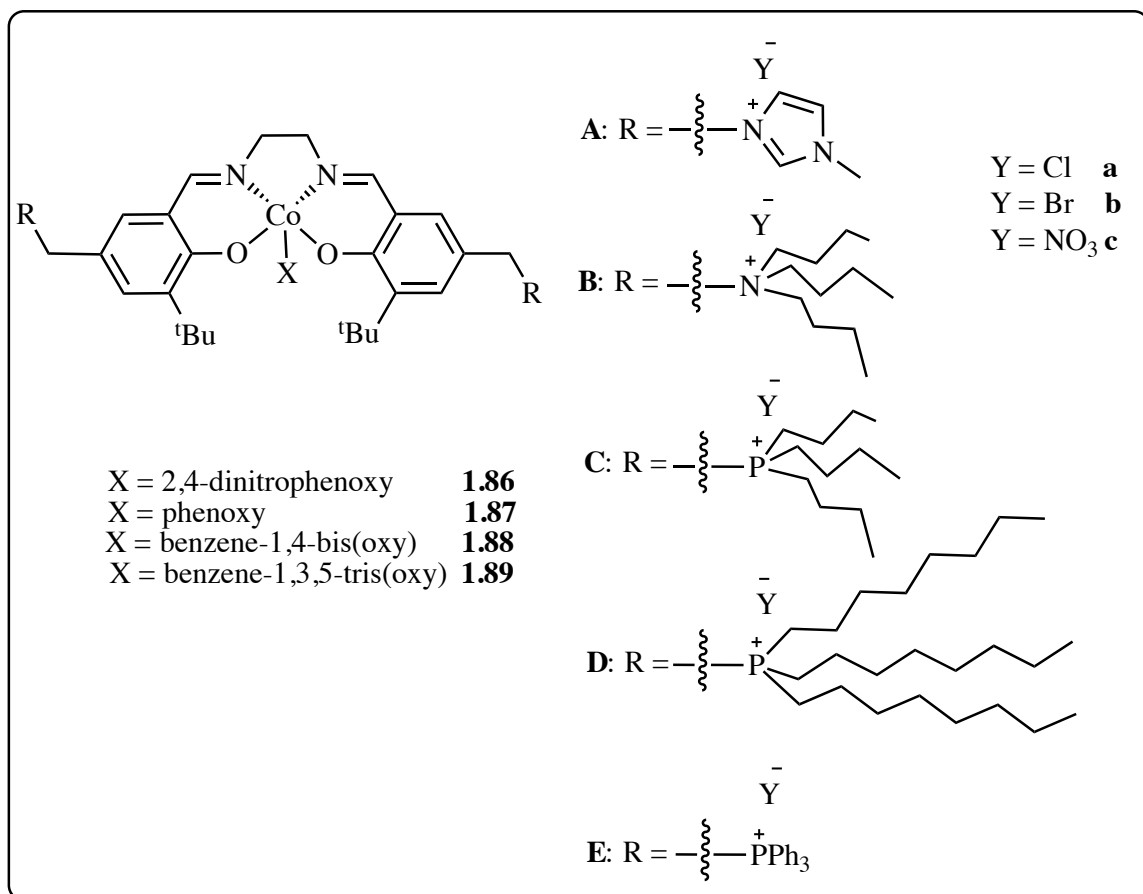


Figure 1.47. Configurations of quaternary onium-modified catalysts.¹⁷³

In summary, the best result (to produce PPC) was achieved using the bifunctional catalyst system Co(III) containing a methyl group at the *ortho* position of the phenyl ring (**1.86c**).¹⁶⁰ The unusual coordination geometry around the metal centre was responsible for the observed high activity and the catalyst could be recycled without loss in activity. The highest production of CPC was obtained using Co(II) complexes bearing amino-bis(phenolate) ligands which were able to furnish CPC with TOF = 52.7 h⁻¹ in the presence of TBAB (**1.81a–1.81d**).¹⁶⁸ In contrast, the Co(III) analogues (**1.82a–1.82b**) showed low activity for CPC production without the addition of cocatalyst (TOF = 4 h⁻¹). The addition of cocatalyst increased the activity to 22 h⁻¹.

1.5 Objectives

The principal goal of this research is the preparation and characterization of novel metal catalysts, and study of their reactivity in polymerization processes and reactions of CO₂. Specifically, the catalysts investigated in this study are built on the structure of tetradentate amino-bis(phenolate) ligands. The design of these complexes benefit from the ease of isolation of tetradentate amino-bisphenol protio-ligands prepared using a modified Mannich condensation reaction which allows for control over the electronic and steric features of the complex by allowing variation of substituents on the phenolate groups or the amine unit of the ligand. In this thesis, data on the use of lithium, sodium, iron and cobalt complexes supported by tetradentate amino-bis(phenolate) ligands in the ring-opening polymerization of *rac*-lactide as well as the reactions of CO₂ with epoxides is presented and discussed. These data lend further support to the existing literature which demonstrates the value of metal catalysts in polymerization processes and transformations of CO₂.

Chapter 2 describes the synthesis and characterization of a series of amino-bis(phenolate) lithium and sodium complexes. The catalytic activity of these complexes towards the ROP of *rac*-lactide in solution and in bulk conditions in the presence and absence of benzyl alcohol is described. Factors such as the type of metal centre, solvents, temperature and time proved to be important in controlling the polymerization. Mechanistic studies in the presence and absence of benzyl alcohol were also investigated and are described in Chapter 2. Excellent results were obtained for the reactions performed in the solution phase using sodium complexes and these data are compared to their lithium analogues.

The objective in Chapter 3 is the synthesis and characterization of iron(III)

containing amino-bis(phenolate) ligands and the study of these complexes as homogeneous catalysts for CO₂/epoxide coupling reactions, especially propylene oxide. Several parameters are shown to play an important role in the catalytic activity such as the substituents in the phenol ring and reaction conditions such as temperature, pressure, and reaction time. Besides this, kinetic studies of the formation of CPC was investigated using *in situ* infrared spectroscopy using iron(III) complexes. The best results for the formation of CPC were observed in the presence of electron-withdrawing substituents on the phenolate groups leading to more active catalysts. It is presumed that this is due to the metal centre being more Lewis acidic (*i.e.*, the epoxide is more easily activated). Reactivity towards seven epoxide substrates was studied, with propylene oxide being examined extensively in terms of reaction condition optimization and kinetics. Both electronic and steric properties of the epoxide substrate influence their conversion via catalysis, *e.g.*, activated epoxides bearing electron-withdrawing groups are more readily converted (a maximum TOF was found for glycidol and epichlorohydrin under our standardized conditions, 142 h⁻¹).

Chapter 4 introduces the synthesis and characterization of dinuclear Co(II) and monometallic Co(III) complexes containing amino-bis(phenolate) ligands. The catalytic activity of these cobalt complexes toward the CO₂/epoxide reactions is described. The influence of the ligand substituents and reaction conditions were also studied. The results demonstrated that dinuclear Co(II) complexes were more active than the monometallic Co(III) and afforded CPC with higher conversion level.

1.6 References

1. C. M. Thomas, *Chem. Soc. Rev.*, **2010**, 39, 165-173.
2. N. R. Nair, R. P. John and K. Madhavan Nampoothiri, *Bioresour. technol.*, **2010**, 101, 8493-8501.
3. A. Arbaoui and C. Redshaw, *Polym. Chem.*, **2010**, 1, 801-826.
4. M. A. Hillmyer and C. Williams, *Polym. Rev.*, **2008**, 48, 1-10.
5. R. H. Platel, L. M. Hodgson and C. K. Williams, *Polym. Rev.*, **2008**, 48, 11-63.
6. M. J. L. Tschan, E. Brule, P. Haquette and C. M. Thomas, *Polym. Chem.*, **2012**, 3, 836-851.
7. X.-B. Lu and D. J. Darensbourg, *Chem. Soc. Rev.*, **2012**, 41, 1462-1484.
8. M. R. Kember, A. Buchard and C. K. Williams, *Chem. Commun.*, **2011**, 47, 141-163.
9. M. M. Reddy, S. Vivekanandhan, M. Misra, S. K. Bhatia and A. K. Mohanty, *Prog. Polym. Sci.*, **2013**, 38, 1653-1689.
10. M. Singhvi and D. Gokhale, *RSC Adv.*, **2013**, 3, 13558-13568.
11. B. Gupta, N. Revagade and J. Hilborn, *Prog. Polym. Sci.*, **2007**, 32, 455-482.
12. C. K. Williams, *Chem. Soc. Rev.*, **2007**, 36, 1573-1580.
13. S. Slomkowski, S. Penczek and A. Duda, *Polym. Adv. Technol.*, **2014**, 25, 436-447.
14. M. J. Stanford and A. P. Dove, *Chem. Soc. Rev.*, **2010**, 39, 486-494.
15. A.-C. Albertsson and I. K. Varma, *Biomacromolecules*, **2003**, 4, 1466-1486.
16. J.-W. Rhim, H.-M. Park and C.-S. Ha, *Prog. Polym. Sci.*, **2013**, 38, 1629-1652.
17. I. Armentano, N. Bitinis, E. Fortunati, S. Mattioli, N. Rescignano, R. Verdejo, M. A. Lopez-Manchado and J. M. Kenny, *Prog. Polym. Sci.*, **2013**, 38, 1720-1747.
18. R. A. Auras, B. Harte, S. Selke and R. Hernandez, *J. Plast. Film. Sheet.*, **2003**, 19, 123-135.
19. Y. Ohya, A. Takahashi and K. Nagahama, in *Polym. Nanomed.*, eds. S. Kunugi and T. Yamaoka, Springer Berlin Heidelberg, **2012**, vol. 247, ch. 160, pp. 65-114.
20. K. Hamad, M. Kaseem, H. W. Yang, F. Deri and Y. G. Ko, *Express Polym. Lett.*, **2015**, 9, 435-455.
21. A. K. Sutar, T. Maharana, S. Dutta, C.-T. Chen and C.-C. Lin, *Chem. Soc. Rev.*, **2010**, 39, 1724-1746.
22. R. E. Drumright, P. R. Gruber and D. E. Henton, *Adv. Mater.*, **2000**, 12, 1841-1846.
23. C. A. Wheaton, P. G. Hayes and B. J. Ireland, *Dalton Trans.*, **2009**, 4832-4846.
24. O. Dechy-Cabaret, B. Martin-Vaca and D. Bourissou, *Chem. Rev.*, **2004**, 104, 6147-6176.
25. N. Ajellal, J.-F. Carpentier, C. Guillaume, S. M. Guillaume, M. Helou, V. Poirier, Y. Sarazin and A. Trifonov, *Dalton Trans.*, **2010**, 39, 8363-8376.
26. C. E. Willans, M. A. Sinenkov, G. K. Fukin, K. Sheridan, J. M. Lynam, A. A. Trifonov and F. M. Kerton, *Dalton Trans.*, **2008**, 3592-3598.
27. M. A. Hillmyer, W. B. Tolman and B. J. O'Keefe, *J. Chem. Soc., Dalton Trans.*, **2001**, 2215-2224.
28. E. E. Delbridge and M. H. Chisholm, *New J. Chem.*, **2003**, 27, 1177-1183.

29. H. R. Kricheldorf, I. Kreiser-Saunders and A. Stricker, *Macromolecules*, **2000**, 33, 702-709.
30. J. Coudane, R. Engel, M. Vert and G. Schwach, *Polym. Int.*, **1998**, 46, 177-182.
31. R. Jerome, P. Teyssie, P. Dubois, R. Jérôme and P. Teyssié, *Makromol. Chem-M Symp.*, **1991**, 42-3, 103-116.
32. A. Kowalski, A. Duda and S. Penczek, *Macromolecules*, **2000**, 33, 7359-7370.
33. A. Kowalski, A. Duda and S. Penczek, *Macromolecules*, **2000**, 33, 689-695.
34. H. Du, J. Feijen and P. J. Dijkstra, *Polym. Chem.*, **2011**, 2, 520-527.
35. F. Schue, G. A. George and J. H. Khan, *Polym. Int.*, **2009**, 58, 296-301.
36. M. Cheng, A. B. Attygalle, E. B. Lobkovsky and G. W. Coates, *J. Am. Chem. Soc.*, **1999**, 121, 11583-11584.
37. M. H. Chisholm, N. W. Eilerts, J. C. Huffman, S. S. Iyer, M. Pacold and K. Phomphrai, *J. Am. Chem. Soc.*, **2000**, 122, 11845-11854.
38. K. Devaine-Pressing, J. H. Lehr, M. E. Pratt, L. N. Dawe, A. A. Sarjeant and C. M. Kozak, *Dalton Trans.*, **2015**, 44, 12365-12375.
39. Y. Sarazin, V. Poirier, T. Roisnel and J.-F. Carpentier, *Eur. J. Inorg. Chem.*, **2010**, 2010, 3423-3428.
40. W. Yi and H. Ma, *Dalton Trans.*, **2014**, 43, 5200-5210.
41. J. P. Davin, J.-C. Buffet, T. P. Spaniol and J. Okuda, *Dalton Trans.*, **2012**, 41, 12612-12618.
42. H.-Y. Chen, L. Mialon, K. A. Abboud and S. A. Miller, *Organometallics*, **2012**, 31, 5252-5261.
43. D. J. Darensbourg, W. Choi, O. Karroonnirun and N. Bhuvanesh, *Macromolecules*, **2008**, 41, 3493-3502.
44. B. Liu, T. Roisnel, J.-P. Guégan, J.-F. Carpentier and Y. Sarazin, *Chem. Eur. J.*, **2012**, 18, 6289-6301.
45. B. Gao, R. Duan, X. Pang, X. Li, Z. Qu, Z. Tang, X. Zhuang and X. Chen, *Organometallics*, **2013**, 32, 5435-5444.
46. Z. Qu, R. Duan, X. Pang, B. Gao, X. Li, Z. Tang, X. Wang and X. Chen, *J. Polym. Sci., Part A: Polym. Chem.*, **2014**, 52, 1344-1352.
47. N. Ikpo, S. M. Barbon, M. W. Drover, L. N. Dawe and F. M. Kerton, *Organometallics*, **2012**, 31, 8145-8158.
48. X. Pang, R. Duan, X. Li, Z. Sun, H. Zhang, X. Wang and X. Chen, *Polym. Chem.*, **2014**, 5, 6857-6864.
49. D. J. H. Emslie and W. Piers, *Coord. Chem. Rev.*, **2002**, 233, 131-155.
50. R. Sillanpää, A. Lehtonen, O. Wichmann and R. Sillanpää, *Coord. Chem. Rev.*, **2012**, 256, 371-392.
51. G. Peng, R. Singh, J. T. Spence, J. H. Enemark, C. J. Hinshaw, M. Bruck, J. Kristofzski, S. L. Merbs, R. B. Ortega and P. A. Wexler, *Inorg. Chem.*, **1989**, 28, 4483-4491.
52. E. L. M. Glennie, W. J. Burke and C. Weatherbee, *J. Org. Chem.*, **1964**, 29, 909-912.
53. M. Versano, I. Goldberg, M. Kol, E. Y. Tshuva, H. Weitman and Z. Goldschmidt, *Inorg. Chem. Commun.*, **1999**, 2, 371-373.
54. I. Goldberg, M. Kol, Z. Goldschmidt and E. Y. Tshuva, *Organometallics*, **2001**,

- 20, 3017-3028.
55. S. Groysman, E. Sergeeva, I. Goldberg and M. Kol, *Inorg. Chem.*, **2005**, 44, 8188-8190.
 56. L. J. Corbett, S. M. Butt, G. Madhurambal, K. L. Collins and F. M. Kerton, *Green Chem. Lett. Rev. J.*, **2007**, 1, 31-35.
 57. S. Holloway, A. Power, R. G. Soper, K. Sheridan, F. M. Kerton, J. M. Lynam, A. C. Whitwood and C. E. Willans, *Can. J. Chem.*, **2008**, 86, 435-443.
 58. D. T. Dugah, B. W. Skelton and E. E. Delbridge, *Dalton Trans.*, **2009**, 1436-1445.
 59. K. Nie, X. Gu, Y. Yao, Y. Zhang and Q. Shen, *Dalton Trans.*, **2010**, 39, 6832-6840.
 60. T. Feng, F. Song, Y. Zhang, H. Sun, K. Nie, D. Yuan, Y. Yao and Q. Shen, *Sci. China Chem.*, **2014**, 57, 1106-1116.
 61. E. Y. Tshuva, I. Goldberg, M. Kol, H. Weitman and Z. Goldschmidt, *Chem. Commun.*, **2000**, 379-380.
 62. E. Y. Tshuva, I. Goldberg, M. Kol and Z. Goldschmidt, *Organometallics*, **2001**, 20, 3017-3028.
 63. E. Y. Tshuva, S. Groysman, I. Goldberg, M. Kol and Z. Goldschmidt, *Organometallics*, **2002**, 21, 662-670.
 64. S. Groysman, E. Y. Tshuva, I. Goldberg, M. Kol, Z. Goldschmidt and M. Shuster, *Organometallics*, **2004**, 23, 5291-5299.
 65. S. E. Reybuck, A. L. Lincoln, S. Ma and R. M. Waymouth, *Macromolecules*, **2005**, 38, 2552-2558.
 66. C. Lorber, F. Wolff, R. Choukroun and L. Vendier, *Eur. J. Inorg. Chem.*, **2005**, 2005, 2850-2859.
 67. C. Lorber, E. Despagnet-Ayoub, L. Vendier, A. Arbaoui and C. Redshaw, *Catal. Sci. Technol.*, **2011**, 1, 489-494.
 68. G. Gunn, *Critical Metals Handbook*, John Wiley & Sons, Oxford, **2014**, ch. 10, pp. 230-260.
 69. R. M. Izatt, J. S. Bradshaw, N. K. Dalley and U. Olsher, *Chem. Rev.*, **1991**, 91, 137-164.
 70. Sodium (**2016**). [Online]. In *The Columbia Encyclopedia*. New York, NY: Columbia University Press. Available from: <http://qe2a-proxy.mun.ca/login?url=http://search.credoreference.com/content/entry/columency/sodium/0> [Accessed 16 May 2016].
 71. J. E. Kasperczyk, *Macromolecules*, **1995**, 28, 3937-3939.
 72. M. Bero, P. Dobrzyński and J. Kasperczyk, *J. Polym. Sci., Part A: Polym. Chem.*, **1999**, 37, 4038-4042.
 73. I. Kreiseraunders, *Makromol. Chem.*, **1990**, 191, 1057-1066.
 74. W. Xie, D. Chen, X. Fan, J. Li, P. G. Wang, H. N. Cheng and R. G. Nickol, *J. Polym. Sci., Part A: Polym. Chem.*, **1999**, 37, 3486-3491.
 75. J. Kasperczyk and M. Bero, *Polymer*, **2000**, 41, 391-395.
 76. B.-T. Ko and C.-C. Lin, *J. Am. Chem. Soc.*, **2001**, 123, 7973-7977.
 77. M. H. Chisholm, C.-C. Lin, J. C. Gallucci and B.-T. Ko, *Dalton Trans.*, **2003**, 406-412.
 78. M.-L. Hsueh, B.-H. Huang, J. Wu and C.-C. Lin, *Macromolecules*, **2005**, 38,

- 9482-9487.
79. C.-A. Huang and C.-T. Chen, *Dalton Trans.*, **2007**, 5561-5566.
 80. C.-A. Huang, C.-L. Ho and C.-T. Chen, *Dalton Trans.*, **2008**, 3502-3510.
 81. Y. Huang, Y.-H. Tsai, W.-C. Hung, C.-S. Lin, W. Wang, J.-H. Huang, S. Dutta and C.-C. Lin, *Inorg. Chem.*, **2010**, 49, 9416-9425.
 82. B. Calvo, M. G. Davidson and D. García-Vivó, *Inorg. Chem.*, **2011**, 50, 3589-3595.
 83. J. Zhang, C. Wang, M. Lu, Y.-M. Yao, Y. Zhang and Q. Shen, *Polyhedron*, **2011**, 30, 1876-1883.
 84. L. N. Saunders, L. N. Dawe and C. M. Kozak, *J. Organomet. Chem.*, **2014**, 749, 34-40.
 85. X. Xu, X. Pan, S. Tang, X. Lv, L. Li, J. Wu and X. Zhao, *Inorg. Chem. Commun.*, **2013**, 29, 89-93.
 86. R. K. Dean, A. M. Reckling, H. Chen, L. N. Dawe, C. M. Schneider and C. M. Kozak, *Dalton Trans.*, **2013**, 42, 3504-3520.
 87. J. Zhang, C. Jian, Y. Gao, L. Wang, N. Tang and J. Wu, *Inorg. Chem.*, **2012**, 51, 13380-13389.
 88. S.-C. Rosca, D.-A. Rosca, V. Dorcet, C. M. Kozak, F. M. Kerton, J.-F. Carpentier and Y. Sarazin, *Dalton Trans.*, **2013**, 42, 9361-9375.
 89. Z. Liu, H.-X. Chen, D. Huang, Y. Zhang and Y.-M. Yao, *J. Organomet. Chem.*, **2014**, 749, 7-12.
 90. F. M. García-Valle, R. Estivill, C. Gallegos, T. Cuenca, M. E. G. Mosquera, V. Tabernero and J. Cano, *Organometallics*, **2015**, 34, 477-487.
 91. J. Zhang, J. Xiong, Y. Sun, N. Tang and J. Wu, *Macromolecules*, **2014**, 47, 7789-7796.
 92. E. Kober, R. Petrus, P. Kocięcka, Z. Janas and P. Sobota, *Polyhedron*, **2015**, 85, 814-823.
 93. S. Ghosh, D. Chakraborty and B. Varghese, *Eur. Polym. J.*, **2015**, 62, 51-65.
 94. M. Poliakoff, W. Leitner and E. S. Streng, *Farad. Discuss.*, **2015**, 183, 9-17.
 95. I. Omae, *Coord. Chem. Rev.*, **2012**, 256, 1384-1405.
 96. I. Omae, *Cata. Today*, **2006**, 115, 33-52.
 97. S. Klaus, M. W. Lehenmeier, C. E. Anderson and B. Rieger, *Coord. Chem. Rev.*, **2011**, 255, 1460-1479.
 98. P. P. Pescarmona and M. Taherimehr, *Catal. Sci. Technol.*, **2012**, 2, 2169-2187.
 99. T. Sakakura and K. Kohno, *Chem. Commun.*, **2009**, 1312-1330.
 100. B. Schäffner, F. Schäffner, S. P. Verevkin and A. Börner, *Chem. Rev.*, **2010**, 110, 4554-4581.
 101. H. Arakawa, M. Aresta, J. N. Armor, M. A. Barteau, E. J. Beckman, A. T. Bell, J. E. Bercaw, C. Creutz, E. Dinjus, D. A. Dixon, K. Domen, D. L. DuBois, J. Eckert, E. Fujita, D. H. Gibson, W. A. Goddard, D. W. Goodman, J. Keller, G. J. Kubas, H. H. Kung, J. E. Lyons, L. E. Manzer, T. J. Marks, K. Morokuma, K. M. Nicholas, R. Periana, L. Que, J. Rostrup-Nielson, W. M. H. Sachtler, L. D. Schmidt, A. Sen, G. A. Somorjai, P. C. Stair, B. R. Stults and W. Tumas, *Chem. Rev.*, **2001**, 101, 953-996.
 102. A. I. Cooper, *J. Mater. Chem.*, **2000**, 10, 207-234.

103. H. Yasuda, L.-N. He, T. Sakakura and C. Hu, *J. Catal.*, **2005**, 233, 119-122.
104. O. V. Zalomaeva, A. M. Chibiryaev, K. A. Kovalenko, O. A. Kholdeeva, B. S. Balzhinimaev and V. P. Fedin, *J. Catal.*, **2013**, 298, 179-185.
105. D. J. Darensbourg and M. W. Holtcamp, *Coord. Chem. Rev.*, **1996**, 153, 155-174.
106. S. S. Murphree, *Arkivoc*, **2006**, 6-33.
107. Y. Liu, K. Murata and M. Inaba, *Chem. Commun.*, **2004**, 582-583.
108. M. G. Finn, H. C. Kolb, M. G. Finn and K. B. Sharpless, *Angew. Chem. Int. Ed.*, **2001**, 40, 2004-2021.
109. K. Nakano and K. Nozaki, in *11.17- Polymerization of Epoxides, Comprehensive Organometallic Chemistry III*, Elsevier Ltd, **2007**, vol. 13, chapter. 11.17, pp. 595-621.
110. A. Gansäuer, *Angew. Chem. Int. Ed.*, **2006**, 45, 5733-5733.
111. M. B. Smith, *Organic Synthesis*, Elsevier Science, Burlington, 3rd ed., **2011**.
112. M. Beller, *Catalytic Carbonylation Reactions*, Springer Heidelberg, Berlin, **2006**.
113. A. Wurtz, *Ann. Chim. phys.*, **1863**, 69, 330-334.
114. A. Walti, *J. Biol. Chem.*, **1927**, 75, 325-336.
115. S. Rajaraman, W. A. Mowers, S. S. Liu and J. V. Crivello, *Macromol. Symp.*, **2000**, 157, 109-120.
116. M. Yus and I. Pastor, *Curr. Org. Chem*, **2005**, 9, 1-29.
117. G. W. Coates, *Chem. Rev.*, **2000**, 100, 1223-1252.
118. X.-B. Lu, L. Shi, Y.-M. Wang, R. Zhang, Y.-J. Zhang, X.-J. Peng, Z.-C. Zhang and B. Li, *J. Am. Chem. Soc.*, **2006**, 128, 1664-1674.
119. M. F. Llauro, T. Hamaide and V. Jacquier-Gonod, *Macromol. Chem. Phys.*, **2000**, 201, 12-20.
120. X.-B. Lu, W.-M. Ren and G.-P. Wu, *Acc. Chem. Res.*, **2012**, 45, 1721-1735.
121. R. Petiaud, M. F. Llauro, T. Hamaide and R. Goriot, *Macromol. Symp.*, **1997**, 119, 173-188.
122. S. J. Wilson and D. J. Darensbourg, *Green Chem.*, **2012**, 14, 2665-2671.
123. K. Vierling and I.G. Farbenindustrie, German Pat., 740,366, **1943**.
124. M. Dekker, *Handbook of Polycarbonate Science and Technology* D. G. Legrand, J. T. Bendler, Eds., New York, **2000**.
125. I. Fukawa, M. Tojo, K. Oonishi, H. Hachiya, S. Fukuoka, M. Aminaka, K. Hasegawa and K. Komiyama, *Catal. Surv. Asia*, **2010**, 14, 146-163.
126. D. Flowers, G. Roberts, D. J. Kiserow, J. M. DeSimone and S. M. Gross, *Macromolecules*, **1999**, 32, 3170-3170.
127. M. Kawamura, K. Komiyama, M. Tojo, H. Hachiya, S. Fukuoka, K. Hasegawa, M. Aminaka, H. Okamoto, I. Fukawa and S. Konno, *Green Chem.*, **2003**, 5, 497-507.
128. M. V. Maffini, B. S. Rubin, C. Sonnenschein and A. M. Soto, *Mol. Cell. Endocrinol.*, **2006**, 254-255, 179-186.
129. C. M. Markey, B. S. Rubin, A. M. Soto and C. Sonnenschein, *J. Steroid Biochem. Mol. Biol.*, **2002**, 83, 235-244.
130. M. Wagner and J. Oehlmann, *Environ. Sci. Pollut. Res*, **2009**, 16, 278-286.
131. M. North, R. Pasquale and C. Young, *Green Chem.*, **2010**, 12, 1514-1539.
132. H. Koinuma, T. Tsuruta, S. Inoue, H. Koinuma and T. Tsuruta, *J. Polym. Sci., Part B: Polym. Chem.*, **1969**, 7, 287-292.

133. T. Sakakura, J.-C. Choi and H. Yasuda, *Chem. Rev.*, **2007**, 107, 2365-2387.
134. B. Plietker, *Iron Catalysis in Organic Chemistry : Reactions and Applications*, Weinheim : Wiley-VCH, Weinheim, **2008**.
135. J. C. Bailar and A. F. Trotman-Dickenson, in *Comprehensive Inorganic Chemistry, Iron*, Pergamon Press, Oxford,, **1973**, vol. 3.
136. J. A. Mcleverty and T. J. Meyer, in *Comprehensive Coordination Chemistry II, Iron*, Elsevier Ltd., New York, **2004**, vol. 5.
137. B. Plietker, *Iron Catalysis: Fundamentals and Applications*, Springer, New York, **2011**.
138. W. J. Kruper and D. J. Swart, *The Dow Chemical Company*, US. Pat., 4,500,704, **1985**.
139. D. J. Darensbourg, M. J. Adams and J. C. Yarbrough, *Inorg. Chem.*, **2001**, 40, 6543-6544.
140. D. J. Darensbourg, M. J. Adams, J. C. Yarbrough and A. L. Phelps, *Inorg. Chem.*, **2003**, 42, 7809-7818.
141. A. Buchard, M. R. Kember, K. G. Sandeman and C. K. Williams, *Chem. Commun.*, **2011**, 47, 212-214.
142. M. W. Lehenmeier, S. Klaus, C. E. Anderson, E. Herdtweck, J. E. Dengler, and B. Rieger, *Eur. J. Inorg. Chem.*, **2011**, 2011, 336-343.
143. C. J. Whiteoak, B. Gjoka, E. Martin, M. M. Belmonte, E. C. Escudero-Adán, C. Zonta, G. Licini and A. W. Kleij, *Inorg. Chem.*, **2012**, 51, 10639-10649.
144. S. M. Al-Amsyar, C. J. Whiteoak, A. W. Kleij, P. P. Pescarmona and M. Taherimehr, *Green Chem.*, **2013**, 15, 3083-3090.
145. M. A. Fuchs, T. A. Zevaco, E. Ember, O. Walter, I. Held, E. Dinjus and M. Döring, *Dalton Trans.*, **2013**, 42, 5322-5329.
146. K. Nakano, K. Kobayashi, T. Ohkawara, H. Imoto and K. Nozaki, *J. Am. Chem. Soc.*, **2013**, 135, 8456-8459.
147. L. Qiao, Y. Qin, X. Wang, F. Wang and X. Sheng, *Polyhedron*, **2014**, 74, 129-133.
148. A. De Nisi, A. Grassi, S. Milione, C. Capacchione, A. Buonerba, S. Vagin and B. Rieger, *Catal. Sci. Technol.*, **2015**, 5, 118-123.
149. A. Buonerba, F. Della Monica, A. De Nisi, E. Luciano, S. Milione, A. Grassi, C. Capacchione and B. Rieger, *Farad. Discuss.*, **2015**, 183, 83-95.
150. M. Taherimehr, J. P. C. C. Sertã, A. W. Kleij, C. J. Whiteoak and P. P. Pescarmona, *ChemSusChem*, **2015**, 8, 1034-1042.
151. F. A. Cotton, G. Wilkinson, C. A. Murillo and M. Bochmann, in *Advanced Inorganic Chemistry*, John Wiley & Sons Inc, New York, 6th ed., **1999**, ch. 17.
152. W. Betteridge, *Cobalt and Its Alloys*, John Wiley & Sons, New York, **1982**.
153. G. Btackman, *Cobalt: Inorganic & Coordination Chemistry* in "Encyclopedia of Inorganic Chemistry" online resource, John Wiley & Sons Inc., Hoboken, NJ, **2006**.
154. J. Emsley, *Nature's Building Blocks: An A-Z Guide to the Elements*, Oxford University Press, Oxford and Toronto, **2001**.
155. Z. Qin, C. M. Thomas, S. Lee and G. W. Coates, *Angew. Chem. Int. Ed.*, **2003**, 42, 5484-5487.

156. X.-B. Lu and Y. Wang, *Angew. Chem. Int. Ed.*, **2004**, 43, 3574-3577.
157. R. L. Paddock and S. T. Nguyen, *Chem. Commun.*, **2004**, 1622-1623.
158. A. Berkessel and M. Brandenburg, *Org. Lett.*, **2006**, 8, 4401-4404.
159. E. K. Noh, S. J. Na, S. S. S.-W. Kim and B. Y. Lee, *J. Am. Chem. Soc.*, **2007**, 129, 8082-8083.
160. S. Sujith, J. K. Min, J. E. Seong, S. J. Na and B. Y. Lee, *Angew. Chem. Int. Ed.*, **2008**, 47, 7306-7309.
161. W.-M. Ren, Z.-W. Liu, Y.-Q. Wen, R. Zhang and X.-B. Lu, *J. Am. Chem. Soc.*, **2009**, 131, 11509-11518.
162. L. Jin, H. Jing and T. Chang, *ChemCatChem*, **2009**, 1, 379-383.
163. Y. Niu and H. Li, *Appl. Organomet. Chem.*, **2011**, 25, 424-428.
164. Y. Niu and H. Li, *React. Funct. Polym.*, **2011**, 71, 121-125.
165. D. J. Darensbourg and S. J. Wilson, *J. Am. Chem. Soc.*, **2011**, 133, 18610-18613.
166. F. Jutz, A. Buchard, A. J. P. White, C. K. Williams and M. R. Kember, *Chem. Sci.*, **2012**, 3, 1245-1255.
167. G.-P. Wu, W.-M. Ren, Y. Luo, B. Li, W.-Z. Zhang and X.-B. Lu, *J. Am. Chem. Soc.*, **2012**, 134, 5682-5688.
168. N. Ikpo, C. F. Petten, U. K. Das, L. N. Dawe, L. N. Saunders, C. M. Kozak and F. M. Kerton, *Catal. Commun.*, **2012**, 18, 165-167.
169. G.-P. Wu, F. Lin, J.-Y. Jiang, C. Liu, W.-M. Ren, Y. Luo and X.-B. Lu, *Chem. Sci.*, **2012**, 3, 2094-2102.
170. S. J. Wilson, D. J. Darensbourg and S. J. Wilson, *Macromolecules*, **2013**, 46, 5929-5934.
171. F. Gou, H. Jing and X. Jiang, *J. Catal.*, **2014**, 313, 159-167.
172. W.-C. Chung, A. D. Yeung, M. Luna and D. J. Darensbourg *Macromolecules*, **2015**, 48, 1679-1687.
173. H. Jing and X. Fu, *J. Catal.*, **2015**, 329, 317-324.
174. D. J. Darensbourg, J. C. Yarbrough, C. Ortiz and C. C. Fang, *J. Am. Chem. Soc.*, **2003**, 125, 7586-7591.

Co-Authorship Statement

Chapter 2: Ring-opening polymerization of *rac*-lactide mediated by tetrametallic lithium and sodium diamino-bis(phenolate) complexes

This chapter contains some of the results published in the full article “Ring-opening polymerization of *rac*-lactide mediated by tetrametallic lithium and sodium diamino-bis(phenolate) complexes”, *Dalton Transactions*, **2015**, 44, 20216–20231.

Authors: Dalal Alhashmialameer, Nduka Ikpo, Julie Collins, Louise N. Dawe, Karen Hattenhauer and Francesca M. Kerton.

The first author (Dalal Alhashmialameer) contributed 90% of the content of the article as the main researcher including: performing experiments, collecting data, and writing parts of the paper (including creating ORTEP images, experimental sections and the results and discussion).

The second author (Nduka Ikpo) was a graduate student in the Kerton group who crystallized the lithium complex for X-ray analysis.

Julie Collins and Louise N. Dawe were the crystallographers on the paper. The other co-authors are Francesca M. Kerton and Karen Hattenhauer, my supervisors, who assisted in writing and editing the paper, and designing experiments. PGSE NMR data were collected by Dr. Céline M. Schneider and analyzed by Schneider and Kerton with advice from Y. Sarazin (Université de Rennes).

Chapter 2 Ring-opening polymerization of *rac*-lactide mediated by tetrametallic lithium and sodium diamino-bis(phenolate) complexes

2.1 Introduction

Ligands with diverse combinations of N- and/or O-donor atoms have been used extensively in transition metal coordination chemistry in catalyst development, particularly amino-phenolate ligands, due to their ability to coordinate to a wide range of metal centres. Variation of the steric properties of the ligand is also readily achieved by changing either the backbone and/or the phenolate substituent, causing variations in the catalytic properties of the complexes formed.¹

In the search for efficient, cheap, stable and non-toxic catalysts, alkali metals have emerged as very attractive catalysts for initiating the ring opening polymerization (ROP) of lactides.^{2,3} Simple alkali metal compounds, like butyllithium,^{4,5} lithium *tert*-butoxide^{5,6} and potassium *tert*-butoxide^{5,7} are reported to be highly active in ROP of cyclic esters; however, they suffer from undesirable side reactions such as backbiting and transesterifications, which lead to uncontrollable polymerizations. Sterically bulky ligands around the alkali metal centre have been reported to minimize the intra- and intermolecular transesterification side reactions during polymerization.^{3-5,8-10} Alkali metals such as lithium and sodium have become increasingly important due to their biocompatibility and success in various catalytic polymerization processes. In addition to having catalytic capability, they tend to form multinuclear aggregates in solution and in the crystalline state depending on the steric properties of the ligand or solvent used.^{8,10-24} This made the study of the structure and reactivity of these multinuclear and/or polymeric

compounds attractive. For example, isomeric diamino-bis(phenol) ligands were used by Kerton, Kozak *et al.* to obtain lithium complexes in the presence of 1,4-dioxane (**Figure 2.1**).¹⁷ Both complexes **2.1** and **2.2** are dioxane adducts, however, the solid state structures confirmed dimeric (tetralithium) and polymeric arrangements, respectively.

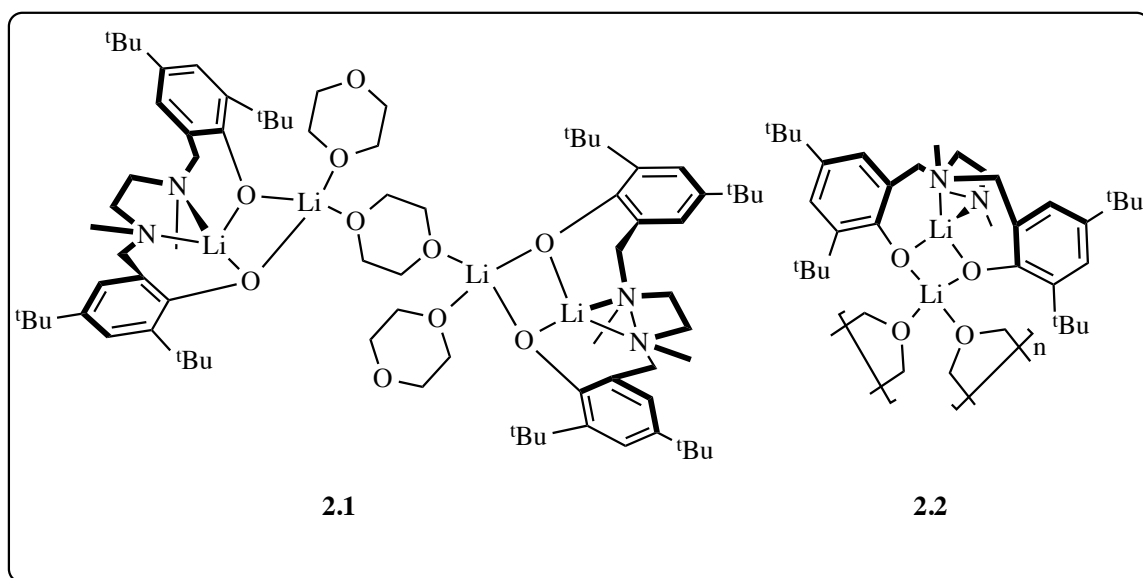


Figure 2.1. Dimeric $\text{Li}_2[\text{O}_2\text{N}_2]^{\text{BuBu}}$ complex (**2.1**) and single unit of $\text{Li}_2[\text{O}_2\text{NN}']^{\text{BuBu}}$ complex (**2.2**).¹⁷

The groups of Chen,¹⁰ O'Hara¹⁸ and Kozak¹¹ reported tetralithium complexes (**Figure 2.2**) have open ladder-like arrangements and dimeric structures in the solid state. They were found to have two amino-bis(phenolate) ligands capped onto the end of the ladder-like core. Compounds **1.8a–1.8c** and **2.3** were able to better control the polymerization reactions as evidenced by the resulting lower polymer dispersities ($D = 1.09\text{--}1.05$) compared with the related tridentate ligand complexes, **1.28a** ($D = 1.3\text{--}2.4$). In later mechanistic studies by Chen and coworkers, using different lithium amino-phenolate complexes, they were able to show that BnOH is activated by the lithium first, followed

by insertion of the resulting benzyl alkoxy group to the carbonyl group of LA.¹⁶

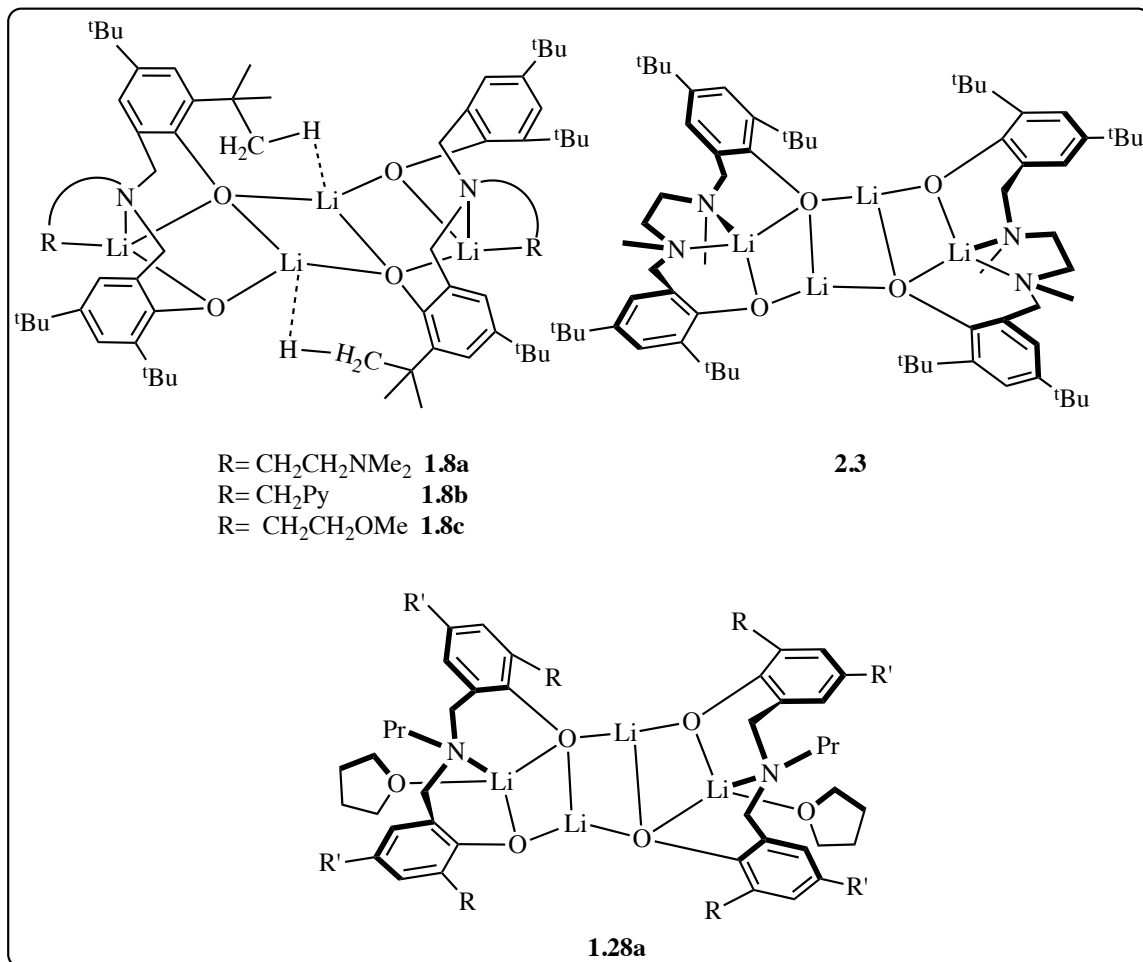


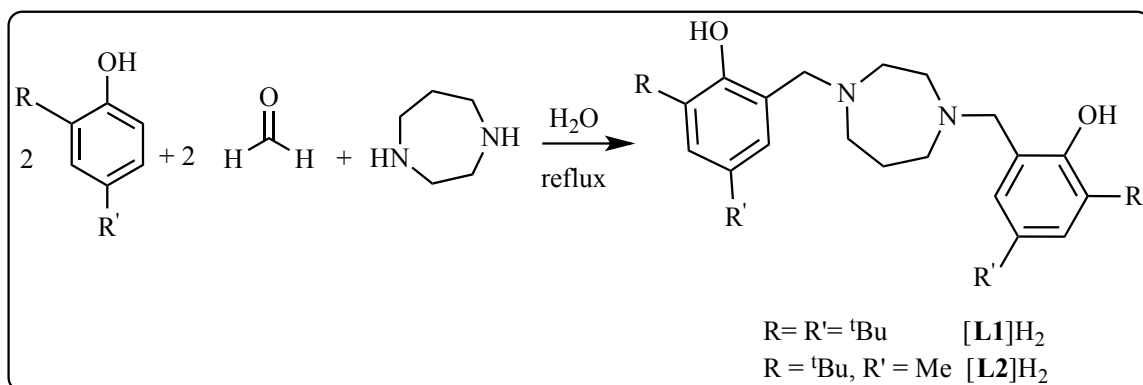
Figure 2.2. Compounds **1.8a–1.8c** reported by Chen and coworkers.¹⁰ **2.3** reported by O'Hara¹⁸ while **1.28a** used by Kozak¹¹ *et al.*

In this chapter, the synthesis and structural characterization of lithium and sodium complexes with tetradentate amino-bis(phenolate) ligands are described. In order to gain insight into the reactivity of these Group 1 complexes, their reactivity as catalysts for the ROP of lactide (LA) under various conditions was explored including catalyst loading, amount of co-initiator, temperature and reaction time.

2.2 Results and discussion

2.2.1 Synthesis and characterization of ligands, lithium and sodium complexes

The tetradentate amino-bis(phenol) ligands were synthesized via a modified Mannich condensation reaction in water.^{25,26} The ligands were prepared by refluxing aqueous formaldehyde, 2 equivalents of the appropriate phenol (2,4-di-*tert*-butylphenol or 2-*tert*-butyl-4-methylphenol) and 1 equivalent of homopiperazine using water as a reaction medium, to afford the products shown in **Scheme 2.1**. These and closely related ligands have previously been used to prepare complexes of Ti,²⁷⁻³⁰ Mn,³¹ Al,³² Zr,³³ Hf,³³ Mo,³⁴ and Fe.³⁵⁻³⁷



Scheme 2.1. Synthesis of amino-bis(phenol) ligands.

The structure of the ligand $[\mathbf{L1}]H_2$ with *t*Bu groups in the *ortho* and *para* positions was confirmed from its ¹H NMR spectrum (**Figure 2.3**) in which two singlets (a) and (b) at 1.25 and 1.40 ppm were assigned to *t*Bu protons. A quintet at 1.89 ppm was assigned to the CH₂ protons (c) that couple with four adjacent CH₂ protons within the homopiperazine ring ($J = 6.0$ Hz). A singlet at 2.75 ppm corresponds to four CH₂ protons

(d). Two overlapping triplet peaks ($J = 6.0$ Hz) at 2.80 ppm were assigned to the remaining four CH_2 protons (e) adjacent to (c). A singlet at 3.75 ppm was assigned to $\text{Ar}-\text{CH}_2-\text{N}$ (f), and two aromatic resonances at 6.79 and 7.19 ppm were assigned to $\text{Ar}-\text{H}$ protons (g and h). The structure was also confirmed by $^{13}\text{C}\{^1\text{H}\}$ NMR spectroscopy and authenticated by the MALDI-TOF mass spectrum with a peak at m/z 536 $[\text{M}]^+$, which corresponds to the molecular weight of the ligand (**Figure 2.4**).

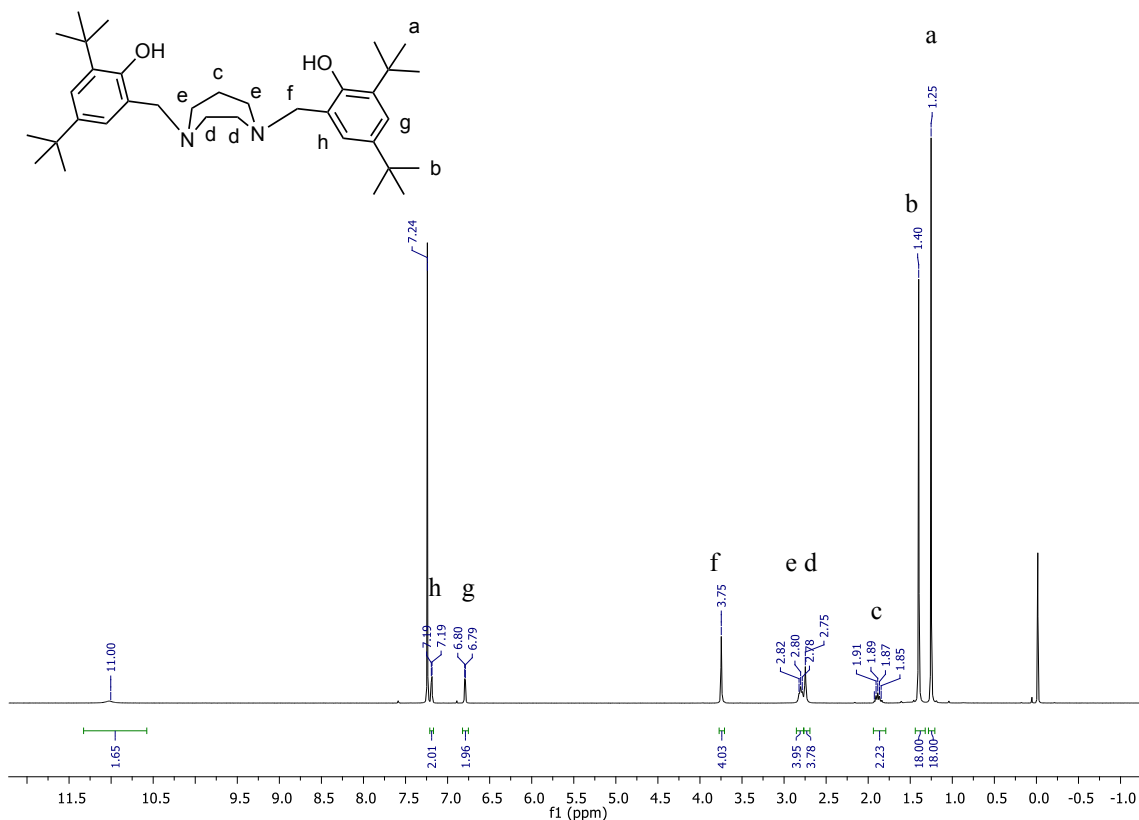


Figure 2.3. ^1H NMR spectrum (300 MHz, 298 K, CDCl_3) of $[\text{L1}]\text{H}_2$.

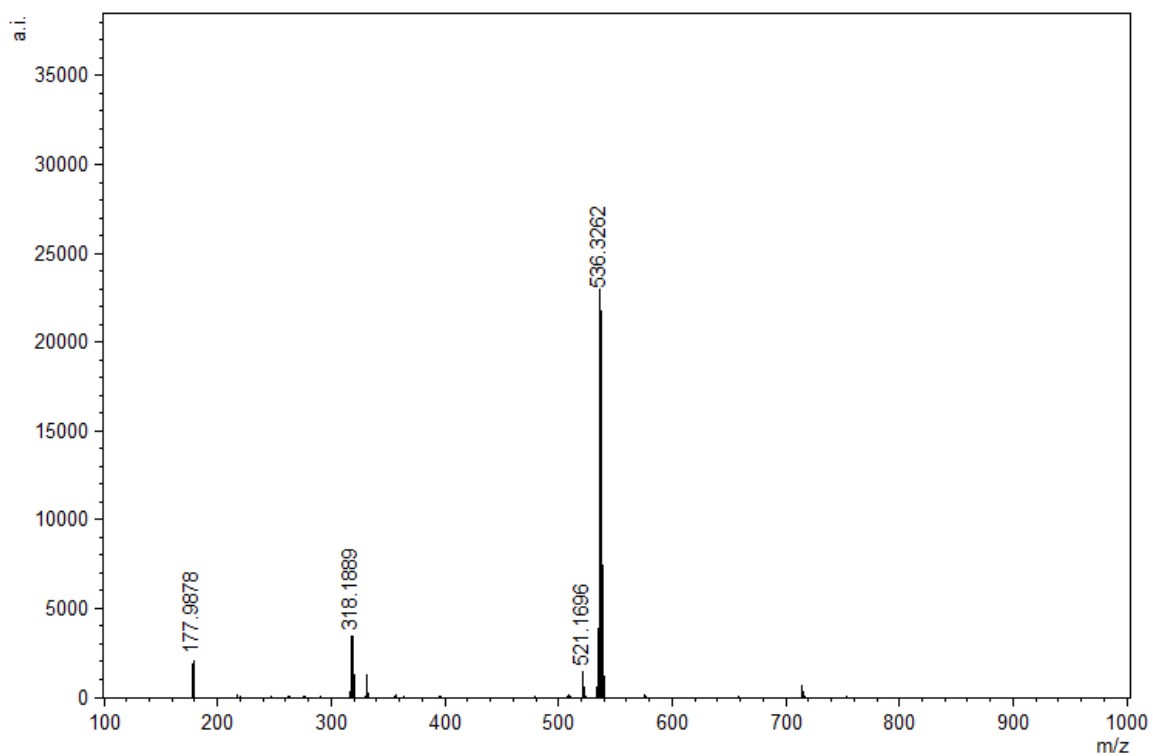


Figure 2.4. MALDI-TOF mass spectrum of [L1]H₂.

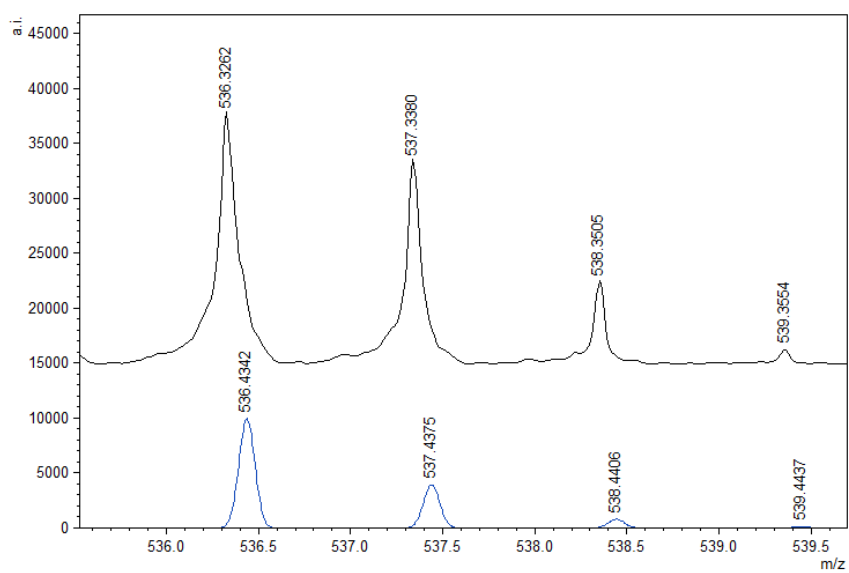
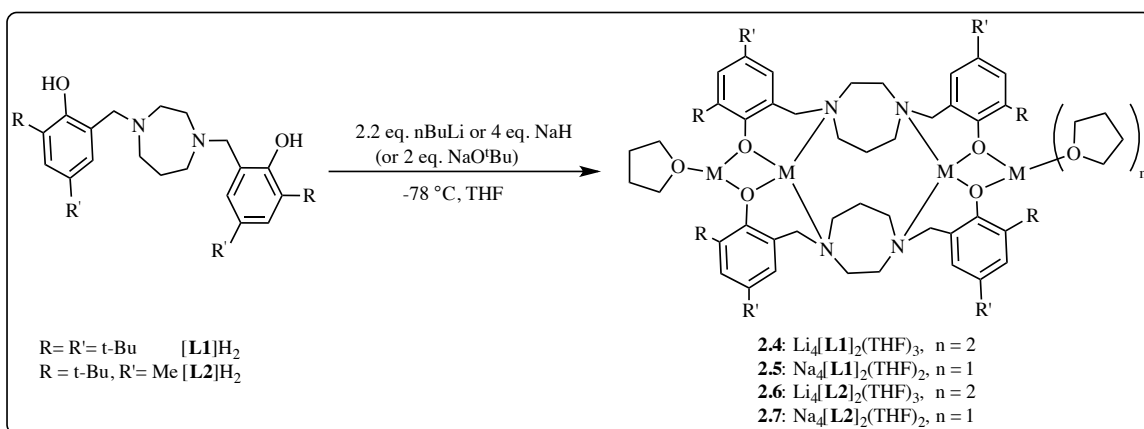


Figure 2.5. Experimental (top) and calculated (bottom) isotopic distribution pattern for [L1]H₂.

As shown in **Scheme 2.2**, lithium complexes with the formulation $\text{Li}_4[\text{L1}]_2(\text{THF})_3$ and $\text{Li}_4[\text{L2}]_2(\text{THF})_3$ were synthesized by the reaction of **[L1]** and **[L2]** with 2.2 equiv. *n*-BuLi in THF. Tetranuclear sodium complexes were produced by reacting the appropriate ligand with an excess of NaH as shown in **Scheme 2.2** but could also be prepared via reaction of ligands with two equiv. of sodium *tert*-butoxide. It is worth noting that the formulation for the sodium complexes is consistent with two equivalents of THF per tetranuclear sodium species in contrast to three for the analogous lithium compounds. The complexes **2.4–2.7** were characterized using X-ray diffraction, MALDI-TOF MS and ^1H , ^{13}C and ^7Li NMR spectroscopy and for **2.5** and **2.7** elemental analyses. Unfortunately, satisfactory elemental analysis could not be obtained for complexes **2.4** and **2.6**.



Scheme 2.2. Synthesis of lithium and sodium complexes.

2.2.2 Crystal structure determination

For complex **2.4**, crystals suitable for single crystal X-ray diffraction were formed by slow evaporation of an equal volume mixture of toluene/pentane under an inert atmosphere at $-35\text{ }^\circ\text{C}$. The ORTEP structure of complex **2.4** $\{\text{Li}_4[\text{L1}]_2(\text{THF})_3\}$ is shown

in **Figure 2.6** and the crystallographic data are collected in **Table 2.1**. The compound contains four Li atoms, capped by two amino-bis(phenolate) ligands. At its core, only three of the four Li centres are tetracoordinate, with the fourth being tricoordinate. Selected bond lengths (Å) and angles (°) for **2.4** are presented in **Table 2.2**. The two terminal lithium centres Li(1) and Li(4) are bonded to two phenolate oxygen atoms (Li(1)–O(1), 1.804 Å, Li(1)–O(3), 1.848 Å, Li(4)–O(2), 1.899 Å, Li(4)–O(4) 1.922 Å) with distances in agreement to those reported by Chen *et al.* for a series of tetranuclear ladder-like lithium phenolates,¹⁰ and other similar species.^{11,18} The terminal Li atoms are bound by one or two THF molecules (Li(1)–O(5), 1.934 Å, Li(4)–O(7), 2.085 Å, Li(4)–O(6) 2.009 Å) resulting in pseudo-trigonal planar (Li(1)) and tetrahedral (Li(4)) coordination environments. Each central Li atom is bound by two N atoms and bridging phenolate O atoms. Li–O and Li–N bond lengths are in good agreement with previously observed literature values for similar systems.^{10,17} Each of these lithium atoms interacts weakly with an adjacent terminal lithium atom (Li(1)–Li(2), 2.493 Å, Li(3)–Li(4), 2.583 Å) and agrees with the values reported by Chen *et al.* for analogous Li-containing compounds (2.403(7)–2.444(4) Å).^{10,11} The weak interaction may be enforced by the structure of the ligands but an interaction is evident due to the Li–Li distances being less than the sum of the Van der Waals radii of lithium.

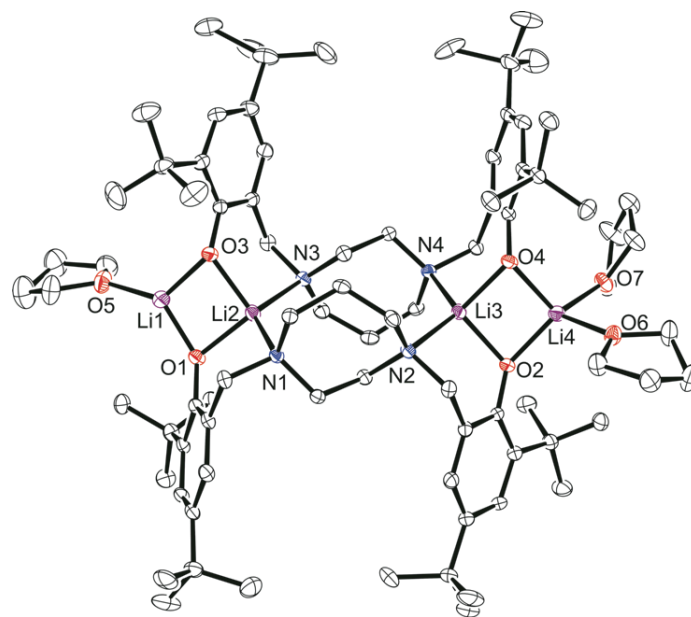


Figure 2.6. Molecular structure (ORTEP) and partial numbering scheme for **2.4**. Ellipsoids are shown at the 50% probability level (H-atoms omitted for clarity).

Table 2.1. Crystallographic data and structure refinement for **2.4** and **2.7**.

Compound	2.4 (CCDC 1410026)	2.7 (CCDC 1410027)
Empirical Formula	C ₈₂ H ₁₃₂ Li ₄ N ₄ O ₇ ·3(C ₇ H ₈)	C ₆₆ H ₁₀₀ Na ₄ N ₄ O ₆
Formula Weight	1590.15	1137.51
Temperature/K	163	163
Crystal Colour	Colorless	Colorless
Crystal System	Triclinic	Monoclinic
Crystal Dimensions	0.38 × 0.35 × 0.34 mm	0.5 × 0.43 × 0.35 mm
Lattice Parameters	a = 16.592(2) Å b = 18.655(2) Å c = 19.067(2) Å α = 103.219(7)° β = 98.581(7)° γ = 109.095(8)° V = 5265.8(10) Å ³	a = 12.898(4) Å b = 13.741(4) Å c = 18.695(6) Å α = 90° β = 101.518(4)° γ = 90° V = 3246.7(17) Å ³
Space Group	P-1 (#2)	P2 ₁ /n(#14)
Z value	2	2
D _{calc}	1.003 g/cm ³	1.164 g/cm ³
F ₀₀₀	1740	1232.0
μ(MoKα)	0.61 cm ⁻¹	0.096 cm ⁻¹
Reflections collected	43063	24304
Independent reflections	21429	7155
R _{int}	0.0454	0.0374
R, wR ₂ (all) ^a	0.1462, 0.3597	0.0604, 0.1653
R, wR ₂ [I ≥ 2σ(I)] ^a	0.1130, 0.3441	0.0543, 0.1580
GOF-fit on F ²	1.060	1.084

$$^a R_1 = \Sigma(|F_o| - |F_c|) / \Sigma|F_o| ; wR_2 = [\Sigma(w(F_o^2 - F_c^2)^2) / \Sigma w(F_o^2)^2]^{1/2}$$

Table 2.2. Selected bond lengths (Å) and angles (°) for **2.4** and **2.7**.

2.4		2.7	
Li(1)–O(1)	1.804(8)	Na(1)–O(1)	2.3450(14)
Li(2)–O(1)	1.932(7)	Na(1)–O(2)	2.3176(14)
Li(1)–O(3)	1.849(8)	Na(1)–O(4)	2.3956(13)
Li(2)–O(3)	1.924(7)	Na(1)–N(2)	2.6392(16)
Li(1)–O(5)	1.932(8)	Na(2)–O(4)	2.1825(14)
Li(2)–N(1)	2.268(8)	Na(2)–O(2)	2.2369(17)
Li(2)–N(3)	2.295(7)	Na(1)–N(1)	2.6761(16)
O(1)–Li(1)–O(3)	100.0(4)	O(1)–Na(1)–O(4)	89.16(4)
O(1)–Li(1)–O(5)	130.5(4)	O(1)–Na(1)–N(2)	134.44(5)
O(1)–Li(2)–O(3)	93.0(3)	O(4)–Na(1)–N(2)	123.34(5)
Li(1)–O(1)–Li(2)	50.3(2)	O(1)–Na(1)–N(1)	77.30(4)
Li(1)–O(3)–Li(2)	50.0(2)	O(2)–Na(1)–O(4)	92.48(5)
O(1)–Li(2)–N(1)	95.5(3)	O(2)–Na(1)–N(2)	77.34(5)
O(1)–Li(2)–N(3)	123.4(3)	O(2)–Na(1)–N(1)	139.96(5)
O(3)–Li(2)–N(1)	118.7(3)	N(1)–Na(1)–N(2)	62.65(5)
O(3)–Li(2)–N(3)	94.3(3)	O(2)–Na(1)–O(4)	35.63(4)
N(1)–Li(2)–N(3)	128.0(3)		

Colourless crystals of complex **2.7** were collected upon recrystallization from an equal volume mixture of a toluene/pentane under an inert atmosphere at $-35\text{ }^{\circ}\text{C}$. The molecular structure of complex **2.7** $\{\text{Na}_4[\text{L}2]_2(\text{THF})_2\}$ is shown in **Figure 2.7** and the crystallographic parameters are given in **Table 2.1**. The arrangement of the metal centres is different to compound **2.4** due to the larger size of sodium compared to lithium. Complex **2.7** is dimeric with the sodium atoms forming a tetranuclear core, with THF

molecules bonded to the terminal sodium atoms in a symmetric arrangement. A simplified illustration of the bonding in **2.7** is shown in **Figure 2.8**. Two sodium atoms Na(1) and Na(3) form a rhomboid structure with two bridging phenolate oxygen donors, O(1) and O(4). Atoms Na(1) and Na(3) are each five coordinate and bonded to both the amine nitrogen atoms and the other phenolate oxygen donors of the tetradentate ligand. Selected bond lengths (Å) and angles (°) for compound **2.7** are presented in **Table 2.2**. According to the calculated tau parameter ($\tau = (\beta - \alpha)/60$), the geometry around the inner sodium centres can be described as distorted square pyramidal.³⁸⁻⁴⁰ The τ value is close to 0, as β the largest angle is $139.96(5)^\circ$ and α the second largest angle in the coordination sphere is $134.44(5)^\circ$ as shown in **Figure 2.8(b)**. A Na(1)–Na(3) interatomic distance of 3.3769 \AA is observed which is within the typical range observed for related complexes.²³ In comparison to the bonding observed in **2.4**, the bond distances for Na(1)–O(4), Na(1)–O(1), Na(1)–N(1) and Na(1)–N(2) are longer than expected at $2.3957(13)$, $2.3450(14)$, $2.6761(16)$ and $2.6392(16) \text{ \AA}$. Yet, all values are in statistical agreement with previously observed related bond distances in the literature.^{14,21,22,24,41} The phenyl rings of the ligand display π interactions with the outer sodium atoms and this is attributed to the flexibility of the aromatic rings to bend toward the metal centres. The Na \cdots C π bond is supported by the short distances between the sodium and carbon atoms, with Na(2)–C(21), Na(2)–C(26), Na(2)–C(8), Na(2)–C(7) bond distances of $2.6683(18)$, $2.7093(19)$, $2.8526(19)$, $2.8788(19) \text{ \AA}$, respectively. These are comparable to those reported in previous studies.^{14,24,41}

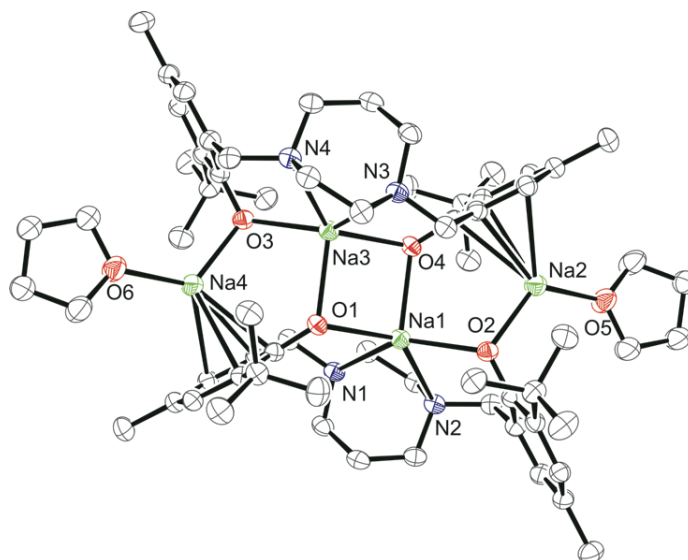


Figure 2.7. Molecular structure (ORTEP) and partial numbering scheme for **2.7**. Ellipsoids are shown at the 50% probability level (H-atoms omitted for clarity).

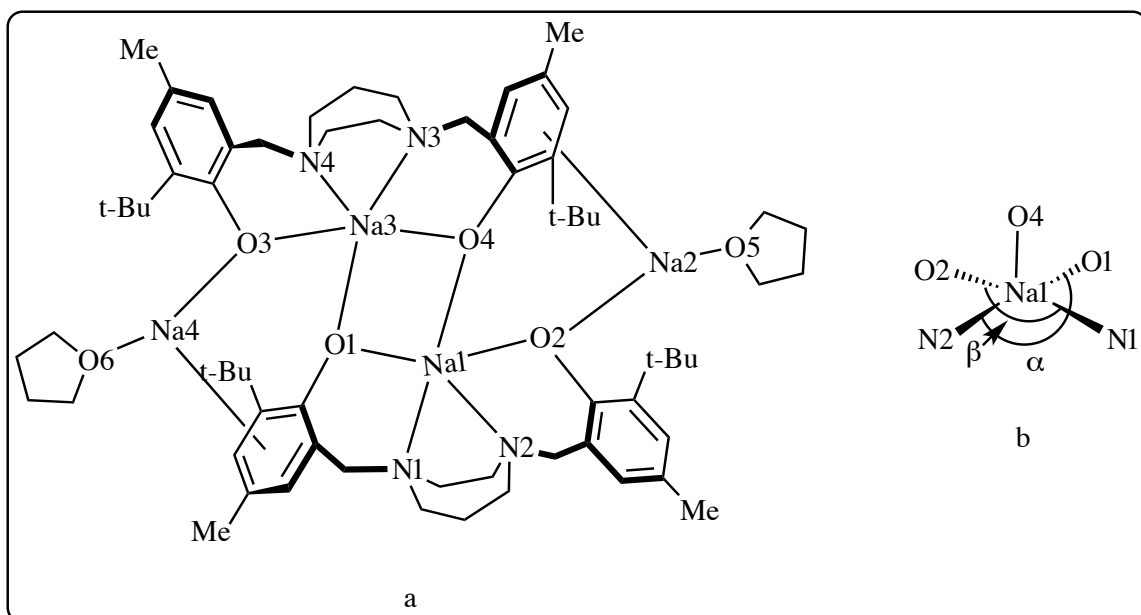


Figure 2.8. [a] Schematic representation of **2.7**. [b] Representation of the five-coordinate environment of Na(1).

2.2.3 Solution-state NMR spectroscopy

The solution structures of complexes **2.4**, **2.5**, **2.6** and **2.7** in C_6D_6 and C_5D_5N

were investigated by ^1H and, where appropriate, ^7Li NMR spectroscopy. For complexes **2.4** and **2.5** in C_6D_6 at 298 K, only one set of ArCH_2 , ^tBu and homopiperazine (CH_2) resonances are observed in the ^1H NMR spectrum (**Figure 2.9**), which is indicative of a centrosymmetric species.

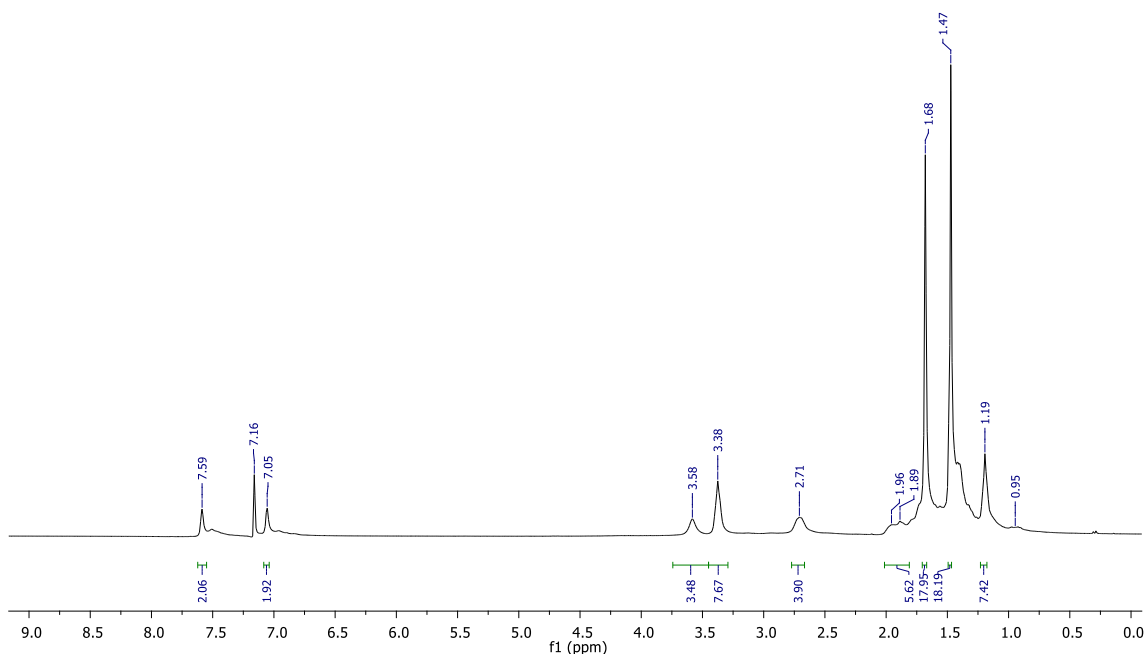


Figure 2.9. ^1H NMR spectrum (300 MHz, 298 K, C_6D_6) of **2.4**.

We assumed that disaggregation might be occurring as a result of steric crowding/congestion, wherein the structure of the ligand causes the degree of Li–O aggregation to be less in solution than the solid-state. The dissociation behavior of related tetranuclear lithium compounds in C_6D_6 and $\text{C}_5\text{D}_5\text{N}$ at 296.2 K has previously been noted by others^{11,18} in which ladder complexes undergo dissociation in solution rather than remaining intact. To further study the aggregation behavior of complex **2.4**, variable-temperature (VT) ^1H and ^7Li NMR spectra were obtained in $\text{C}_5\text{D}_5\text{N}$ from 233 to 318 K

(shown in **Figure 2.10** and **Figure 2.12**, respectively). At room temperature, the proton resonances are noticeably sharper in C_5D_5N compared to those seen in C_6D_6 (**Figure 2.11**), suggesting that the pyridine preferentially coordinates to the metal centre and reduces fluxionality in the complexes.

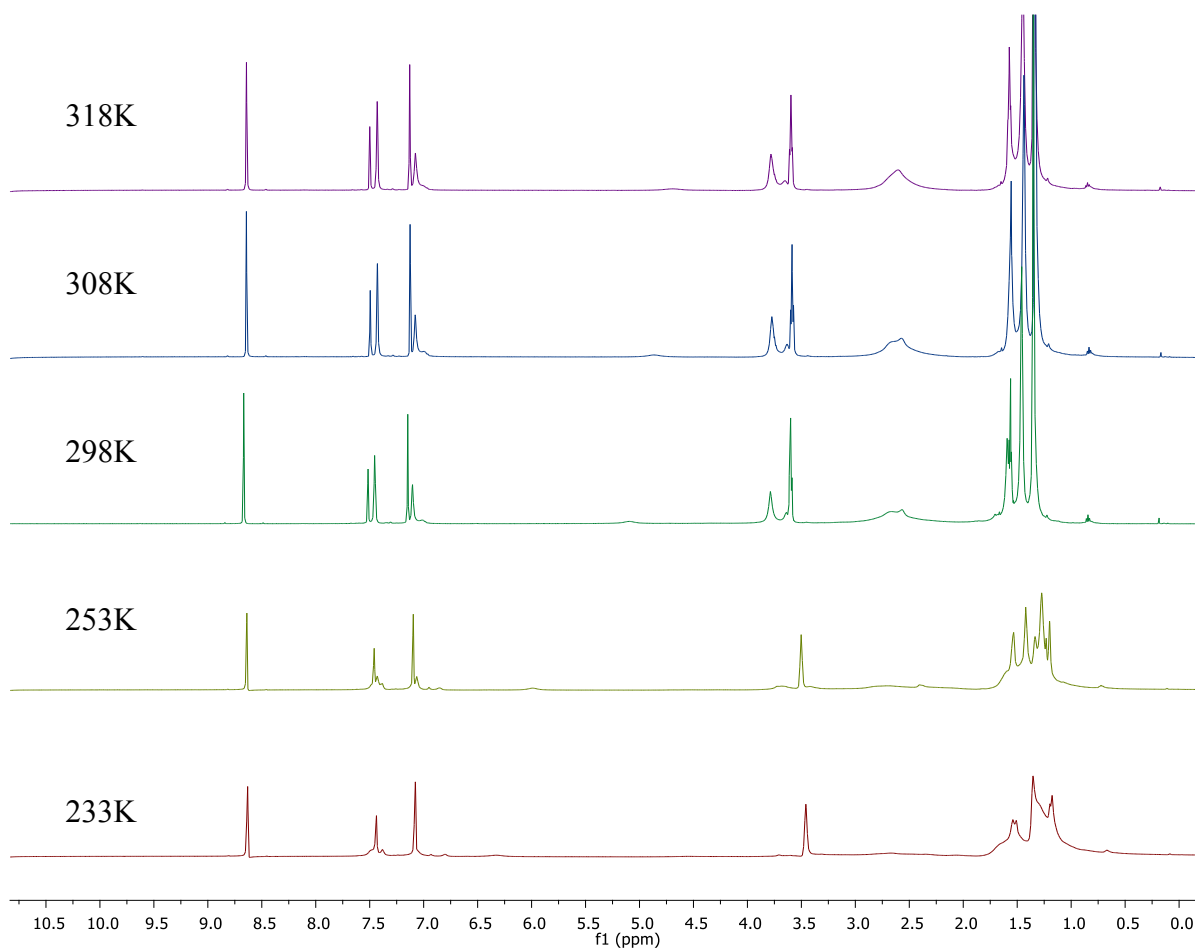


Figure 2.10. VT 1H NMR spectra (500 MHz, C_5D_5N) of **2.4**.

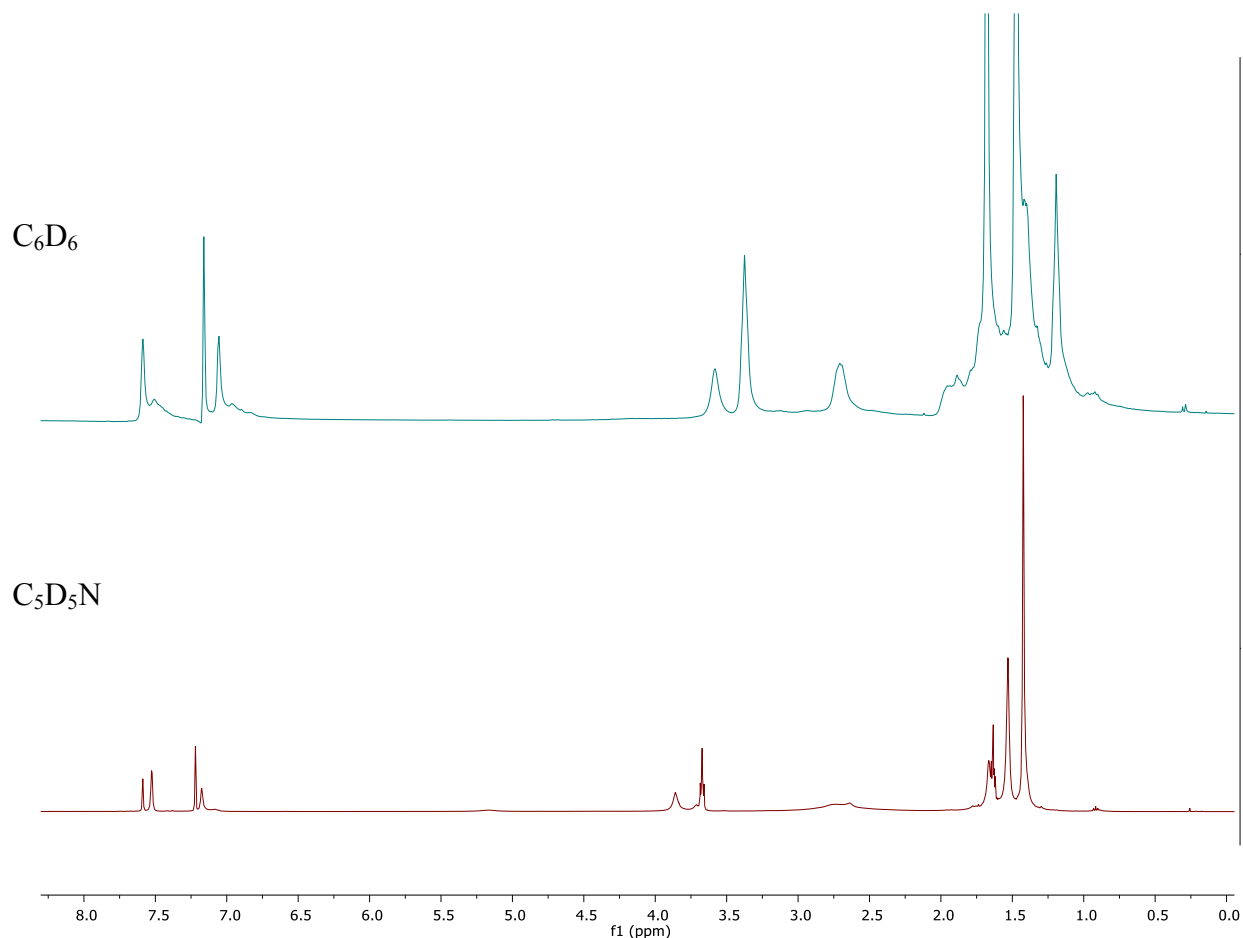


Figure 2.11. ^1H NMR spectra (500 MHz, 298 K, C_6D_6 and $\text{C}_5\text{D}_5\text{N}$) of **2.4**.

As seen in **Figure 2.12**, at room temperature and above, the ^7Li NMR spectra display a single peak at approximately 3.8 ppm ($\omega_{1/2} = 29.6$ Hz), corresponding to a single type of lithium environment, which contrasts with the solid-state structure where two environments are present. However, at low temperature (233 K), four Li environments were observed at 4.0 ($\omega_{1/2} = 70.6$ Hz), 3.8 ($\omega_{1/2} = 10.01$ Hz), 3.6 ($\omega_{1/2} = 27.2$ Hz) and 3.3 ($\omega_{1/2} = 94.5$ Hz) ppm as determined by a line fitting program. Our results contrast with the previously reported work by both the Kozak¹¹ and Chen¹⁰ groups, who observed symmetric Li environments for similar complexes. This unique observation is likely

because at low temperatures the tetralithium adduct is the dominant species present. On going from 233 K to 333 K, a small change in the chemical shift was observed which is consistent with those reported for other Li-based phenolates.^{10,11} ^7Li NMR spectra were also obtained in the formally non-coordinating solvent deuterated benzene. As expected, a major lithium environment at lower frequency, 1.58 ppm was observed (**Figure 2.13**).

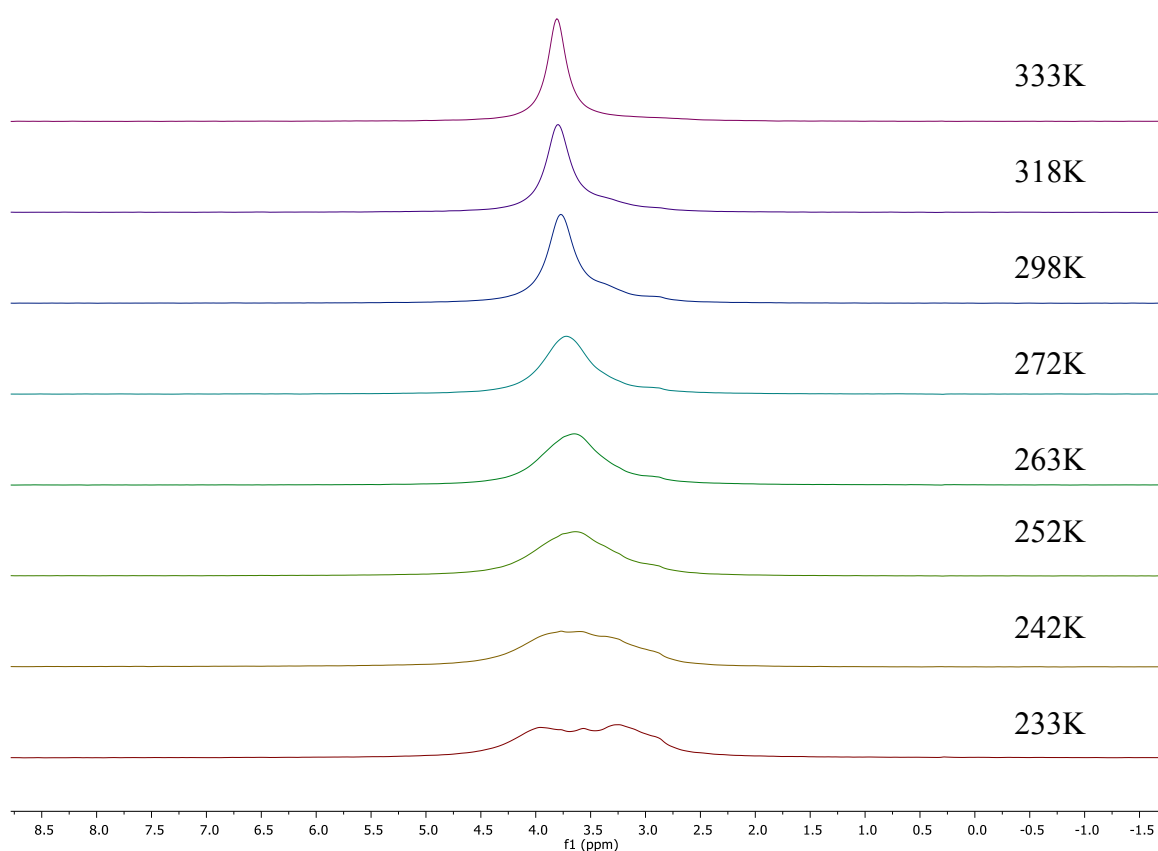


Figure 2.12. VT ^7Li NMR spectra (116.6 MHz, $\text{C}_5\text{D}_5\text{N}$) of **2.4** ($\omega_{1/2}$ values were calculated from the line fitting program in MestReNova NMR processing software).

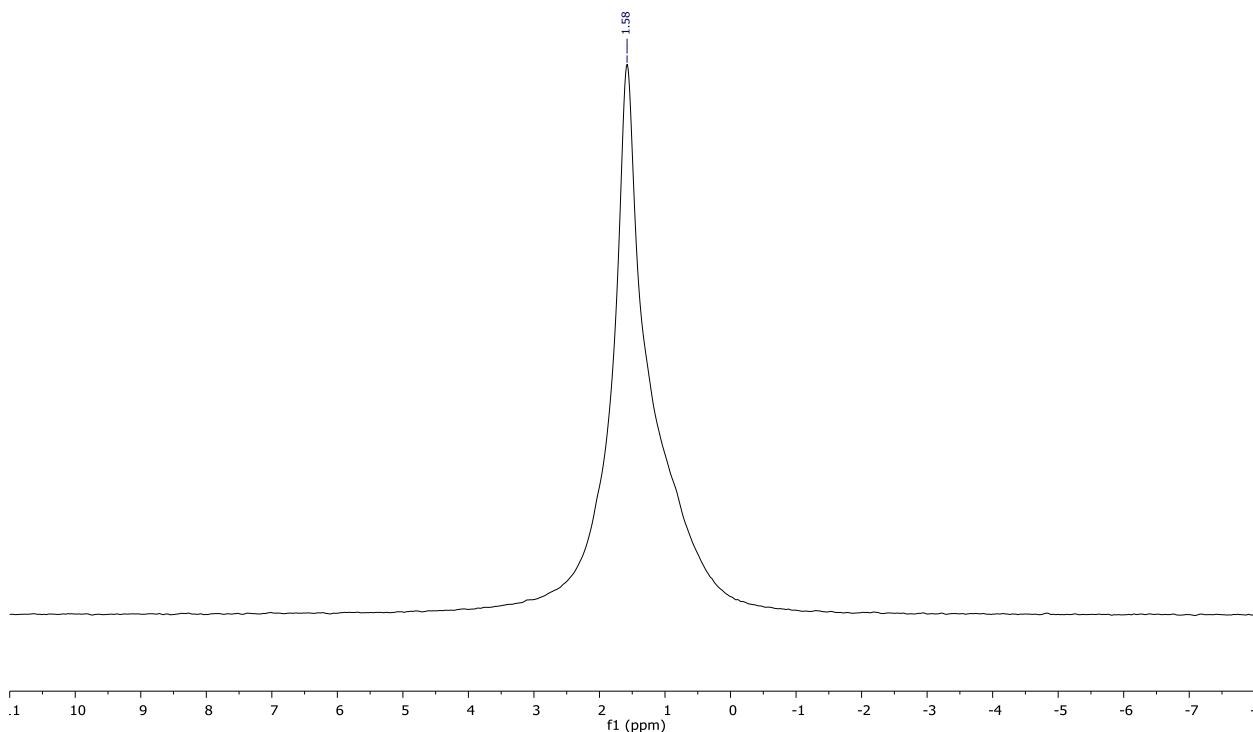


Figure 2.13. ^7Li NMR spectrum (116.6 MHz, 298 K, C_6D_6) of **2.4**.

For complex **2.7**, the spectra in C_6D_6 solutions showed broad peaks indicative of fluxional behavior (**Figure 2.14**) and this led us to pursue VT experiments in $\text{C}_5\text{D}_5\text{N}$ as shown in **Figure 2.15**. The methylene groups of the homopiperazine and those between the nitrogen and the aromatic ring are twisted and averaged at high temperatures but at low temperatures (233 and 253 K) the spectrum contains well separated peaks. At room and high temperature, the separate peaks coalesce to yield single broad peaks. As a result of the fluxional nature of compound **2.7** at room temperature and high temperature, the peaks in the ^1H NMR are broad and difficult to assign specifically. However, it is possible to predict the approximate regions that particular protons may absorb based on

comparisons of chemical shifts in similar compounds. Clearly, the most challenging portion of the spectrum to deal with are the numerous peaks observed in **Figure 2.16** between 1.0 and 4.0 ppm which are typical chemical shift regions attributed to methylene protons of which there are many in compound **2.7**. Although for some of the broad regions between 1.0 and 4.0 ppm it may be possible to make cautious peak assignments based on a comparison with the ligand spectrum in **Figure 2.3** and known chemical shifts of THF in pyridine, without further investigation of compound **2.7** utilizing 2-D NMR experiments, it is not possible to assign the peaks with certainty.

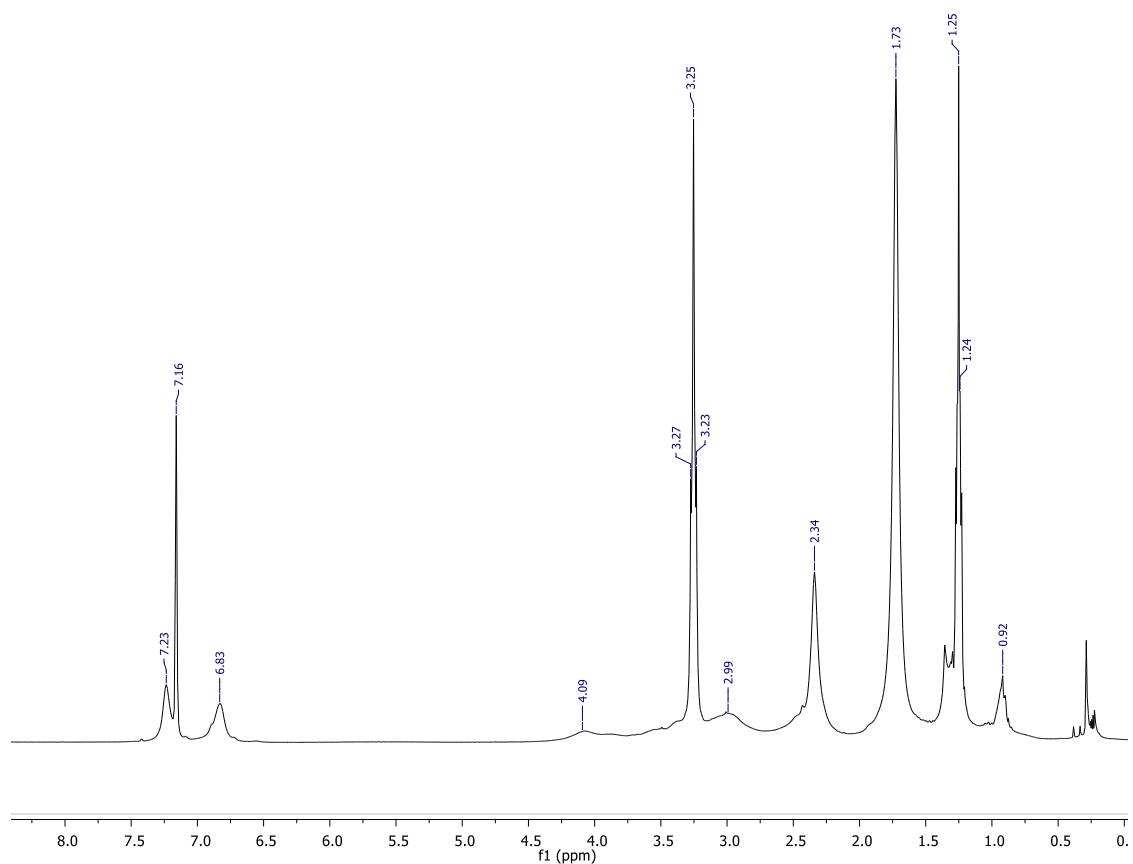


Figure 2.14. ¹H NMR spectrum (300 MHz, 298 K, C₆D₆) of **2.7**.

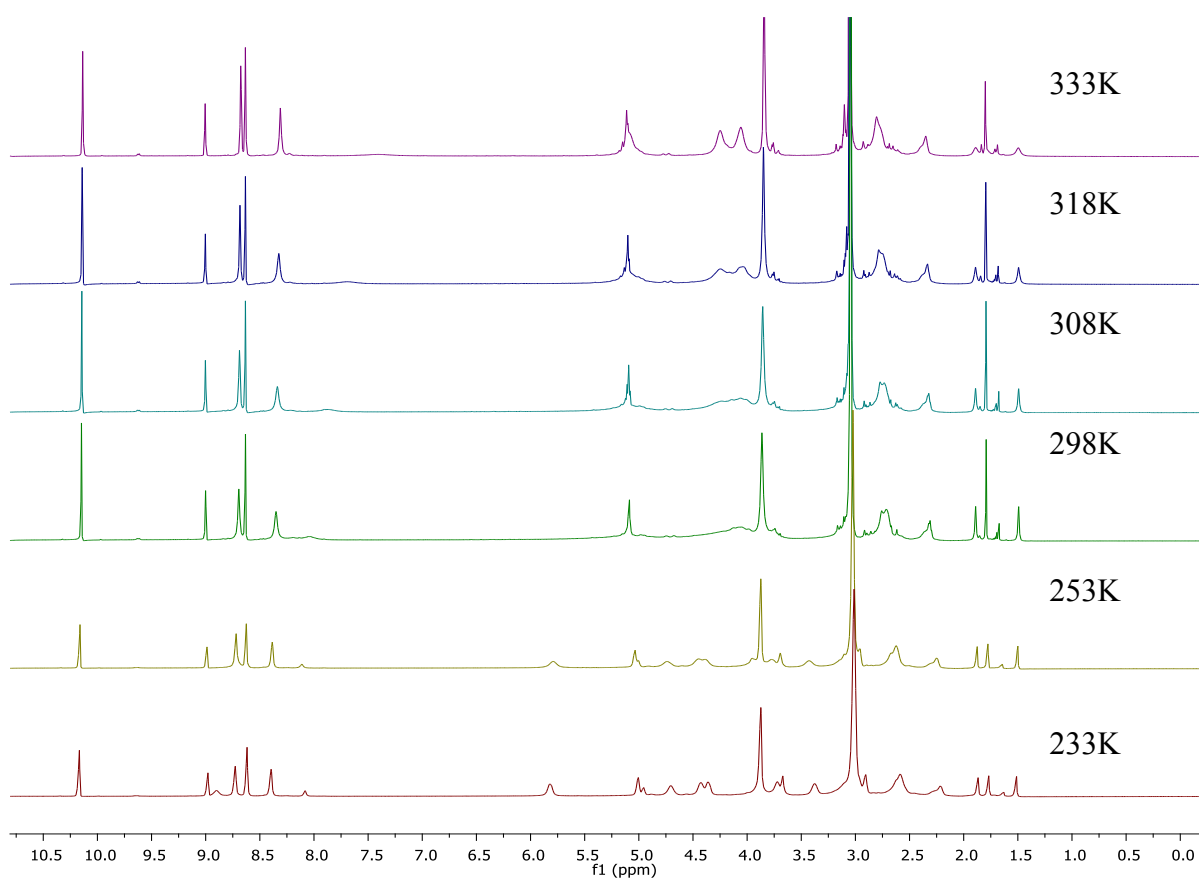


Figure 2.15. VT ¹H NMR spectra (500 MHz, C₅D₅N) of **2.7**.

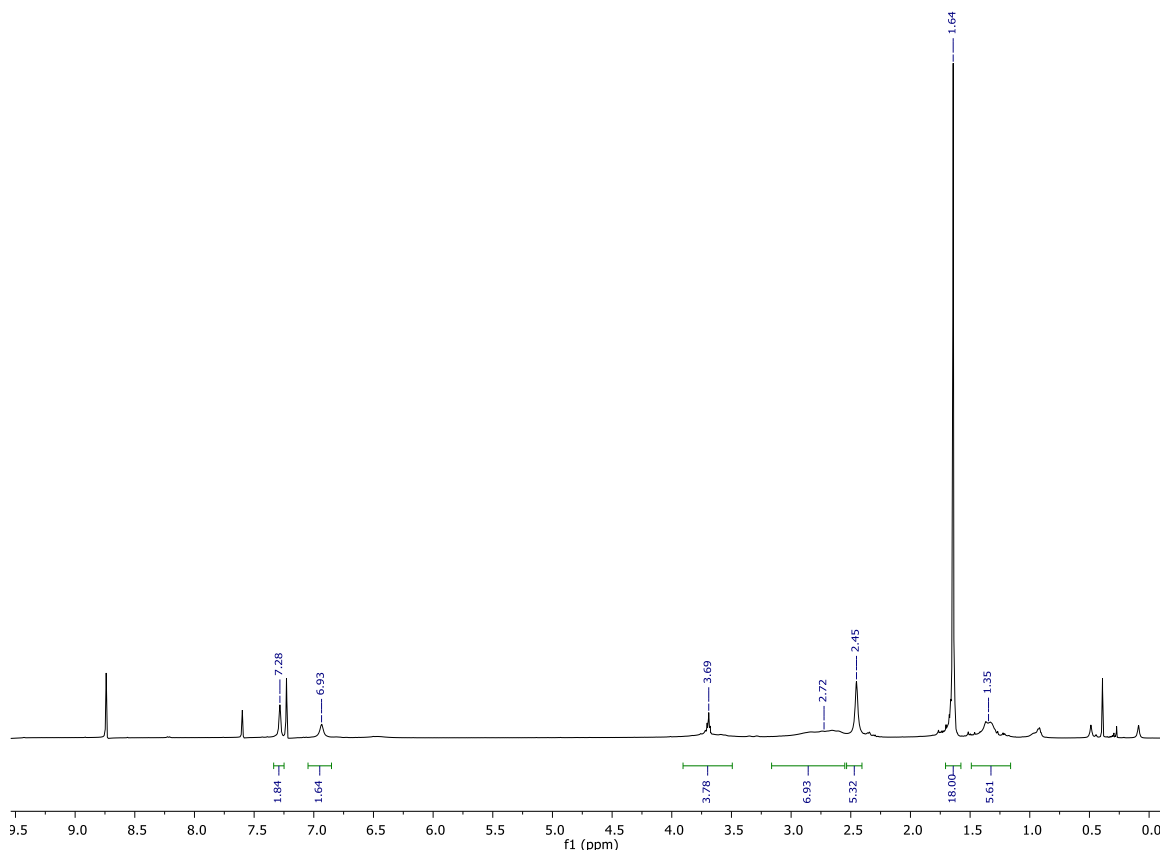


Figure 2.16. ^1H NMR spectrum (500 MHz, 308 K, $\text{C}_5\text{D}_5\text{N}$) of **2.7**. (Labels as shown in inset).

Pulse-gradient spin-echo (PGSE) NMR spectroscopy is a useful way to determine the size of molecules in solution.⁴² As polymerization reactions were performed in dichloromethane, the nuclearity of **2.4** in CD_2Cl_2 was assessed by PGSE NMR spectroscopy. The value of the hydrodynamic radius ($r_{\text{H,PGSE}}$) of **2.4** was calculated using a previously described method and found to be 15.1 Å.¹² This is moderately smaller than $r_{\text{X-ray}} = 18.76$ Å, which was calculated according to $r_{\text{X-ray}} = (a^2b)^{1/3}$ where a and b are the major and minor semi-axes of the prolate ellipsoid formed by the complex, as determined

from the solid-state structure ($a = 19.94 \text{ \AA}$, $b = 16.61 \text{ \AA}$). This indicates that **2.4** likely retains its tetrametallic structure in this noncoordinating solvent. However, it should be noted that this data reflects the solution-state structure at room temperature and the dinuclear species may exist at elevated temperatures. Although many previously reported Li_4 phenolate complexes disaggregate in solution, the Kerton group has recently published a closely related Li_4 complex that also retains its aggregated state at room temperature in solution.⁴³

2.2.4 Polymerization of *rac*-lactide

The catalytic behavior of **2.4**, **2.5**, **2.6** and **2.7** in the ring-opening polymerization of *rac*-lactide in the presence and absence of benzyl alcohol as co-initiator was investigated.

2.2.4.1 Solvent free polymerization

In order to reduce reaction times and achieve higher turnover frequencies,^{44,45} polymerization reactions were conducted under bulk/melt conditions at high temperatures. The results are summarized in **Table 2.3**. ROP reactions were performed with **2.4**, **2.5**, **2.6** and **2.7** at $150 \text{ }^\circ\text{C}$ and no significant differences in reactivity were observed. All complexes were stable and capable of initiating the ROP of *rac*-lactide, with benzyl alcohol (BnOH) (entries 5–8) or without benzyl alcohol (BnOH) (entries 1–4). Under these conditions, PLA molecular weights were slightly lower for reactions in the presence of BnOH. Compared to work done previously with main group metals under the same conditions but with higher monomer loadings (greater than 50), higher conversions could be achieved in shorter reaction times with lower dispersity values using

these complexes.⁴⁶⁻⁴⁸ To study the effect of the temperature and the co-initiator, **2.6** was further scrutinized (entries 9–12). The complex was able to efficiently polymerize *rac*-lactide at 130 °C, which is particularly relevant to industry.⁴⁴ For bulk polymerization, studies indicate a pseudo first-order dependence on monomer concentration as shown in conversion vs. time plots (**Figure 2.17**). However, kinetic data cannot be obtained from such graphs because the reaction proceeds too quickly to ascertain initial rates where *rac*-lactide concentrations will still be high.

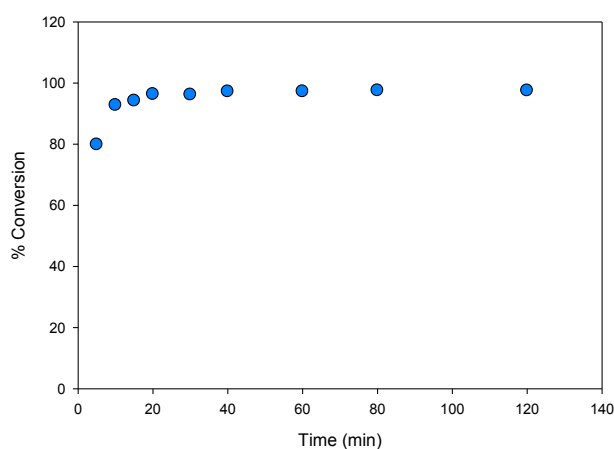


Figure 2.17. Conversion (%) vs. time for the ROP of LA initiated by **2.6** under the conditions in **Table 2.3**, entry 9.

As expected it was found that the conversion rates were greater with BnOH than without it (entries 9 and 11). The control of macromolecular features is also much improved when BnOH is used, both in terms of dispersities and agreement between M_{ncal} vs. M_n . All the generated polymers have molecular weights higher than the theoretical values (M_{ncal}), which might be attributed to intermolecular transesterification reactions,^{49,50} but are less significant in reactions when BnOH is present. Notably, the obtained dispersities (with or without BnOH) were more narrow than previously reported

values⁴⁶⁻⁴⁸ for polymers prepared in the melt-phase, suggesting a more controlled polymerization. It should be noted that the M_n values increase moderately with longer reaction times (entries 11 and 12). In addition, there was no significant difference in the molecular weights between the polymers produced at 150 °C and 130 °C. However, lower molecular weights were observed when polymerizations were run with higher monomer loadings (entries 13 and 14).

Table 2.3. Polymerization of *rac*-lactide using **2.4**, **2.5**, **2.6** and **2.7** in the presence and absence of BnOH in the melt phase

Entry	Complex	[LA] ₀ /[M] ₀ /[BnOH] ₀	t/min	T/°C	Conv /% ^[a]	$M_{n,cal}^{[b]} \times 10^3$	$M_n^{[c]} \times 10^3$	$M_w/M_n^{[c]}$
1	2.4	50/1/0	90	150	98	7.1	13.0	1.30
2	2.5	50/1/0	90	150	97	7.0	10.2	1.10
3	2.6	50/1/0	90	150	99	7.1	12.0	1.14
4	2.7	50/1/0	90	150	96	7.0	11.3	1.20
5	2.4	50/1/1	90	150	98	7.1	8.2	1.05
6	2.5	50/1/1	90	150	98	7.2	9.2	1.06
7	2.6	50/1/1	90	150	99	7.2	9.0	1.20
8	2.7	50/1/0	90	150	99	7.2	10.3	1.10
9	2.6	50/1/0	10	130	93	6.7	14.0	1.14
10	2.6	50/1/0	120	130	98	7.0	16.2	1.21
11	2.6	50/1/1	5	130	97	7.1	9.4	1.04
12	2.6	50/1/1	120	130	99	7.2	11.0	1.18
13	2.5	250/1/0	90	150	73	26.3	8.0	1.22
14	2.5	250/1/1	90	150	99	35.8	6.4	1.18

[a] Determined by ¹H NMR spectroscopy. [b] The $M_{n,cal}$ value of the polymer was calculated with $M_{n,cal} = ([LA]_0/[M]_0) \times 144.13 \times \text{conv. \%}/[BnOH] + 108.14$. [c] M_n (g mol⁻¹) determined by triple detection gel permeation chromatography (GPC) in THF using a dn/dc value of 0.049 mL g⁻¹.

2.2.4.2 Polymerizations in solution

2.4–2.7 were examined for ROP of *rac*-lactide in CH₂Cl₂ at room temperature. To examine solvent effects that may influence activities in these reactions, polymerization with **2.6** was further explored in THF and toluene. Representative results are reported in **Table 2.4**. Comparison between melt phase and solution polymerization data (**Table 2.3**, melt phase, entries 13 and 14, and **Table 2.4**, CH₂Cl₂, entries 7 and 8) shows that although polymer dispersities are similar, the molecular weights of polymers prepared in solution are higher and in closer agreement with theoretically predicted values than those obtained under melt phase conditions. This difference is seen both in the presence and absence of BnOH. All solution polymerizations showed a first-order dependence on lactide concentration in the form of a linear relationship of $\ln([LA]_0/[LA]_t)$ versus time as shown in **Figure 2.18–Figure 2.28**.

Table 2.4. Polymerization of *rac*-lactide using **2.4**, **2.5**, **2.6** and **2.7** in the presence and absence of BnOH

Entry	Complex	[LA] ₀ /[M] ₀ /[BnOH] ₀	t/min	Conv /% ^[d]	$M_{\text{ncal}}^{[e]} \times 10^3$	$M_n^{[f]} \times 10^3$	$M_w/M_n^{[f]}$
1	2.4	250/1/0 ^[a]	80	92	33.1	28.0	1.31
2	2.4	250/1/1 ^[a]	80	93	33.6	17.2	1.29
3	2.4	250/1/2 ^[a]	40	92	16.7	8.00	1.15
4	2.4	250/1/2 ^[a]	300	99	17.9	12.1	1.24
5	2.4	250/1/4 ^[a]	30	90	8.2	4.00	1.19
6	2.4	250/1/4 ^[a]	300	95	8.7	7.80	1.15
7	2.5^k	250/1/0 ^[a]	40	73	26.3	24.0	1.30
8	2.5^k	250/1/1 ^[a]	7	93	33.6	19.0	1.18
9 ^h	2.5^k	250/1/0 ^[a]	60	53	19.1	13.0	1.11
10	2.5^k	250/1/0 ^[c]	180	55	19.8	21.0	1.10
11	2.6^k	50/1/0 ^[a]	5	100	7.2	ND	–
12	2.6^k	250/1/0 ^[a]	80	94	33.9	33.4	1.33
13	2.6^k	250/1/1 ^[a]	80	91	33.0	29.6	1.32
14	2.6^k	250/1/0 ^[b]	180	69	24.9	ND ^[g]	-
15	2.6^k	250/1/1 ^[b]	120	93	33.6	ND ^[g]	-
16	2.6^k	250/1/0 ^[c]	240	52	18.7	ND ^[g]	-
17	2.6^k	250/1/1 ^[c]	3	98	35.4	ND ^[g]	-
18	2.7	250/1/0 ^[a]	40	91	32.8	26.3	1.20
19	2.7	250/1/1 ^[a]	5	94	34.1	22.4	1.36
20	2.7	250/1/1 ^[a]	300	99	35.8	34.8	1.22
21	2.7	250/1/0 ^[c]	3	90	32.4	36.2	1.41
22	2.7	250/1/1 ^[c]	3	100	36.1	20.2	1.10
23 ⁱ	n-BuLi	250/1/1 ^[a]	60	96	34.7	11.8	1.13
24 ^j	NaH	250/1/1 ^[a]	>540	65	23.5	11.7	1.47

All reactions performed at 25 °C [a] CH₂Cl₂ (5 mL). [b] Toluene (30 mL). [c] THF (20 mL). [d] Determined by ¹H NMR spectroscopy. [e] The M_{ncal} value of the polymer was calculated with $M_{\text{ncal}} = ([\text{LA}]_0/[\text{M}]_0) \times 144.13 \times \text{conv. \%}/[\text{BnOH}] + 108.14$. [f] The M_n (g mol⁻¹) determined by triple detection gel permeation

chromatography (GPC) in THF using a dn/dc value of 0.049 mL g^{-1} . [g] Low molecular weight oligomers formed. Data from NMR end group analysis: $M_n \sim 5384 \text{ g mol}^{-1}$. [h] CH_2Cl_2 (20 mL). [i] 0.2 mL $n\text{-BuLi}$ (0.16 M, 0.02 mmol) was added to CH_2Cl_2 solution (5 mL) containing *rac*-lactide (2.95 mmol) and BnOH (0.0118) at 25 °C. [j] NaH (0.16 M, 0.047 mmol) was added to CH_2Cl_2 solution (5 mL) containing *rac*-lactide (2.95 mmol) and BnOH (0.0118 mmol) at 25 °C. [k] P_r values for polymers produced by **2.5** and **2.6** were typically 0.44-0.47.

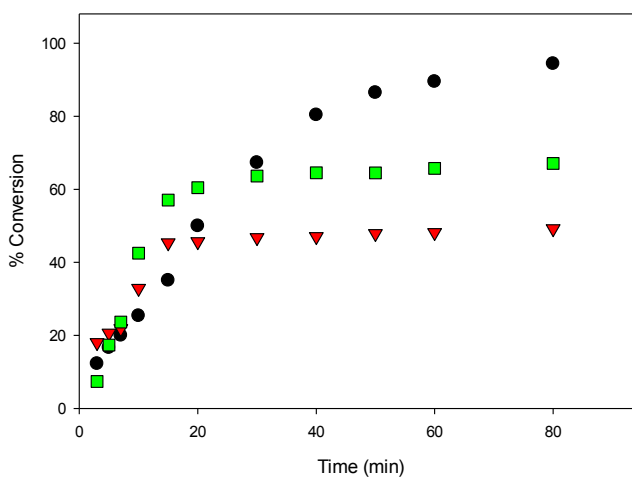


Figure 2.18. Conversion (%) vs. time for the ROP of LA initiated by **2.6** [conditions: 2.95 mmol LA, 250 LA :1 Li :0 BnOH, 25 °C]. ● CH_2Cl_2 (5 mL), ■ Toluene (30 mL), ▼ THF (20 mL).

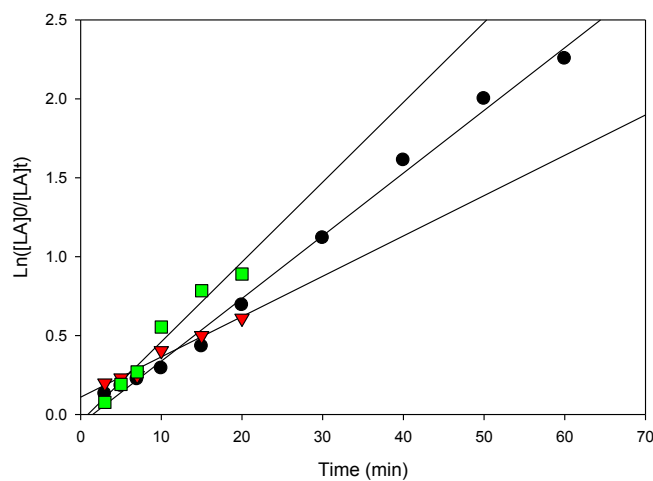


Figure 2.19. First-order plot of LA consumption initiated by **2.6** [conditions: 2.95 mmol LA, 250 LA :1 Li :0 BnOH, 25 °C]. ● CH₂Cl₂ (5 mL, $y = 0.0397x - 0.0594$, $R^2 = 0.9933$), ■ Toluene (30 mL, $0.0506x - 0.0448$, $R^2 = 0.96$), ▼ THF (20 mL $y = 0.0255x + 0.1097$, $R^2 = 0.9742$).

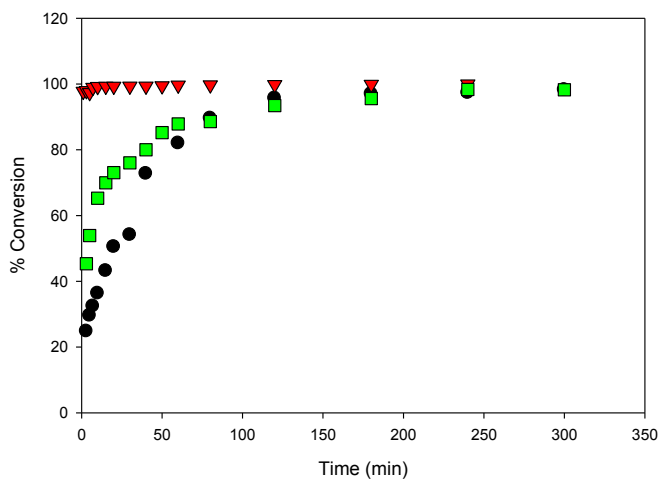


Figure 2.20. Conversion (%) vs. time for the ROP of LA initiated by **2.6** under the conditions in **Table 2.4**, entries 13, 15 and 17. ● CH₂Cl₂, ■ Toluene, ▼ THF.

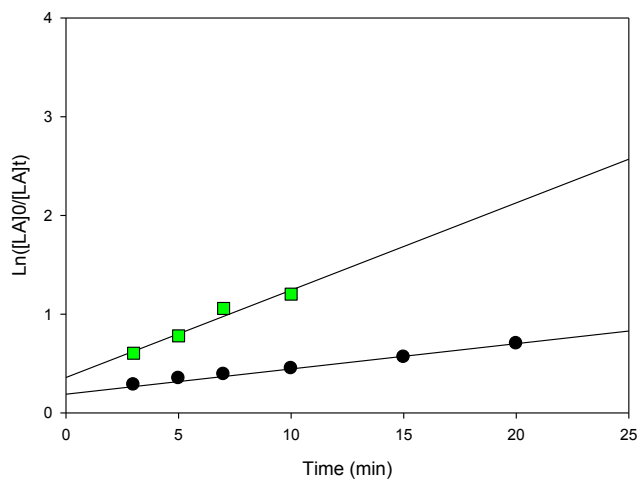


Figure 2.21. First-order plot of LA consumption initiated by **2.6** according to the conditions in **Table 2.4**, entries 13 and 15. ● CH₂Cl₂ ($y = 0.0256x + 0.1897$, $R^2 = 0.9894$), ■ Toluene ($y = 0.0884x + 0.3487$, $R^2 = 0.9593$).

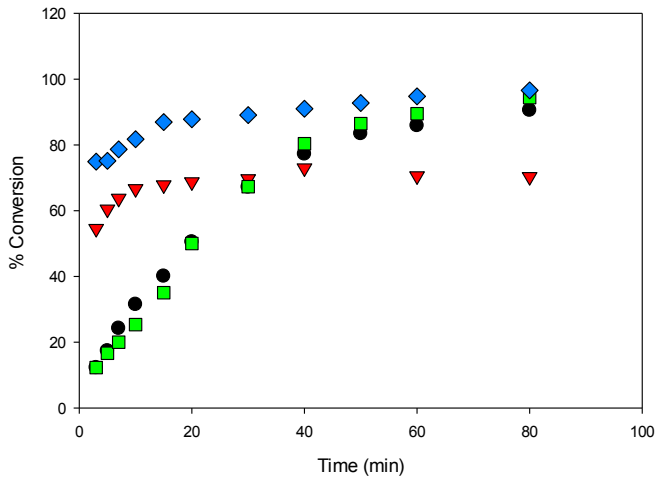


Figure 2.22. Conversion (%) vs. time for the ROP of LA initiated by **2.4**, **2.5**, **2.6** and **2.7** in CH₂Cl₂ (5 mL) [conditions: 2.95 mmol LA, 250 LA :1 M :0 BnOH, 25 °C]. ● **2.4**, ▼ **2.5**, ■ **2.6**, ◆ **2.7**.

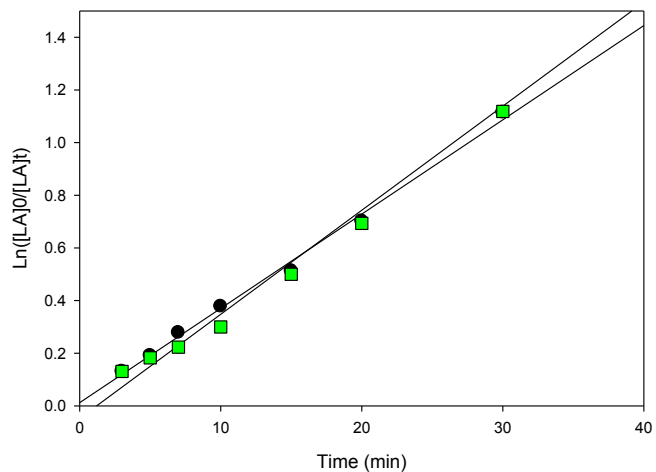


Figure 2.23. First-order plot of LA consumption initiated by **2.4** and **2.6** in CH₂Cl₂ (5 mL) [conditions: 2.95 mmol LA, 250 LA :1 Li :0 BnOH, 25 °C]. ● **2.4** ($y = 0.0358x + 0.0123$, $R^2 = 0.9954$), ■ **2.6** ($y = 0.0395x - 0.0471$, $R^2 = 0.9951$).

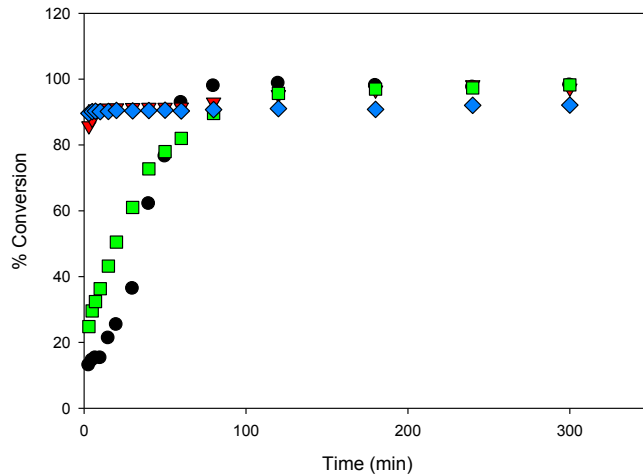


Figure 2.24. Conversion (%) vs. time for the ROP of LA initiated by **2.4**, **2.5**, **2.6** and **2.7** in CH₂Cl₂ under the conditions in **Table 2.4**, entries 2, 8, 13 and 19. ● **2.4**, ▼ **2.5**, ■ **2.6**, ◆ **2.7**.

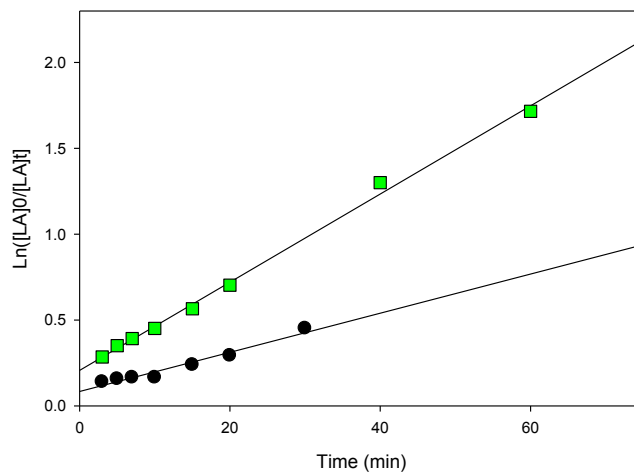


Figure 2.25. First-order plot of LA consumption initiated by **2.4** and **2.6** in CH_2Cl_2 under the conditions in **Table 2.4**, entries 2 and 13. ● **2.4** ($y = 0.0114x + 0.0834$, $R^2 = 0.96$), ■ **2.6** ($y = 0.0257x + 0.2068$, $R^2 = 0.9983$).

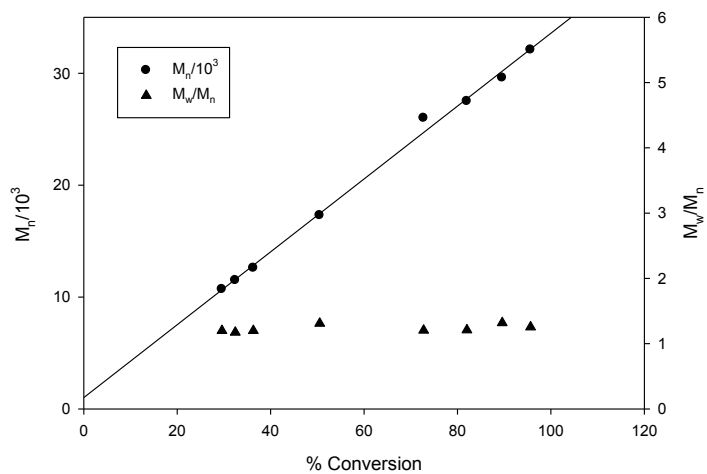


Figure 2.26. Plot of PLA M_n and dispersity (M_w/M_n) as a function of *rac*-lactide conversion under the conditions in **Table 2.4**, entries 13. Line shown to indicate the linear trend and proportional increases in M_n as conversion increases.

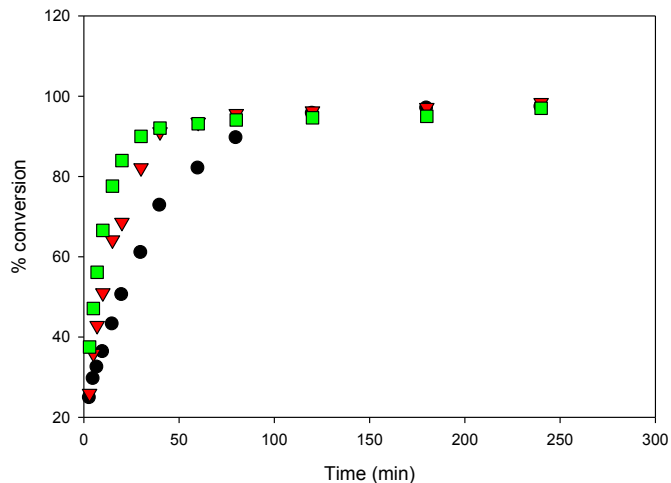


Figure 2.27. Conversion (%) vs. time for the ROP of LA initiated by **2.4** in CH_2Cl_2 under the conditions in **Table 2.4**, entries 2, 3 and 5. ● 1 eq. BnOH, ▼ 2 eq. BnOH, ■ 4 eq. BnOH.

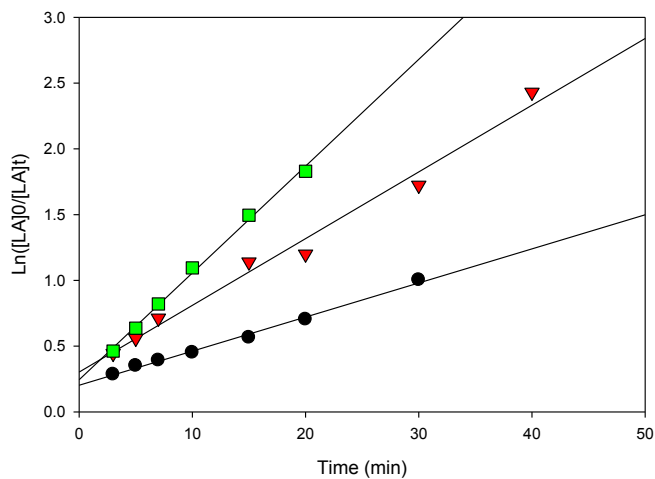


Figure 2.28. First-order plot of LA consumption initiated by **2.4** with different quantities of BnOH [conditions: CH_2Cl_2 (5 mL), 2.95 mmol LA, 250 LA : 1 Li : n BnOH, 25 °C]. ● CH_2Cl_2 1 eq. BnOH ($y = 0.0507x + 0.3033$, $R^2 = 0.9858$), ▼ 2 eq. BnOH ($y = 0.0259x + 0.2026$, $R^2 = 0.9944$), ■ 4 eq. BnOH ($y = 0.0812x + 0.2446$, $R^2 = 0.9963$).

Polymerization data (**Table 2.4**) shows that catalytic activities were strongly influenced by the nature of the solvent and the presence of BnOH (co-initiator). It should be noted that a large amount of toluene (30 mL) was essential due to the low solubility of

LA in toluene at room temperature. Performing the reaction in CH₂Cl₂ (entry 12) in the absence of BnOH using **2.6** resulted in a much faster reaction compared to toluene and THF (entries 14 and 16) with high conversion after only 80 min. Furthermore, the molecular weights of the polymers obtained in toluene and THF were very low (~5384 g mol⁻¹) despite moderate conversion levels (entries 14-17). Due to the high solubility of both LA and catalysts in CH₂Cl₂, reactions in this solvent normally contained 2.95 mmol of LA and the desired amount of catalyst in 5 mL. When reactions were performed using **2.5** under similar conditions (entries 7 and 9) but using different volumes of CH₂Cl₂ (30 mL), *M_n* values were lower than theoretically predicted under more dilute reaction conditions whereas good agreement with calculated *M_n* values was seen when only 5 mL CH₂Cl₂ was used. This shows that in addition to rate effects, the volume of solvent used can also affect polymerization reactions in terms of polymer properties. Compared to CH₂Cl₂ and toluene, lower conversions were observed when THF was employed and this could be due to the coordinating nature of THF, which competes with the incoming monomer for coordination at the metal centre (entry 16 compared with entries 12 and 14).^{13,48,51} Moreover, BnOH is able to significantly speed up the polymerizations carried out in THF (entry 17), whereas little difference in activities were observed for both CH₂Cl₂ and toluene (entries 13 and 15). Therefore, kinetic data for reactions performed in THF in the presence of BnOH could not be accurately obtained, as assumptions regarding the steady-state concentration of *rac*-lactide could not be made (**Figure 2.20**). It should be noted that with **2.6** low molecular weight oligomers were likely obtained when toluene and THF were used (entries 14–17) because no polymer precipitated upon the addition of cold methanol to reaction mixtures and therefore, GPC data were not obtained for these

samples. The formation of low molecular weight species was confirmed by end group analysis using ^1H NMR of the polymers. Integration of the $-\text{OH}$ end group resonance relative to the CH_3 group showed that low molecular weight polymer formed ($M_n = 5384 \text{ g mol}^{-1}$). The steric bulk of substituents on the aromatic rings was found to have less influence on the activity compared to the identity of the metal centre (entries 1 and 12). That is, the activity trend decreases in the order $2.7 > 2.5 > 2.6 \geq 2.4$ and can be partially explained by the larger ionic radius of sodium compared to lithium.^{14,21,22,52} It is not surprising that the co-initiator is not required for ROP catalyzed by **2.4** and **2.6** as the same observation was reported by Kozak's group for related amino-bis(phenolate) lithium complexes.¹¹ In contrast, the presence of the co-initiator was necessary to accelerate reactions using sodium complexes (entries 18 and 19) and this has also been reported by others.^{23,41} The observed M_n values of these solution-phase polymers are in some cases close to the expected molecular weights and the low dispersities obtained (ranging from 1.10–1.36) indicated that the polymerization has characteristics of controlled propagation. The controlled behavior is also demonstrated by the linear relationship between M_n and % conversion, and the narrow dispersity of the polymers throughout their chain growth (**Figure 2.26**).^{12,50,53} Increasing the amount of BnOH can be used to control both the molecular weight and the polymerization rate. For instance, upon doubling the amount of alcohol to two equiv. per lithium centre, the molecular weight of the polymer diminished to half its original value (entries 2 and 3), while it decreased to one quarter with the addition of four equiv. of BnOH (entries 2 and 4). In addition, as shown in **Figure 2.27** and **Figure 2.28**, in both cases, the reaction rates are faster compared to performing the reaction with one equiv. of BnOH. Such observations are an important feature of well-

behaved immortal ROP with reversible and fast chain transfer between dormant and growing macroalcohols.^{12,50} Performing the reaction at longer times gives higher molecular weight compared with short reaction times (*e.g.* entries 3 and 4) suggesting the occurrence of chain transfer reactions during polymerization.^{12,46} We propose that once LA conversion is close to completion, the lithium-polymeryl species undergo intermolecular chain transfer (as there is little remaining monomer to react with) and this leads to higher M_n values. Moreover, a comparison of the catalytic activities of **2.4–2.7** and diamino-bis(phenolate)-free systems (*i.e.*, control reactions) has been undertaken under identical ROP conditions. These polymerization systems use the precursor metal reagents as initiators and no phenolic ligand. One equiv. of *n*-BuLi or four equiv. NaH was added into a CH₂Cl₂ solution containing 250 equiv. of *rac*-lactide and one equiv. of BnOH (entries 23 and 24). ROP of lactide using the *in situ* formed lithium alkoxide was complete within 60 min with a conversion of 96% whereas the sodium alkoxide exhibited lower efficiency with moderate conversion (65%) and a more disperse polymer was produced. All the generated polymers from phenolate-free systems had lower molecular weights than those produced with **2.4–2.7**.

2.2.4.3 NMR spectroscopy of polymers in bulk and solvent polymerization

Similar signals were found in ¹H NMR spectra for the polymers from reactions performed in both the absence and the presence of one equiv. BnOH: a hydroxyl group (d) at 2.72 ppm, a hydroxymethine group (HOCH–) (c) at 4.35 ppm, methyl groups (CH–CH₃) (a) between 1.50 and 1.55 ppm (**Figure 2.29**).¹¹ No evidence for benzyl ester group formation could be found when one equiv. BnOH was added, suggesting the presence of

inter or intratransesterification reactions. However, a benzyl ester group (OCH₂Ph) (e) at 7.32 ppm, hydroxyl group (f) and hydroxymethine group (HOCH-) (c) at 4.33 ppm were observed as end-groups with the addition of two and four equiv. BnOH (**Figure 2.30**). Determination of the polymer tacticity was achieved by homodecoupled ¹H and ¹³C NMR experiments (**Figure 2.31** and **Figure 2.32** respectively). The probability of racemic enchainment (probability of forming a new racemic diad) was calculated from the deconvoluted homonuclear decoupled ¹H NMR spectra.⁵⁴ The *P_r* values for polymers produced by **2.5** and **2.6** are within the range of 0.44–0.47, which indicates a negligible isotactic bias (a value of 0.5 is expected for a perfectly atactic polymer).⁴¹ Isotactic polymers have previously been reported, in some cases, for lithium and sodium phenolates.^{11,41} In the ¹³C NMR spectra, the signal assignments in the methine region show multiple possible tetrad sequences *iii*, *iis*, *sii* and *isi* which is in good agreement with previously reported ROP of *rac*-lactide by an achiral catalyst.⁵⁵ However, the unusual increase in the intensity of the *iss*, *sss* and *ssi* tetrads in **Figure 2.31** and the presence of weaker peaks at 69.58, 69.47 and 69.25 ppm in **Figure 2.32** indicate stereorandom transesterification during the course of the polymerization reactions.^{11,41,56}

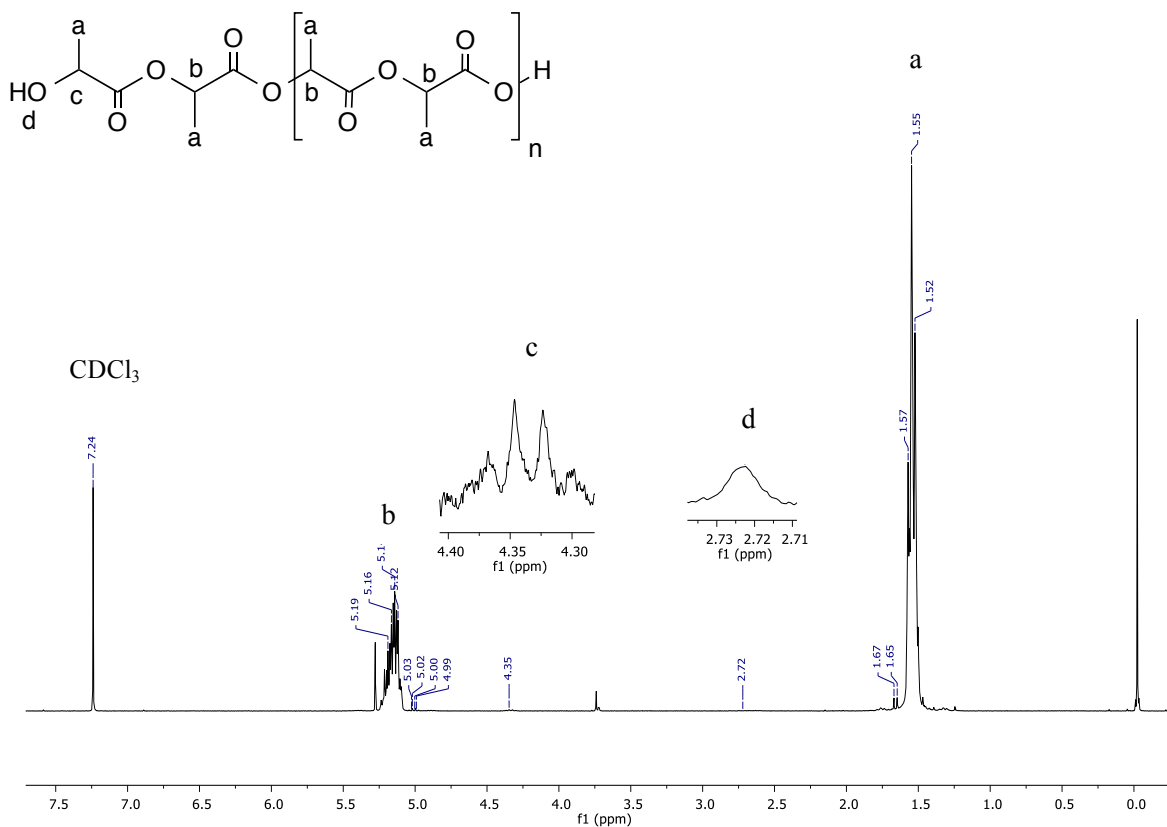


Figure 2.29. ¹H NMR spectrum in CDCl₃ of PLA obtained under the conditions in **Table 2.4**, entry 12, similar spectra also obtained for entries 13, 18 and 19.

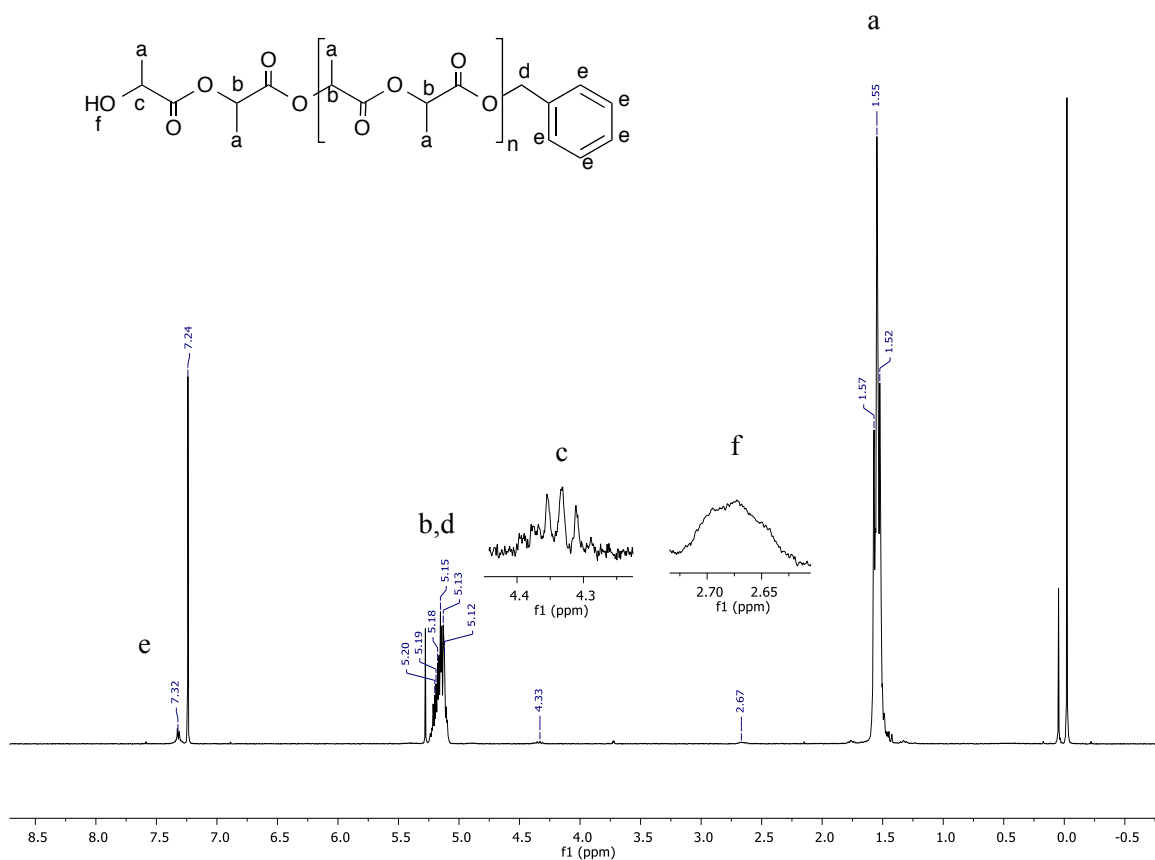


Figure 2.30. ¹H NMR spectrum in CDCl₃ of PLA obtained under the conditions in **Table 2.4**, entry 3, similar spectrum obtained for entry 5.

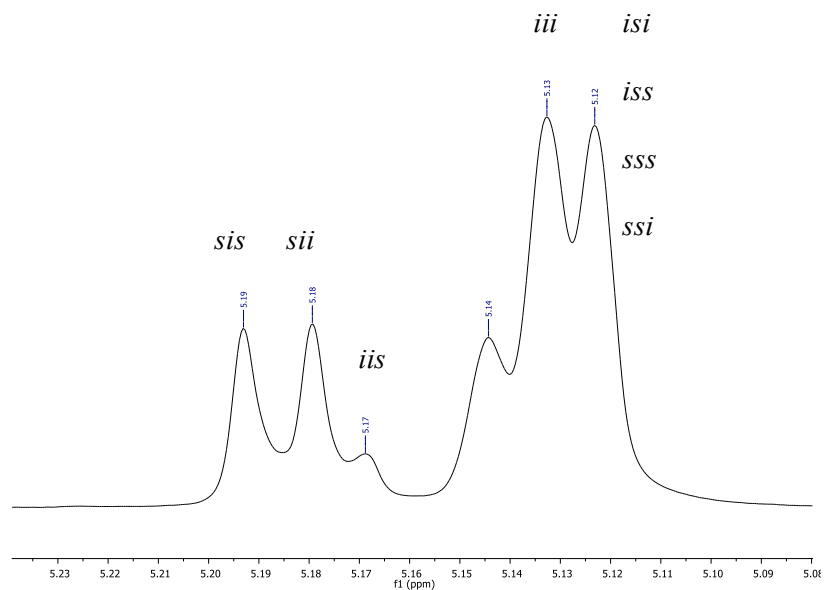


Figure 2.31. $^1\text{H}\{^1\text{H}\}$ NMR spectrum (500 MHz, CDCl_3) of the methine region of PLA produced under the conditions in **Table 2.4**, entry 7, similar results were obtained for entries 8, 12 and 13.

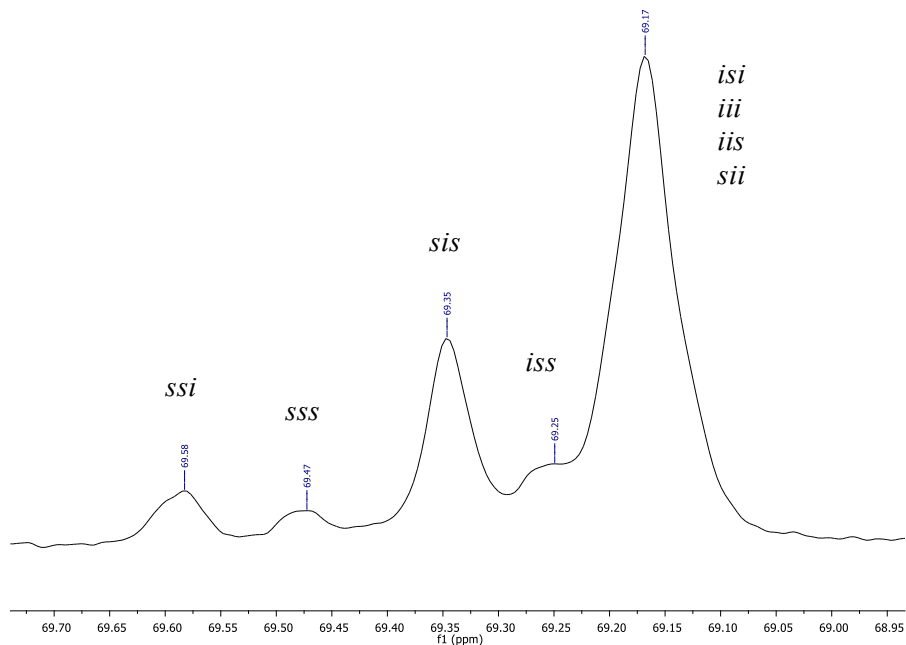


Figure 2.32. ^{13}C NMR spectrum (500 MHz, CDCl_3) of the methine region of PLA produced under the conditions in **Table 2.4**, entry 7, similar results were obtained for entries 8, 12 and 13.

2.2.4.4 Mass spectrometry of polymers

MALDI-TOF analysis of PLA was conducted with 2,5-dihydroxybenzoic acid (DHBA) as the matrix with a ratio of 5:1 (matrix:PLA). Using reflectron mode, the peaks are separated by 72 mass units and three major repeating masses were observed in the case of polymers obtained in the absence of BnOH and 1 equiv. BnOH. As shown in **Figure 2.33**, two intense peaks (B and C, $n = 12$, $m/z = 919$ and 935) were assigned as $\text{CH}_3\text{O}[(\text{C}=\text{O})\text{-CHMeO}]_n\text{H}\cdot\text{Na}^+$ and $\text{CH}_3\text{O}[(\text{C}=\text{O})\text{CHMeO}]_n\text{H}\cdot\text{K}^+$. In addition, a less intense series of peaks for cyclic polymer (A, $n = 12$, $m/z = 903$) clustered with a K^+ ion were seen, pointing to the presence of intrachain transesterification side reactions. The termination with methoxy groups probably stems from initiation of polymerization by nucleophilic attack of the phenolate oxygen on the carbonyl followed by quenching with methanol. Similar end-groups have been observed by others recently.⁵⁷ The polymers formed with 2 and 4 equiv. BnOH show only one major repeating series (A, $n = 12$, $m/z = 919$) that corresponds to polymers capped with methoxy groups $\text{CH}_3\text{O}[(\text{C}=\text{O})\text{-CHMeO}]_n\text{H}\cdot\text{Na}^+$ without any evidence for cyclic formation or the benzyl ester groups (**Figure 2.34**). This contrasts with the NMR data obtained, which showed the presence of the expected benzyl ester groups.

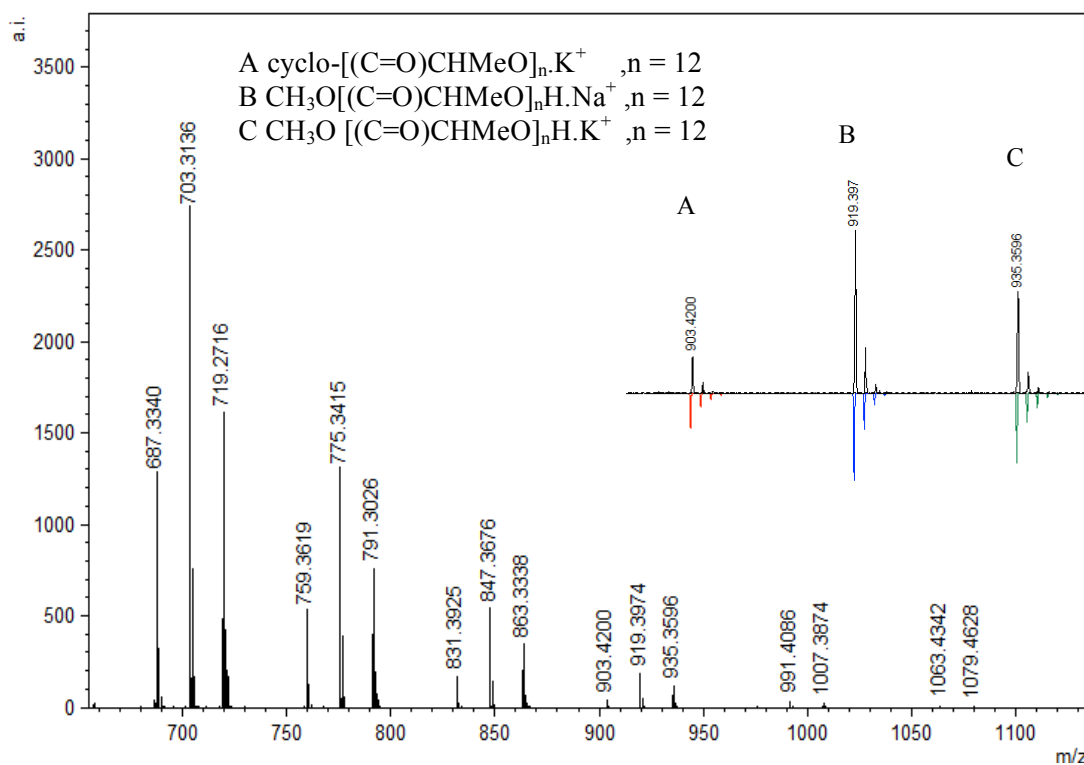


Figure 2.33. Representative region of the MALDI-TOF mass spectrum (reflectron mode) of PLA formed using **2.6** under the following conditions: CH₂Cl₂ (5 mL), 2.95 mmol LA, 250 LA :1 Li :0 BnOH, 25 °C (similar spectra obtained for PLA from other reactions using no BnOH).

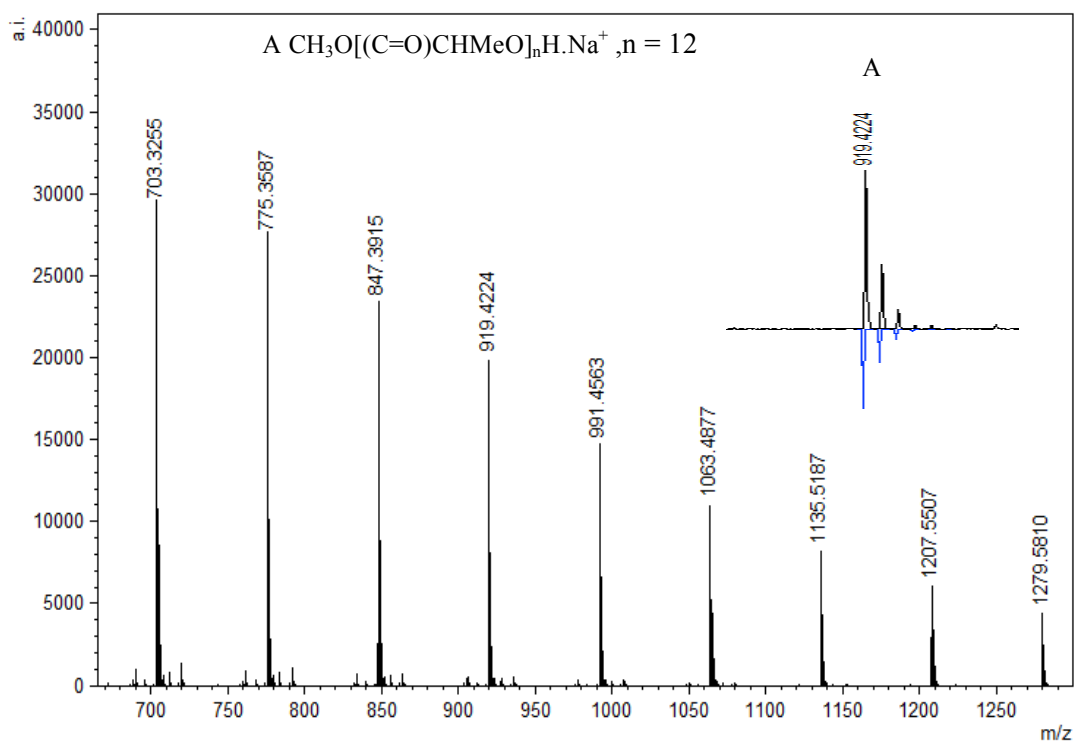


Figure 2.34. Representative region of the MALDI-TOF mass spectrum (reflectron mode) of PLA formed using **2.4** under the following conditions: CH₂Cl₂ (5 mL), 2.95 mmol LA, 250 LA :1 Li :2 BnOH, 25 °C.

2.1.1 Proposed Mechanism

In the absence of BnOH, the initiation step in the ROP of *rac*-lactide could be proceeding via coordination insertion of the monomer into the metal–phenoxide bond as shown in **Figure 2.35** and described in the literature for related metal–phenolate systems.^{3,10,11,13,20,58-60} Comparison of ⁷Li NMR spectra recorded in the absence and presence of *rac*-lactide suggests the formation of an additional Li species upon addition of a small amount of *rac*-lactide with the growth of a new peak at 1.30 ppm (**Figure 2.36**). This supports the monomer coordination step of the mechanisms described herein, but it should also be noted that these ⁷Li NMR spectra were obtained without BnOH. To investigate the ROP reaction in the presence of BnOH, stoichiometric reactions with **2.4** in CD₂Cl₂ at room temperature were monitored by ¹H NMR spectroscopy. The spectra of a 1:1 (per 2 metal centres) reaction of **2.4** and BnOH confirms the formation of both {L1}H (11.05 ppm) and BnO–Li, the latter appearing as overlapping peaks around 7.34 ppm (**Figure 2.38**, **Figure 2.39** and **Figure 2.40**). Similar observations have also been reported for related amino-phenolate systems by Chen and coworkers.¹⁶ Addition of 1 equiv. of *rac*-lactide should yield benzyl-2-((2-hydroxypropano-yl)oxy)propanoate, the product of lactide ring-opening. Unfortunately, we were unable to isolate this or identify resonances belonging to this species. In spite of this, we propose that ring-opening polymerization is occurring through a coordination–insertion mechanism, where benzyl alcohol is sufficiently activated by the lithium centres and protonates the phenolate group to yield a new lithium complex, followed by attack of the benzyl alkoxide group at the carbonyl group of *rac*-lactide (**Figure 2.37**).^{3,10,11,13,20,58-60} We also note that the reactivity of BnOLi formed in situ affords similar polymerization data (**Table 2.4**, entry 23). From

the DOSY NMR experiments above, the predominant Li species present in CD₂Cl₂ (in the absence of lactide and BnOH) is the tetralithium complex. Therefore, it is likely that the alcohol also plays a role in assisting the dissociation process in solution, as we assume this will occur under reaction conditions to allow space for the growing polymer chain. Further data would be required in order to confirm this assumption.

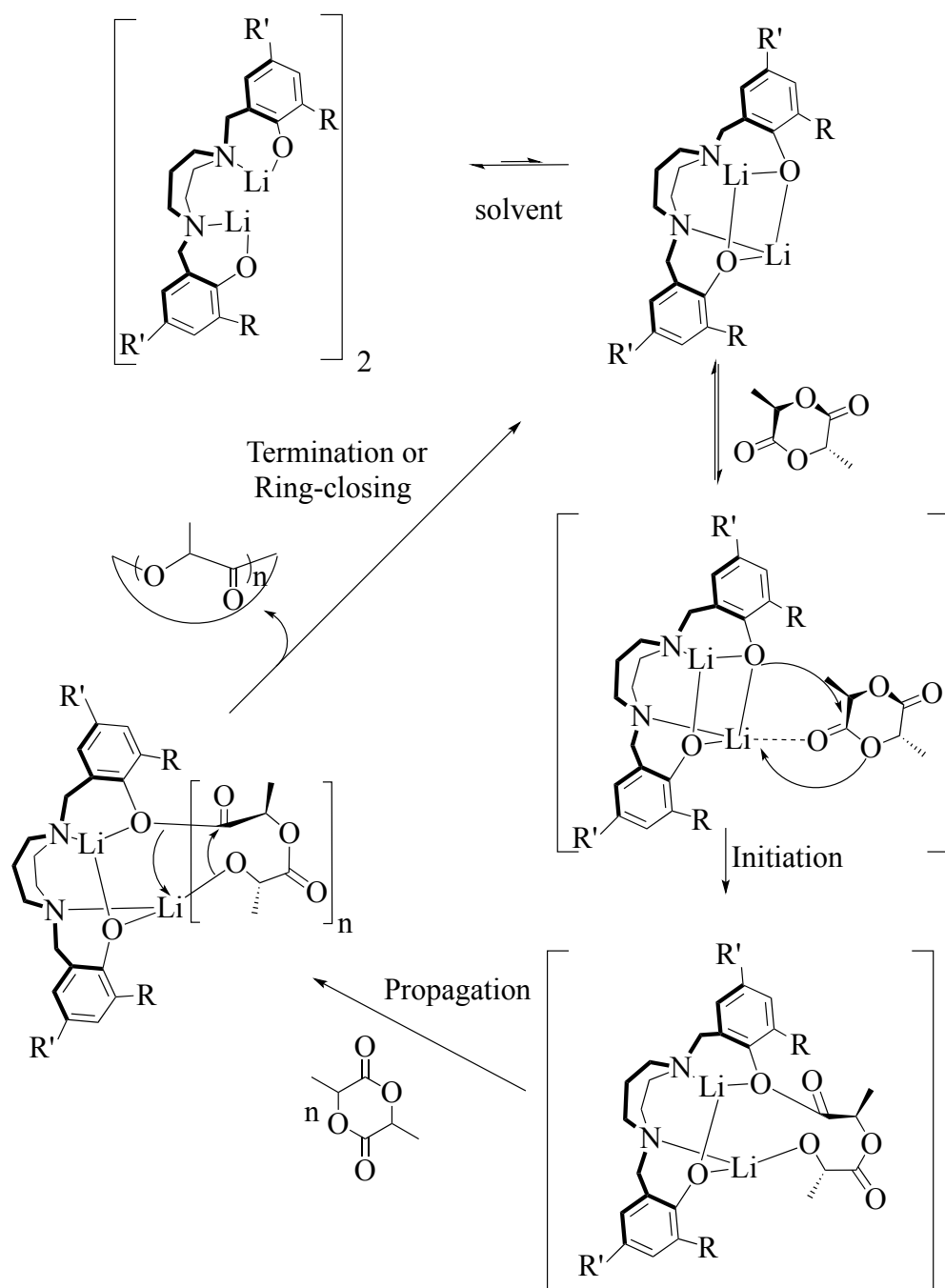


Figure 2.35. Proposed mechanism of the ROP of *rac*-LA in the absence of BnOH initiated by lithium and sodium diamino-bis(phenolate) complexes (THF omitted for clarity, coordination sphere of the metals will be completed by either LA or THF).

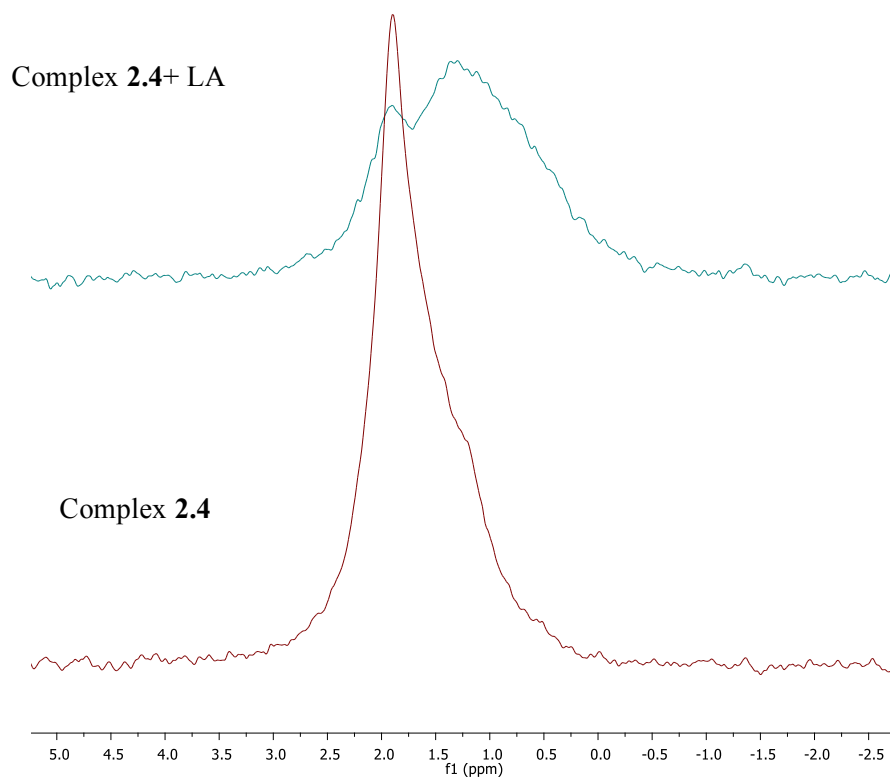


Figure 2.36. ^7Li NMR spectrum (116.6 MHz, C_6D_6) of **2.4**.

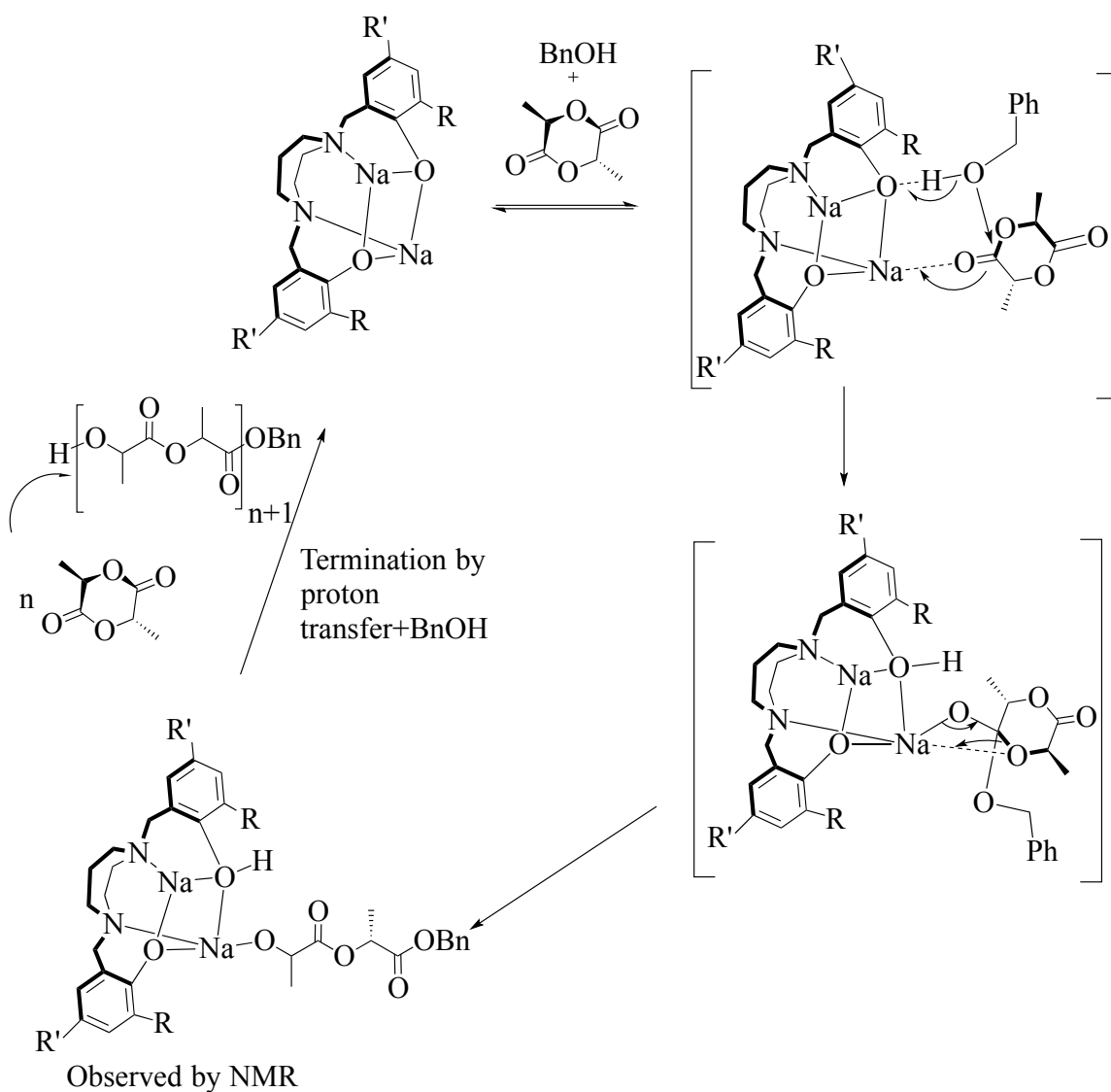


Figure 2.37. Proposed mechanism of the ROP of *rac*-LA in the presence of BnOH initiated by sodium diamino-bis(phenolate) complexes (THF omitted for clarity, coordination sphere of the metals will be completed by either LA or THF).

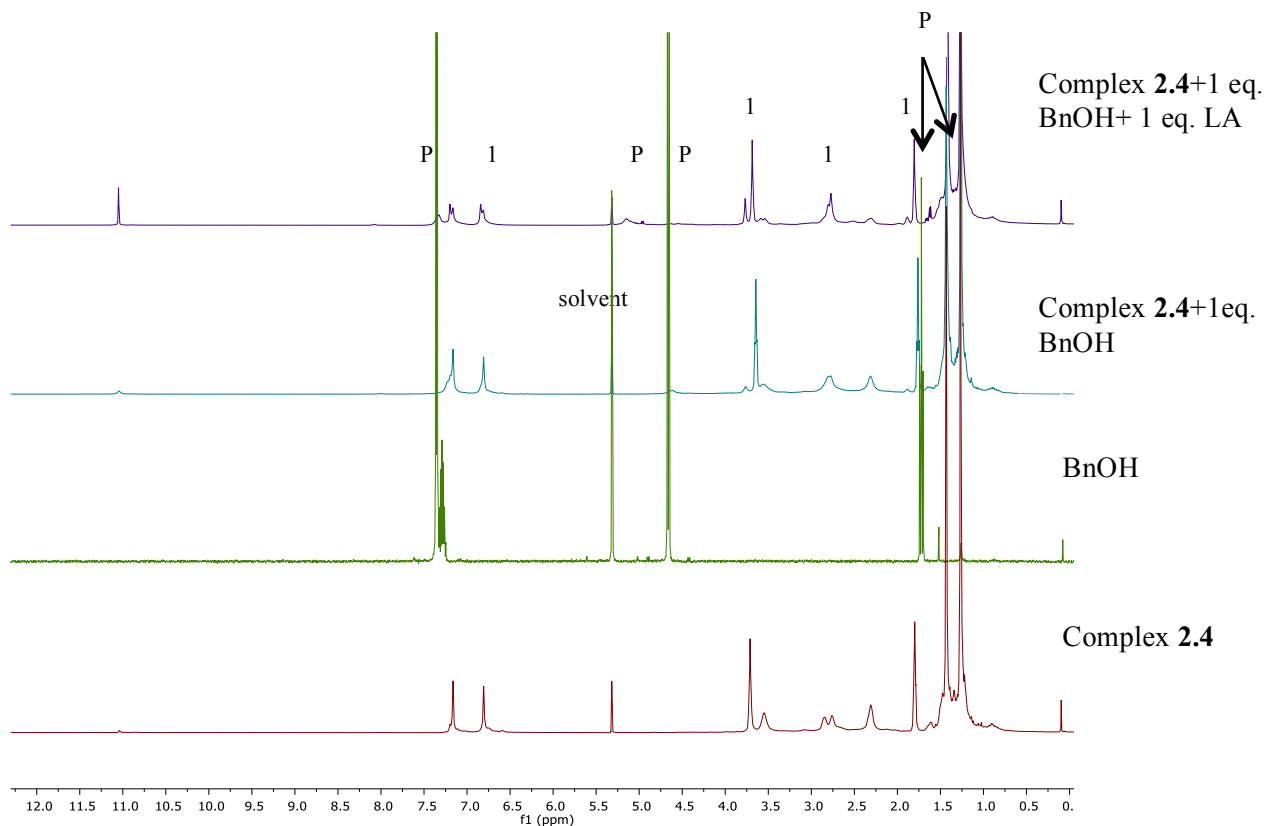


Figure 2.38. Monitoring of stoichiometric (M:BnOH:LA, 1:1 and 1:1:1) model reactions by ^1H NMR spectroscopy in dichloromethane- d_2 at 298 K (500 MHz).

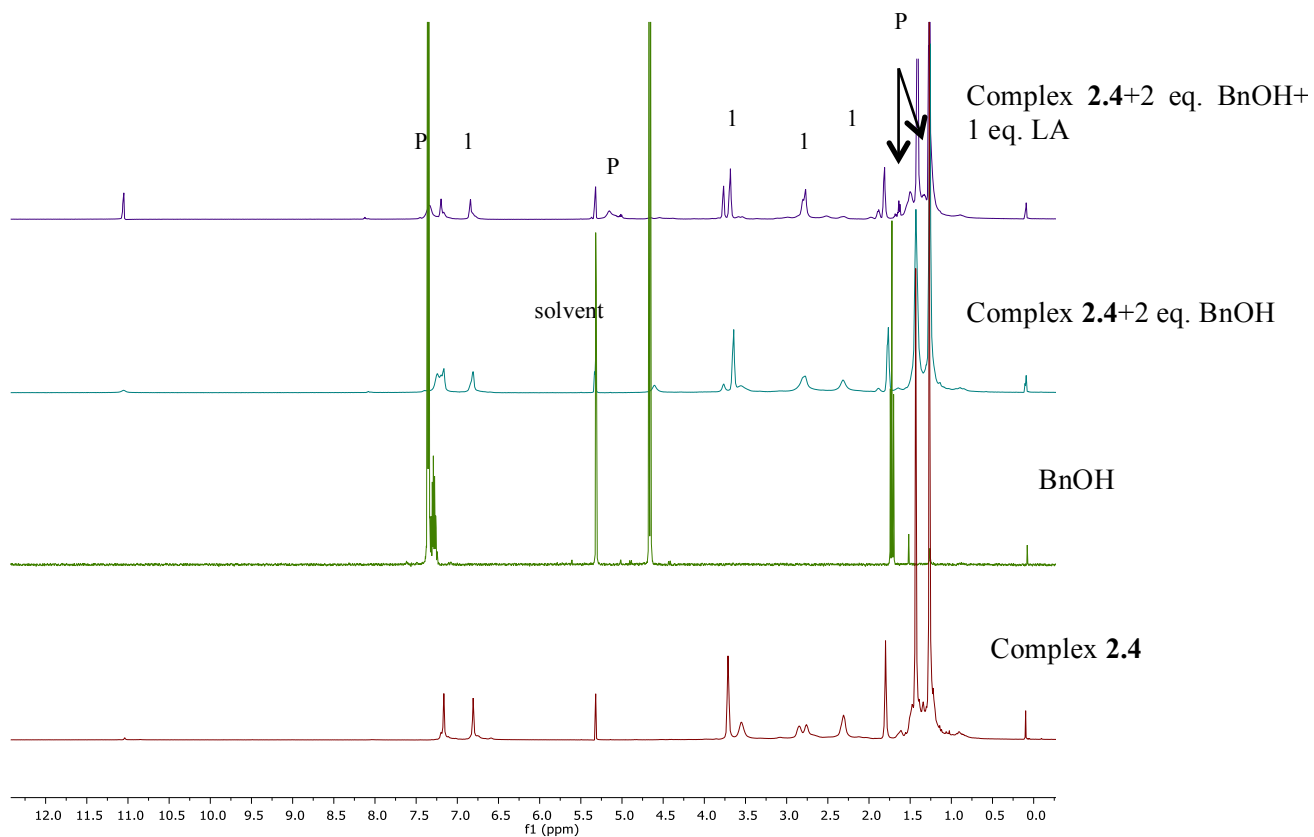


Figure 2.39. Monitoring of stoichiometric (M:BnOH:LA, 1:2 and 1:2:1) model reactions by ^1H NMR spectroscopy in dichloromethane- d_2 at 298 K (500 MHz).

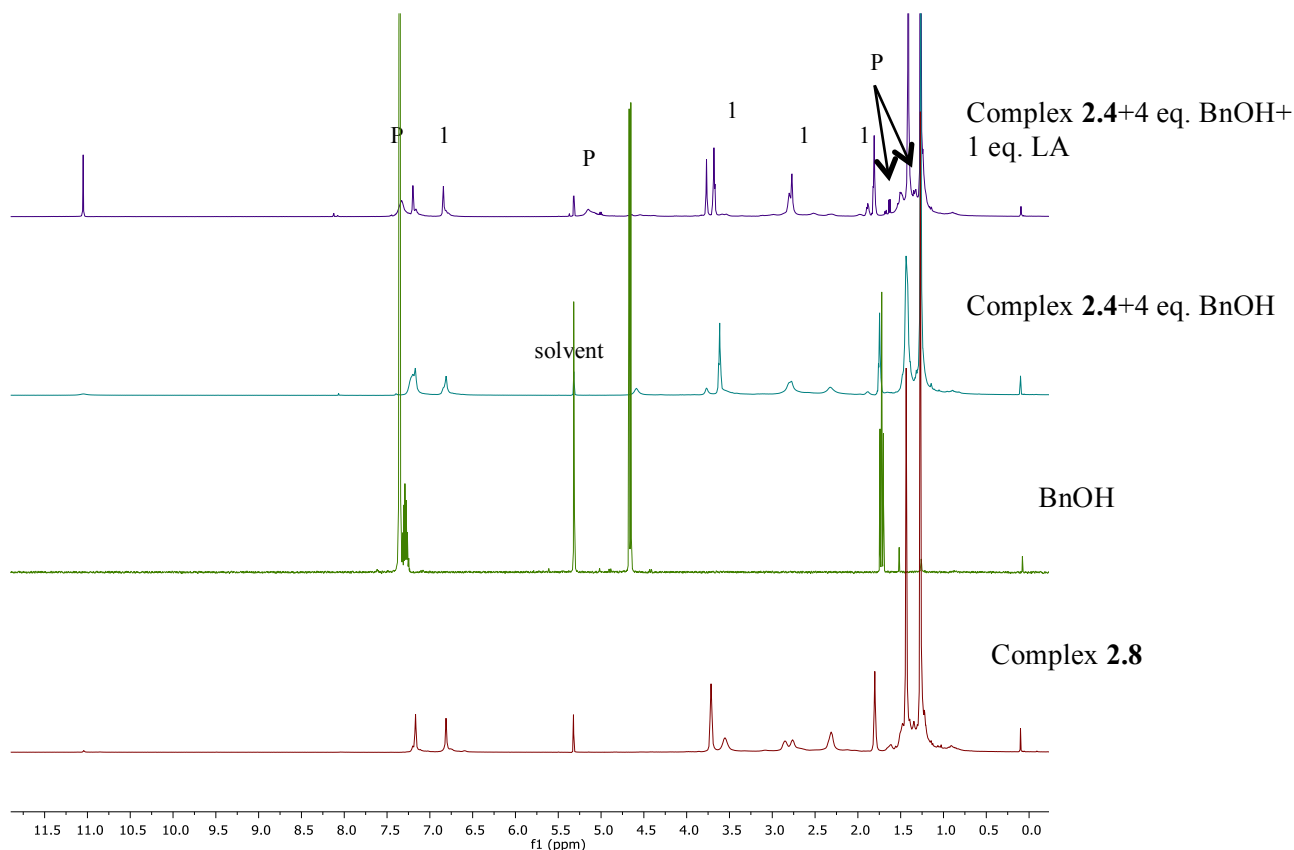


Figure 2.40. Monitoring of stoichiometric (M:BnOH:LA, 1:4 and 1:4:1) model reactions by ^1H NMR spectroscopy in dichloromethane- d_2 at 298 K (500 MHz).

2.3 Conclusions

In conclusion, we have prepared and characterized tetrametallic lithium and sodium diamino-bis(phenolate) complexes. At room temperature, these complexes demonstrate good activity for ring-opening polymerization of *rac*-lactide both in the absence and presence of benzyl alcohol to yield polymers with narrow dispersities. The effect of solvents on the ROP reactions was studied. The sodium complexes outperform their lithium analogues especially in the presence of BnOH. We note that the effect of BnOH on the lithium initiators is negligible. The molecular weight of PLAs can be tuned according to the monomer: alcohol ratio, where increasing the amount of BnOH results in

proportionally lower molecular weight polymers. GPC data of the produced polymers point to well-controlled polymerizations but evidence for transesterification is seen in the mass spectra of the polymers. On the basis of preliminary stoichiometric model reactions, the polymerization appears to occur via a coordination–insertion mechanism.

2.4 Experimental

2.4.1 General experimental conditions

All operations were carried out under an atmosphere of dry, oxygen-free nitrogen using standard Schlenk techniques or an MBraun Labmaster glove box. Anhydrous THF and benzene were distilled from sodium benzophenone ketyl under nitrogen. Toluene and pentane were purified by an MBraun Manual Solvent Purification System. Most reagents were purchased either from Aldrich or Alfa Aesar and used without further purification. *rac*-Lactide was purchased from Alfa Aesar and dried over Na₂SO₄ in THF, recrystallized from toluene twice, subsequently sublimed under vacuum and then stored under nitrogen in a glove box. Benzyl alcohol was purchased from Alfa Aesar and dried over activated 4 Å molecular sieves, distilled under reduced pressure and stored under nitrogen in an ampule prior to use. Deuterated solvents were purchased from Cambridge Isotope Laboratories and purified and degassed through freeze–vacuum–thaw cycles three times and stored under nitrogen in ampules fitted with Teflon valves. NaH was washed twice with hexane, as it was purchased as a suspension in mineral oil. Aqueous formaldehyde (37 wt%) was purchased from Fisher Scientific and used without further purification.

2.4.2 Instrumentation

^1H , ^{13}C and $^1\text{H}\{^1\text{H}\}$ NMR spectra were recorded on a Bruker Avance 500 or 300 MHz spectrometer at 25 °C (unless otherwise stated) and were referenced internally using the residual proton and ^{13}C resonances of the solvent. ^7Li NMR was recorded on a Bruker 300 MHz spectrometer and referenced externally to LiCl in D_2O . MALDI-TOF MS spectra were obtained using an Applied Biosystems 4800 MALDI TOF/TOF Analyzer equipped with a reflectron, delayed ion extraction and high performance nitrogen laser (200 Hz operating at 355 nm). Samples were prepared in a glove box and sealed under nitrogen in a Ziploc© bag for transport to the instrument at a concentration of 10.0 mg mL^{-1} in toluene. For ligands and complexes, anthracene was used as the matrix, which was mixed at a concentration of 10.0 mg mL^{-1} . For the polymers, mass spectra were recorded in reflectron mode and DHBA was used as the matrix and purified tetrahydrofuran was used as the solvent for depositing analytes onto the instrument's plate. The matrix was dissolved in THF at a concentration of 10 mg mL^{-1} . Polymer was dissolved in THF at approximately 1 mg mL^{-1} . The matrix and polymer solutions were mixed together at a ratio of 5 to 1; 1 μL of this was spotted on the MALDI plate and left to dry. Images of mass spectra were prepared using mMass™ software (<http://www.mmass.org>). GPC analysis was performed in THF at 25 °C on a Wyatt Triple Detection (triple angle light scattering, viscometry and refractive index) system with an Agilent 2600 series LC for sample and solvent handling, and two Phenogel 10³ Å 300 × 4.60 mm columns. Samples were dissolved in THF at a concentration of 1 mg mL^{-1} , left to equilibrate for ~2 h and passed through syringe filters before analysis. An eluent flow

rate of 0.30 mL min^{-1} and $100 \text{ }\mu\text{L}$ injection volume were used. Molecular weights (g mol^{-1}) were determined by triple detection using a dn/dc value of 0.049 mL g^{-1} . Conversions were determined by integration of the methyl signals due to the residual *rac*-lactide and produced poly-(*rac*-lactide). Elemental analyses were performed by Canadian Microanalytical Service Ltd, Delta, BC Canada or at the Ocean Sciences Centre, St. John's, NL Canada. Diffusion NMR measurements were performed on a Bruker Avance 500 MHz NMR spectrometer equipped with a 5 mm TXI probe and a z-gradient coil with a maximum strength of 5.35 G cm^{-1} at 298 K. The sample was run in CD_2Cl_2 at a concentration of 10.0 mM. The 90° pulse length and the relaxation time T_1 of the sample were determined before running the DOSY experiment. A standard 2D sequence with double stimulated echo and spoil gradient (DSTEBPGP3s) was used. The relaxation delay was set at 10 s. The gradient strength was calibrated by using the self-diffusion coefficient of residual HOD in D_2O ($1.9 \text{ \AA} \sim 10^{-9} \text{ m}^2 \text{ s}^{-1}$). For each experiment, the gradient strength was increased from 2–95% in 32 equally spaced steps with 16 scans per increment. Values of δ (gradient pulse length) and Δ (diffusion time) were optimized on the sample to give an intensity of between 5 and 10% of the initial intensity at 95% gradient strength and were set to 1 ms and 100 ms respectively. The solvent peak was used as an internal standard to measure the viscosity of each sample, $D_0(\text{CD}_2\text{Cl}_2) = 3.28 \text{ \AA} \sim 10^{-9} \text{ m}^2 \text{ s}^{-1}$ and $\eta_0 = 0.413 \text{ cp}$ at 298 K.⁶¹ The data were plotted using DynamicCenter (Bruker) and the diffusion coefficient (D) was extracted by fitting a mono exponential function ($\ln(I/I^0) = -\gamma^2 \delta^2 G^2 (\Delta - \delta/3) D t$) with the data analysis component of the software. The hydrodynamic radius of the complex ($r_{\text{H,PGSE}}$) was calculated using the procedure

outlined by Carpentier, Sarazin and coworkers.¹² An average of the values of D_t ($9.86 \text{ \AA} \sim 10^{-10} \text{ m}^2 \text{ s}^{-1} \pm 0.65$) found for 3 separate peaks in the ^1H PGSE NMR spectrum was used in the calculations. $r_{\text{H}}(\text{CD}_2\text{Cl}_2) = 2.49 \text{ \AA}$ was used.⁶²

2.4.3 X-ray crystallography

Crystals of **2.4** and **2.7** were mounted on low temperature diffraction loops. All measurements were made on a Rigaku Saturn70 CCD diffractometer using graphite monochromated Mo-K α radiation, equipped with a SHINE optic. A summary of the collection details and refinement results can be found in **Table 2.1**. For both structures, H-atoms were introduced in calculated positions and refined on a riding model while all nonhydrogen atoms were refined anisotropically. While refinement of **2.7** proceeded normally, in the structure of **2.4**, two disordered t-butyl groups were present ([C60–C62] and [C63–65] with respective occupancies 0.647(14) : 0.353(14), and [C67–69] and [C70–72] with respective occupancies 0.761(10) : 0.239(10)). Similar anisotropic restraints were applied to these groups, as well as to one THF molecule (O5, C77–C80). Further disorder was treated by the Platon⁶³ Squeeze procedure which was applied to recover 119 electrons per unit cell in two voids (total volume 813 \AA^3); that is 59.5 electrons per formula unit. Disordered lattice solvent toluene molecules (50 electrons per C_7H_8 ; one molecule per formula unit) were present prior to the application of Squeeze, however, a satisfactory point atom model could not be achieved. Note that there are two well ordered toluene molecules associated with each formula unit that were not removed from the model using Squeeze.

Crystal data for 2.4. $\text{C}_{103}\text{H}_{156}\text{Li}_4\text{N}_4\text{O}_7$ ($M = 1590.15 \text{ g mol}^{-1}$), triclinic, space

group $P1^-$ (no. 2), $a = 16.592(2) \text{ \AA}$, $b = 18.655(2) \text{ \AA}$, $c = 19.067(2) \text{ \AA}$, $\alpha = 103.219(7)^\circ$, $\beta = 98.581(7)^\circ$, $\gamma = 109.095(8)^\circ$, $V = 5265.8(10) \text{ \AA}^3$, $Z = 2$, $T = 163(2) \text{ K}$, $\mu(\text{MoK}\alpha) = 0.061 \text{ mm}^{-1}$, $D_{\text{calc}} = 1.003 \text{ g cm}^{-3}$, 43 063 reflections measured ($6^\circ \leq 2\theta \leq 53^\circ$), 21 429 unique ($R_{\text{int}} = 0.0454$) which were used in all calculations. The final R_1 was 0.1130 ($>2\sigma(I)$) and wR_2 was 0.3597 (all data). CCDC no. 1410026.

Crystal data for 2.7. $\text{C}_{66}\text{H}_{100}\text{N}_4\text{Na}_4\text{O}_6$ ($M = 1137.45 \text{ g mol}^{-1}$), monoclinic, space group $P21/n$ (no. 14), $a = 12.898(4) \text{ \AA}$, $b = 13.741(4) \text{ \AA}$, $c = 18.695(6) \text{ \AA}$, $\beta = 101.518(4)^\circ$, $V = 3246.7(17) \text{ \AA}^3$, $Z = 2$, $T = 163 \text{ K}$, $\mu(\text{MoK}\alpha) = 0.096 \text{ mm}^{-1}$, $D_{\text{calc}} = 1.164 \text{ g cm}^{-3}$, 24 304 reflections measured ($4.61^\circ \leq 2\theta \leq 54.206^\circ$), 7155 unique ($R_{\text{int}} = 0.0374$) which were used in all calculations. The final R_1 was 0.0543 ($I > 2\sigma(I)$) and wR_2 was 0.1653 (all data). CCDC no. 1410027.

2.4.4 Polymerization procedures

Typical bulk polymerization procedure. A monomer:initiator ratio employed was 100: 1 and the reactions were conducted at $130 \text{ }^\circ\text{C}$. A Schlenk tube equipped with a magnetic stir bar was charged in a glovebox with the required amount of LA (0.50 g, 3.5 mmol) and initiator (0.02–0.023 g, 0.035 mmol). The reaction vessel was sealed, brought out of the glovebox and immersed in an oil bath that was preheated to $130 \text{ }^\circ\text{C}$. At the desired time, an aliquot was withdrawn from the flask for ^1H NMR analysis to determine the monomer conversion. The vial was then placed in an ice bath to halt the reaction and solidify the polymer. The resulting solid was dissolved in dichloromethane and the polymer, precipitated with acidified methanol. Centrifugation was applied where needed for better separation of the solids. Solvents were decanted and the white solids were dried

in vacuo followed by drying in a vacuum oven at 40 °C overnight.

Typical solution polymerization procedure. The reaction mixtures were prepared in a glovebox and subsequent operations were performed with standard Schlenk techniques. A Schlenk tube containing a stir bar and the monomer (0.85 g, 5.9 mmol) in solvent (CH₂Cl₂, toluene or THF) was prepared. A second Schlenk tube was prepared containing a stir bar and the catalyst (0.007–0.0085 g, 0.0118 mmol) and a solution of BnOH (127 μL, 0.0118 mmol), if appropriate, in 10 mL of solvent (CH₂Cl₂, toluene). Then the lactide solution was transferred by cannula to the complex mixture. Timing of the reaction began when all the lactide was transferred. An aliquot of the reaction solution was taken for NMR spectroscopic analysis, and the reaction was quenched immediately by the addition of methanol. The resulting solid was dissolved in dichloromethane and the polymer precipitated with excess cold methanol. Solvents were decanted and the white solids were dried in vacuo followed by drying in a vacuum oven at 40 °C overnight.

2.4.5 Synthesis and characterization

Synthesis of [L1]H₂. A mixture of 2,4-di-*tert*-butylphenol (24.4 g, 0.123 mol), 37% w/w aqueous formaldehyde (10.0 mL, 123 mmol) and homopiperazine (6.22 g, 0.0615 mol) in water (100 mL) was stirred and heated to reflux for 24 h. Upon cooling to room temperature, solvents were decanted from the resulting white solid, which was recrystallized from methanol and chloroform to afford a pure white powder (32.4 g, 98%). Anal. calc'd for C₃₅H₅₆N₂O₂: C, 78.31; H, 10.51; N, 5.22. Found: C, 78.19; H, 10.33; N, 5.11. ¹H NMR (300 MHz, 298 K, CDCl₃) δ 11.03 (2H, s, OH), 7.19 (2H, d, ²J_{HH} = 2.3, ArH), 6.79 (2H, d, ²J_{HH} = 2.3 Hz, ArH), 3.75 (4H, s, ArC–CH₂–N), 2.80 (4H,

t, $^3J_{\text{HH}} = 6$ Hz, N-CH₂{CH₂}CH₂-N), 2.75 (4H, s, N-CH₂CH₂-N), 1.89 (2H, quintet, $^3J_{\text{HH}} = 6.04$ Hz, N-CH₂{CH₂}CH₂-N), 1.40 (18H, s, ArC-C(CH₃)₃), 1.25 (18H, s, ArC-C(CH₃)₃). ¹³C{¹H} NMR (75.4 MHz, 298 K, C₆D₆) δ 155.6 (ArC-O), 141.1 (ArC-C(CH₃)₃), 136.5 (ArC-C(CH₃)₃), 124.0 (ArCH), 123.6 (ArCH), 122.1 (ArC-CH₂-N), 63.1 (ArC-CH₂-N), 54.9 (N-CH₂{CH₂}CH₂-N), 53.2 (N-CH₂CH₂-N), 35.7 (ArC-C(CH₃)₃), 34.7 (ArC-C(CH₃)₃), 32.4 (ArC-C(CH₃)₃), 30.4 (ArC-C(CH₃)₃), 27.2 (N-CH₂{CH₂}CH₂-N). MS (MALDI-TOF) *m/z* (% ion): 536.32 (100, [H₂[L1]]⁺).

Synthesis of [L2]H₂. [L2]H₂ was prepared in an identical manner to [L1]H₂ using 2-*tert*-butyl-4-methylphenol to yield a pure white powder (26.1 g, 93.6%). Anal. calc'd for C₂₉H₄₄N₂O₂: C, 76.95; H, 9.80; N, 6.19. Found: C, 77.11; H, 9.87; N, 6.12. ¹H NMR (300 MHz, 298 K, CDCl₃) δ 11.0 (2H, s, OH), 7.01 (2H, s, ArH), 6.66 (2H, s, ArH), 3.75 (4H, s, ArC-CH₂-N), 2.82 (4H, t, $^3J_{\text{HH}} = 6.1$ Hz, N-CH₂{CH₂}CH₂-N), 2.77 (4H, s, N-CH₂CH₂-N), 2.25 (6H, s, ArC-CH₃), 1.89 (2H, quintet, $^3J_{\text{HH}} = 6.01$ Hz, N-CH₂{CH₂}CH₂-N), 1.43 (18H, s, ArC-C(CH₃)₃). ¹³C{¹H} NMR (75.4 MHz, 298 K, CDCl₃) δ 154.6 (ArC-O), 136.6 (ArC-C(CH₃)₃), 127.5 (ArC-CH₃), 127.4 (ArCH), 127.0 (ArCH), 122.1 (ArC-CH₂-N), 62.2 (ArC-CH₂-N), 54.6 (N-CH₂{CH₂}CH₂-N), 53.2 (N-CH₂CH₂-N), 34.8 (ArC-C(CH₃)₃), 29.7 (ArC-C(CH₃)₃), 27.0 (N-CH₂{CH₂}CH₂-N), 21.0 (ArC-CH₃). MS (MALDI-TOF) *m/z* (% ion): 452.31(100, [H₂[L2]]⁺).

Synthesis of 2.4. [L1]H₂ (2.01 g, 3.7 mmol) was dissolved in THF (50 mL) and cooled to -78 °C. *n*-Butyllithium (1.6 M, 5.0 mL, 8.14 mmol) was slowly added via cannula to afford a yellow solution, which was warmed to room temperature and stirred for 72 h. Solvent was removed under vacuum; the product was washed with cold pentane (10 mL). The product was then filtered and dried under vacuum to yield (2.36 g, 97%) of

a pale yellow product. ^1H NMR (300 MHz, 298 K, C_6D_6) δ 7.6 (2H, d, $^2J_{\text{HH}} = 2.2$ Hz, ArH). 7.05 (2H, d, $^2J_{\text{HH}} = 2.2$ Hz, ArH), 3.58 (4H, s, ArC-CH₂-N), 3.38 (8H, s, CH₂, THF), 2.71 (4H, s, N-CH₂CH₂-N), 1.89 (6H, br, N-CH₂{CH₂}CH₂-N), 1.68 (18H, s, ArC-C(CH₃)₃), 1.47 (18H, s, ArC-C(CH₃)₃), 1.19 (8H, s, CH₂, THF). ^1H NMR (500 MHz, 298 K, $\text{C}_5\text{D}_5\text{N}$) δ 7.53 (2H, s, ArH), 7.18 (2H, s, ArH), 3.86 (4H, s, ArC-CH₂-N), 2.77 (4H, br, N-CH₂CH₂-N), 1.68 (6H, s, CH₂{CH₂}CH₂-N), 1.63 (4H, m, CH₂, $^3J_{\text{HH}} = 6.5$ Hz, THF), 1.53 (18H, s, ArC-C(CH₃)₃), 1.42 (18H, s, ArC-C(CH₃)₃). $^{13}\text{C}\{^1\text{H}\}$ NMR (75.4 MHz, 298 K, CDCl_3) δ 140.8 (ArC-C(CH₃)₃), 135.9 (ArC-C(CH₃)₃), 123.6 (ArCH), 121.4 (ArCH), 100.2 (ArC-CH₂-N), 62.7 (ArC-CH₂-N), 54.7 (N-CH₂{CH₂}CH₂-N), 53.3 (N-CH₂CH₂-N), 35.1 (ArC-C-(CH₃)₃), 34.4 (ArC-C-(CH₃)₃), 31.9 (ArC-C-(CH₃)₃), 29.8 (ArC-C-(CH₃)₃), 27.0 (CH₂, THF). $^{13}\text{C}\{^1\text{H}\}$ NMR (75.4 MHz, 298 K, C_6D_6) δ 164.2 (ArC-O), 136.9 (ArC-C(CH₃)₃), 134.0 (ArC-C(CH₃)₃), 127.2 (ArCH), 126.1 (ArCH), 123.9 (ArC-CH₂-N), 68.5 (CH₂, THF), 62.8 (ArC-CH₂-N), 53.4 (N-CH₂{CH₂}CH₂-N), 51.0 (N-CH₂CH₂-N), 35.7 (ArC-C-(CH₃)₃), 34.5 (ArC-C-(CH₃)₃), 32.8 (ArC-C-(CH₃)₃), 31.0 (ArC-C-(CH₃)₃), 27.4 (N-CH₂{CH₂}CH₂-N), 25.6 (CH₂, THF). $^{13}\text{C}\{^1\text{H}\}$ NMR (75.4 MHz, 298 K, $\text{C}_5\text{D}_5\text{N}$) δ 166.0 (ArC-O), 137.5 (ArC-C(CH₃)₃), 132.8 (ArC-C(CH₃)₃), 127.5 (ArCH), 126.4 (ArCH), 68.3 (CH₂, THF), 62.8 (ArC-CH₂-N), 53.9 (N-CH₂{CH₂}CH₂-N), 51.8 (N-CH₂CH₂-N), 35.9 (ArC-C-(CH₃)₃), 34.5 (ArC-C-(CH₃)₃), 32.8 (ArC-C-(CH₃)₃), 31.1 (ArC-C-(CH₃)₃), 27.4 (N-CH₂{CH₂}CH₂-N), 26.3 (CH₂, THF). $^7\text{Li}\{^1\text{H}\}$ NMR (C_6D_6 , 298 K, δ) 1.58. MS (MALDI-TOF) m/z (% ion): 548.4 (100, $[\text{Li}_2[\text{L1}]]^+$).

Synthesis of 2.5. $[\text{L1}]\text{H}_2$ (2.01 g, 3.7 mmol) was dissolved in THF (50 mL) and cooled to -78 °C. Sodium hydride (0.357 g, 14.8 mmol) was dissolved in THF (20 mL)

and slowly added via cannula to afford a white suspension solution, which was warmed and stirred for 72 h. Solvent was removed under vacuum; the product was washed with cold pentane (10 mL). The product was then filtered and dried under vacuum to yield (2.36 g, 98%) of a deep yellow product. Anal. calc'd for $C_{70}H_{108}Na_4N_4O_4$ ($3C_4H_8O$): C, 71.48; H, 9.66; N, 4.07. Found: C, 71.78; H, 9.38; N, 4.14. 1H NMR (300 MHz, 298 K, C_6D_6) δ 7.51 (2H, d, $^2J_{HH} = 2.3$ Hz, ArH), 6.99 (2H, d, $^2J_{HH} = 2.3$ Hz, ArH), 4.02 (4H, br, ArC-CH₂-N), 3.25 (8H, m, $^3J_{HH} = 6.6$ Hz, CH₂, THF), 3.03 (2H, br, N-CH₂{CH₂}CH₂-N), 2.81 (2H, br, N-CH₂{CH₂}CH₂-N), 2.47 (4H, br, N-CH₂CH₂-N), 1.90 (2H, br, N-CH₂{CH₂}CH₂-N), 1.70 (18H, s, ArC-C(CH₃)₃), 1.29 (18H, s, ArC-C(CH₃)₃), 1.28 (8H, m, $^3J_{HH} = 6.6$ Hz, CH₂, THF). $^{13}C\{^1H\}$ NMR (75.4 MHz, 298 K, C_5D_5N) δ 168.8 (ArC-O), 137.7 (ArC-C(CH₃)₃), 130.4 (ArC-C(CH₃)₃), 127.1 (ArCH), 126.7 (ArCH), 123.3 (ArC-CH₂-N), 68.3 (CH₂, THF), 64.7 (ArC-CH₂-N), 56.7 (N-CH₂{CH₂}CH₂-N), 54.2 (N-CH₂CH₂-N), 36.1 (ArC-C-(CH₃)₃), 34.5 (ArC-C-(CH₃)₃), 33.1 (ArC-C-(CH₃)₃), 31.2 (ArC-C-(CH₃)₃), 27.9 (N-CH₂{CH₂}CH₂-N), 26.3 (CH₂, THF). $^{13}C\{^1H\}$ NMR (75.4 MHz, 298 K, $CDCl_3$) δ 154.3(ArC-O), 140.9 (ArC-C(CH₃)₃), 135.8 (ArC-C(CH₃)₃), 123.7 (ArCH), 121.5 (ArCH), 100.2 (ArC-CH₂-N), 68.2 (CH₂, THF), 62.7 (ArC-CH₂-N), 54.7 (N-CH₂{CH₂}CH₂-N), 53.3 (N-CH₂CH₂-N), 35.1 (ArC-C-(CH₃)₃), 34.4 (ArC-C-(CH₃)₃), 31.9 (ArC-C-(CH₃)₃), 29.8 (ArC-C-(CH₃)₃), 27.0 (N-CH₂{CH₂}CH₂-N), 25.8 (CH₂, THF). MS (MALDI-TOF) *m/z* (% ion): 580.3 (100, [Na₂[L1]]⁺).

Synthesis of 2.6. Complex **2.6** was prepared in an identical manner to **2.4** using [L2]H₂ to yield (2.06 g, 97%) of a pale yellow product. 1H NMR (300 MHz, 298 K, C_6D_6) δ 7.35 (2H, d, $^2J_{HH} = 2.3$ Hz, ArH), 6.85 (2H, d, $^2J_{HH} = 2.3$ Hz, ArH), 3.61 (4H, s,

ArC-CH₂-N), 3.51 (8H, m, ³J_{HH} = 6.6 Hz, CH₂, THF), 2.75 (4H, m, N-CH₂CH₂-N), 2.41 (6H, s, ArC-CH₃), 1.96 (6H, m, N-CH₂{CH₂}CH₂-N), 1.66 (18H, s, ArC-C(CH₃)₃), 1.30 (8H, m, ³J_{HH} = 6.6 Hz, CH₂, THF). ¹³C{¹H} NMR (75.4 MHz, 298 K, C₆D₆) δ 164.5 (ArC-O), 137.6 (ArC-C-(CH₃)₃), 131.3 (ArC-CH₃), 126.5 (ArCH), 120.4 (ArC-CH₂-N), 68.5 (CH₂, THF), 62.2 (ArC-CH₂-N), 53.5 (N-CH₂{CH₂}CH₂-N), 51.1 (N-CH₂CH₂-N), 35.4 (ArC-C-(CH₃)₃), 30.8 (ArC-CH₃), 27.7 (N-CH₂{CH₂}CH₂-N), 25.8 (CH₂, THF), 21.6 (ArC-CH₃). ⁷Li{¹H} NMR (C₆D₆, 298 K, δ) 1.60. MS (MALDI-TOF) *m/z* (% ion): 464.3 (100, [Li₂[L2]]⁺).

Synthesis of 2.7. Complex **2.7** was prepared in an identical manner to **2.5** using [L2]H₂ to yield (2.02 g, 96%) of a yellow product. Anal. calc'd for C₅₈H₈₄Na₄N₄O₄ (3C₄H₈O): C, 69.51; H, 9.00; N, 4.63. Found: C, 69.23; H, 9.03; N, 4.94. ¹H NMR (300 MHz, 298 K, C₆D₆) δ 7.23 (2H, s, ArH), 6.83 (2H, s, ArH), 4.09 (4H, br, ArC-CH₂-N), 3.25 (8H, m, ³J_{HH} = 6.7 Hz, CH₂, THF), 2.99 (4H, br, N-CH₂{CH₂}CH₂-N), 2.34 (6H, s, ArC-CH₃), 1.73 (18H, s, ArC-C(CH₃)₃), 1.25 (8H, m, ³J_{HH} = 6.7 Hz, CH₂, THF). ¹³C{¹H} NMR (75.4 MHz, 298 K, CDCl₃) δ 154.41 (ArC-O), 136.55 (ArC-C-(CH₃)₃), 127.47 (ArCH), 126.90 (ArCH), 122.12 (ArC-CH₂-N), 68.13 (CH₂, THF), 62.12 (ArC-CH₂-N), 54.66 (N-CH₂{CH₂}CH₂-N), 53.20 (N-CH₂CH₂-N), 34.74 (ArC-C-(CH₃)₃), 29.72 (ArC-CH₃), 26.98 (N-CH₂{CH₂}CH₂-N), 25.78 (CH₂, THF), 20.96 (ArC-CH₃). MS (MALDI-TOF) *m/z* (% ion): 497.2 (10, [Na₂[L2]]⁺), 475.2 (25, [Na[L2]]⁺).

2.5 References

1. O. Wichmann, R. Sillanpää and A. Lehtonen, *Coord. Chem. Rev.*, **2012**, 256, 371-392.
2. T. L. Yu, C. T. Chen, C. C. Lin, J. Wu and T. Yu, *Coord. Chem. Rev.*, **2006**, 250, 602-626.
3. A. K. Sutar, T. Maharana, S. Dutta, C.-T. Chen and C.-C. Lin, *Chem. Soc. Rev.*, **2010**, 39, 1724-1746.
4. M. Bero and J. Kasperczyk, *Polymer*, **2000**, 41, 391-395.
5. I. Kreisersaunders, *Makromol. Chem.*, **1990**, 191, 1057-1066.
6. H. R. Kricheldorf, I. Kreiser-Saunders and A. Stricker, *Macromolecules*, **2000**, 33, 702-709.
7. J. Penczek, J. Franek, Z. Jedlinski and P. Kurcok, *Macromolecules*, **1992**, 25, 2285-2289.
8. B.-T. Ko and C.-C. Lin, *J. Am. Chem. Soc.*, **2001**, 123, 7973-7977.
9. J. E. Kasperczyk, *Macromolecules*, **1995**, 28, 3937-3939.
10. C.-A. Huang and C.-T. Chen, *Dalton Trans.*, **2007**, 5561-5566.
11. R. K. Dean, A. M. Reckling, H. Chen, L. N. Dawe, C. M. Schneider and C. M. Kozak, *Dalton Trans.*, **2013**, 42, 3504-3520.
12. S.-C. Rosca, D.-A. Rosca, V. Dorcet, C. M. Kozak, F. M. Kerton, J.-F. Carpentier and Y. Sarazin, *Dalton Trans.*, **2013**, 42, 9361-9375.
13. N. Ikpo, C. Hoffmann, L. N. Dawe and F. M. Kerton, *Dalton Trans.*, **2012**, 41, 6651-6660.
14. Y. Huang, Y.-H. Tsai, W.-C. Hung, C.-S. Lin, W. Wang, J.-H. Huang, S. Dutta and C.-C. Lin, *Inorg. Chem.*, **2010**, 49, 9416-9425.
15. L. Wang, X. Pan, L. Yao, N. Tang and J. Wu, *Eur. J. Inorg. Chem.*, **2011**, 2011, 632-636.
16. C.-A. Huang, C.-L. Ho and C.-T. Chen, *Dalton Trans.*, **2008**, 3502-3510.
17. F. M. Kerton, C. M. Kozak, K. Lüttgen, C. E. Willans, R. J. Webster and A. C. Whitwood, *Inorg. Chim. Acta*, **2006**, 359, 2819-2825.
18. W. Clegg, M. G. Davidson, D. V. Graham, G. Griffen, M. D. Jones, A. R. Kennedy, C. T. O'Hara, L. Russo and C. M. Thomson, *Dalton Trans.*, **2008**, 1295-1301.
19. Z. Janas, T. Nerkowski, E. Kober, L. B. Jerzykiewicz and T. Lis, *Dalton Trans.*, **2012**, 41, 442-447.
20. E. Kober, R. Petrus, P. Kocięcka, Z. Janas and P. Sobota, *Polyhedron*, **2015**, 85, 814-823.
21. F. M. García-Valle, R. Estivill, C. Gallegos, T. Cuenca, M. E. G. Mosquera, V. Tabernero and J. Cano, *Organometallics*, **2015**, 34, 477-487.
22. W.-Y. Lu, M.-W. Hsiao, S. C. N. Hsu, W.-T. Peng, Y.-J. Chang, Y.-C. Tsou, T.-Y. Wu, Y.-C. Lai, Y. Chen and H.-Y. Chen, *Dalton Trans.*, **2012**, 41, 3659-3667.
23. X. Xu, X. Pan, S. Tang, X. Lv, L. Li, J. Wu and X. Zhao, *Inorg. Chem. Commun.*, **2013**, 29, 89-93.
24. X. Xu, Y. Yao, Y. Zhang and Q. Shen, *Inorg. Chem.*, **2007**, 46, 3743-3751.
25. L. J. Corbett, S. M. Butt, G. Madhurambal, K. L. Collins and F. M. Kerton, *Green*

- Chem. Lett. Rev. J.*, **2007**, 1, 31-35.
26. S. Holloway, A. Power, R. G. Soper, K. Sheridan, F. M. Kerton, J. M. Lynam, A. C. Whitwood and C. E. Willans, *Can. J. Chem.*, **2008**, 86, 435-443.
 27. S. L. Hancock, R. Gati, M. F. Mahon, E. Y. Tshuva and M. D. Jones, *Dalton Trans.*, **2014**, 43, 1380-1385.
 28. S. L. Hancock, M. F. Mahon and M. D. Jones, *Chem. Cent. J.*, **2013**, 7, 135-135.
 29. S. L. Hancock, M. F. Mahon and M. D. Jones, *Dalton Trans.*, **2011**, 40, 2033-2037.
 30. J. Baldamus and E. Hecht, *Z. Anorg. Allg. Chem.*, **2003**, 629, 188-191.
 31. M. Sankaralingam and M. Palaniandavar, *Dalton Trans.*, **2014**, 43, 538-550.
 32. S. L. Hancock, M. D. Jones, C. J. Langridge and M. F. Mahon, *New J. Chem.*, **2012**, 36, 1891-1896.
 33. S. L. Hancock, M. F. Mahon, G. Kociok-Köhn and M. D. Jones, *Eur. J. Inorg. Chem.*, **2011**, 2011, 4596-4602.
 34. R. Mayilmurugan, B. N. Harum, M. Volpe, A. F. Sax, M. Palaniandavar and N. C. Mösch-Zanetti, *Chem. Eur. J.*, **2011**, 17, 704-713.
 35. C. Fernandes, R. W. A. Franco, L. M. Lube, S.-H. Wei, L. L. Mendes, R. W. A. Franco, L. M. Lube, J. H. Reibenspies, D. J. Darensbourg and A. Horn Jr, *J. Braz. Chem. Soc.*, **2014**, 25, 1050-1061.
 36. R. Mayilmurugan, M. Sankaralingam, E. Suresh and M. Palaniandavar, *Dalton Trans.*, **2010**, 39, 9611-9625.
 37. R. Mayilmurugan, H. Stoeckli-Evans, E. Suresh and M. Palaniandavar, *Dalton Trans.*, **2009**, 5101-5114.
 38. T. N. Rao, J. Reedijk, J. Vanrijn, A. W. Addison and G. C. Verschoor, *J. Chem. Soc., Dalton Trans.*, **1984**, 1349-1356.
 39. R. Wegner, B. Krebs and S. Uhlenbrock, *J. Chem. Soc., Dalton Trans.*, **1996**, 3731-3736.
 40. G. Murphy, C. O'Sullivan, B. Murphy and B. Hathaway, *Inorg. Chem.*, **1998**, 37, 240-248.
 41. B. Calvo, M. G. Davidson and D. García-Vivó, *Inorg. Chem.*, **2011**, 50, 3589-3595.
 42. A. Macchioni, G. Ciancaleoni, C. Zuccaccia and D. Zuccaccia, *Chem. Soc. Rev.*, **2008**, 37, 479-489.
 43. M. W. Drover, J. N. Murphy, J. C. Flogeras, C. M. Schneider, L. N. Dawe and F. M. Kerton, *Polyhedron*, **2015**, 102, 60-68.
 44. B. Gupta, N. Revagade and J. Hilborn, *Prog. Polym. Sci.*, **2007**, 32, 455-482.
 45. R. E. Drumright, P. R. Gruber and D. E. Henton, *Adv. Mater.*, **2000**, 12, 1841-1846.
 46. K. Devaine-Pressing, J. H. Lehr, M. E. Pratt, L. N. Dawe, A. A. Sarjeant and C. M. Kozak, *Dalton Trans.*, **2015**, 44, 12365-12375.
 47. C. Paetz and R. Hagen, *Chem. Ing. Tech.*, **2014**, 86, 519-523.
 48. S. Bian, S. Abbina, Z. Lu, E. Kolodka and G. Du, *Organometallics*, **2014**, 33, 2489-2495.
 49. N. Ikpo, L. N. Saunders, J. L. Walsh, J. M. B. Smith, L. N. Dawe and F. M. Kerton, *Eur. J. Inorg. Chem.*, **2011**, 2011, 5347-5359.

50. N. Ajellal, J.-F. Carpentier, C. Guillaume, S. M. Guillaume, M. Helou, V. Poirier, Y. Sarazin and A. Trifonov, *Dalton Trans.*, **2010**, 39, 8363-8376.
51. B. Liu, T. Roisnel, J.-P. Guégan, J.-F. Carpentier and Y. Sarazin, *Chem. Eur. J.*, **2012**, 18, 6289-6301.
52. H.-Y. Chen, L. Mialon, K. A. Abboud and S. A. Miller, *Organometallics*, **2012**, 31, 5252-5261.
53. Z. Qu, R. Duan, X. Pang, B. Gao, X. Li, Z. Tang, X. Wang and X. Chen, *J. Polym. Sci., Part A: Polym. Chem.*, **2014**, 52, 1344-1352.
54. M. J. Stanford and A. P. Dove, *Chem. Soc. Rev.*, **2010**, 39, 486-494.
55. K. A. M. Thakur, R. T. Kean, E. S. Hall, J. J. Kolstad, T. A. Lindgren, M. A. Doscotch, J. I. Siepmann and E. J. Munson, *Macromolecules*, **1997**, 30, 2422-2428.
56. M.-H. Thibault and F.-G. Fontaine, *Dalton Trans.*, **2010**, 39, 5688-5697.
57. N. Maudoux, T. Roisnel, J.-F. Carpentier and Y. Sarazin, *Organometallics*, **2014**, 33, 5740-5748.
58. M. A. Sinenkov, G. K. Fukin, A. V. Cherkasov, N. Ajellal, T. Roisnel, F. M. Kerton, J.-F. Carpentier and A. A. Trifonov, *New J. Chem.*, **2011**, 35, 204-212.
59. C. E. Willans, M. A. Sinenkov, G. K. Fukin, K. Sheridan, J. M. Lynam, A. A. Trifonov and F. M. Kerton, *Dalton Trans.*, **2008**, 3592-3598.
60. H. E. Dyer, S. Huijser, A. D. Schwarz, C. Wang, R. Duchateau and P. Mountford, *Dalton Trans.*, **2008**, 32-35.
61. H. Kato, T. Saito, M. Nabeshima, K. Shimada and S. Kinugasa, *J. Magn. Reson.*, **2006**, 180, 266-273.
62. D. Zuccaccia and A. Macchioni, *Organometallics*, **2005**, 24, 3476-3486.
63. A. L. Spek, *J. Appl. Crystallogr.*, **2003**, 36, 7-13.

Co-Authorship Statement

Chapter 3: Iron amino-bis(phenolate) complexes for the formation of organic carbonates from CO₂ and oxiranes

This chapter contains some of the results published in the full article “Iron amino-bis(phenolate) complexes for the formation of organic carbonates from CO₂ and oxiranes”, *Catal. Sci. Technol.*, **2016**, DOI: 10.1039/C6CY00477F.

Authors: Dalal Alhashmialameer, Julie Collins, Karen Hattenhauer and Francesca M. Kerton.

The first author Dalal Alhashmialameer contributed 95% of the content of the article as a main researcher including: performing experiments, collecting data, and writing all parts of the paper in collaboration with her supervisors

Julie Collins and Louise N. Dawe were the crystallographers on the paper. The other co-authors are Francesca M. Kerton and Karen Hattenhauer, who assisted in writing and editing the paper, and designing experiments.

Chapter 3 Iron amino-bis(phenolate) complexes for the formation of organic carbonates from CO₂ and oxiranes

3.1 Introduction

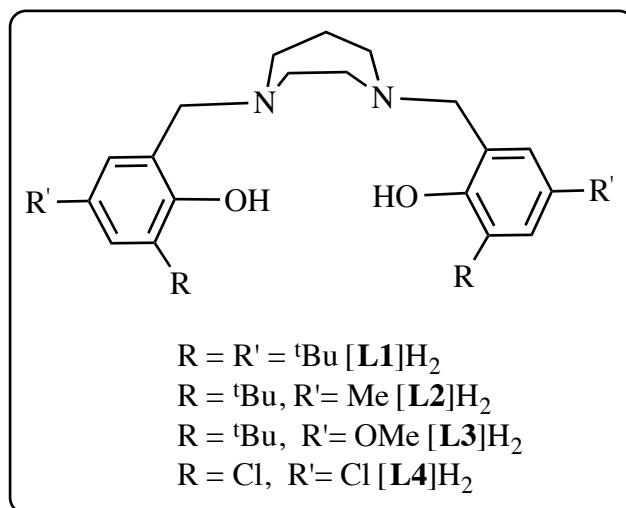
Utilization of carbon dioxide (CO₂) in the preparation of chemicals with commercial value has become important as it is a green, cheap, non-toxic and abundant feedstock.¹⁻⁸ Highly reactive substrates such as epoxides allow for the thermodynamic stability of CO₂ to be overcome.^{1,2,9} The interest in cyclic carbonates as CO₂-derived molecules is driven by their wide applications as aprotic solvents (including their use to prepare electrolyte solutions in lithium ion batteries) and as starting materials for polycarbonates.¹⁰ Industrially, the production of cyclic carbonates requires demanding reaction conditions such as elevated CO₂ pressures and high temperatures. Therefore, numerous efforts have been devoted to the design of efficient catalysts for this transformation under mild reaction conditions,¹⁰ including catalysts of aluminum,¹¹⁻¹⁴ chromium,¹⁵⁻¹⁸ cobalt,¹⁷⁻²² zinc,^{23,24} manganese²⁵ and magnesium.²⁶ In order to address the potential toxicity associated with some of these metals, iron complexes have been used as a promising class of catalyst. Moreover, compared to some catalysts, because of iron's high natural abundance they are often cheap and some recent examples have shown exceptional catalytic activity in the conversion of CO₂ and epoxides to carbonates.²⁷⁻²⁹

This chapter describes the synthesis, structural, spectroscopic and magnetic properties of iron(III) complexes possessing tetradentate amino-bis(phenolate) ligands and their catalytic activity for the coupling reaction of CO₂ and various epoxides.

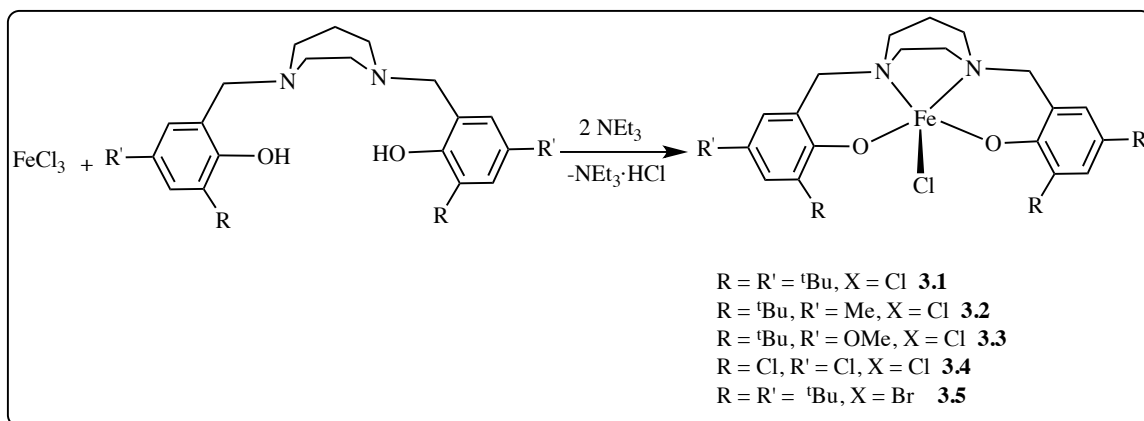
3.2 Results and discussion

3.2.1 Synthesis and characterization of iron complexes

A series of tetradentate amino-bis(phenol) compounds $H_2[L]^{RR'Pip}$ (**Scheme 3.1**) were synthesized using a method similar to literature procedures reported by Kerton and coworkers.³⁰ As shown in **Scheme 3.2**, the desired iron(III) complexes were obtained *via* a method reported by Kozak and coworkers,³¹ which employs dropwise addition of a methanol solution of anhydrous FeX_3 ($X = Cl$ or Br) to a methanolic slurry of the ligand at room temperature. The resulting solution was neutralized using NEt_3 and evaporated to dryness. Extraction into an appropriate solvent, such as acetone, followed by filtration and removal of the solvent afforded analytically pure paramagnetic complexes with the formulation $Fe[L]X$.³²⁻³⁴ The complexes were characterized using MALDI-TOF mass spectrometry, elemental analysis, X-ray diffraction and UV-vis spectroscopy.



Scheme 3.1. Proligands used with iron(III) in this study.



Scheme 3.2. Synthesis of iron(III) complexes.

3.2.2 Crystal structure determination

Single crystals of **3.1** and **3.2** suitable for X-ray diffraction analysis were obtained by slow evaporation and cooling of a saturated methanol or acetone solution at $-20\text{ }^\circ\text{C}$. The ORTEP diagrams of the structures are shown in **Figure 3.1** and **Figure 3.2** and the crystallographic data are collected in **Table 3.1**. Both complexes exhibit monometallic structures with the iron centres bonded to the two phenolate oxygen atoms and two amine nitrogen atoms of the ligand, which define the basal plane of the square pyramid. The apical sites are occupied by chloride ions and the coordination geometry around each iron atom can be described as a distorted square pyramid for both complexes. Selected bond lengths (\AA) and angles ($^\circ$) for compounds **3.1** and **3.2** are given in **Table 3.2**. Since both of these complexes are structurally identical except for one substituent, namely a methyl group instead of *tert*-butyl group on the phenolate rings, the observed bond lengths and angles are very similar. For **3.1**, the phenolate oxygen atoms exhibit bond distances to iron of 1.869(12) and 1.8734(11) \AA for Fe–O(1) and Fe–O(2). These Fe–O(1) and Fe–O(2) distances lie within the range observed for **3.2** [1.8690(12) to 1.8805(12) \AA]. These

values are similar to those observed in related square pyramidal geometry iron(III) complexes containing salen and bis(phenolate) ligands.³⁵⁻³⁹ However, they are longer than the corresponding Fe–O bond lengths observed in 5-coordinate iron(III) complexes possessing diamino-bis(phenolate) ligands^{33,34,40,41} and salan complexes^{42,43} in which the iron(III) ion adopts a trigonal bipyramidal. Moreover, the Fe–O distances are shorter than the average bond length of 1.92 Å observed in octahedral iron(III) complexes,^{40,44-47} suggesting relatively strong iron–oxygen overlap which is consistent with the lower coordination number (five rather than six).^{40,44} The short Fe–O bond distance is also supported by the high molar absorptivity of the LMCT band (UV-section below). The Fe–Cl(1) distance of 2.2466(6) Å in **3.1** and 2.2488(8) Å in **3.2** are shorter than those in the trigonal bipyramidal complexes but similar to the Fe–Cl lengths observed in other square pyramidal iron(III) complexes possessing salen or diamino-bis(phenolate) ligands.^{33,36,38,39} The nitrogen donors in the ligand backbone exhibit bond lengths of 2.1864(13) and 2.1681(13) Å for Fe–N(1) and Fe–N(2) in **3.1**, and lengths of 2.1826(14) and 2.1902(14) Å for Fe–N(1) and Fe–N(2) in **3.2**. The Fe–N bond distances in both complexes were close to the Fe–N distances in the related square pyramidal complexes.^{33,36,38,39} The Fe–O(1)–C_(ipso) and Fe–O(2)–C_(ipso) angles in **3.1** are 138.27(10)° and 137.92(10)° while **3.2** gives angles of 137.50(10)° and 138.15(10)°, which are identical to those observed in square pyramidal iron(III) complexes of phenolate ligands.³³ The distortion of the coordination around the iron centre was determined by the trigonality parameter τ , (where $\tau = (\beta - \alpha)/60$), the largest angle β is O(2)–Fe–N(1) and the second largest angle α in the coordination sphere is O(1)–Fe–N(2).⁴⁸ For both

complexes, the trigonality index is close to zero.

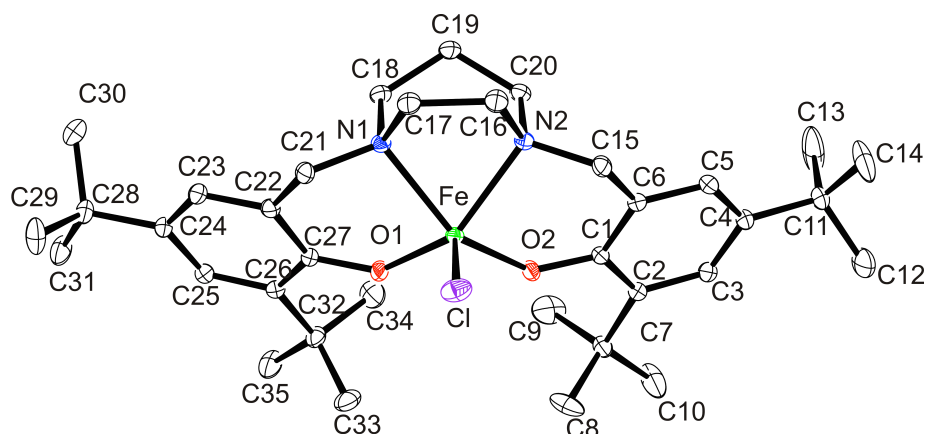


Figure 3.1. Molecular structure (ORTEP) and partial numbering scheme for **3.1**. Ellipsoids are shown at the 50% probability level (H-atoms omitted for clarity).

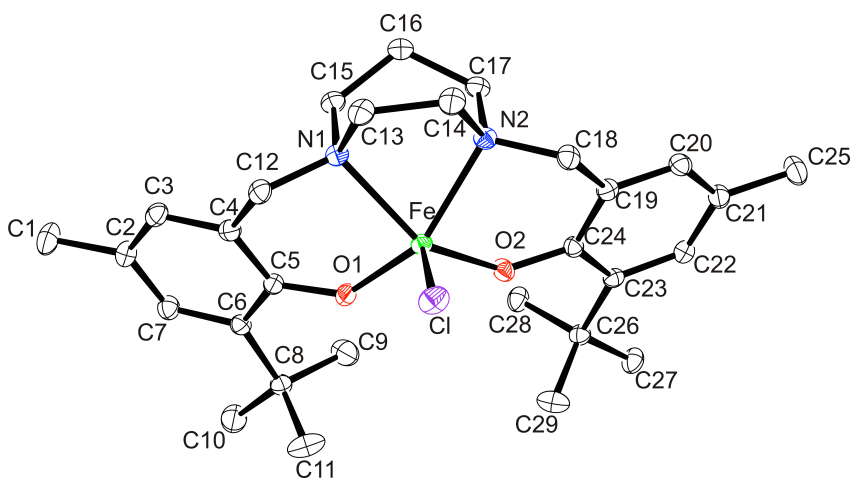


Figure 3.2. Molecular structure (ORTEP) and partial numbering scheme for **3.2**. Ellipsoids are shown at the 50% probability level (H-atoms omitted for clarity).

Table 3.1. Crystallographic data and structure refinement for **3.1** and **3.2**.

Compound	3.1	3.2
Empirical Formula	C ₃₅ H ₅₄ FeClN ₂ O ₃ .C ₃ H ₆ O	C ₂₉ H ₄₂ FeClN ₂ O ₂ .CH ₄ O
Formula Weight	684.18	570.98
Temperature/K	138	168
Crystal Colour	Purple	Purple
Crystal System	Monoclinic	Monoclinic
Crystal Dimensions	0.3 × 0.3 × 0.17 mm	0.29 × 0.2 × 0.2 mm
Lattice Parameters	a = 12.492(3) Å b = 9.7027(19) Å c = 31.799(6) Å α = 90° β = 94.843(3)° V = 3840.6(13) Å ³	a = 27.898(9) Å b = 9.683(3) Å c = 23.472(8) Å α = 90° β = 110.032(4)° V = 5957(3) Å ³
Space Group	P2 ₁ /n (#14)	C2/c (#15)
Z value	4	8
D _{calc}	1.183 g/mm ³	1.273 g/cm ³
F ₀₀₀	1476.0	2440.0
μ(MoKα)	0.498 mm ⁻¹	0.627 cm ⁻¹
Reflections collected	34918	27235
Independent reflections	8486	6525
R _{int}	0.0417	0.0380
R, wR ₂ (all) ^a	0.0417, 0.1025	0.0392, 0.1006
R, wR ₂ [I >= 2σ(I)] ^a	0.0400, 0.1039	0.0375, 0.0988
GOF-fit on F ²	1.051	1.051

$$^a R_1 = \Sigma(|F_o| - |F_c|) / \Sigma|F_o| ; wR_2 = [\Sigma(w(F_o^2 - F_c^2)^2) / \Sigma w(F_o^2)]^{1/2}$$

Table 3.2. Selected bond lengths (Å) and angles (°) for **3.1** and **3.2**.

	3.1	3.2
Fe–O(1)	1.8696(12)	1.8805(12)
Fe–O(2)	1.8734(11)	1.8690(12)
Fe–N(1)	2.1864(13)	2.1826(14)
Fe–N(2)	2.1681(13)	2.1902(14)
Fe–Cl	2.2466(6)	2.2488(8)
O(1)–Fe–O(2)	97.34(5)	98.85(5)
O(1)–Fe–Cl	111.90(4)	109.07(4)
O(2)–Fe–Cl	110.54(4)	110.41(4)
N(1)–Fe–Cl	97.84(4)	99.25(4)
N(2)–Fe–Cl	98.54(4)	96.29(4)
O(1)–Fe–N(1)	86.06(5)	87.84(5)
O(1)–Fe–N(2)	145.15(5)	145.20(5)
O(2)–Fe–N(2)	87.01(5)	86.22(5)
O(2)–Fe–N(1)	147.45(5)	150.19(5)
N(1)–Fe–N(2)	72.93(5)	72.46(5)

3.2.3 UV-visible spectroscopic and magnetic data

Based on previous work with iron(III) compounds supported by tetradentate amino-bis(phenolate) ligands, similar electronic absorption spectra were obtained for all of the present complexes.^{31,33,46} Since all of these complexes showed similar absorption bands, we can assume that the compounds contain Fe in similar geometries. Complexes **3.1–3.5** are intensely purple-coloured solids and their UV-vis spectra exhibit multiple intense bands in the UV and visible regions. Electronic absorption spectra of **3.1–3.5** are shown in **Figure 3.3–Figure 3.7**. The highest energy bands (<300 nm) are caused by $\pi \rightarrow \pi^*$ transitions involving the phenolate units. Strong bands in this region are also observed between 330 and 450 nm which are assigned to charge transfer transitions from the out-of-plane $p\pi$ orbital (HOMO) of the phenolate oxygen to the half-filled $d_{x^2-y^2}/d_{z^2}$ orbital of high-spin iron(III). The lowest energy bands (visible region) between 450 and 700 nm arise from charge-transfer transitions from the in-plane $p\pi$ orbital of the phenolate to the half-filled $d\pi^*$ orbital of iron(III) and account for the intense blue/purple colour of the complexes. The halide ligands are anticipated to be labile in solution.^{40,46} Changing the halide from chloride to bromide resulted in the lowest energy band appearing at a longer wavelength for the bromide complex compared to the chloride analogue. The lower energy of absorption in **3.4** (with electron withdrawing groups) reflects the higher Lewis acidity of the iron centre in this complex compared with **3.1–3.3** and **3.5**.

Magnetic susceptibility data for powdered samples were measured at room temperature using a Johnson-Matthey balance. All compounds **3.1–3.3** and **3.5** exhibited moments in the range of 4.6–5.1 μ_B , consistent with high spin d^5 ions. Complex **3.4**,

however, exhibited a lower magnetic moment than expected ($2.3 \mu_B$) which we postulate is due to the presence of diamagnetic impurities (*e.g.* unreacted ligand), which was supported by MALDI-TOF mass spectrometric data. Another possibility for the lower than expected magnetic moment may be spin-spin coupling if a dinuclear complex was formed – however, we observed no peaks for Fe_2 -species in the mass spectra of **3.4**. More in depth studies on **3.4** including variable temperature magnetic susceptibility measurements would be needed to confirm the assumptions made herein.

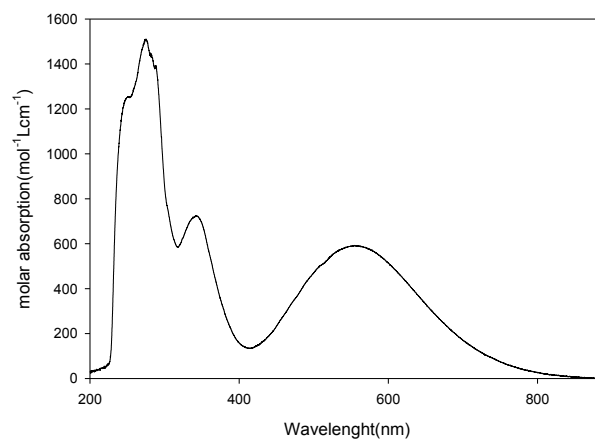


Figure 3.3. Electronic absorption spectrum of **3.1** in dichloromethane.

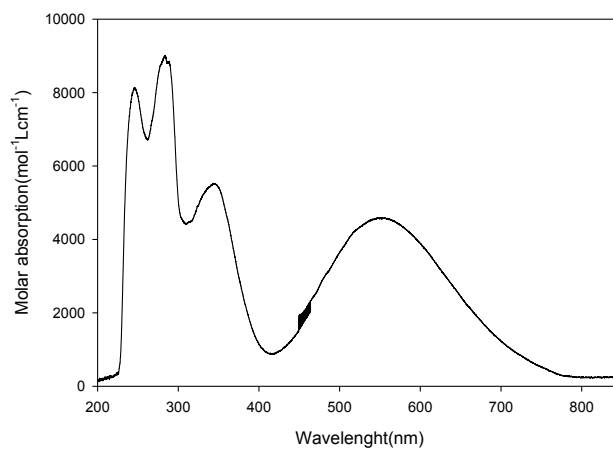


Figure 3.4. Electronic absorption spectrum of **3.2** in dichloromethane.

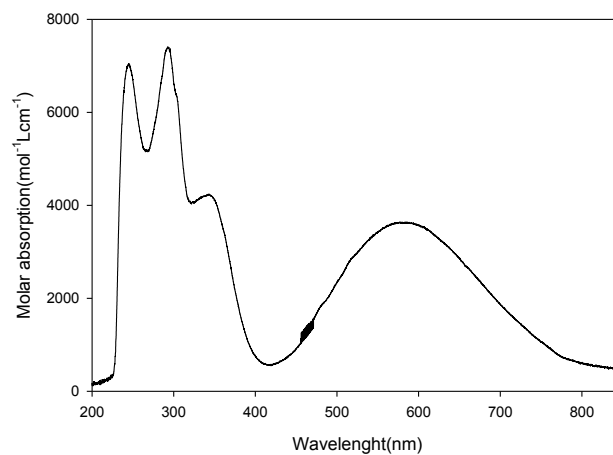


Figure 3.5. Electronic absorption spectrum of **3.3** in dichloromethane.

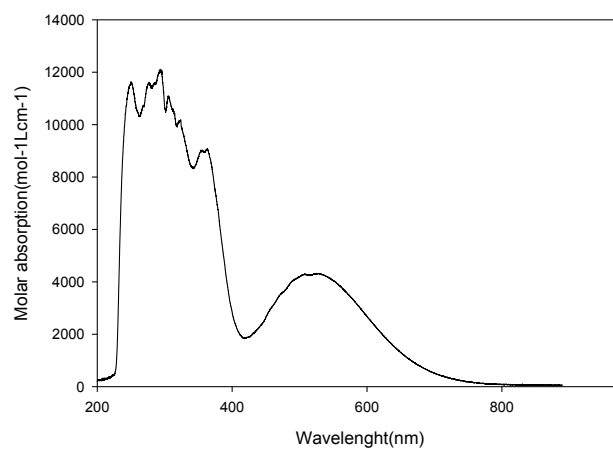


Figure 3.6. Electronic absorption spectrum of **3.4** in dichloromethane.

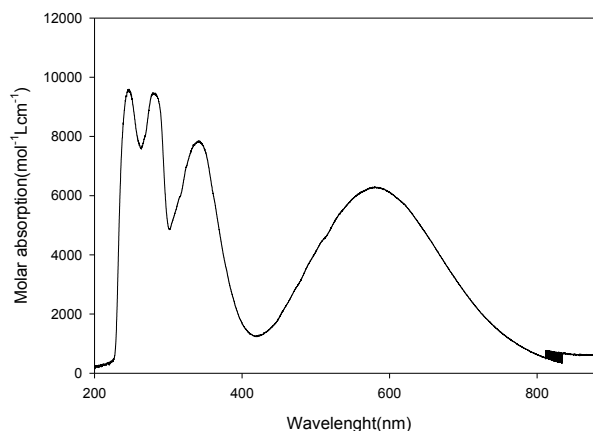


Figure 3.7. Electronic absorption spectrum of **3.5** in dichloromethane.

3.2.4 Cyclization of propylene oxide with carbon dioxide

Inspired by the promising results reported by the Wang,⁴⁹ Capacchione and Rieger³⁵ groups, complexes **3.1–3.5** were evaluated as catalysts under similar conditions but longer reaction times. The results are summarized in **Table 3.3**. Complex **3.1** was studied most extensively in order to get baseline results for comparison with other related catalysts. Tetrabutylammonium bromide (TBAB) was used as a cocatalyst and the influence of the reaction temperature, CO₂ pressure and mole ratio of Fe:PO was studied. The presence of the cocatalyst was necessary since no reactivity was observed when catalyst was used alone (entry 1 vs. entry 3). Ionic and neutral cocatalysts such as TBAB, bis(triphenylphosphine)iminium chloride (PPNCl), PPN azide (PPNN₃) and 4-dimethylaminopyridine (DMAP) were investigated with **3.1** and compared. The results show that the combination of **3.1** and TBAB or PPNCl gives the highest activity and conversion compared to other cocatalysts (entries 3 and 5 vs. entries 6 and 8). It is well known that the anionic group of the cocatalyst can function as a nucleophile for the ring-

opening reaction of the epoxides.^{50,51} It should be noted that TBAB and PPnCl salts alone have been reported to yield only small amounts of cyclic carbonate indicating the necessity of an active catalyst for carbonate formation in addition to the ionic cocatalyst.^{28,35,49,52,53} For example, cyclic propylene carbonate (CPC) was produced with a conversion of 33% in the absence of an Fe catalyst in the present study (entry 2). Under the applied conditions, one equivalent of the neutral Lewis base cocatalyst (DMAP) produced only small amounts of CPC, with an increase to four equivalents inhibiting the reaction (entry 7 vs. 8). This can be explained by the ability of DMAP to coordinate to the metal centre which then competes with the incoming epoxide.^{1,21} In addition, the ratio between cocatalyst and catalyst was also evaluated under the same conditions using TBAB as the cocatalyst. At higher ratios of cocatalyst, the conversion of cyclic carbonate increased from 63% to 74% which corresponds to an increase in TOF from 115 h⁻¹ to 135 h⁻¹ (entry 3 vs. 9). However, a drop in the conversion and the catalytic activity was observed with further increase of TBAB loading (entry 10). Therefore, all reactions were performed with four equivalents of TBAB.

Table 3.3. Cycloaddition reactions of propylene oxide and carbon dioxide catalyzed by iron(III) complexes **3.1–3.5**.

Entry ^[a]	Catalyst	Co-catalyst	[Fe]:[PO]: [Cocat]	Time (h)	T (°C)	Pressure (bar)	Conv. (yield)/ % ^[h]	TON ^[i]	TOF (h ⁻¹) ^[j]
1	3.1	-	1:4000:0	22	100	20	0	-	-
2	-	TBAB	0:4000:4	22	100	20	33	1320	60
3	3.1	TBAB	1:4000:4	22	100	20	74(70)	2960	135
4	3.1	PPNCl	1:4000:4	6	100	20	27	1080	180
5	3.1	PPNCl	1:4000:4	22	100	20	70	2800	127
6	3.1	PPNN ₃	1:4000:4	22	100	20	18	720	33
7	3.1	DMAP	1:4000:1	22	100	20	14	560	26
8	3.1	DMAP	1:4000:4	22	100	20	0	-	-
9 ^[b]	3.1	TBAB	1:4000:2	22	100	20	63	2520	115
10 ^[c]	3.1	TBAB	1:4000:10	22	100	20	58	2320	106
11 ^[d]	3.1	TBAB	1:4000:4	22	25	20	0	-	-
12 ^[e]	3.1	TBAB	1:4000:4	22	100	40	84	3360	153
13 ^[f]	3.1	TBAB	1:4000:4	6	100	20	25	1000	167
14 ^[g]	3.1	TBAB	1:1000:4	22	100	20	58	580	26
15	3.2	TBAB	1:4000:4	22	100	20	30	1200	55
16	3.3	TBAB	1:4000:4	22	100	20	34	1360	62
17	3.4	TBAB	1:4000:4	22	100	20	95	3800	173
18	3.5	TBAB	1:4000:4	22	100	20	34	1360	62

[a] Reaction conditions (unless otherwise stated): PO (7.0×10^{-2} mol), catalyst (1.75×10^{-5} mol), 0.025

mol%), TBAB (7.0×10^{-5} mol, 0.1 mol%), CO₂ (20 bar); 100 °C, 22 h. [b, c] Reactions performed with 2 and 10 equivalents of TBAB respectively. [d] Reaction at room temperature. [e] At 40 bar CO₂. [f] 6 h. [g] Reaction conducted with 1000 equivalents of PO. [h] Determined by ¹H NMR spectroscopy. [i] Overall turnover number ($\text{mol}_{\text{PC}} \text{mol}_{\text{Cat}}^{-1}$). [j] Overall turnover frequency (TON/reaction time) observed.

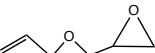
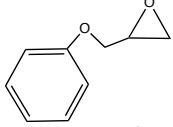
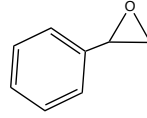
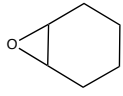
Cycloadditions, as with most reactions, are strongly influenced by temperature. At elevated temperature (100 °C), a conversion of 74% was reached in 22 h with a corresponding TOF value of 135 h^{-1} (entry 3) confirming the thermal stability of the catalytic system. However, conducting the reaction at room temperature afforded no conversion of PO (entry 11). A similar trend has previously been noted for iron complexes by Wang and coworkers.⁴⁹ Therefore, the cycloaddition reaction of PO and CO₂ to form PC typically requires high temperatures and this is in agreement with the fact that selectivity towards formation of the cyclic carbonate product is thermodynamically favored at high temperature. It can also be seen that the pressure of CO₂ has a significant influence on the conversion of PO. When the reaction is conducted at 20 bar P_{CO_2} , conversion levels of 74% were achieved. At higher pressure, $P_{\text{CO}_2} = 40$ bar, it increased from 74% to 84% (entry 3 vs. 12) possibly due to the increased solubility of CO₂ in the epoxide at higher pressure.² As expected, the PO conversion was time-dependent as shortening reaction times from 22 h to 6 h led to decreases in the amount of PC obtained (entry 3 and 13, respectively). In addition, the epoxide loading has a significant influence on the reaction course with an increase in conversion being observed with increasing amounts of PO from 1000 to 4000 (entry 14 vs. 3, respectively).

The cycloaddition reaction was also tested for complexes **3.2–3.5**, in order to identify the most active catalyst and any ligand effects (entries 15-18). As previously reported by others, introducing electron-withdrawing substituents in the *ortho* and *para*-positions of the phenolate ring generates more reactive complexes for use in the coupling reaction of CO₂ and epoxides.⁵³⁻⁵⁵ Our results are in good agreement with this observation as **3.4** displays the highest catalytic activity with a TOF of 173 h⁻¹ (entry 17). A possible explanation is that a decrease in the donor ability of the ligand leads to increased Lewis acidity of the metal centre and enhances the ability of the metal to bind to the epoxide.^{1,2} The substitution of the axial ligand by a bromide led to a drop in the catalytic activity with conversions achieving only 34% (entry 18 *cf.* entry 3 for the corresponding chloride complex, conversion 74%). A similar trend was also observed by Pescarmona and coworkers.⁵³ and they attributed the low activity to the larger radius of bromide which causes steric repulsion for the incoming epoxide substrate when approaching the metal centre. Other reasons for the decrease in activity may be a difference in lability or nucleophilicity of the halide anion. Therefore, overall in the present work activity decreased in the order **3.4** > **3.1** > **3.3** ≥ **3.5** > **3.2**. In contrast to the work reported by Pescarmona's group, only a small amount of polypropylene carbonate (PPC) (4%) could be produced at higher temperature and pressure conditions (70 °C and 70 bar of CO₂).⁵³

To expand the scope of the catalytic system, several commercially available epoxides with different electronic and steric properties were examined as substrates using **3.1** (**Table 3.4**). The reaction conditions were chosen according to the conditions presented in **Table 3.3**. Complex **3.1** was able to produce cyclic carbonate from various terminal epoxides containing functional groups. It has recently been noted that the

presence of such groups can have a significant effect on the underlying mechanism of the reaction and functional groups such as –OH in glycidol can serve a role in activating carbon dioxide.⁵⁶ In our study, epichlorohydrin and glycidol reached conversions higher than those observed for PO (**Table 3.4**, entry 1 vs. 2 and 3). Such observations have already been documented in earlier studies.^{29,35,49,57} Reducing the electron-withdrawing nature of the substituents on the oxirane ring resulted in the production of cyclic carbonate in smaller amounts and low catalytic activity (**Table 3.4**, entries 4 and 5). Styrene oxide (SO) exhibited lower reactivity with conversion reaching only 31% (entry 6). This might be due to electronic effects that have been studied computationally, which show that the alkoxide formed from ring-opening of SO is less nucleophilic and therefore less reactive towards carbon dioxide.⁵⁸ Further to this, switching the substrate to cyclohexene oxide led to very low conversions compared to all other epoxides used and no polymer was formed (**Table 3.4**, entry 7). These results are in agreement with the ones reported by the groups of Kleij,²⁹ Wang,⁴⁹ Capacchione and Rieger.³⁵

Table 3.4. Catalytic cyclization of carbon dioxide and epoxides using **3.1**.

Entry ^[a]	Catalyst	Substrate	Conv./ % ^[b]	TON ^[c]	TOF (h ⁻¹) ^[d]
1	3.1		74	2960	135
2	3.1		78	3120	142
3	3.1		78	3120	142
4	3.1		52	2080	95
5	3.1		53	2120	96.4
6	3.1		31	1240	57
7	3.1		9	364	17

[a] Reaction conditions: substrate (7.0×10^{-2} mol), catalyst (1.75×10^{-5} mol, 0.025 mol%), TBAB (7.0×10^{-5} mol, 0.1 mol%), Fe:[epoxide]:[Cocatalyst] = 1:4000:4, CO₂ (20 bar); 100 °C, 22 h. [b] Overall turnover number ($\text{mol}_{\text{PC}} \text{mol}_{\text{Cat}}^{-1}$). [d] Overall turnover frequency (TON/reaction time) observed.

3.2.5 Kinetic measurements

At elevated temperatures, it is known that CPC is produced as the dominant product in the coupling reaction of PO and CO₂.¹⁹ The production of cyclic carbonates is proposed to occur via a backbiting mechanism from either a carbonate or an alkoxide chain end during the coupling process.^{19,27} In an effort to better understand the mechanistic aspects of the propylene oxide/carbon dioxide coupling process, a kinetic study for the formation of CPC catalyzed by **3.1** and TBAB was undertaken. **Figure 3.8** shows the reaction profile obtained using *in situ* infrared spectroscopy. During the course of the reaction, a strong absorption band at 1806 cm⁻¹ was seen to increase in intensity and can be assigned to the cyclic carbonate carbonyl group.

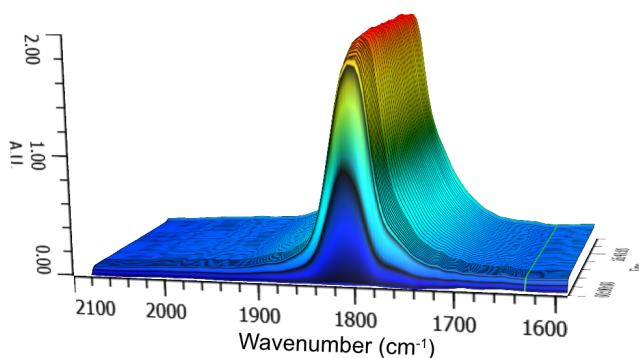


Figure 3.8. Three-dimensional stack plots of IR spectra using **3.1** at 20 bar, 100 °C and [Fe]:[PO]:[Cocat] 1:4000:4.

Furthermore, as discussed above, temperature has a clear influence on the reaction; therefore, the formation of cyclic carbonate was monitored with respect to increases in temperature (**Figure 3.9**). During the course of the reaction, the temperature was gradually increased and maintained for approximately 25 minutes at each temperature. Therefore, the slopes of the straight lines (superimposed on the data points)

at each temperature within Figure 3.9 do not pass through the origin ($t = 0$ min). However, the observed rate of formation of the cyclic carbonate could be obtained from them. Similar experiments have been performed in this way by other researchers including Darensbourg and coworkers.⁵⁹ In the current study, no cyclic carbonate was observed at room temperature and a small amount formed at 30 and 40 °C. As expected, increasing the temperature further resulted in significant increases in the rate of cyclic carbonate formation. In addition, as shown in the Arrhenius plot (**Figure 3.10**), the activation energy for the formation of the cyclic carbonate could be calculated from the kinetic data. The activation barrier using the **3.1**/TBAB catalytic system was determined to be 98.4 kJ mol⁻¹, which is in good agreement with the values reported by the groups of Rieger (93.8 kJ mol⁻¹) and Darensbourg (100 kJ mol⁻¹),^{28,59} for the cycloaddition of PO with CO₂ using an iron(II) complex containing a tetradentate bis(amino)-bis(pyridyl) ligand and chromium(III) salen complex, respectively. Thus implying that the reaction pathways followed by these catalytic systems are likely similar.

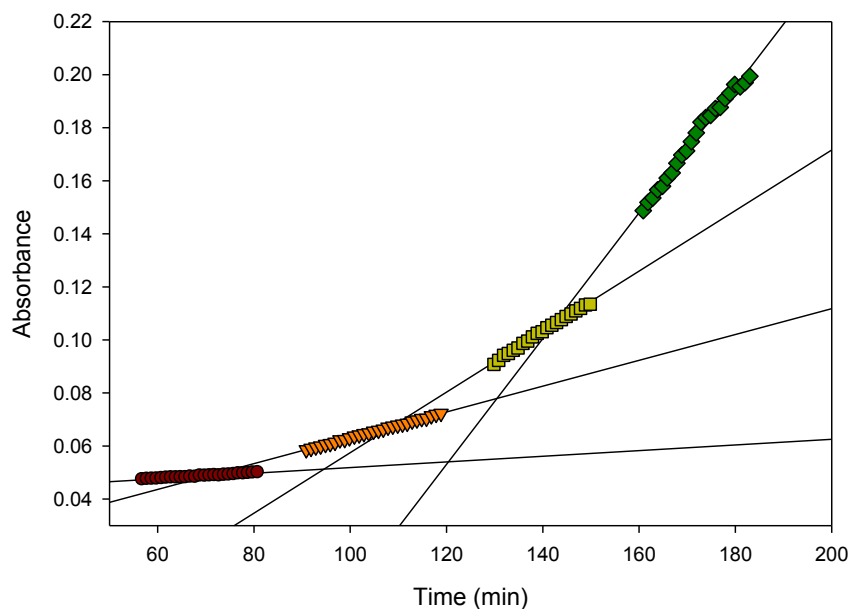


Figure 3.9. Initial rates profile at various temperature based on the absorbance of the $\nu(\text{C}=\text{O})$ of the cyclic propylene carbonate (CPC). All measurements performed on the same reaction mixture and therefore different $t = 0$ for each temperature. \bullet At 50 °C ($y = 0.0001066x + 0.04121$, $R^2 = 0.9838$), \blacktriangledown At 60 °C ($y = 0.0004866x + 0.01444$, $R^2 = 0.9987$), \blacksquare At 70 °C ($y = 0.001141x - 0.05657$, $R^2 = 0.9971$), \blacklozenge At 80 °C ($y = 0.002372x - 0.2107$, $R^2 = 0.988$).

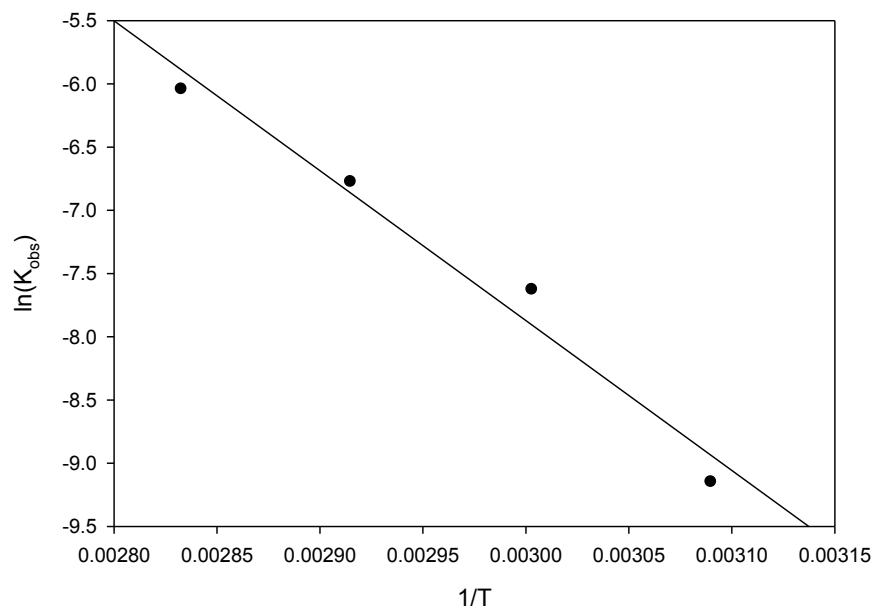


Figure 3.10. Arrhenius plot for the formation of PC. Straight line: $y = -11840x + 27.25$, $R^2 = 0.9713$.

3.3 Conclusions

New air stable iron(III) complexes based on amino-bis(phenolate) ligands were prepared and characterized. The structures of **3.1** and **3.2** were determined and reveal iron(III) centres in square pyramidal environments. The complexes in combination with TBAB exhibit promising activity towards the catalytic formation of cyclic carbonates. It was found that the presence of electron withdrawing groups in the *ortho*- and *para*-positions of the phenolate rings increases the reactivity of catalysts. On the basis of the kinetic data at different temperatures, the activation energy determined for cyclic carbonate formation was close to those previously reported.

3.4 Experimental

3.4.1 General experimental conditions

Reagents were purchased from either Sigma-Aldrich or Alfa Aesar and used without further purification. Commercially available solvents were used without further purification. Reactions for synthesizing ligands and iron complexes were performed in air. [L1]H₂ and [L2]H₂ were prepared using a previously described procedure described in Chapter 2.⁶⁰

3.4.2 Instrumentation

¹H and ¹³C{¹H} NMR spectra were recorded on a Bruker Avance 300 MHz spectrometer at 25 °C and were referenced internally using the residual proton and ¹³C resonances of the solvent. MALDI-TOF MS spectra were obtained using an Applied Biosystems 4800 MALDI TOF/TOF Analyzer equipped with a reflectron, delayed ion

extraction and high performance nitrogen laser (200 Hz operating at 355 nm). Samples were prepared at a concentration of 10.0 mg/mL in toluene. Matrix (anthracene) was mixed at a concentration of 10.0 mg/mL to promote desorption and ionization. Separate vials were used to mix 20 μ L of the sample solution with 20 μ L of the matrix solution. 1 μ L of the sample and matrix mixture were spotted on a MALDI plate and left to dry. Images of mass spectra were prepared using mMassTM software (www.mmass.org). The crystal structures were collected on a AFC8-Saturn 70 single crystal X-ray diffractometer from Rigaku/MSK, equipped with an X-stream 2000 low temperature system (CCDC numbers: 1452392-3). UV-vis spectra were recorded on an Ocean Optics USB4000+ fiber optic spectrophotometer. The room temperature magnetic measurements were obtained using a Johnson-Matthey magnetic susceptibility balance. The data were corrected for the diamagnetism of all atoms and the balance was calibrated using Hg[Co(NCS)₄]. In addition to reactions described below that use a 100 mL pressure vessel equipped for IR-monitoring, cycloaddition reactions were also carried out in a 300 mL stainless steel Parr® 5500 autoclave reactor with a Parr® 4836 controller.

3.4.3 *In situ* monitoring of the cycloaddition reaction by IR spectroscopy

In situ monitoring was carried out using a modified 100 mL stainless steel reactor vessel (Parr Instrument Company) equipped with a silicon sensor (SiComp), motorized mechanical stirrer and a heating mantle. The silicon sensor was connected to a ReactIR 15 base unit (Mettler-Toledo) through a DS silver-halide Fiber-to-Sentinel conduit. The reactor vessel was cleaned and heated under vacuum at 80 °C for 24 h before experiments. The appropriate amount of complex and cocatalyst were weighed and then

dissolved in 4 g PO which afforded a purple solution. The mixture was stirred for about 10 min and the reaction solution was transferred into a 5 mL syringe with a cannula needle attached. The syringe was injected into the vessel through a port. Then the vessel was pressurized with 20 bar CO₂. Heating and stirring were started and the reaction was monitored for the allotted time. After venting the reaction vessel, it was noted that the mixture had changed colour - a brown solution had formed.

3.4.4 Synthesis and characterization of ligands and catalysts

Synthesis of [L3]H₂. A mixture of 3-*tert*-butyl-4-hydroxyanisole (24.4 g, 0.123 mol), 37% w/w aqueous formaldehyde (10.0 mL, 0.123 mol) and homopiperazine (6.22 g, 0.0615 mol) in water (100 mL) was stirred and heated to reflux for 24 h. Upon cooling to room temperature, solvents were decanted from the resulting white solid, which was recrystallized from methanol and chloroform to afford a pure white powder (24 g, 85.7%). ¹H NMR (300 MHz, 298 K, CDCl₃) δ 10.71 (2H, s, OH), 6.80 (2H, d, ²J_{HH} = 2.6, ArH), 6.40 (2H, d, ²J_{HH} = 2.6, ArH), 3.73 (4H, s, ArC-CH₂-N), 3.48 (6H, s, ArC-OCH₃), 2.81 (4H, t, ³J_{HH} = 6.1 Hz, N-CH₂{CH₂}CH₂-N), 2.76 (4H, br, N-CH₂CH₂-N), 1.88 (2H, quintet, ³J_{HH} = 6.01 Hz, N-CH₂{CH₂}CH₂-N), 1.4 (18H, s, ArC-C(CH₃)₃). ¹³C {¹H} NMR (75.4 MHz, 298 K, CDCl₃) δ 151.8 (ArC-O), 150.6 (ArC-OCH₃), 138.0 (ArC-C(CH₃)₃), 122.0 (ArCH), 112.8 (ArCH), 111.2 (ArC-CH₂-N), 62.2 (ArC-CH₂-N), 55.7 (ArC-OCH₃), 54.5 (N-CH₂{CH₂}CH₂-N), 53.0 (N-CH₂CH₂-N), 34.9 (ArC-C-(CH₃)₃), 29.4 (ArC-C-(CH₃)₃), 26.8 (N-CH₂{CH₂}CH₂-N). MS (MALDI-TOF) *m/z* (% ion): 484.3 (100, [H₂[L3]]⁺).

Synthesis of [L4]H₂. A mixture of 2,4-dichlorophenol (24.4 g, 0.123 mol), 37% w/w aqueous formaldehyde (10.0 mL, 0.123 mol) and homopiperazine (6.22 g, 0.0615 mol) in water (50 mL) was stirred and heated to reflux for 72 h. Upon cooling to room temperature, solvents were decanted from the resulting yellow solid (18.5 g, 67%). ¹H NMR (300 MHz, 298 K, CDCl₃) δ 11.65 (2H, s, OH), 7.24 (2H, d, ²J_{HH} = 2.3 Hz, ArH), 6.84 (2H, d, ²J_{HH} = 2.3 Hz, ArH), 3.75 (4H, s, ArC-CH₂-N), 2.83 (4H, t, ³J_{HH} = 6 Hz, N-CH₂{CH₂}CH₂-N), 2.79 (4H, s, N-CH₂CH₂-N), 1.97 (2H, quintet, ³J_{HH} = 6.04 Hz, N-CH₂{CH₂}CH₂-N). ¹³C{¹H} NMR (75.4 MHz, 298 K, CDCl₃) δ 152.40 (ArC-O), 128.70 (ArCCl), 126.51 (ArCCl), 123.43 (ArCH), 123.31 (ArCH), 121.37 (ArC-CH₂-N), 61.11 (ArC-CH₂-N), 54.05 (N-CH₂{CH₂}CH₂-N), 53.59 (N-CH₂CH₂-N), 25.97 (N-CH₂{CH₂}CH₂-N). MS (MALDI-TOF) *m/z* (% ion): 449 (100, [H₂[L4]]⁺⁺).

Synthesis of 3.1. To a methanol solution (30 mL) of recrystallized [L1]H₂ (2.52 g, 4.7 mmol) was added a solution of anhydrous FeCl₃ (0.762 g, 4.7 mmol) in methanol resulting in a purple solution. To this solution was added triethylamine (0.819 g, 9.4 mmol) and the resulting mixture was stirred for 2 h. After stirring, the solvent was removed under vacuum. The purple product was dissolved in acetone (50 mL) and filtered through Celite three times. Removal of solvent under vacuum yielded a black powder (2.61 g, 88%). Anal. calc'd for C₃₅H₅₄FeClN₂O₂·C₃H₆O: C, 66.71; H, 8.84; N, 4.09. Found: C, 66.70; H, 8.80; N, 4.19. MS (MALDI-TOF) *m/z* (% ion): 664.2 (15, [FeCl[L1]+K]⁺⁺), 625.2 (85, [FeCl[L1]]⁺), 590.3 (94.3, [Fe[L1]]⁺). UV-Vis (CH₂Cl₂) λ_{max}, nm (ε): 570 (600). μ_{eff} (solid, 25 °C) = 4.68 μ_B.

Synthesis of 3.2. To a methanol solution (30 mL) of recrystallized [L2]H₂ (2.51 g, 5.5 mmol) was added a solution of anhydrous FeCl₃ (0.899 g, 5.5 mmol) in methanol

resulting in an intense purple solution. To this solution was added triethylamine (0.967 g, 11.1 mmol) and the resulting mixture was stirred for 2 h. After stirring, the solvent was removed under vacuum. The purple product was dissolved in acetone (50 mL) and filtered through Celite. Removal of solvent under vacuum yielded a black powder (2.5 g, 86%). Anal. calc'd for $C_{29}H_{42}FeClN_2O_2$: C, 64.27; H, 7.81; N, 5.17. Found: C, 64.14; H, 8.10; N, 5.37. MS (MALDI-TOF) m/z (% ion): 580.1 (12.2, $[FeCl[L2]+K]^+$), 541.1 (32.4, $[FeCl[L2]]^+$), 506 (63, $[Fe[L2]]^+$). UV-Vis (CH_2Cl_2) λ_{max} , nm (ϵ): 580 (4200). μ_{eff} (solid, 25 °C) = 5.1 μ_B .

Synthesis of 3.3. To a methanol solution (30 mL) of recrystallized $[L3]H_2$ (2.52 g, 5.5 mmol) was added a solution of anhydrous $FeCl_3$ (0.896 g, 5.5 mmol) in methanol resulting in an intense blue solution. To this solution was added triethylamine (0.965 g, 11.1 mmol) and the resulting mixture was stirred for 2 h. After stirring, the solvent was removed under vacuum. The purple product was dissolved in acetone (50 mL) and filtered through Celite. Removal of solvent under vacuum yielded a black powder (2.5 g, 79%). Anal. calc'd for $C_{29}H_{42}FeClN_2O_4 \cdot C_3H_6O$: C, 60.81; H, 7.66; N, 4.43. Found: C, 60.90; H, 7.41; N, 4.63. MS (MALDI-TOF) m/z (% ion): 573.1 (98.6, $[FeCl[L3]]^+$), 538.2 (43.1, $[Fe[L3]]^+$). UV-Vis (CH_2Cl_2) λ_{max} , nm (ϵ): 580 (3700). μ_{eff} (solid, 25 °C) = 5.1 μ_B .

Synthesis of 3.4. To a methanol solution (30 mL) of recrystallized $[L4]H_2$ (2.52 g, 5.6 mmol) was added a solution of anhydrous $FeCl_3$ (0.91 g, 5.6 mmol) in methanol resulting in an intense blue solution. To this solution was added triethylamine (0.977 g, 11.2 mmol) and the resulting mixture was stirred for 2 h. After stirring, the solvent was removed under vacuum. The purple product was dissolved in acetone (50 mL) and

filtered through Celite. Removal of solvent under vacuum yielded a dark black powder (2.9 g, 82%). MS (MALDI-TOF) m/z (% ion): 538.24 (90, [FeCl[L4]]⁺), 503.98 (35, [Fe[L4]]⁺). UV-Vis (CH₂Cl₂) λ_{\max} , nm (ϵ): 550 (4000). μ_{eff} (solid, 25 °C) = 2.3 μ_B .

Synthesis of 3.5. To a methanol solution (30 mL) of recrystallized [L1]H₂ (2.52 g, 4.7 mmol) was added a solution of anhydrous FeBr₃ (1.389 g, 4.7 mmol) in methanol resulting in an intense blue solution. To this solution was added triethylamine (0.819 g, 9.4 mmol) and the resulting mixture was stirred for 2 h. After stirring, the solvent was removed under vacuum. The purple product was dissolved in acetone (50 mL) and filtered through Celite. Removal of solvent under vacuum yielded a dark black powder (2.9 g, 92%). Anal. calc'd for C₃₅H₅₄FeBrN₂O₂: C, 62.69; H, 8.12; N, 4.18. Found: C, 62.87; H, 7.97; N, 4.24. MS (MALDI-TOF) m/z (% ion): 669.29 (45.5, [FeBr[L1]]⁺), 590.38 (81.8, [Fe[L1]]⁺). UV-Vis (CH₂Cl₂) λ_{\max} , nm (ϵ): 580 (6000). μ_{eff} (solid, 25 °C) = 4.85 μ_B .

3.4.5 Spectroscopic data for carbonate products

4-methyl-1,3-dioxolan-2-one (Table 3.4, entry 1).^{54,61} ¹H NMR (300 MHz, 298 K, CDCl₃): δ 4.7 (1H, m, CHO), 4.4 (1H, t, ³ J_{HH} = 7.1 Hz, OCH₂), 3.8 (1H, t, ³ J_{HH} = 7.1 Hz, OCH₂), 1.26 (3H, d, ³ J_{HH} = 6 Hz, CH₃). ¹³C{¹H} NMR (75.4 MHz, 298 K, CDCl₃) δ 154.9 (C-CO), 73.5 (C-CH), 70.5 (C-CH₂), 18.9 (C-CH₃).

4-chloromethyl-1,3-dioxolan-2-one (Table 3.4, entry 2).^{35,54,61} ¹H NMR (300 MHz, 298 K, CDCl₃) δ 4.94 (1H, m, CHO), 4.54 (1H, t, ³ J_{HH} = 8.9 Hz, OCH₂), 4.35 (1H, dd, ³ J_{HH} = 9.2 Hz, OCH₂), 3.7-3.9 (2H, m, CH₂Cl). ¹³C{¹H} NMR (75.4 MHz, 298 K, CDCl₃) δ 154.5 (C-CO), 74.5 (C-CH), 67.0 (C-CH₂Cl), 44.1 (C-CH₂).

4-hydroxymethyl-1,3-dioxolan-2-one (Table 3.4, entry 3).^{35,54} ¹H NMR (300 MHz, 298 K, CDCl₃) δ 4.8 (1H, m, CHO), 4.4-4.6 (2H, m, OCH₂), 3.6-4.1 (1H, m, CH₂OH). ¹³C{¹H} NMR (75.4 MHz, 298 K, CDCl₃) δ 155.6 (C-CO), 75.27 (C-CH), 66.02 (C-CH₂OH), 44.01 (C-CH₂).

4-allyloxymethyl-1,3-dioxolan-2-one (Table 3.4, entry 4).^{35,54} ¹H NMR (300 MHz, 298 K, CDCl₃) δ 5.8 (1H, m, CH), 5.0-5.15 (2H, m, CH₂), 4.71 (1H, s, OCH), 4.4 (1H, t, ³J_{HH} = 8.5 Hz, OCH₂), 4.2 (1H, dd, ³J_{HH} = 8.5 Hz, OCH₂), 3.9 (2H, d, OCH₂), 3.4-3.6 (2H, m, CH₂O). ¹³C{¹H} NMR (75.4 MHz, 298 K, CDCl₃) δ 155.0 (C-CO), 133.7 (C-CHCH₂), 117.3 (C-CHCH₂), 75.2 (C-CH), 72.2 (C-CH₂O), 66.1 (C-CH₂O), 44.0 (C-CH₂).

4-phenoxyethyl-1,3-dioxolan-2-one (Table 3.4, entry 5).^{35,61} ¹H NMR (300 MHz, 298 K, CDCl₃) δ 7.3 (5H, m, ArH), 5.3 (1H, s, ArCH), 5.0 (1H, m, OCH), 4.6 (2H, m, PhCH₂O), 4.2 (2H, m, OCH₂). ¹³C{¹H} NMR (75.4 MHz, 298 K, CDCl₃) δ 155.0 (C-CO), 129.8 (Ar-CO), 122.0 (ArCH), 121.3 (Ar-CH), 114.7 (ArCH), 75.7 (C-CH), 66.2 (C-CH₂O), 44.8 (C-CH₂).

4-phenyl-1,3-dioxolan-2-one (Table 3.4, entry 6).^{35,54,61} ¹H NMR (300 MHz, 298 K, CDCl₃) δ 7.3 (5H, m, ArH), 4.7 (1H, t, ³J_{HH} = 8.7 Hz, OCH), 4.2 (2H, t, ³J_{HH} = 8.7 Hz, OCH₂). ¹³C{¹H} NMR (75.4 MHz, 298 K, CDCl₃) δ 154.9 (C-CO), 137.6 (Ar-CO), 128.5 (ArCH), 128.2 (Ar-CH), 125.5 (Ar-CH), 71.1 (C-CH), 51.1 (C-CH₂).

cis-1,2-cyclohexene carbonate (Table 3.4, entry 7).^{35,61} ¹H NMR (300 MHz, 298 K, CDCl₃) δ 2.89 (1H, m, OCHCH₂CH₂), 1.63 (4H, m, OCHCH₂CH₂), 1.20 (2H, m, OCHCH₂CH₂), 1.03 (2H, m, OCHCH₂CH₂). ¹³C{¹H} NMR (75.4 MHz, 298 K, CDCl₃) δ 154.9 (C-CO), 75.5 (OCHCH₂CH₂), 26.6 (OCHCH₂CH₂), 19.1 (OCHCH₂CH₂).

3.5 References

1. S. Klaus, M. W. Lehenmeier, C. E. Anderson and B. Rieger, *Coord. Chem. Rev.*, **2011**, 255, 1460-1479.
2. P. P. Pescarmona and M. Taherimehr, *Catal. Sci. Technol.*, **2012**, 2, 2169-2187.
3. T. Sakakura and K. Kohno, *Chem. Commun.*, **2009**, 1312-1330.
4. B. Schöffner, F. Schöffner, S. P. Verevkin and A. Börner, *Chem. Rev.*, **2010**, 110, 4554-4581.
5. H. Arakawa, M. Aresta, J. N. Armor, M. A. Barteau, E. J. Beckman, A. T. Bell, J. E. Bercaw, C. Creutz, E. Dinjus, D. A. Dixon, K. Domen, D. L. DuBois, J. Eckert, E. Fujita, D. H. Gibson, W. A. Goddard, D. W. Goodman, J. Keller, G. J. Kubas, H. H. Kung, J. E. Lyons, L. E. Manzer, T. J. Marks, K. Morokuma, K. M. Nicholas, R. Periana, L. Que, J. Rostrup-Nielson, W. M. H. Sachtler, L. D. Schmidt, A. Sen, G. A. Somorjai, P. C. Stair, B. R. Stults and W. Tumas, *Chem. Rev.*, **2001**, 101, 953-996.
6. A. I. Cooper, *J. Mater. Chem.*, **2000**, 10, 207-234.
7. H. Yasuda, L.-N. He, T. Sakakura and C. Hu, *J. Catal.*, **2005**, 233, 119-122.
8. O. V. Zalomaeva, A. M. Chibiryaev, K. A. Kovalenko, O. A. Kholdeeva, B. S. Balzhinimaev and V. P. Fedin, *J. Catal.*, **2013**, 298, 179-185.
9. D. J. Darensbourg and M. W. Holtcamp, *Coord. Chem. Rev.*, **1996**, 153, 155-174.
10. M. North, R. Pasquale and C. Young, *Green Chem.*, **2010**, 12, 1514-1539.
11. X.-B. Lu, Y.-J. Zhang, B. Liang, X. Li and H. Wang, *J. Mol. Catal. A: Chem.*, **2004**, 210, 31-34.
12. G. A. Luinstra, G. R. Haas, F. Molnar, V. Bernhart, R. Eberhardt and B. Rieger, *Chem. Eur. J.*, **2005**, 11, 6298-6314.
13. S. H. Kim, D. Ahn, M. J. Go, M. H. Park, M. Kim, J. Lee and Y. Kim, *Organometallics*, **2014**, 33, 2770-2775.
14. I. S. Metcalfe, M. North and P. Villuendas, *J. CO₂ Util.*, **2013**, 2, 24-28.
15. S. Iksi, A. Aghmiz, R. Rivas, M. D. González, L. Cuesta-Aluja, J. Castilla, A. Orejón, F. El Guemmout and A. M. Masdeu-Bultó, *J. Mol. Catal. A: Chem.*, **2014**, 383-384, 143-152.
16. Y. Niu, W. Zhang, H. Li, X. Chen, J. Sun, X. Zhuang and X. Jing, *Polymer*, **2009**, 50, 441-446.
17. M. Adolph, T. A. Zevaco, C. Altesleben, O. Walter and E. Dinjus, *Dalton Trans.*, **2014**, 43, 3285-3296.
18. M. Sunjuk, A. Abu-Surrah, E. Al-Ramahi, A. Qaroush and A. Saleh, *Transition Met. Chem.*, **2013**, 38, 253-257.
19. X.-B. Lu and D. J. Darensbourg, *Chem. Soc. Rev.*, **2012**, 41, 1462-1484.
20. L. N. Saunders, N. Ikpo, C. F. Petten, U. K. Das, L. N. Dawe, C. M. Kozak and F. M. Kerton, *Catal. Commun.*, **2012**, 18, 165-167.
21. R. L. Paddock, Y. Hiyama, J. M. McKay and S. T. Nguyen, *Tetrahedron Lett.*, **2004**, 45, 2023-2026.
22. K. L. Peretti, H. Ajiro, C. T. Cohen, E. B. Lobkovsky and G. W. Coates, *J. Am. Chem. Soc.*, **2005**, 127, 11566-11567.
23. A. Decortes, M. Martinez Belmonte, J. Benet-Buchholz and A. W. Kleij, *Chem.*

- Commun.*, **2010**, 46, 4580-4582.
24. S.-i. Fujita, M. Nishiura and M. Arai, *Catal. Lett.*, **2010**, 135, 263-268.
 25. P. Ramidi, C. M. Felton, B. P. Subedi, H. Zhou, Z. R. Tian, Y. Gartia, B. S. Pierce and A. Ghosh, *J. CO₂ Util.*, **2015**, 9, 48-57.
 26. C.-Y. Li, C.-R. Wu, Y.-C. Liu and B.-T. Ko, *Chem. Commun.*, **2012**, 48, 9628-9630.
 27. A. Buchard, M. R. Kember, K. G. Sandeman and C. K. Williams, *Chem. Commun.*, **2011**, 47, 212-214.
 28. J. E. Dengler, M. W. Lehenmeier, S. Klaus, C. E. Anderson, E. Herdtweck and B. Rieger, *Eur. J. Inorg. Chem.*, **2011**, 2011, 336-343.
 29. C. J. Whiteoak, B. Gjoka, E. Martin, M. M. Belmonte, E. C. Escudero-Adán, C. Zonta, G. Licini and A. W. Kleij, *Inorg. Chem.*, **2012**, 51, 10639-10649.
 30. K. L. Collins, L. J. Corbett, S. M. Butt, G. Madhurambal and F. M. Kerton, *Green Chem. Lett. Rev.*, **2007**, 1, 31-35.
 31. X. Qian, L. N. Dawe and C. M. Kozak, *Dalton Trans.*, **2011**, 40, 933-943.
 32. R. R. Chowdhury, A. K. Crane, C. Fowler, P. Kwong and C. M. Kozak, *Chem. Commun.*, **2008**, 94-96.
 33. K. Hasan, C. Fowler, P. Kwong, A. K. Crane, J. L. Collins and C. M. Kozak, *Dalton Trans.*, **2008**, 2991-2998.
 34. R. K. Dean, C. I. Fowler, K. Hasan, K. Kerman, P. Kwong, S. Trudel, D. B. Leznoff, H.-B. Kraatz, L. N. Dawe and C. M. Kozak, *Dalton Trans.*, **2012**, 41, 4806-4816.
 35. A. Buonerba, A. De Nisi, A. Grassi, S. Milione, C. Capacchione, S. Vagin and B. Rieger, *Catal. Sci. Technol.*, **2015**, 5, 118-123.
 36. L. Dyers Jr, S. Y. Que, D. VanDerveer and X. R. Bu, *Inorg. Chim. Acta*, **2006**, 359, 197-203.
 37. T. Kurahashi, K. Oda, M. Sugimoto, T. Ogura and H. Fujii, *Inorg. Chem.*, **2006**, 45, 7709-7721.
 38. H.-L. Shyu, H.-H. Wei, G.-H. Lee and Y. Wang, *J. Chem. Soc., Dalton Trans.*, **2000**, 915-918.
 39. R. Mayilmurugan, M. Sankaralingam, E. Suresh and M. Palaniandavar, *Dalton Trans.*, **2010**, 39, 9611-9625.
 40. M. Velusamy, M. Palaniandavar, R. S. Gopalan and G. U. Kulkarni, *Inorg. Chem.*, **2003**, 42, 8283-8293.
 41. E. F. Chard, J. R. Thompson, L. N. Dawe and C. M. Kozak, *Can. J. Chem.*, **2014**, 92, 758-764.
 42. J. B. H. Strautmann, S. D. George, E. Bothe, E. Bill, T. Weyhermüller, A. Stammler, H. Bögge and T. Glaser, *Inorg. Chem.*, **2008**, 47, 6804-6824.
 43. P. Mialane, E. Anxolabéhère-Mallart, G. Blondin, A. Nivorojkine, J. Guilhem, L. Tchertanova, M. Cesario, N. Ravi, E. Bominaar, J.-J. Girerd and E. Münck, *Inorg. Chim. Acta*, **1997**, 263, 367-378.
 44. R. Viswanathan, M. Palaniandavar, T. Balasubramanian and T. P. Muthiah, *Inorg. Chem.*, **1998**, 37, 2943-2951.
 45. M. Merkel, F. K. Müller and B. Krebs, *Inorg. Chim. Acta*, **2002**, 337, 308-316.
 46. A. M. Reckling, D. Martin, L. N. Dawe, A. Decken and C. M. Kozak, *J.*

- Organomet. Chem.*, **2011**, 696, 787-794.
47. R. van Gorkum, J. Berding, A. M. Mills, H. Kooijman, D. M. Tooke, A. L. Spek, I. Mutikainen, U. Turpeinen, J. Reedijk and E. Bouwman, *Eur. J. Inorg. Chem.*, **2008**, 2008, 1487-1496.
 48. T. N. Rao, J. Reedijk, J. Vanrijn and G. C. Verschoor, A. W. Addison, *J. Chem. Soc., Dalton Trans.*, **1984**, 1349-1356.
 49. X. Sheng, L. Qiao, Y. Qin, X. Wang and F. Wang, *Polyhedron*, **2014**, 74, 129-133.
 50. T. Aida and S. Inoue, *Acc. Chem. Res.*, **1996**, 29, 39-48.
 51. M. North and R. Pasquale, *Angew. Chem. Int. Ed.*, **2009**, 48, 2946-2948.
 52. M. A. Fuchs, T. A. Zevaco, E. Ember, O. Walter, I. Held, E. Dinjus and M. Döring, *Dalton Trans.*, **2013**, 42, 5322-5329.
 53. M. Taherimehr, J. P. C. C. Sertã, A. W. Kleij, C. J. Whiteoak and P. P. Pescarmona, *ChemSusChem*, **2015**, 8, 1034-1042.
 54. C. J. Whiteoak, N. Kielland, V. Laserna, E. C. Escudero-Adán, E. Martín and A. W. Kleij, *J. Am. Chem. Soc.*, **2013**, 135, 1228-1231.
 55. J. R. Wildeson, J. C. Yarbrough, J. H. Reibenspies and D. J. Darensbourg, *J. Am. Chem. Soc.*, **2000**, 122, 12487-12496.
 56. J. Rintjema, R. Epping, G. Fiorani, E. Martín, E. C. Escudero-Adán and A. W. Kleij, *Angew. Chem. Int. Ed.*, **2016**, 55, 3972-3976.
 57. E. Martín, M. Martínez Belmonte, J. Benet-Buchholz, C. J. Whiteoak and A. W. Kleij, *Adv. Synth. Catal.*, **2012**, 354, 469-476.
 58. F. Castro-Gómez, G. Salassa, A. W. Kleij and C. Bo, *Chem. Eur. J.*, **2013**, 19, 6289-6298.
 59. D. J. Darensbourg, J. C. Yarbrough, C. Ortiz and C. C. Fang, *J. Am. Chem. Soc.*, **2003**, 125, 7586-7591.
 60. D. Alhashmialameer, N. Ikpo, J. Collins, L. N. Dawe, K. Hattenhauer and F. M. Kerton, *Dalton Trans.*, **2015**, 44, 20216-20231.
 61. M. A. Fuchs, T. A. Zevaco, E. Ember, O. Walter, I. Held, E. Dinjus and M. Döring, *Dalton Trans.*, **2013**, 42, 5322-5329.

Chapter 4 Synthesis and reactivity of cobalt amino-bis(phenolate) complexes

4.1 Introduction

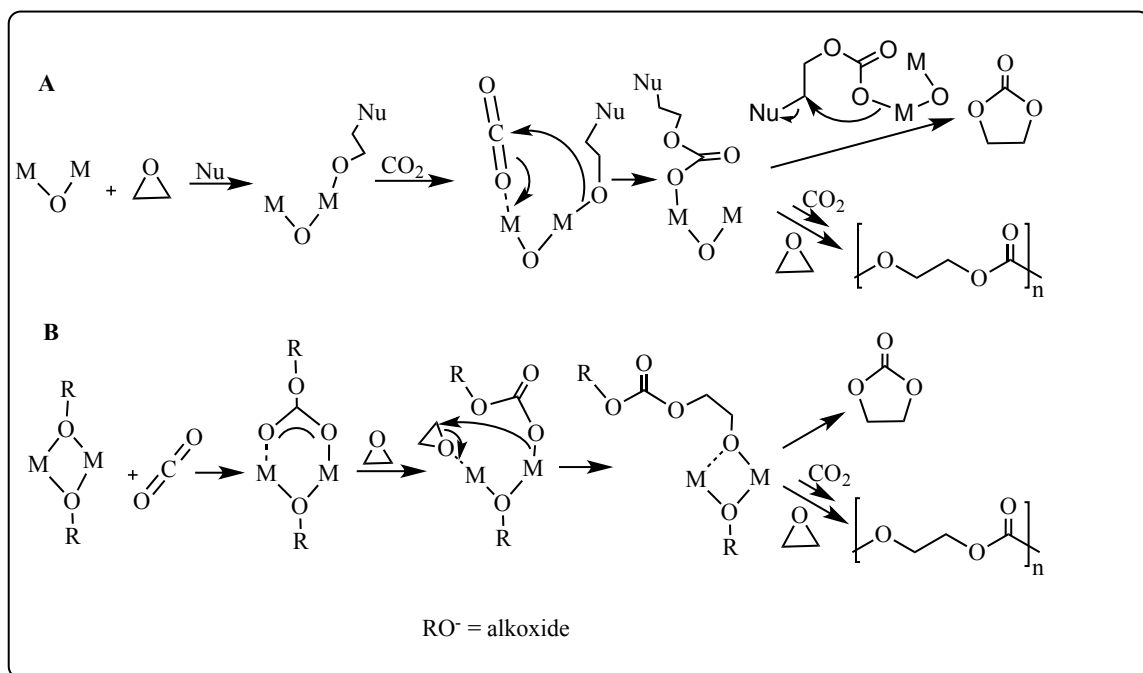
4.1.1 Dinuclear complexes

In the context of coordination chemistry, the term *dinuclear* refers to a metal complex that contains two of the same metal while a *bimetallic* complex is a metal complex containing two different metal centres. In the addition of CO₂ to epoxides, it has been shown that catalytic activity can be efficiently increased by using a catalyst containing two metal centres, which can be the same or different. The mechanism for dinuclear initiation is thought to occur through one of the following two pathways (**Scheme 4.1**):^{1,2}

A- The first step is the activation of the epoxide by coordination to the metal centre.

The presence of two neighbouring metal centres is crucial to activate the epoxide and CO₂ simultaneously, thus enhancing the intramolecular nucleophilic attack of the alkoxide to the carbon atom of the activated CO₂ molecule. This type of mechanism has been proposed for some dinuclear salen complexes as compared to their mononuclear analogues.³

B- Some metal alkoxide complexes bridged by alkoxide or aryloxy groups (-OR) can undergo CO₂ insertion to form bidentate carbonates as the first step instead of epoxide activation. This initial step is followed by coordination of the epoxide to one of the metal centres and then ring opening and insertion into the metal carbonate bond. This mechanism has been proposed for bulky β -diiminate (BDI) zinc complexes bridged by alkoxide (or carboxylate) groups.^{4,5}



Scheme 4.1. Dinuclear catalytic mechanisms for CO₂/epoxide copolymerization. **A.** Dinuclear pathway with simultaneous activation of epoxide and CO₂. **B.** Dinuclear pathway with complexes containing –OR groups.

Dinuclear zinc β-diiminate (BDI) catalysts were first reported by Coates in 1998 (**Figure 4.1**).⁶ The catalyst demonstrated good activity (TOF = 247 h⁻¹) and selectivity for CO₂/CHO copolymerization at 50 °C and 7 bar CO₂. Furthermore, the polymers produced had high molecular weights (31,000 g mol⁻¹) and very narrow dispersities, consistent with a living polymerization process. The mechanism was investigated in 2003, and it was revealed that the two zinc centres interact with each other in the copolymerization, with reaction orders in total zinc 1.8.⁵

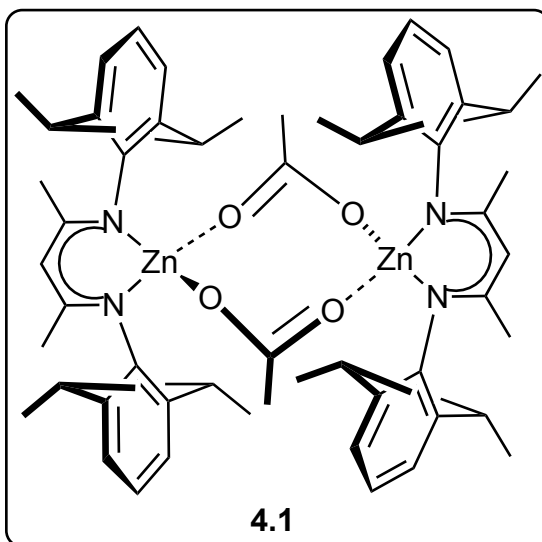


Figure 4.1. β -Diimine zinc acetate complexes used for the alternating copolymerization of CHO and CO₂.⁶

A study of dinuclear Co complexes containing two salen ligands (**4.2**) was undertaken by Nozaki and coworkers towards the copolymerization of PO and CO₂ (**Figure 4.2**).⁷ In the absence of cocatalyst, the tethered catalysts were in fact more reactive than the monometallic species- on the order of 6–11 times faster. In addition, these catalysts were able to operate under high dilution conditions (with low catalyst loadings of up to 20,000:1 epoxide:catalyst).

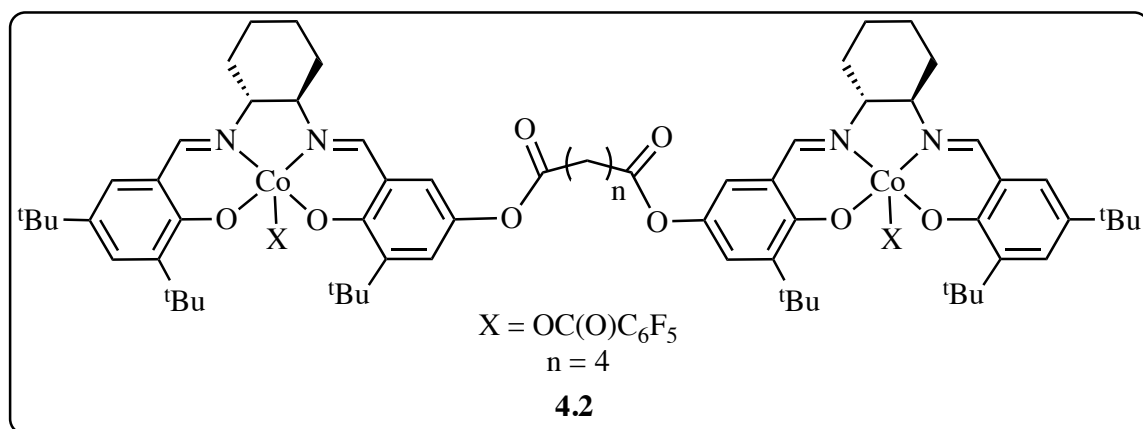


Figure 4.2. Dinuclear cobalt(III) salen complexes.⁷

A series of dinuclear macrocyclic complexes has been developed by Williams and coworkers. A highly active macrocyclic dinuclear cobalt(II,II), cobalt(II,III) complexes (**4.3** and **4.4**, **Figure 4.3**) was shown to catalyze the alternating copolymerization of CHO and CO₂.⁸ The catalyst was effective at 1 bar CO₂, 80–100 °C, and 0.1% catalyst loading with a TOF = 200 and 250 h⁻¹, respectively. The higher activity of these complexes at low pressure was attributed to the macrocyclic ligand environment and dinuclear structure.

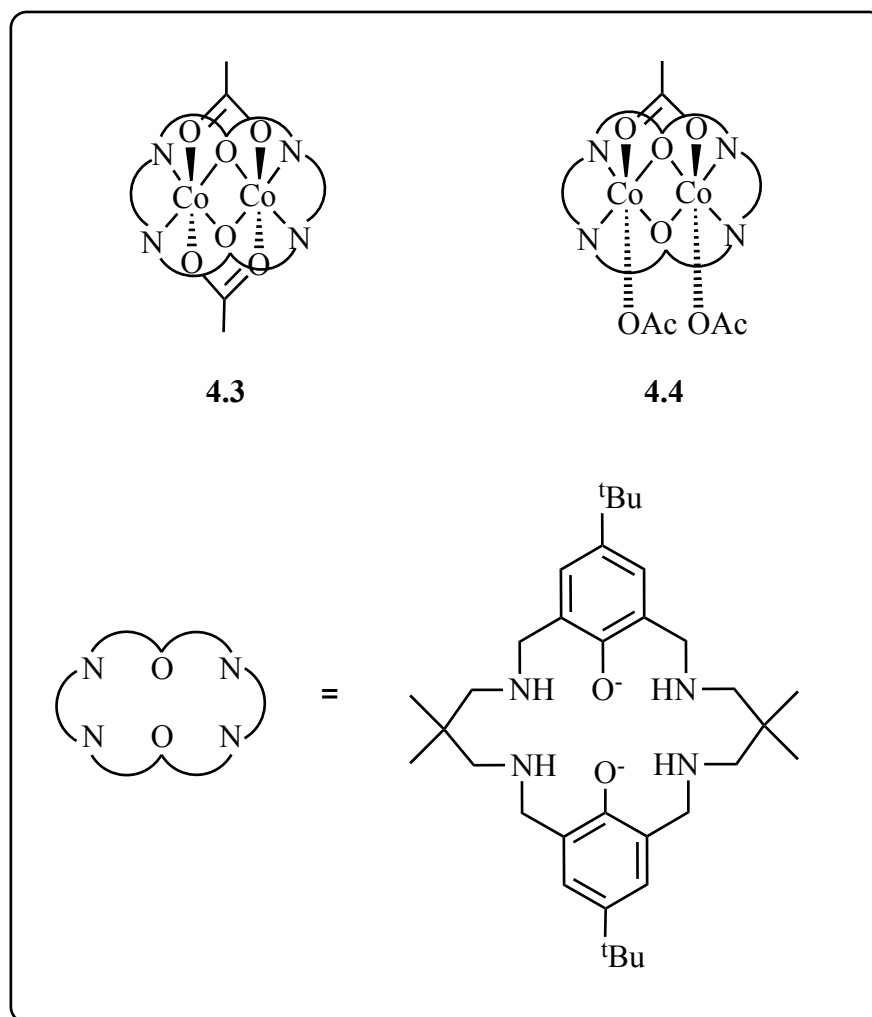


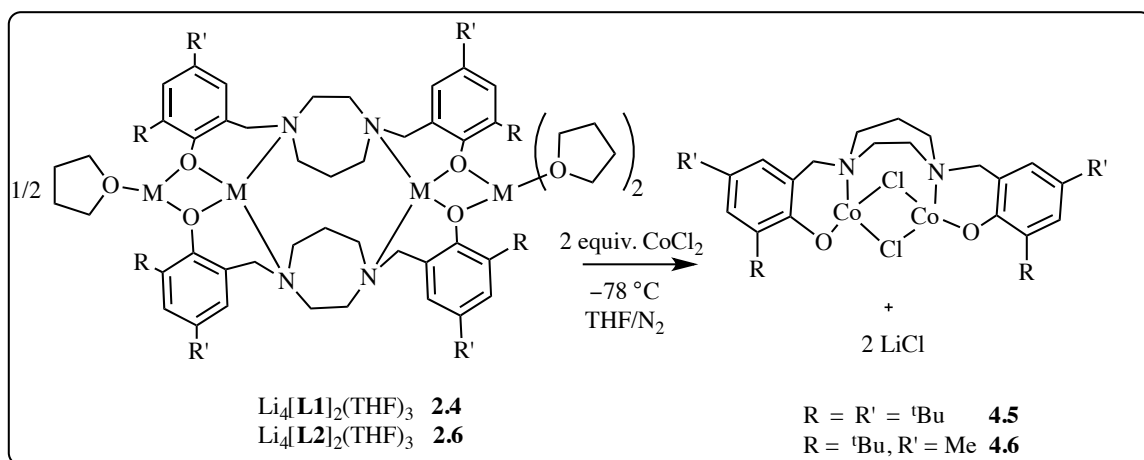
Figure 4.3. Dinuclear macrocyclic cobalt catalyst.⁸

In this chapter, the synthesis and structural characterization of mono- and dinuclear cobalt amino-bis(phenolate) complexes are reported. Their catalytic activities in the cyclization of carbon dioxide–propylene oxide are discussed.

4.2 Results and discussion

4.2.1 Synthesis and characterization of dinuclear cobalt complexes

Co₂(II) complexes were synthesized by salt metathesis, in which the lithium amino-bis(phenolate) complexes (**2.4** and **2.6**) presented in Chapter 2 were used in the preparation of Co(II) complexes. The complexes were reacted with 2 equivalents CoCl₂ per ligand in THF at -78 °C, resulting in the isolation of dark blue powders. Extraction in toluene afforded the formation of the desired dinuclear complexes Co₂Cl₂[L1] (**4.5**) and Co₂Cl₂[L2] (**4.6**) (Scheme 4.2). Their characterization is described in section 4.2.3.



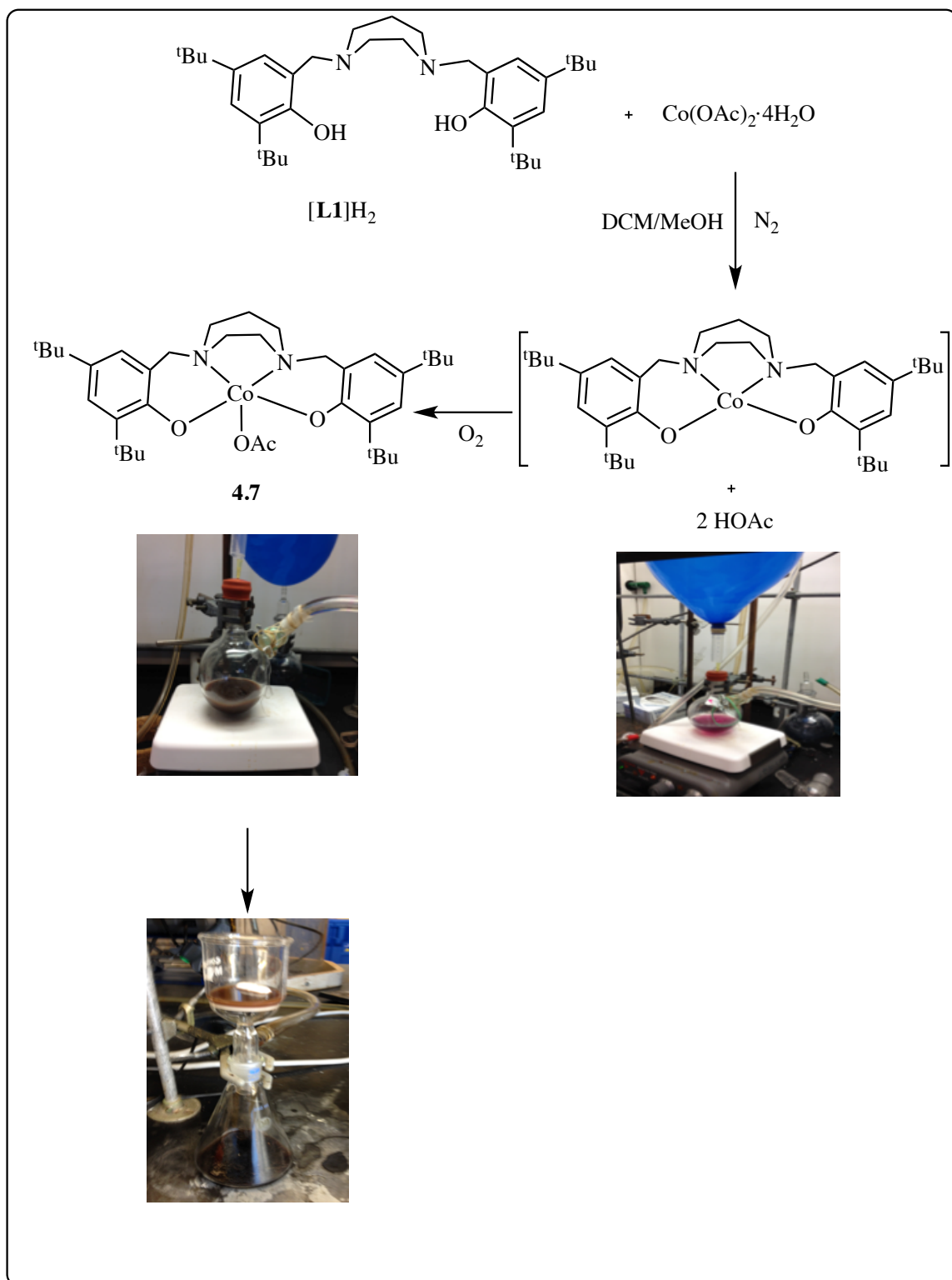
Scheme 4.2. Synthesis of dinuclear Co(II) amino-bis(phenolate) complexes.

4.2.2 Synthesis and characterization of cobalt(III) acetate complex

The literature has reported, in some cases, the complete loss of activity upon

reduction of Co(III) to Co(II) during the copolymerization.⁹ The Lewis acidity of Co(III) is an important factor in enhancing the copolymerization reaction by facilitating the activation and ring opening of the epoxide and suppressing the undesirable dissociation of the growing polymer chain from the metal and as a result, the possibility of subsequent back-biting.¹⁰ Therefore, we were interested in designing Co(III) complexes based on amino-bis(phenolate) ligands and studying their activity in the coupling of CO₂ and epoxides.

As seen in **Scheme 4.3**, [L1]H₂ (2 g, 3.72 mmol) and cobaltous acetate tetrahydrate (0.926 g, 3.72 mmol) were combined under N₂ in a Schlenk flask. A dry, degassed mixture of dichloromethane (20 mL) and methanol (30 mL) was added to the flask. The resulting suspension was stirred under N₂ for 1 h to afford a dark pink solution. Stirring for 1 week under O₂ afforded a dark brown solution and a dark brown solid that was collected on a frit and isolated in 77% yield (1.7 g). Unfortunately, the elemental analysis obtained for this compound was not satisfactory and repeated recrystallizations did not afford material that was superior in this regard.



Scheme 4.3. Synthesis of Co(III) acetate complex (**4.7**).

4.2.3 Characterization of cobalt complexes

4.2.3.1 MALDI-TOF mass spectrometry

The mass spectra of **4.5** is illustrated in **Figure 4.4** and **Figure 4.5**, and of **4.6** in **Figure 4.6** and **Figure 4.7**; anthracene was used as a charge transfer matrix.^{11,12} For complex **4.5**, the molecular ion peak at m/z 722.1 amu correlates well to the calculated molecular weight for the dinuclear cobalt complex (722.2 amu). The isotopic distribution pattern of molecular ion peak agrees well with its calculated value for **4.5**, providing strong evidence for the formulation proposed. The loss of the first chloride ion was observed at 678.1 amu, corresponding to $[\text{Co}_2\text{Cl}[\text{L1}]]^+$, while the peak at 593.2 amu was assigned to the loss of the second chloride ion and a cobalt, $[\text{Co}[\text{L1}]]^+$.

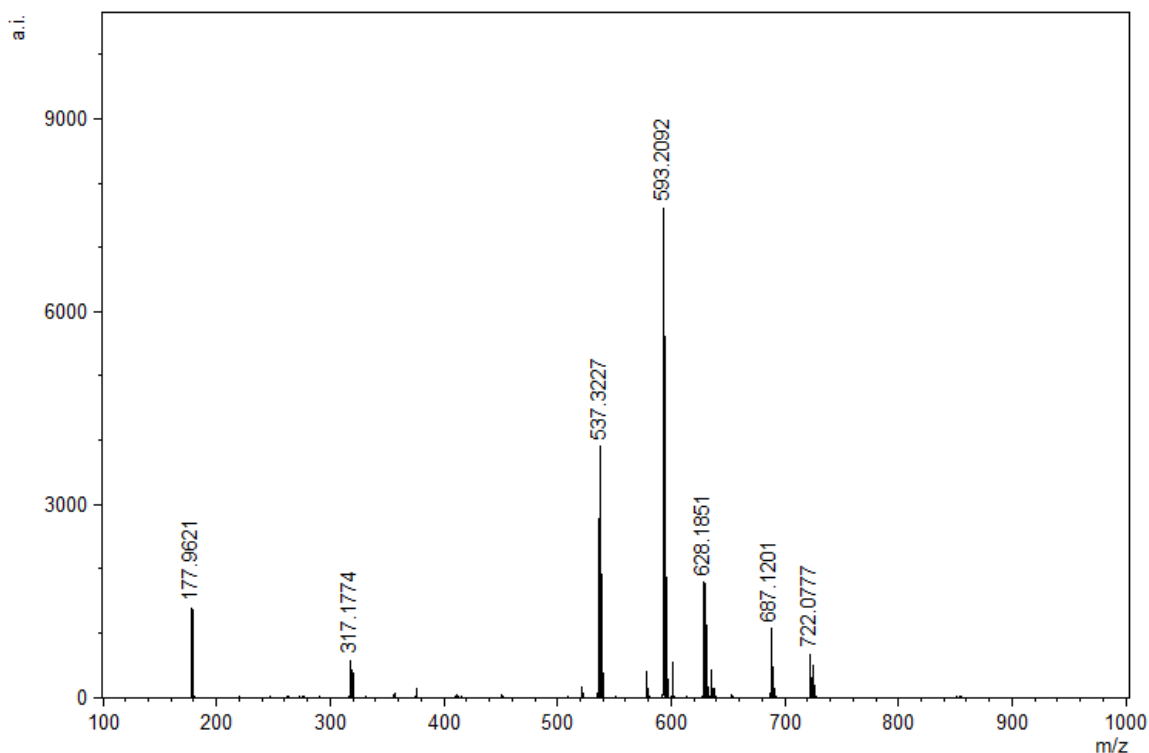


Figure 4.4. MALDI-TOF mass spectrum of $\text{Co}_2\text{Cl}_2[\text{L1}]$ (**4.5**).

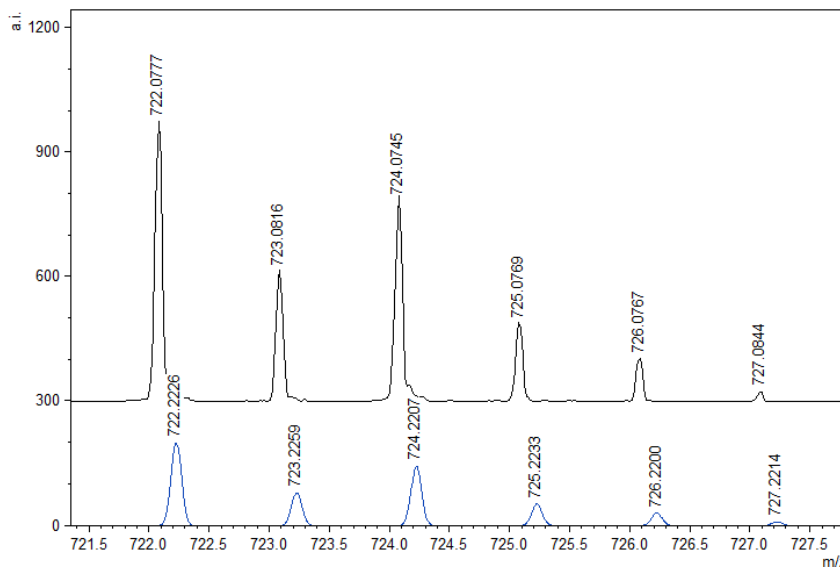


Figure 4.5. Experimental (top) and calculated (bottom) isotopic distribution pattern for **4.5**.

The molecular ion peak of complex **4.6** occurs at m/z 638.12 amu, which matches with the calculated molecular weight for the dinuclear cobalt complex, 638.1 amu (**Figure 4.6**). The isotopic distribution pattern of the molecular ion peak has a close resemblance to its calculated molecular ion peak (**Figure 4.7**). The low intensity peak at 603.1 amu corresponds to the loss of the first Cl^- ion to give $[\text{Co}_2\text{Cl}[\text{L2}]]^+$. However, the most intense peak in the spectrum is observed at m/z 509.2 amu; this corresponds to the $[\text{Co}[\text{L2}]]^+$ ion, which was generated by the loss of the second Cl^- ion and a cobalt from its molecular ion.

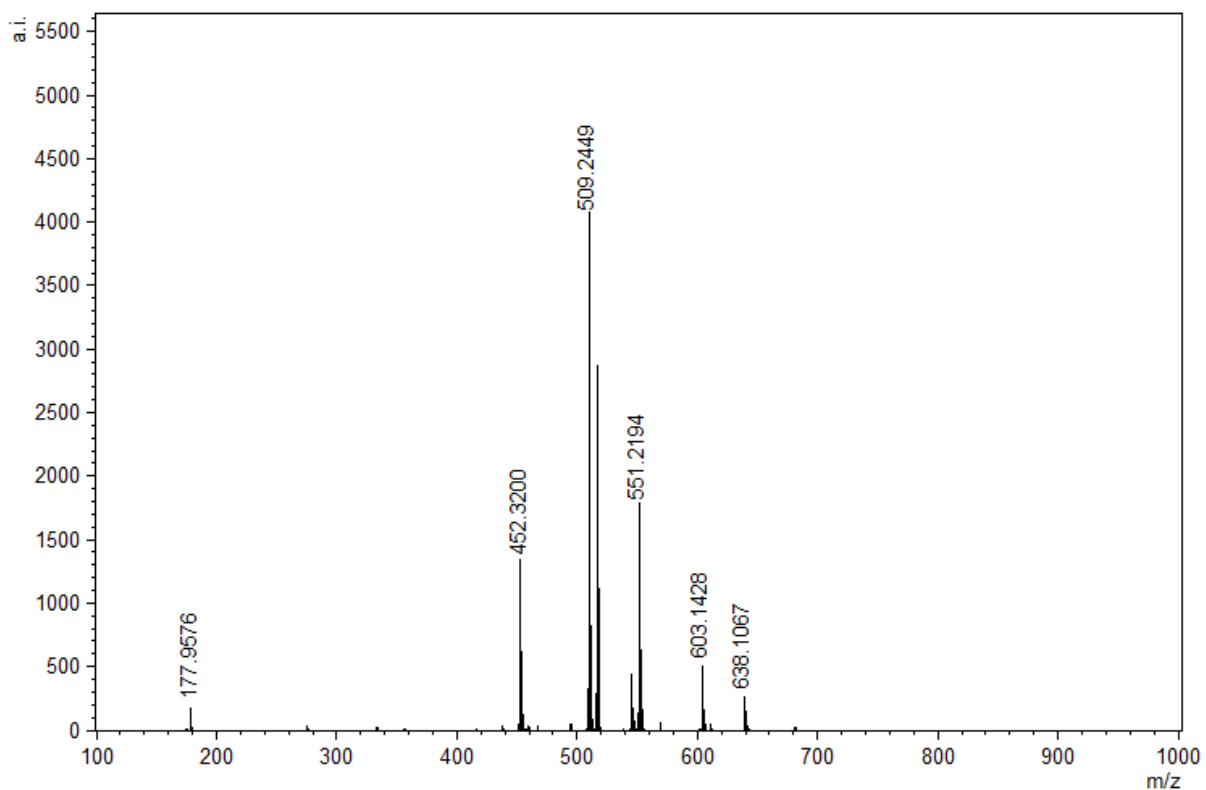


Figure 4.6. MALDI-TOF mass spectrum of $\text{Co}_2\text{Cl}_2[\text{L2}]$ (4.6).

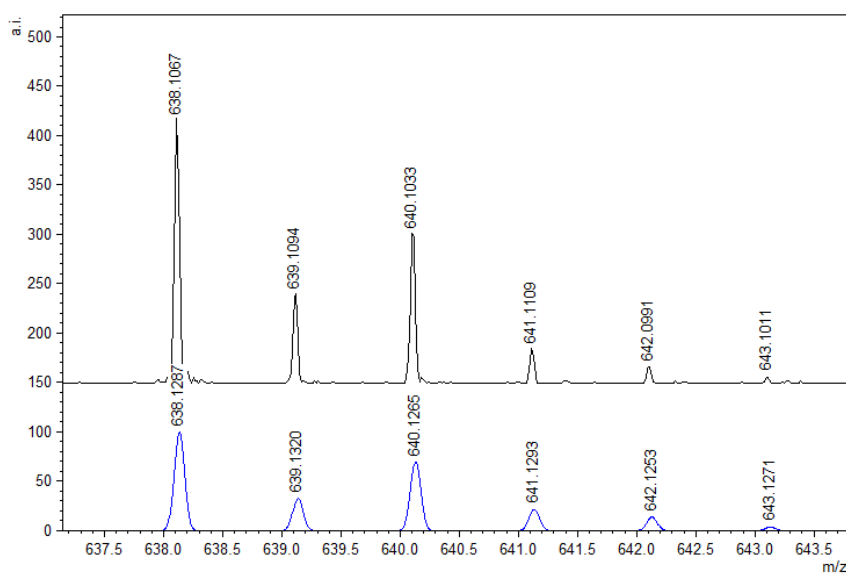


Figure 4.7. Experimental (top) and calculated (bottom) isotopic distribution pattern for 4.6.

The MALDI-TOF mass spectrum of complex CoOAc[L1] (**4.7**) shows the molecular ion peak at m/z 652.46 amu, which is close to the calculated exact mass for that complex, 652.37 amu (**Figure 4.8**). In addition, the loss of acetate was observed at 594.4 amu, corresponding to $[\text{Co}[\text{L1}]]^+$. The isotopic distribution pattern of the experimental $[\text{M}]^+$ ion agrees well with the theoretical peaks for **4.7**, as shown in **Figure 4.9**.

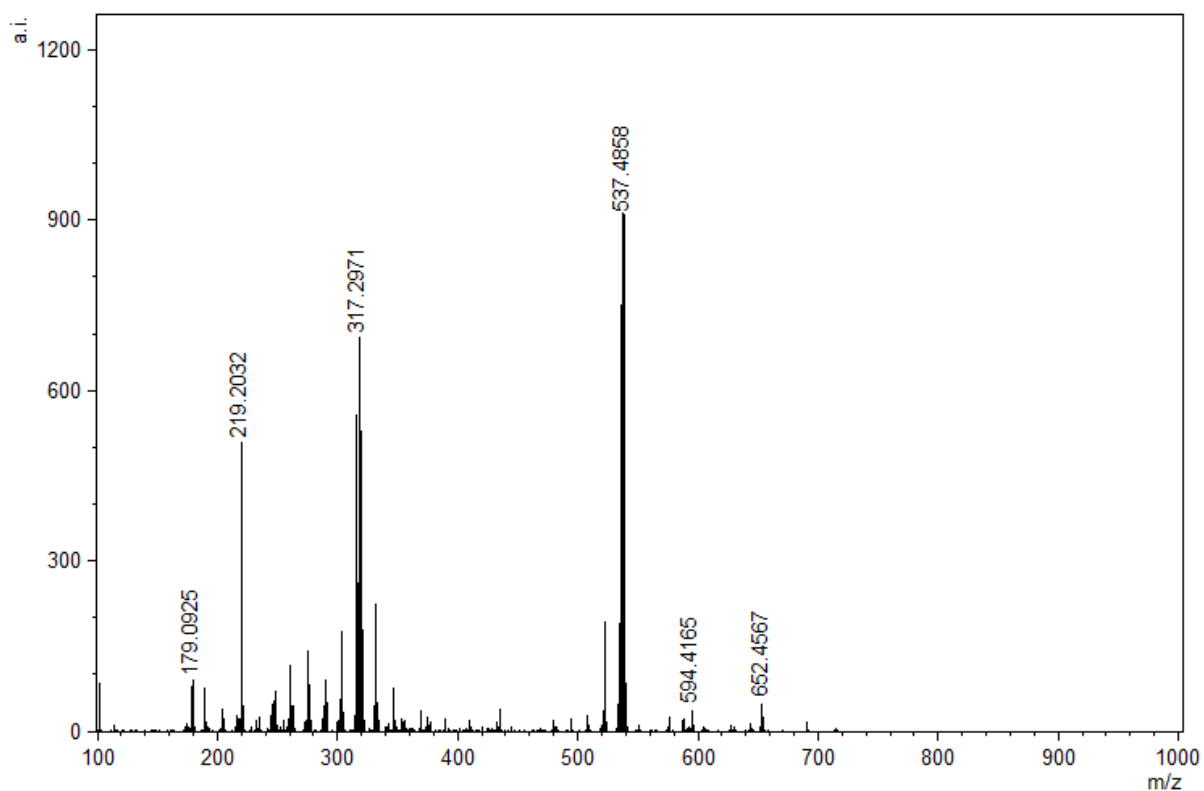


Figure 4.8. MALDI-TOF mass spectrum of CoOAc [L1] (**4.7**).

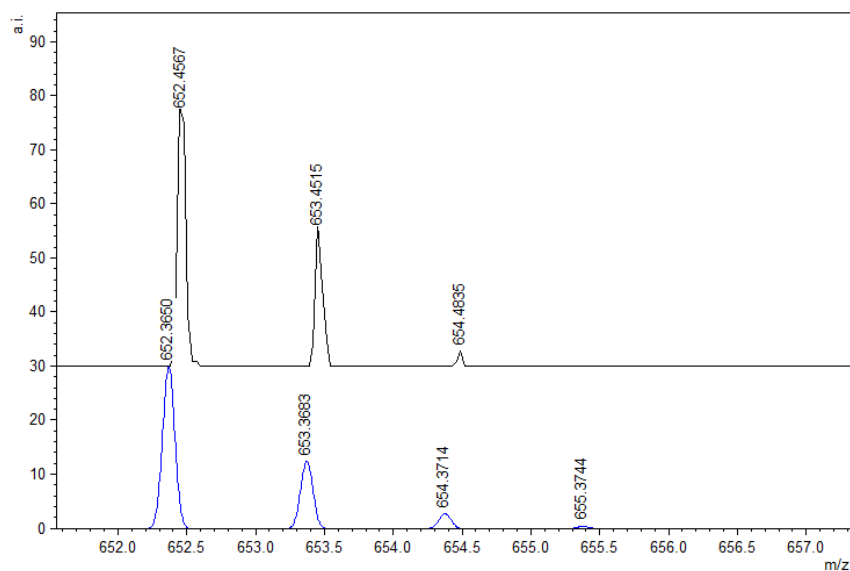


Figure 4.9. Experimental (top) and calculated (bottom) isotopic distribution pattern for **4.7**.

4.2.4 UV-visible spectroscopic and magnetic data

UV-vis spectra of cobalt complexes **4.5–4.7** are shown in **Figure 4.10–Figure 4.12**. The complexes were dissolved in dichloromethane at a concentration of 1×10^{-4} mol L⁻¹ and generated blue solutions. UV-vis spectra of these complexes show four absorption bands in the UV and visible regions: the absorption maxima observed in the near-UV region (below 300 nm) are attributed to π to π^* transitions involving the phenolate units; and intense, high energy bands around 340 nm are associated with the ligand-to-metal charge transfer (LMCT) transition from the highest occupied molecular orbital (HOMO) of the phenolate oxygen to the half-filled $d_{x^2-y^2}/d_{z^2}$ orbitals of the Co(II) or Co(III) centre. The lowest energy bands for **4.5** and **4.6** (~580 nm), and **4.7** (~550 nm) are assigned to the LMCT from the phenolate oxygen to the $d\pi^*$ orbitals of the Co(II) or Co(III) centre, respectively.

The spectra produced by **4.5** showed two d-d transitions at 670 nm and 750 nm,

which correspond, respectively, to the ${}^4T_{1g}(F) \rightarrow {}^4T_{1g}(P)$ and ${}^4T_{1g}(F) \rightarrow {}^4T_{2g}$ transitions of an octahedral, high-spin cobalt(II) centre.⁹ However, **4.6** showed only one d-d transition around 715 nm.

Magnetic susceptibility data for all dinuclear amino-bis(phenolate) Co(II) complexes (**4.5** and **4.6**) were collected at room temperature using a Johnson-Matthey magnetic susceptibility balance. The magnetic moments of these complexes were 5.6 and 6.0 μ_B , respectively, which is expected for dinuclear, high-spin Co(II) species.

Elemental analytical data for **4.5** and **4.6** also agree with the proposed formula. However, unfortunately, crystals suitable for X-ray diffraction analysis could not be obtained.

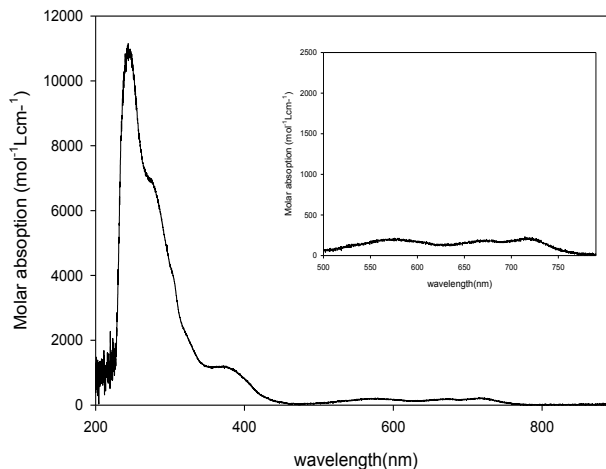


Figure 4.10. Electronic absorption spectrum of $\text{Co}_2\text{Cl}_2[\text{L1}]$ (**4.5**) in dichloromethane.

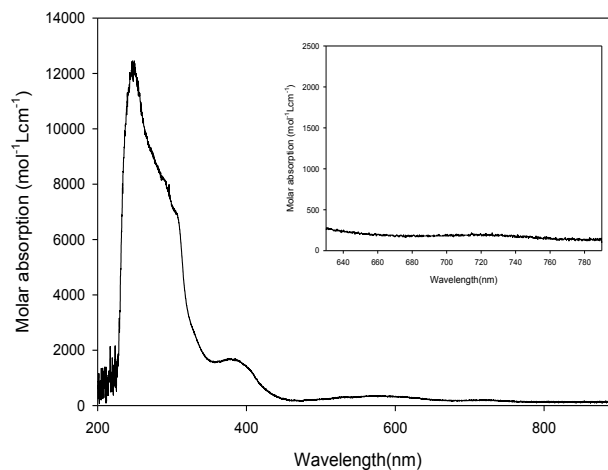


Figure 4.11. Electronic absorption spectrum of $\text{Co}_2\text{Cl}_2[\text{L2}]$ (4.6) in dichloromethane.

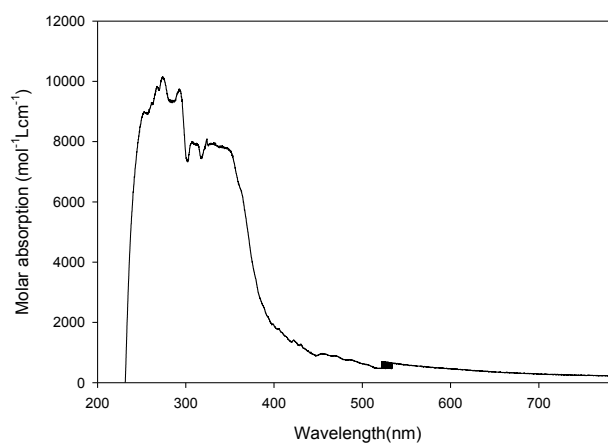


Figure 4.12. Electronic absorption spectrum of $\text{CoOAc}[\text{L1}]$ (4.7) in dichloromethane.

4.2.5 Proton NMR spectroscopy

4.7 is diamagnetic and therefore its ^1H NMR spectrum was obtained. As seen in **Figure 4.13**, the two singlet peaks at δ 1.31 and 1.45 were assigned to ^tBu protons. A singlet at δ 1.94 was assigned to the CH_3 protons of the acetate group (c). A broad peak at 2.32 ppm was assigned to the CH_2 protons within the homopiperazine ring (d). A singlet at 2.83 corresponds to the eight CH_2 protons in the homopiperazine ring (e). A singlet at

3.80 ppm was assigned to Ar-CH₂-N (f), and two aromatic resonances at 6.84 and 7.28 ppm were assigned to Ar-H protons (g and h). The signals in the spectrum of **4.7** are much broader than in the spectrum of the parent protio ligand. The increased signal broadness may be due to fluxionality of the coordination geometry around the cobalt centre and also possibly the presence of paramagnetic impurities.

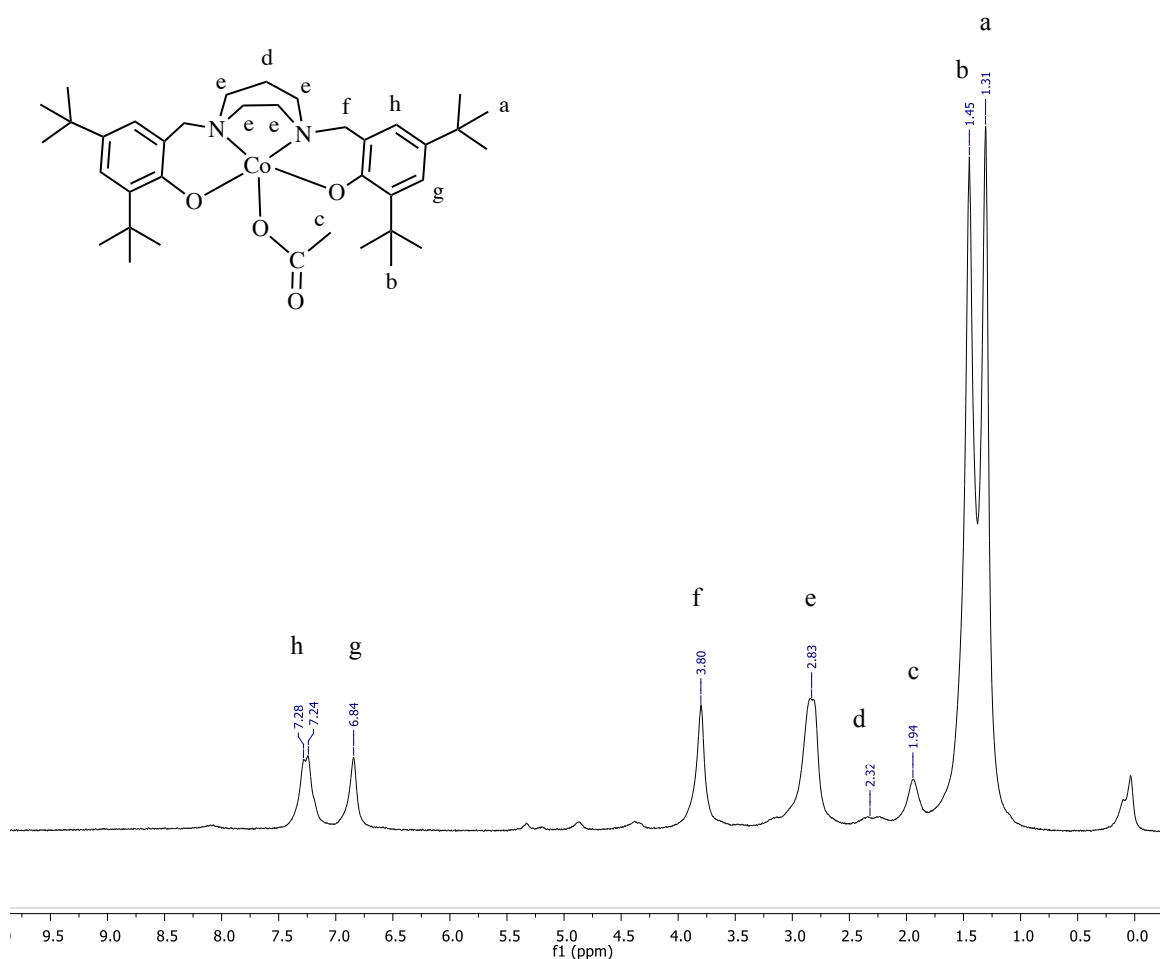


Figure 4.13. ¹H NMR spectrum (300 MHz, 298 K, CDCl₃) of **4.7**.

4.2.6 Cyclization of propylene oxide with carbon dioxide

Dinuclear Co(II) complexes **4.5** and **4.6** and monometallic Co(III) complex **4.7** were tested as catalysts in the reaction of propylene oxide and carbon dioxide. The catalytic screening was carried out in reaction conditions similar to those reported by the Kerton group (**Table 4.1**)¹³ In all cases, no polycarbonate was detected by NMR spectroscopy, and the catalysts produced cyclic carbonates selectively. The catalysts required activation by Bu₄NBr in order to yield cyclic product (entry 1 and 2 vs. entry 3). **4.5** and **4.6** could produce small amounts of cyclic carbonate with a conversion of 20% and 23%, respectively, at room temperature. However, for **4.5**, increasing the temperature up to 60 °C gave higher conversions (52%), which corresponds to an increase in TOF from 17 h⁻¹ to 43 h⁻¹ (entry 3 vs. 5). With further increases in temperature to 80 °C, the formation of cyclic carbonate was enhanced and reached 74%, with a corresponding TOF value of 62 h⁻¹ (entry 7). The formation of thermally stable cyclic carbonates at room temperature by cobalt(II) and (III) complexes has been previously reported.¹³⁻¹⁵ In contrast to the promising results reported by Williams *et al.*⁸ using dicobalt(II) complexes, the production of polypropylene carbonate was not observed. Although the TOFs in the current studies are lower than those observed by Williams group (200 h⁻¹) we performed the reaction at lower temperatures and they required elevated temperature (100 °C). It should be noted that the activities of the dinuclear Co(II) complexes are also lower than those observed by Kerton *et al.*¹³ using Co(II) complexes at room temperature but it could be enhanced at higher temperatures. Furthermore, the effect of CO₂ pressure was investigated; increasing the pressure from 30 to 40 bar enhanced the catalytic activity from 43 h⁻¹ to 55 h⁻¹. Surprisingly, a lower activity was obtained with complex **4.7**,

which gave a conversion of 10% and TOF of 8 h⁻¹. This is in contrast to the high activity reported for Co(III) acetate complexes based on salen ligands.¹⁶⁻¹⁸

Table 4.1. Cycloaddition reactions of propylene oxide and carbon dioxide catalyzed by dicobalt(II) and cobalt(III) complexes **4.5–4.7**.

Entry ^[a]	Catalyst	Co-catalyst	[Co]:[PO]: [Cocat]	Time (h)	T (°C)	Pressure (bar)	Conv. (%) ^[b]	TON ^[c]	TOF (h ⁻¹) ^[d]
1	4.5	-	1:2000:0	24	25	30	0	-	-
1	4.6	-	1:2000:0	24	25	30	0	-	-
3	4.5	TBAB	1:2000:1	24	25	30	20	400	17
4	4.6	TBAB	1:2000:1	24	25	30	23	460	19
5	4.5	TBAB	1:2000:1	24	60	30	52	1040	43
6	4.6	TBAB	1:2000:1	24	60	30	39	780	33
7	4.5	TBAB	1:2000:1	24	80	30	74	1480	62
8	4.5	TBAB	1:2000:1	24	60	40	66	1320	55
9	4.7	TBAB	1:2000:1	24	60	30	10	200	8

[a] Reaction conditions unless otherwise stated: PO (107 mmol), catalyst (0.05 mmol, 0.05 mmol%), TBAB (0.05 mmol, 0.05 mol%), CO₂ (30 bar), 25 °C, 24 h. [b] Determined by ¹H NMR spectroscopy. [c] Overall turnover number (mol_{PC} mol_{Cat}⁻¹). [d] Overall turnover frequency (TON/reaction time) observed.

4.3 Conclusions

Co₂(II) and Co(III) complexes supported by amino-bis(phenolate) ligands were synthesized and characterized; however, no crystal structures were determined. Based on the experimental data, Co₂(II) complexes **4.5** and **4.6** demonstrated good activity

compared to the related monometallic complex. Compared to previously reported Co(III) and Co₂(II) complexes, they exhibit lower reactivity and no formation of polycarbonates was observed under the conditions studied..

4.4 Experimental

4.4.1 General experimental conditions

All manipulations were performed under an atmosphere of dry, oxygen-free nitrogen using standard Schlenk techniques or an MBraun Labmaster glovebox. Most reagents were purchased either from Aldrich or Alfa Aesar and used without further purification. Anhydrous CoCl₂ was purchased from Alfa Aesar. Propylene oxide was purchased from Aldrich and distilled from CaH₂. Tetrahydrofuran was purified by distillation from sodium/benzophenone ketyl under nitrogen. All other solvents were purified by an MBraun Manual Solvent Purification System. All ¹H and ¹³C NMR spectra were obtained in CDCl₃ purchased from Cambridge Isotope Laboratories, Inc. In addition, cycloaddition reactions were carried out in a 300 mL stainless steel Parr® 5500 autoclave reactor with a Parr® 4836 controller.

4.4.2 Synthesis and characterization of catalysts

Synthesis of 4.5. [L1]H₂ (2.06 g, 3.72 mmol) was dissolved in THF (50 mL) and cooled to -78 °C. n-Butyllithium (1.6 M, 4.65 mL, 7.44 mmol) was slowly added via cannula to afford a cloudy, yellow solution, which was warmed to room temperature and stirred for 72 h. This mixture was transferred via cannula to a suspension of CoCl₂ (0.966 g, 7.44 mmol) in THF (50 mL) cooled to -78 °C to give a dark blue mixture. Upon warming to RT and stirring for 18 h, a dark blue solution formed. The solvent was

removed under vacuum and the residue was extracted into toluene (50 mL). The product was then filtered through Celite and the solvent was removed under vacuum. The product was washed with cold pentane (10 mL) and dried under vacuum to yield a dark blue solid (2.30 g, 85.5%). Anal. calc'd for $C_{35}H_{54}Co_2Cl_2N_2O_2$: C, 58.10; H, 7.52; N, 3.87. Found: C, 57.79; H, 7.53; N, 3.65. UV-vis (CH_2Cl_2) λ_{max} , nm (ϵ): 580 (210), 670 (148), 750 (205); μ_{eff} (298 K) = 6.30 μ_B . MS (MALDI-TOF) m/z (% ion): 722 (20, $[Co_2Cl_2[L1]]^+$), 687.1 (25, $[Co_2Cl[L1]]^+$), 628.1 (30, $[CoCl[L1]]^+$), 593.2 (100, $[Co[L1]]^+$).

Synthesis of 4.6. $[L2]H_2$ (2.06 g, 4.4 mmol) was dissolved in THF (50 mL) and cooled to -78 °C. n-Butyllithium (1.6 M, 5.5 mL, 8.8 mmol) was slowly added via cannula to afford a dark yellow solution, which was warmed to room temperature and stirred for 72 h. This mixture was transferred via cannula to a suspension of $CoCl_2$ (1.14 g, 8.8 mmol) in THF (50 mL) cooled to -78 °C to give a dark blue mixture. Upon warming to RT and stirring for 18 h, a dark blue solution formed. The solvent was removed under vacuum and the residue was extracted into toluene (50 mL). The product was then filtered through Celite and the solvent was removed under vacuum. The dark blue solid was washed with cold pentane (10 mL) and dried under vacuum (2.24 g, 92.3%). Anal. calc'd for $C_{29}H_{42}Co_2Cl_2N_2O_2$: C, 54.47; H, 6.62; N, 4.38. Found: 54.67; H, 6.51; N, 4.23. UV-vis (CH_2Cl_2) λ_{max} , nm (ϵ): 580 (185), 720 (120); μ_{eff} (298 K) = 6.02 μ_B . MS (MALDI-TOF) m/z (% ion): 638.1 (9, $[Co_2Cl_2[L2]]^+$), 603 (25, $[Co_2Cl[L2]]^+$), 544 (10, $[CoCl[L2]]^+$), 509.2 (100, $[Co[L2]]^+$).

Synthesis of 4.7. $[L1]H_2$ (2.00 g, 3.72 mmol) and $Co(OAc)_2 \cdot 4H_2O$ (0.926 g, 3.72 mmol) were added under N_2 in a Schlenk flask. A dry, degassed mixture of dichloromethane (20 mL) and methanol (30 mL) was added to the flask. The resulting

suspension was stirred under N₂ for 1 h to afford a dark pink solution. After stirring for 1 week under O₂, a dark brown solution and dark brown solid resulted; the solid was collected on a frit and isolated in 77% yield (1.7 g). ¹H NMR (300 MHz, 298 K, CDCl₃) δ 7.20 (2H, s, ArH), 6.76 (2H, s, ArH), 3.75 (4H, s, ArC-CH₂-N), 2.79 (8H, br, N-CH₂CH₂-N), 2.24 (2H, br, N-CH₂{CH₂}CH₂-N), 1.86 (3H, s, {CH₃}COO), 1.37 (18H, s, ArC-C(CH₃)₃), 1.23 (18H, s, ArC-C(CH₃)₃). UV-vis (CH₂Cl₂) λ_{max}, nm (ε): 550 (155). MS (MALDI-TOF) *m/z* (% ion): 652.4 (20, [CoOAc[L1]]⁺), 594.4 (20, [Co[L1]]⁺).

4.5 References

1. P. P. Pescarmona and M. Taherimehr, *Catal. Sci. Technol.*, **2012**, 2, 2169-2187.
2. S. Klaus, M. W. Lehenmeier, C. E. Anderson and B. Rieger, *Coord. Chem. Rev.*, **2011**, 255, 1460-1479.
3. M. North, R. Pasquale and J. Meléndez, *Eur. J. Inorg. Chem.*, **2007**, 2007, 3323-3326.
4. G. W. Coates and D. R. Moore, *Angew. Chem.*, **2004**, 43, 6618-6639.
5. D. R. Moore, M. Cheng, E. B. Lobkovsky and G. W. Coates, *J. Am. Chem. Soc.*, **2003**, 125, 11911-11924.
6. E. B. Lobkovsky, G. W. Coates and M. Cheng, *J. Am. Chem. Soc.*, **1998**, 120, 11018-11019.
7. S. Hashimoto, K. Nozaki and K. Nakano, *Chem. Sci.*, **2010**, 1, 369-373.
8. F. Jutz, A. Buchard, A. J. P. White, C. K. Williams and M. R. Kember, *Chem. Sci.*, **2012**, 3, 1245-1255.
9. Z. Qin, C. M. Thomas, S. Lee and G. W. Coates, *Angew. Chem. Int. Ed.*, **2003**, 42, 5484-5487.
10. X.-B. Lu and D. J. Darensbourg, *Chem. Soc. Rev.*, **2012**, 41, 1462-1484.
11. N. Ikpo, S. M. Butt, K. L. Collins and F. M. Kerton, *Organometallics*, **2009**, 28, 837-842.
12. M. D. Eelman, J. M. Blacquiere, M. M. Moriarty and D. E. Fogg, *Angew. Chem.*, **2008**, 47, 303-306.
13. N. Ikpo, C. F. Petten, U. K. Das, L. N. Dawe, L. N. Saunders, C. M. Kozak and F. M. Kerton, *Catal. Commun.*, **2012**, 18, 165-167.
14. X. Fu and H. Jing, *J. Catal.*, **2015**, 329, 317-324.
15. G.-P. Wu, F. Lin, J.-Y. Jiang, C. Liu, W.-M. Ren, Y. Luo and X.-B. Lu, *Chem. Sci.*, **2012**, 3, 2094-2102.
16. Y. Niu and H. Li, *Appl. Organomet. Chem.*, **2011**, 25, 424-428.
17. X.-B. Lu and Y. Wang, *Angew. Chem. Int. Ed.*, **2004**, 43, 3574-3577.
18. R. L. Paddock and S. T. Nguyen, *Chem. Commun.*, **2004**, 1622-1623.

Chapter 5 Conclusions

5.1 Summary

Poly lactide (PLA) is a very promising alternative to petrochemical-derived polymer products because it is biodegradable, biocompatible, and derived from natural resources. Furthermore, the transformation of CO₂ into cyclic carbonates is economical and reduces CO₂ emissions. Today, there is strong demand for the development of new catalysts that are environmentally sustainable—non-toxic, cheap, abundant, stable, and efficient for the production of polymers and cyclic carbonates. In response to this demand, we describe in this research the synthesis of inexpensive and active catalysts based on lithium, sodium, iron, and cobalt metals stabilized by amino-bis(phenolate) ligands.

Chapter 1 presents an overview of the main overriding topics of interest in this study. Initially, highlights toward the preparation of PLA using lithium and sodium catalysts via ROP is reviewed with particular attention given to amino-bis(phenolate) ligands. Further review of coupling reactions involving carbon dioxide and epoxides using metal catalysts have been reviewed. In particular, a literature overview on the use of homogenous iron and cobalt catalysts for the production of polycarbonates and cyclic carbonates was given.

A series of tetralithium and sodium complexes based on amino-bis(phenolate) ligands were synthesized and characterized; this is described in Chapter 2. Pulsed gradient spin echo (PGSE) NMR spectroscopy indicates that the Li₄ complex retains its aggregated state in solution at room temperature. At low temperature, four Li

environments were also observed in ^7Li NMR. Further studies on the effect of BnOH on the nuclearity of the complexes is required in order to evaluate their activity and to gain a better understanding of their differences in reactivity. The application of these complexes for the ring-opening-polymerization (ROP) of *rac*-lactide in the presence and absence of benzyl alcohol as co-initiator was investigated. The polymerization data indicated that the presence of an alcohol was necessary to generate an efficient initiator system for sodium complexes, while benzyl alcohol does not affect reactions involving lithium complexes to the same extent. In addition, excellent results were obtained using sodium complex (**2.11**) in THF with BnOH (100% conversion, 3 min, $M_w/M_n = 1.10$). The kinetic analysis revealed that the *rac*-lactide polymerization using these initiator systems are first-order with respect to monomer concentration and demonstrated the living character of the polymerization. Experimental evidence, in the form of stoichiometric reactions, strongly suggest that these reactions proceed via a coordination-insertion mechanism.

Chapter 3 discussed the synthesis of monometallic iron(III) complexes and their utility for the cycloaddition reaction of CO_2 and oxiranes in the presence of TBAB as a cocatalyst. Modifications of the substituents on the phenolate rings by introducing electron withdrawing halides (Cl) and electron donating groups (*t*Bu, Me and OMe) were found to affect the catalytic activity. The highest catalytic activity was observed for complex **3.4** with electron-withdrawing substituents on the phenolate groups (TOF = 135 h^{-1}), which was attributed to the resulting high Lewis acidity of the metal centre. The effect of temperature, pressure, cocatalyst loading, and epoxide loading were studied extensively with propylene oxide. In addition, the electronic and steric properties of the epoxide substrate were found to play a significant role in the catalytic activity; glycidol

and epichlorohydrin, bearing electron-withdrawing groups, led to maximum TOF of 142 h⁻¹ for our catalyst system. The formation of cyclic carbonate was monitored by *in situ* IR spectroscopy, which allowed the determination of the activation energy.

The synthesis, structure, and spectroscopic and magnetic properties of mono- and dinuclear cobalt(III) and cobalt(II) amino-bis(phenolate) complexes were described in Chapter 4. Unfortunately, the solid-state structures for these complexes could not be obtained. The isolated complexes were characterized by mass spectrometry, elemental analysis, UV-vis spectroscopy, and magnetometry. The activity of these complexes was explored in the cyclization reaction of CO₂ and propylene oxide in the presence of TBAB as cocatalyst. The experimental data show that the dinuclear Co(II) complexes have a high catalytic activity compared to monometallic Co(III) complexes, and varying the reaction temperature and pressure influenced the conversion. It would be interesting to study the effects of varying the ratio of catalyst to cocatalyst, as well as monomer ratio and time. This would allow for the determination of the appropriate (optimized) reaction conditions for significant product formation.

Future research in the area of this thesis would be worthwhile in the area of ROP using sodium complexes. For example, other monomers (*e.g.* ϵ -caprolactone) and more in depth structure activity relationships (ligand effects) studied. In the area of CO₂ activation, iron catalysts have shown promise and perhaps dinuclear complexes could be prepared that should exhibit high activity.

Appendix A: NMR spectra

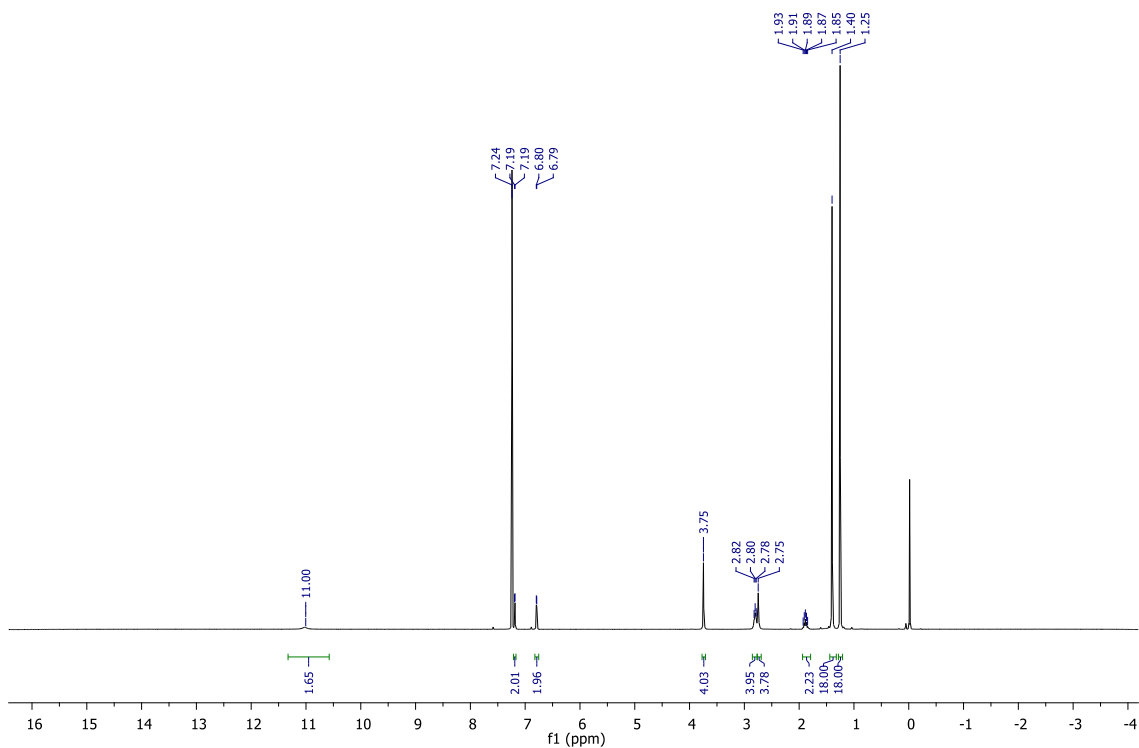


Figure A. 1. ^1H NMR spectrum (300 MHz, 298 K, CDCl_3) of $[\text{L1}]\text{H}_2$.

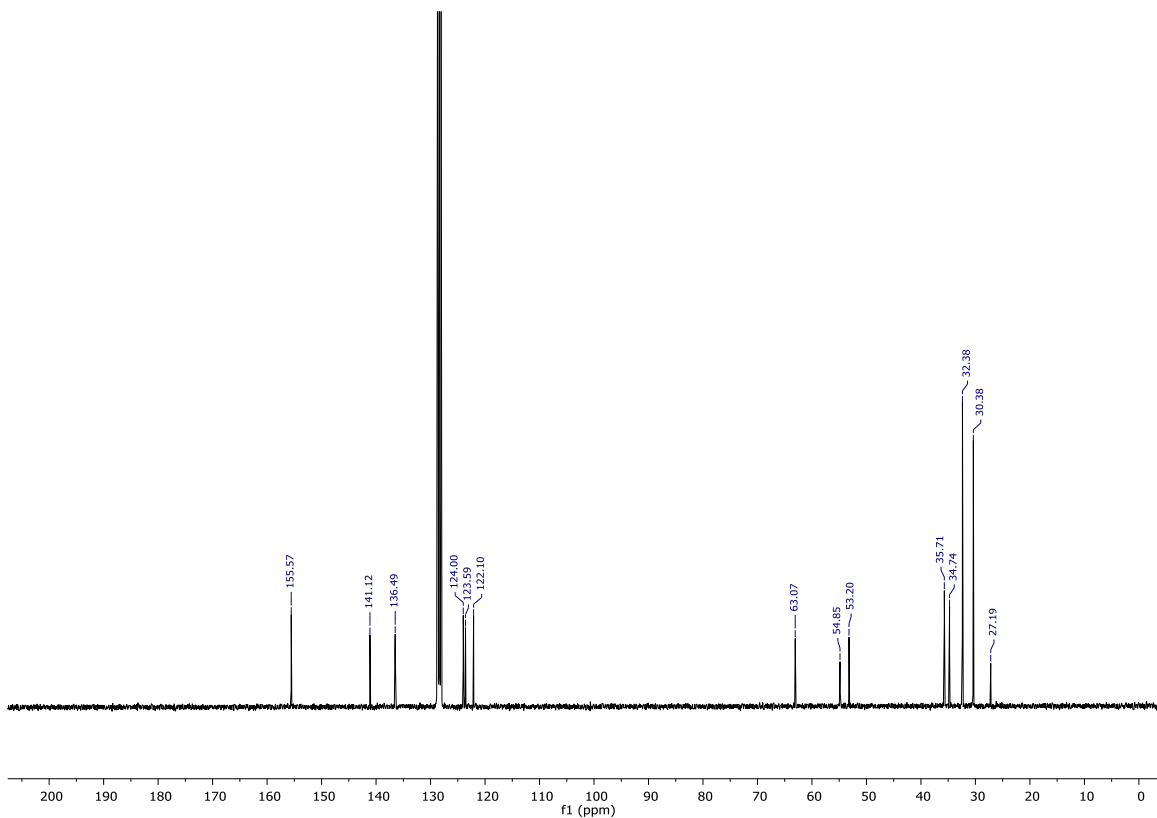


Figure A. 2. ^{13}C NMR spectrum (75.4 MHz, 298 K, C_6D_6) of $[\text{L1}]\text{H}_2$.

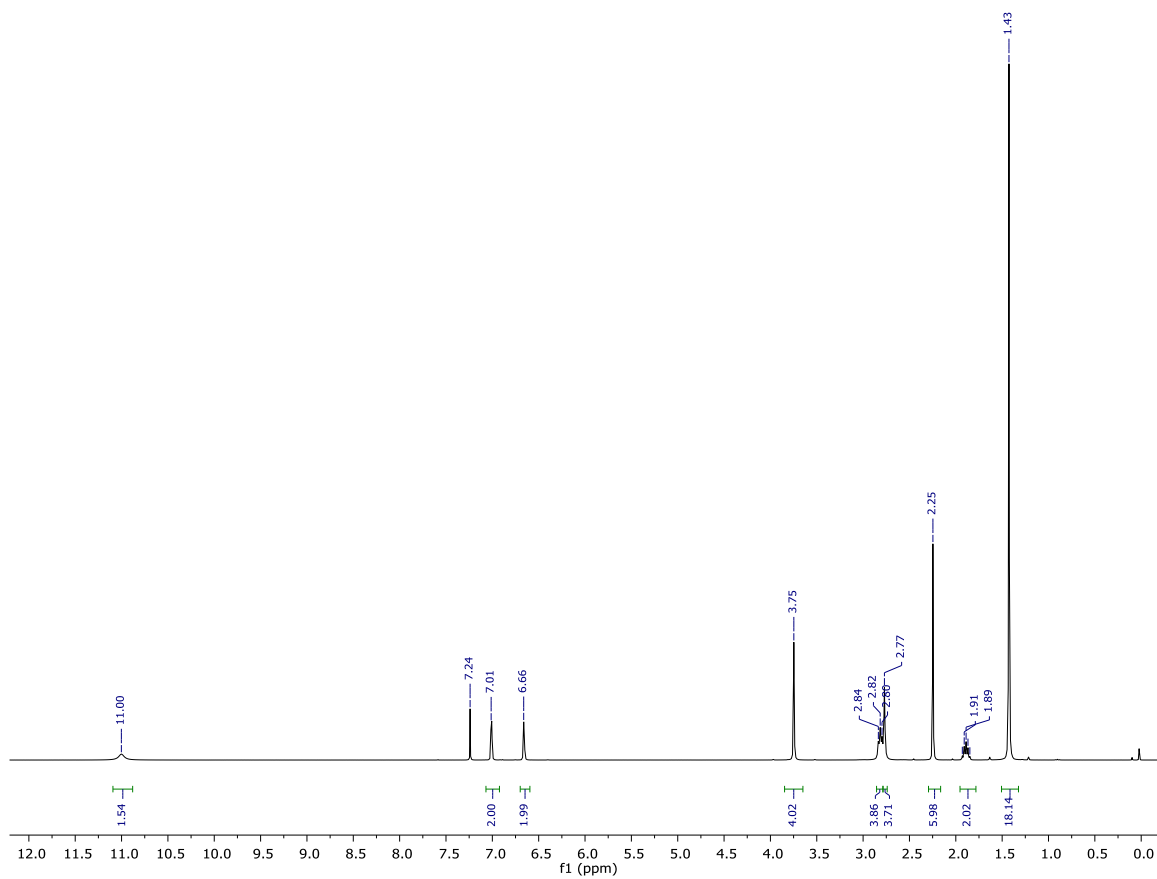


Figure A. 3. ^1H NMR spectrum (300 MHz, 298 K, CDCl_3) of $[\text{L}2]\text{H}_2$.

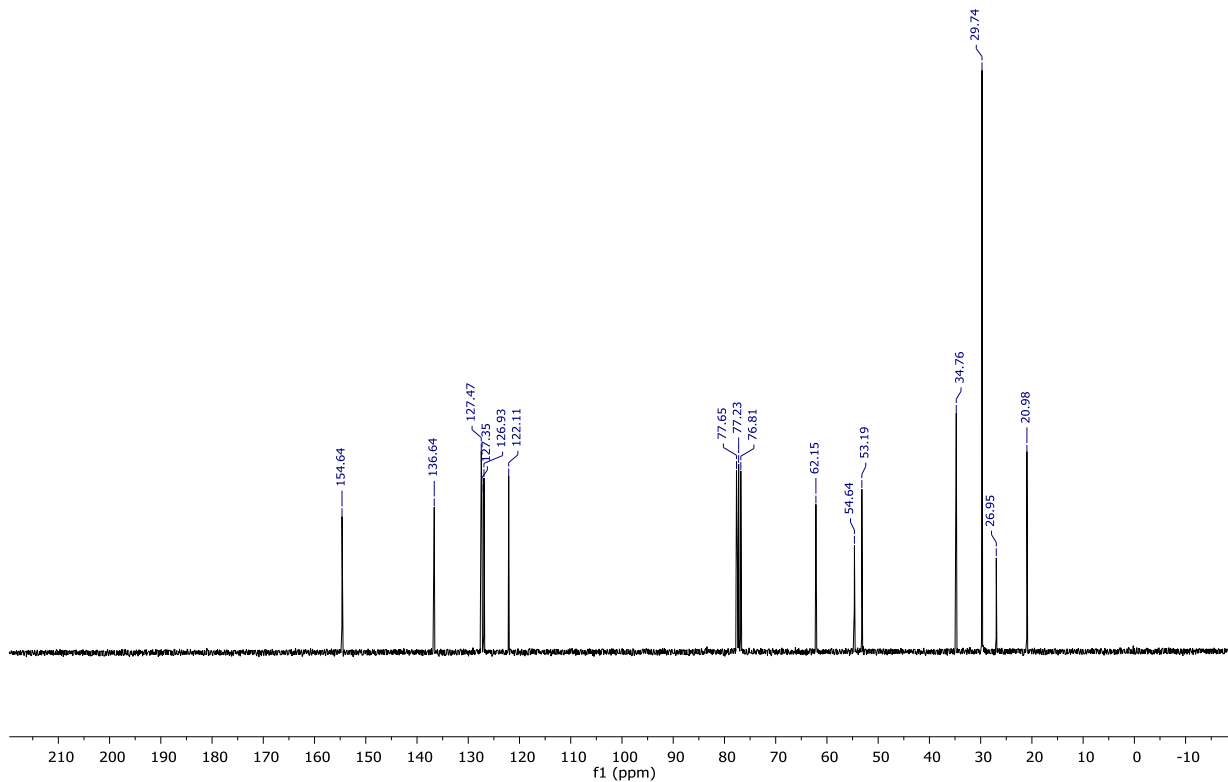


Figure A. 4. ^{13}C NMR spectrum (75.4 MHz, 298 K, CDCl_3) of $[\text{L2}]\text{H}_2$.

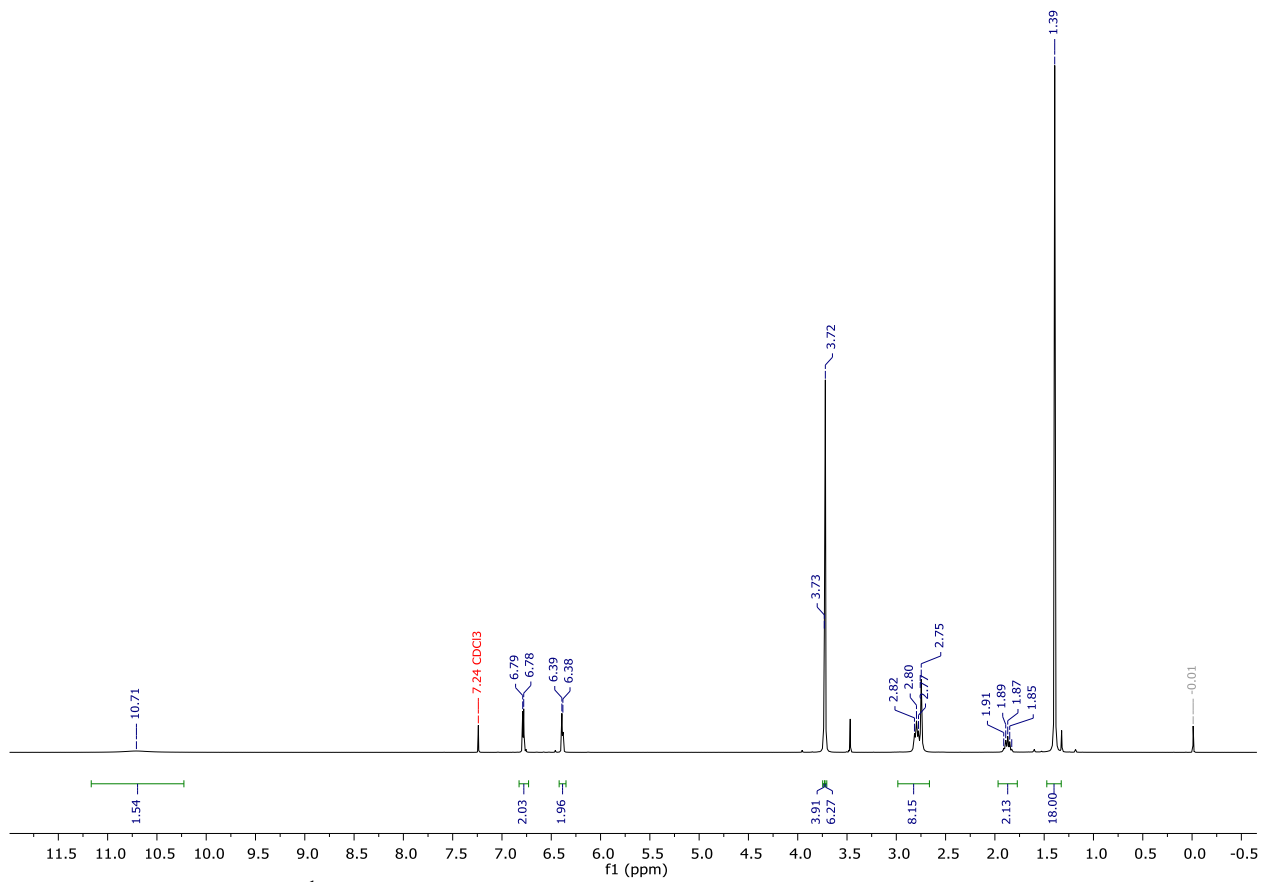


Figure A. 5. ¹H NMR spectrum (300 MHz, 298 K, CDCl₃) of [L3]H₂.

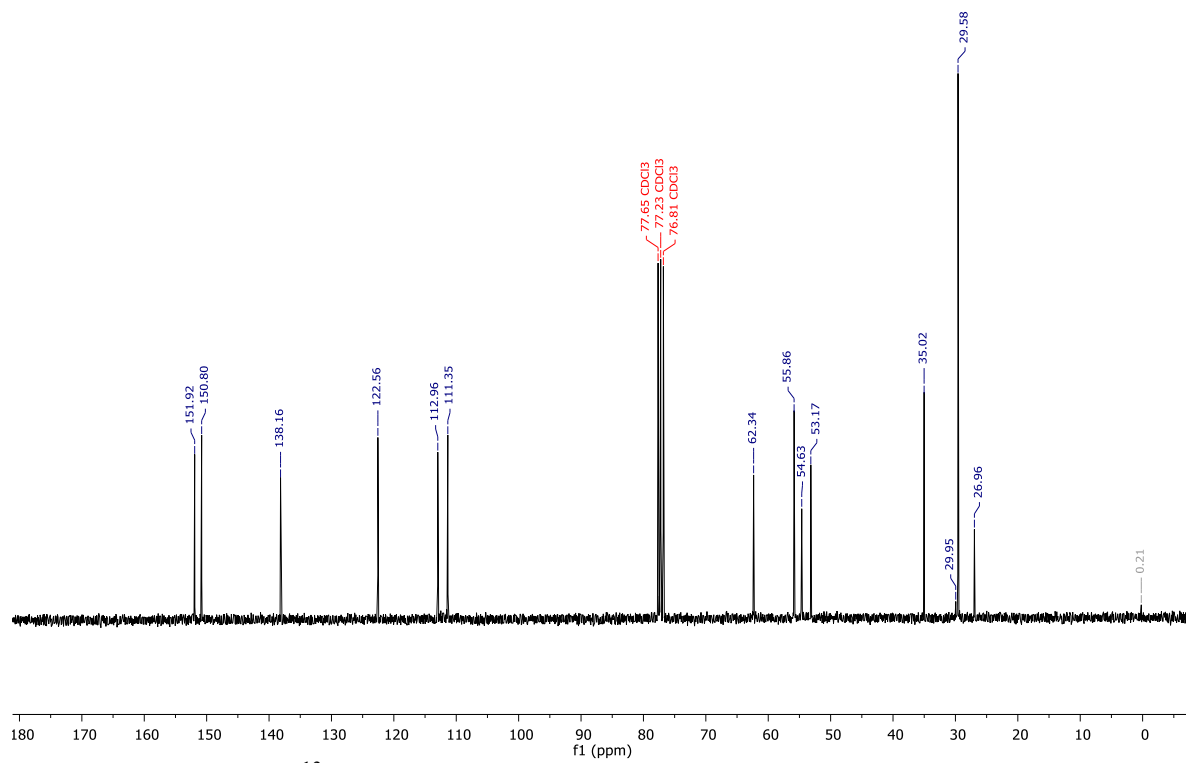


Figure A. 6. ^{13}C NMR spectrum (75.4 MHz, 298 K, CDCl_3) of $[\text{L3}]\text{H}_2$.

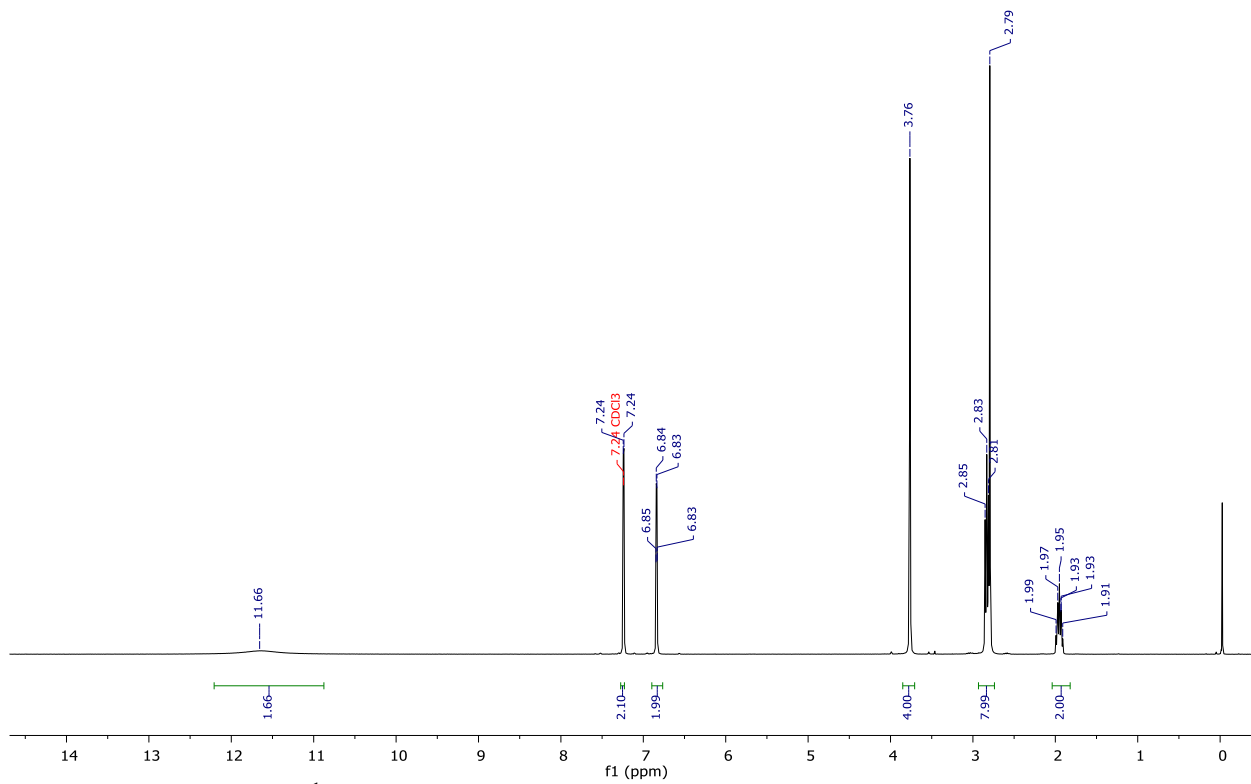


Figure A. 7. ^1H NMR spectrum (300 MHz, 298 K, CDCl_3) of $[\text{L4}]\text{H}_2$.

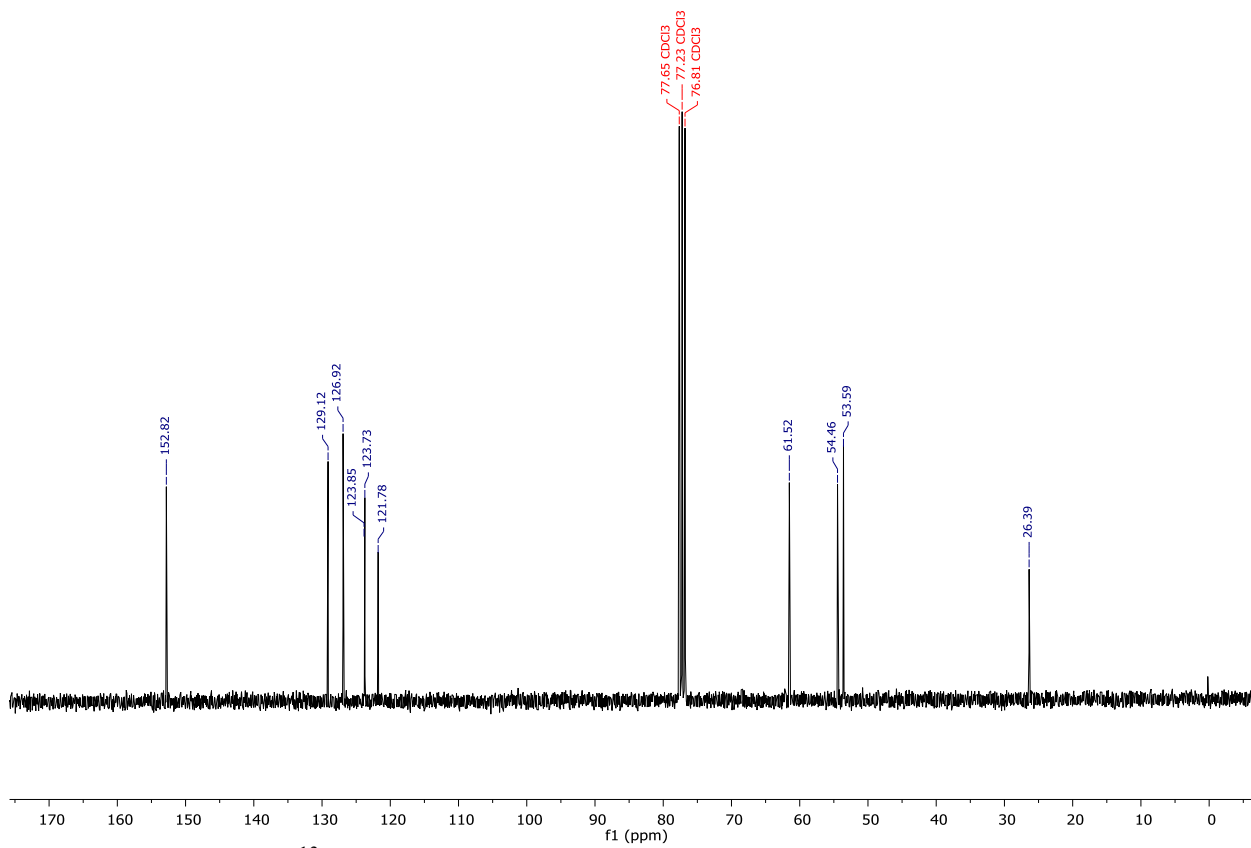


Figure A. 8. ^{13}C NMR spectrum (75.4 MHz, 298 K, CDCl_3) of $[\text{L4}]\text{H}_2$.

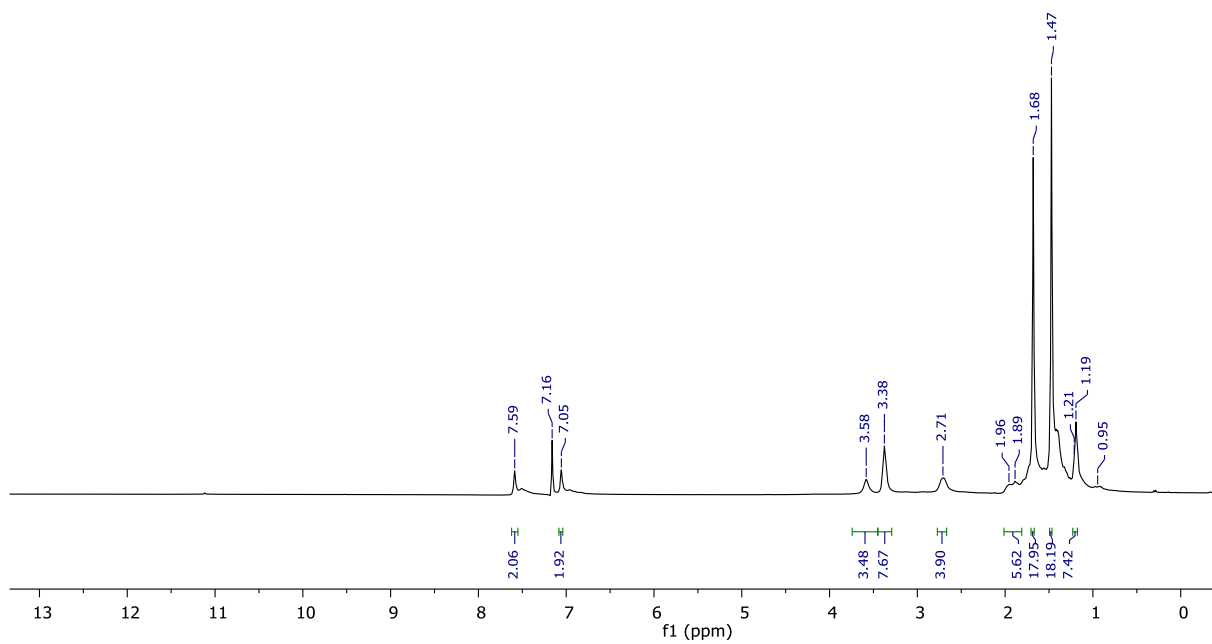


Figure A. 9. ^1H NMR spectrum (300 MHz, 298 K, C_6D_6) of **2.4**.

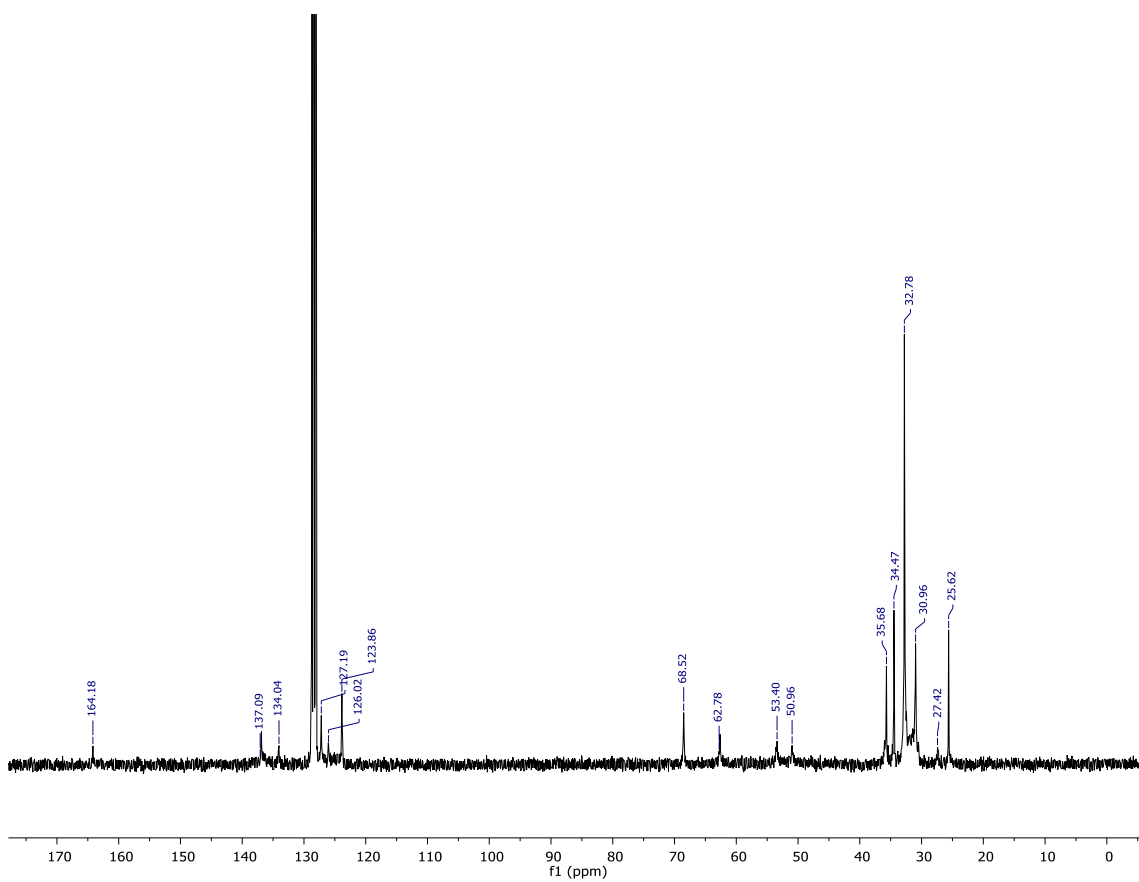


Figure A. 10. ^{13}C NMR spectrum (75.4 MHz, 298 K, C_6D_6) of **2.4**.

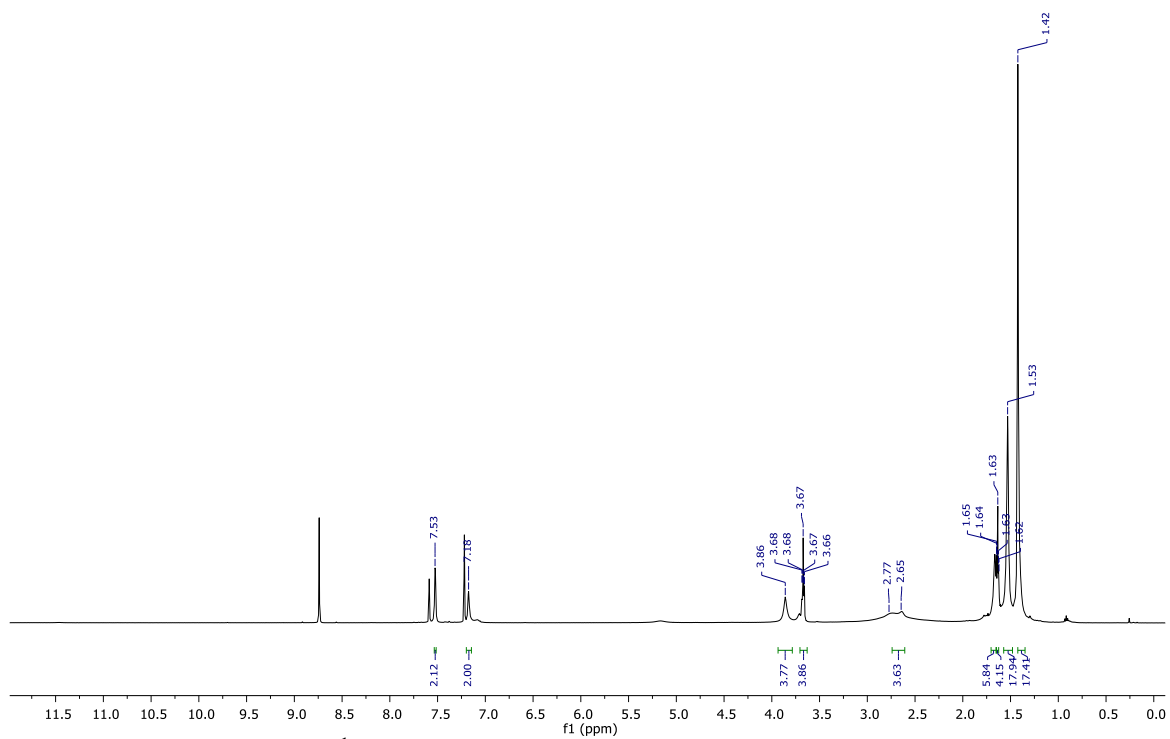


Figure A. 11. ^1H NMR spectrum (500 MHz, 298 K, $\text{C}_5\text{D}_5\text{N}$) of **2.4**.

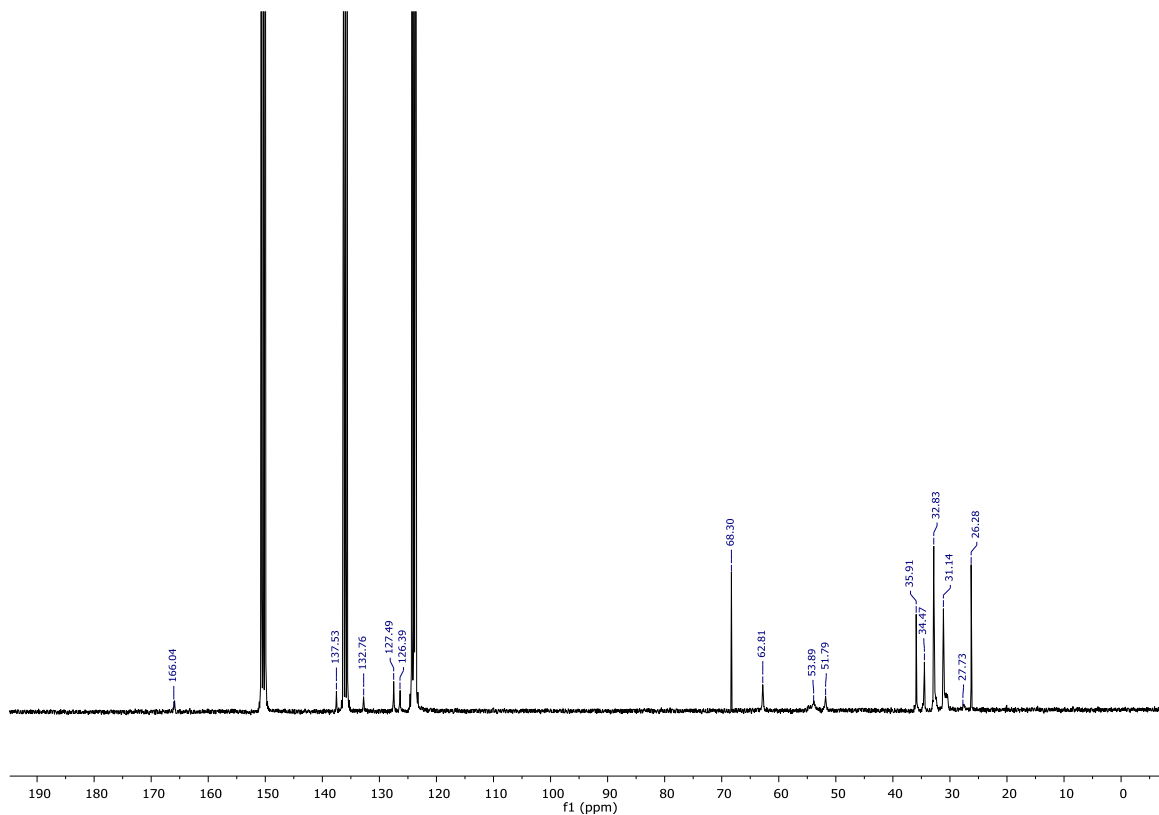


Figure A. 12. ^{13}C NMR spectrum (75.4 MHz, 298 K, $\text{C}_5\text{D}_5\text{N}$) of **2.4**.

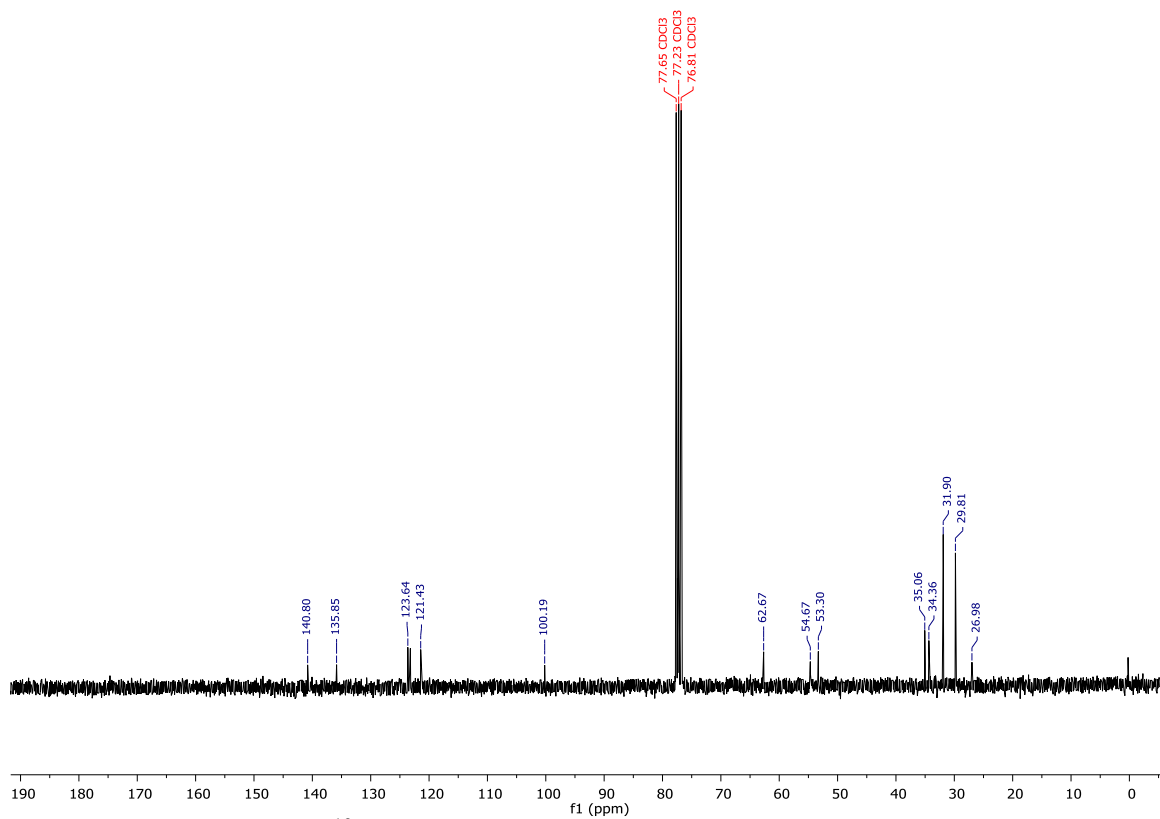


Figure A. 13. ^{13}C NMR spectrum (75.4 MHz, 298 K, CDCl_3) of 2.4.

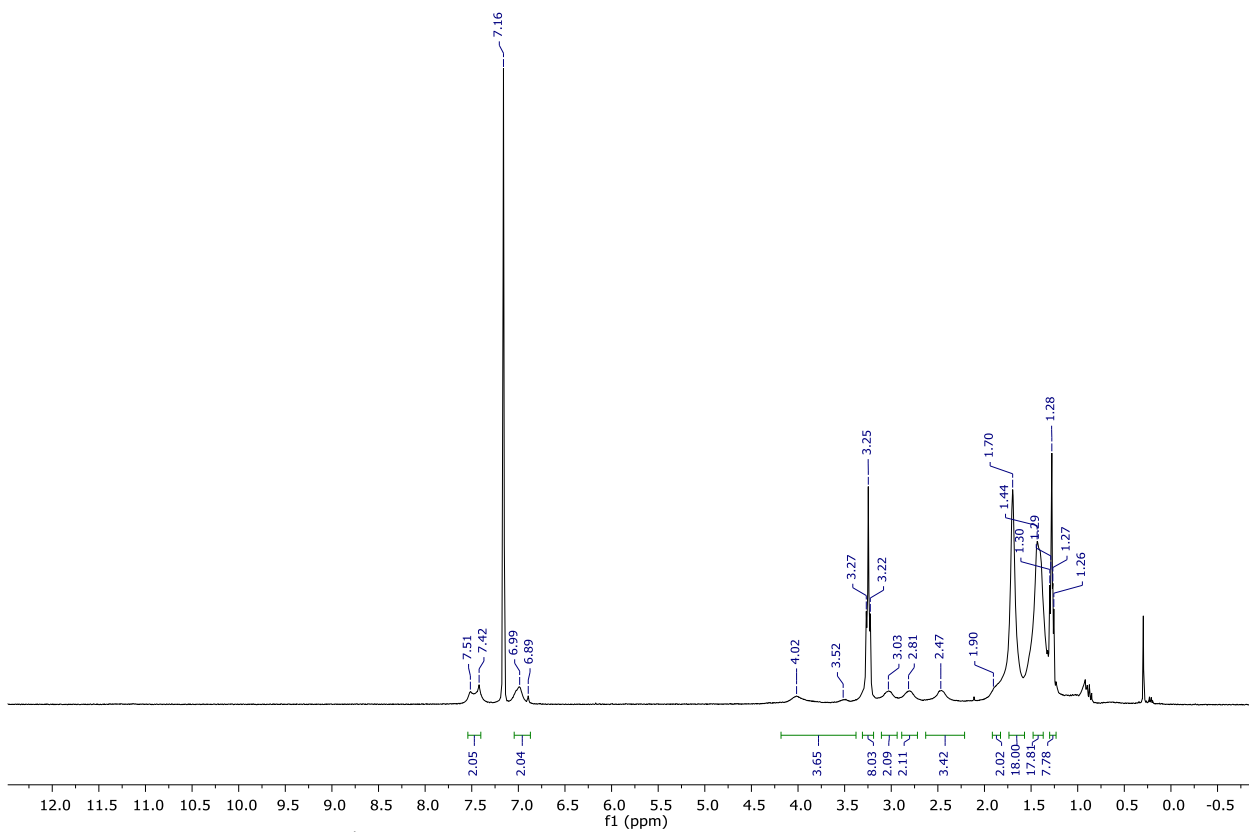


Figure A. 14. ^1H NMR spectrum (300 MHz, 298 K, C_6D_6) of **2.5**.

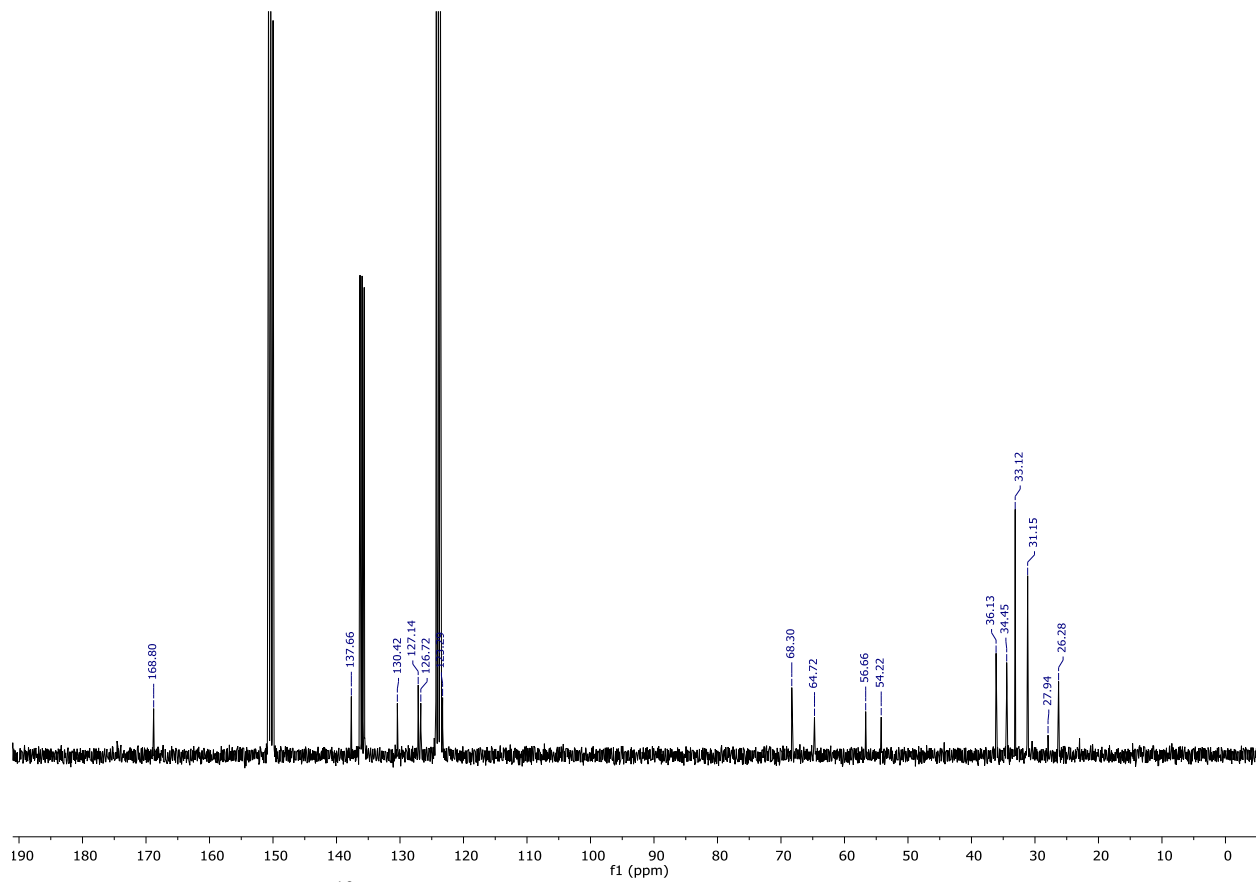


Figure A. 15. ^{13}C NMR spectrum (75.4 MHz, 298 K, $\text{C}_5\text{D}_5\text{N}$) of **2.5**.

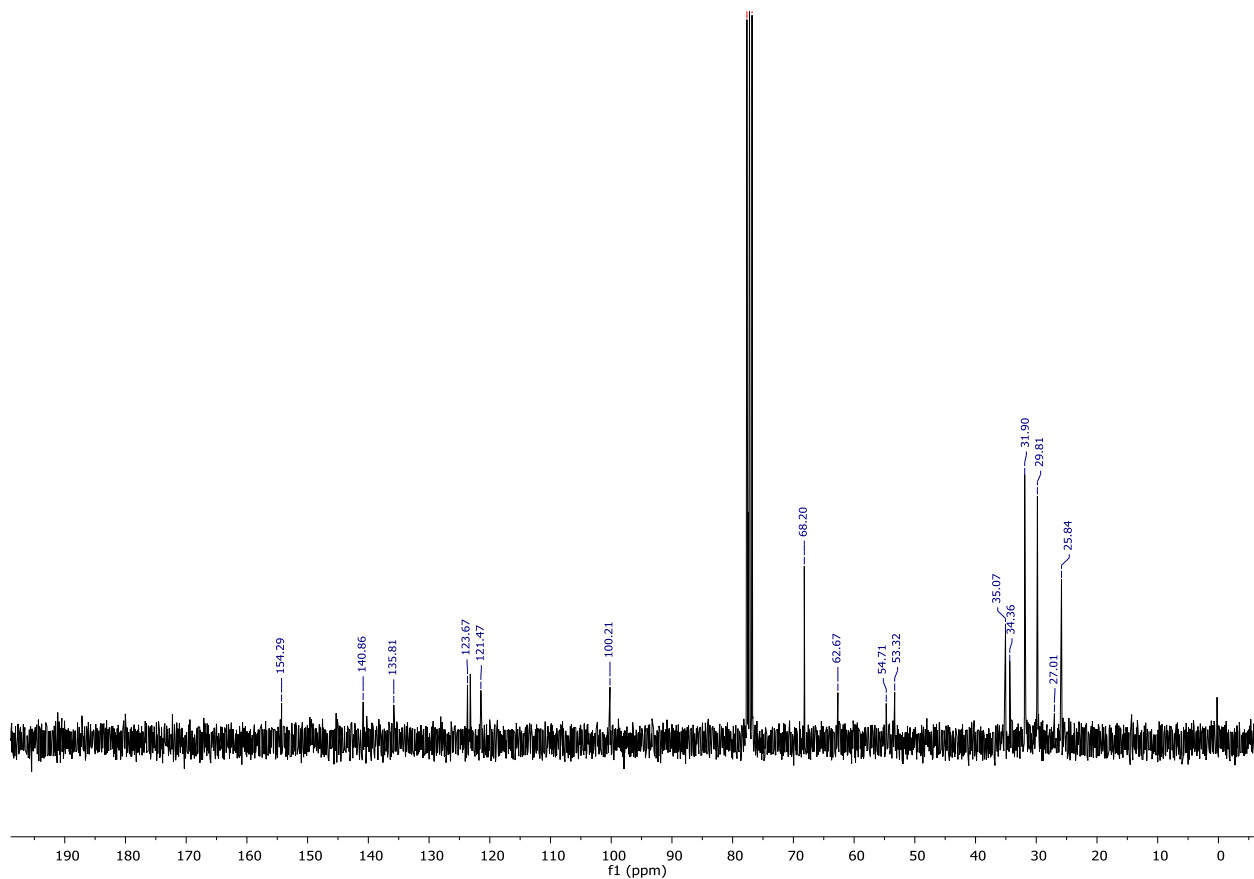


Figure A. 16. ^{13}C NMR spectrum (75.4 MHz, 298 K, CDCl_3) of **2.5**.

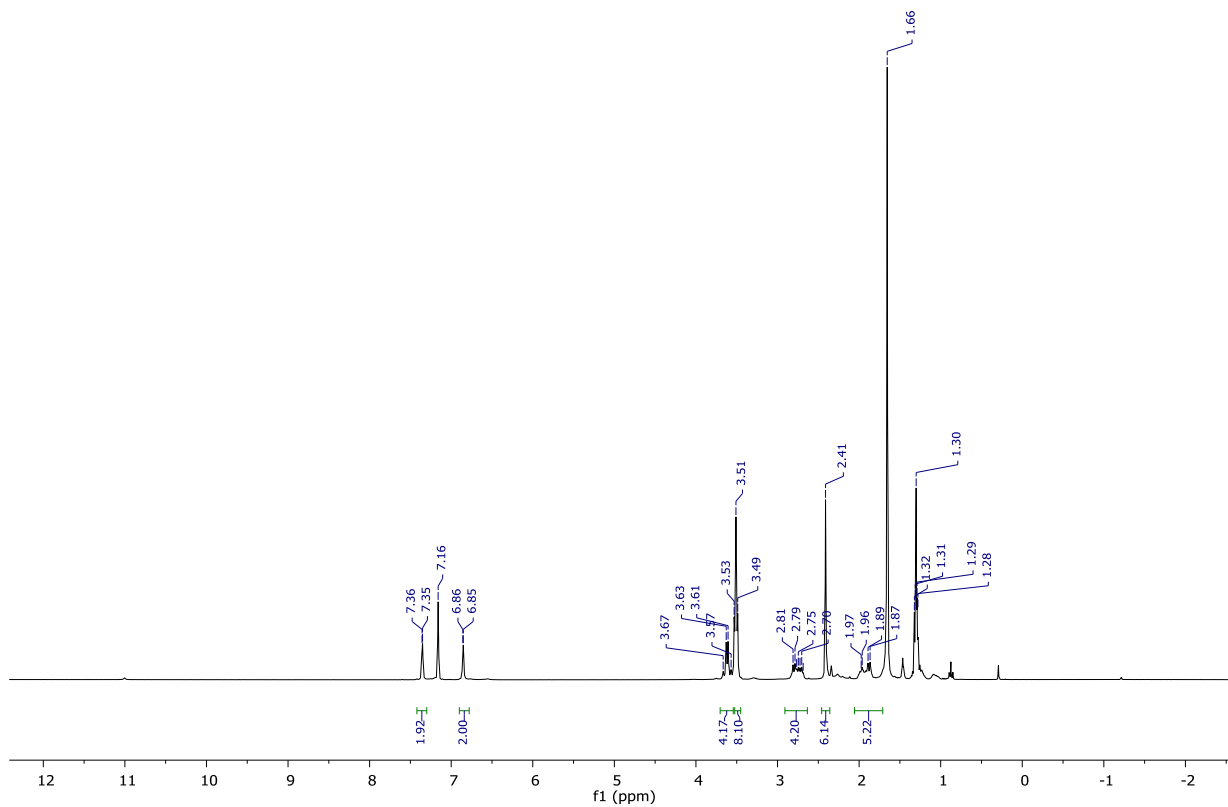


Figure A. 17. ^1H NMR spectrum (300 MHz, 298 K, C_6D_6) of **2.6**.

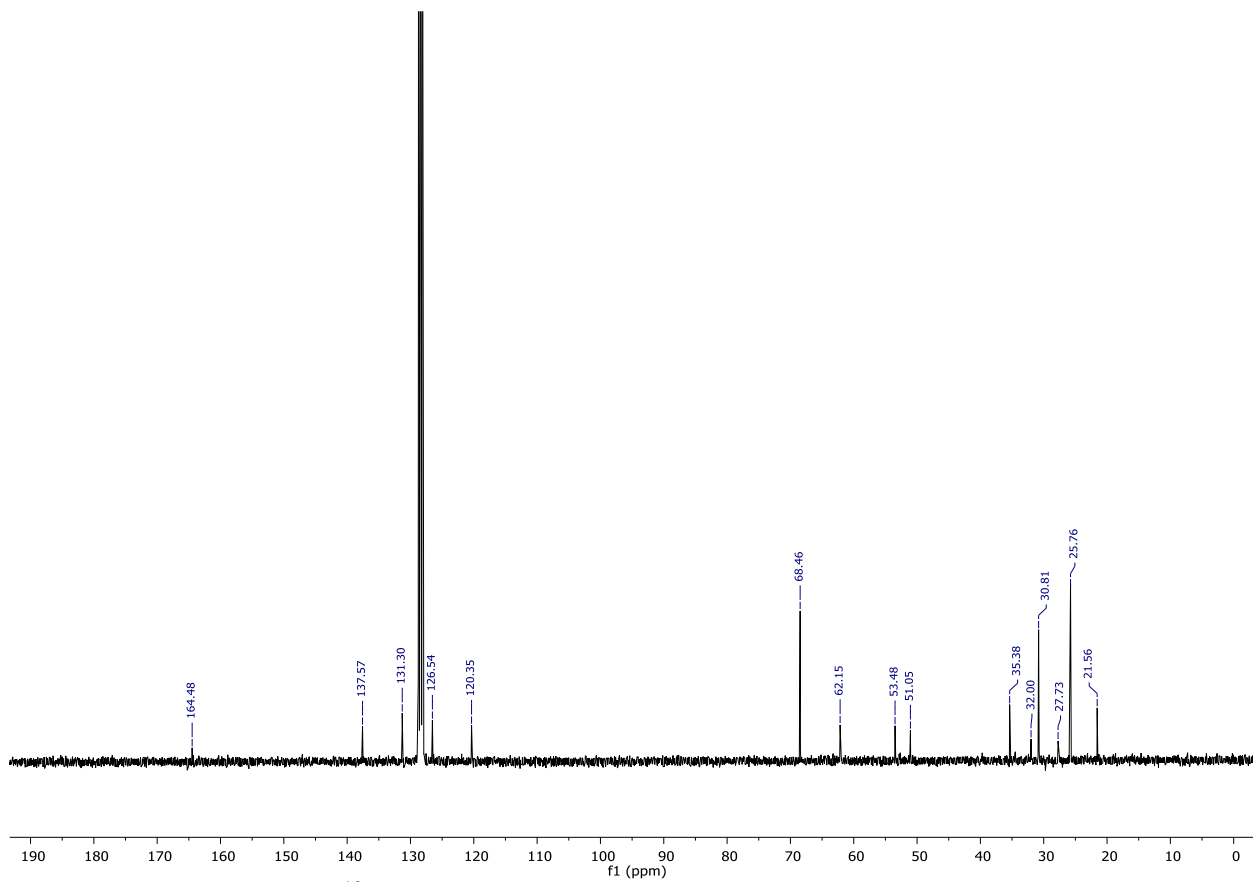


Figure A. 18. ^{13}C NMR spectrum (75.4 MHz, 298 K, C_6D_6) of **2.6**.

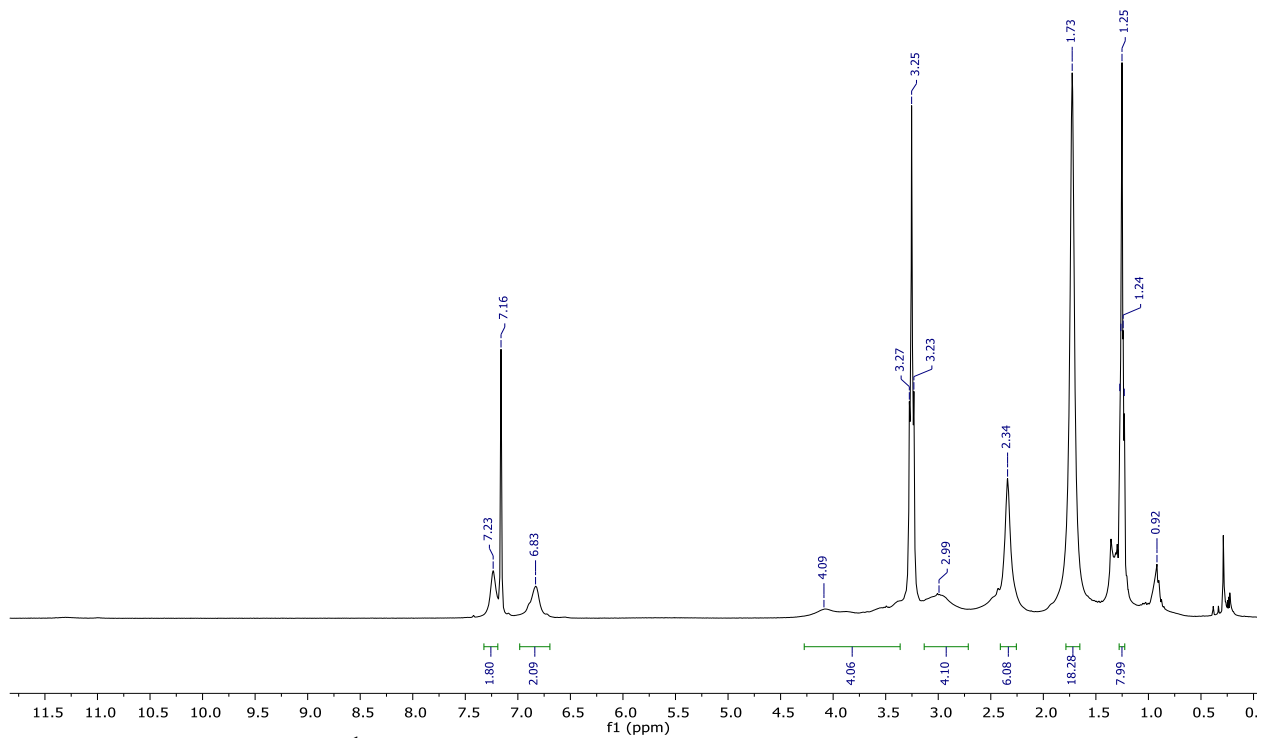


Figure A. 19. ^1H NMR spectrum (300 MHz, 298 K, C_6D_6) of **2.7**.

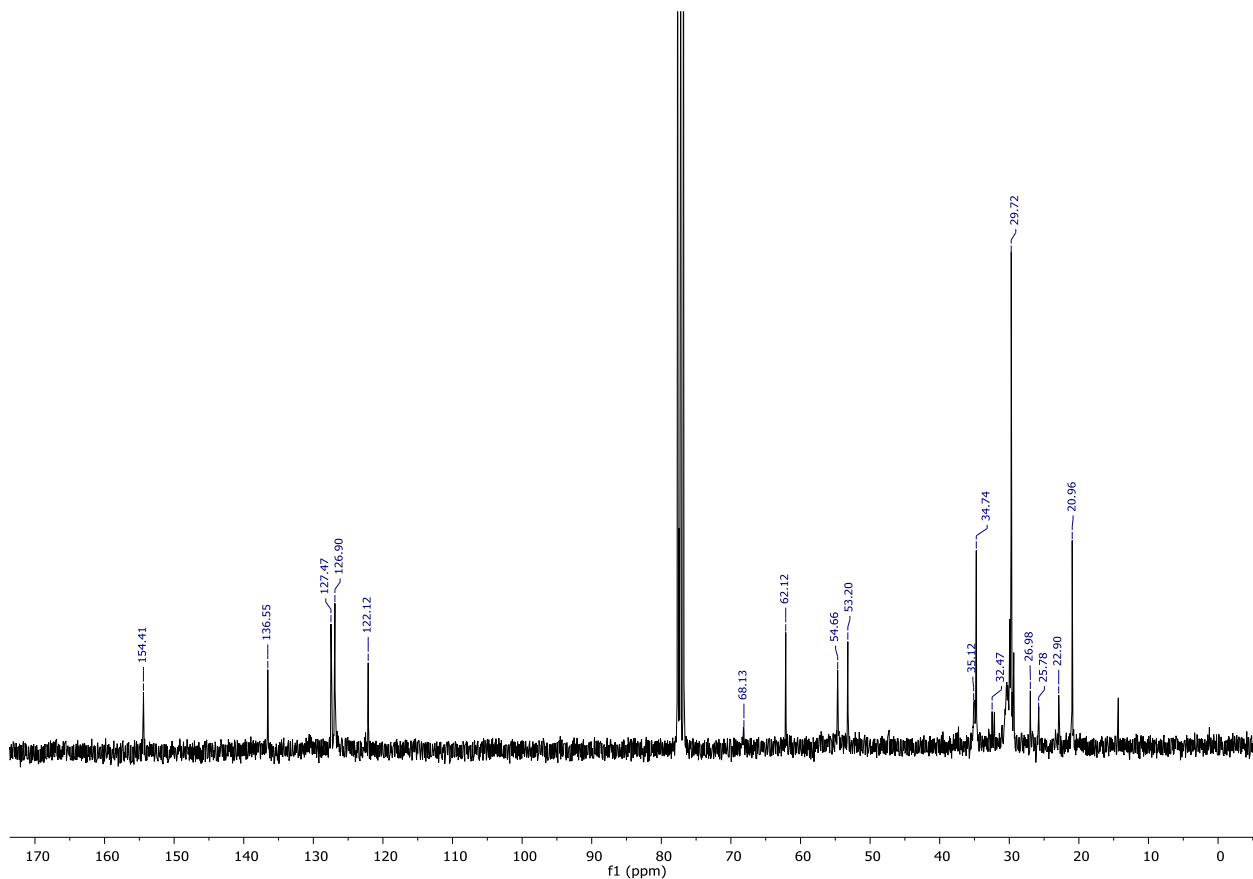


Figure A. 20. ^{13}C NMR spectrum (75.4 MHz, 298 K, CDCl_3) of **2.7**.

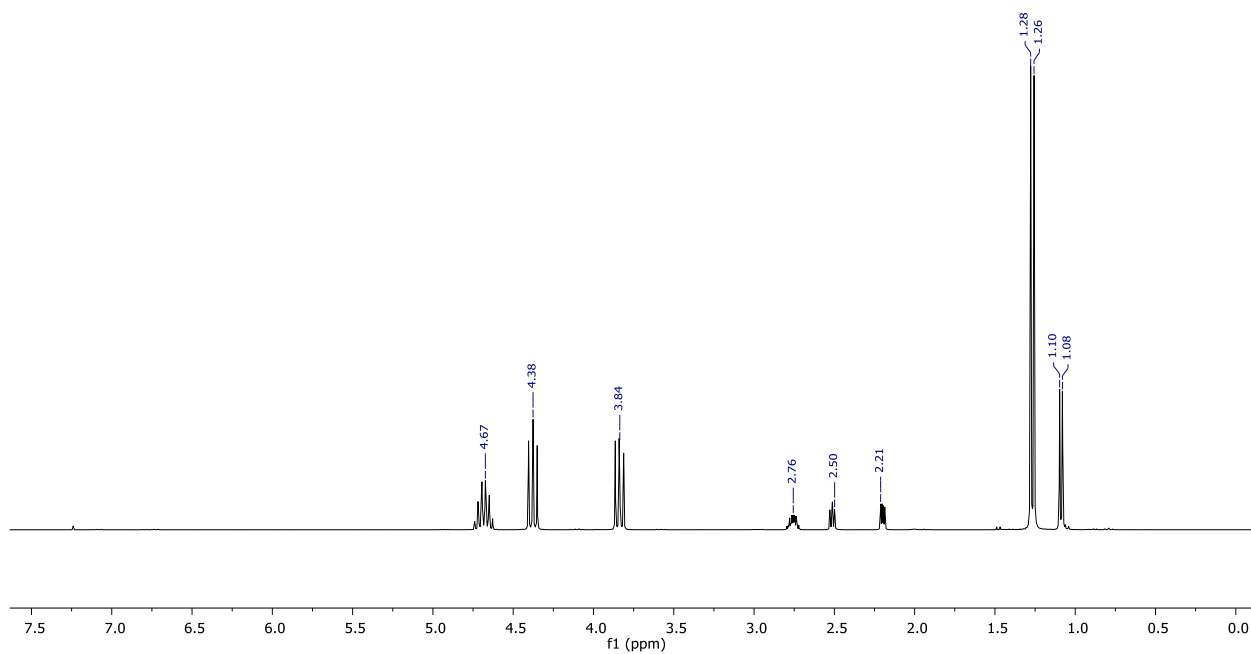


Figure A. 21. ^1H NMR spectrum (300 MHz, 298 K, CDCl_3) of 4-methyl-1,3-dioxolan-2-one (Table 3.4, entry 1).

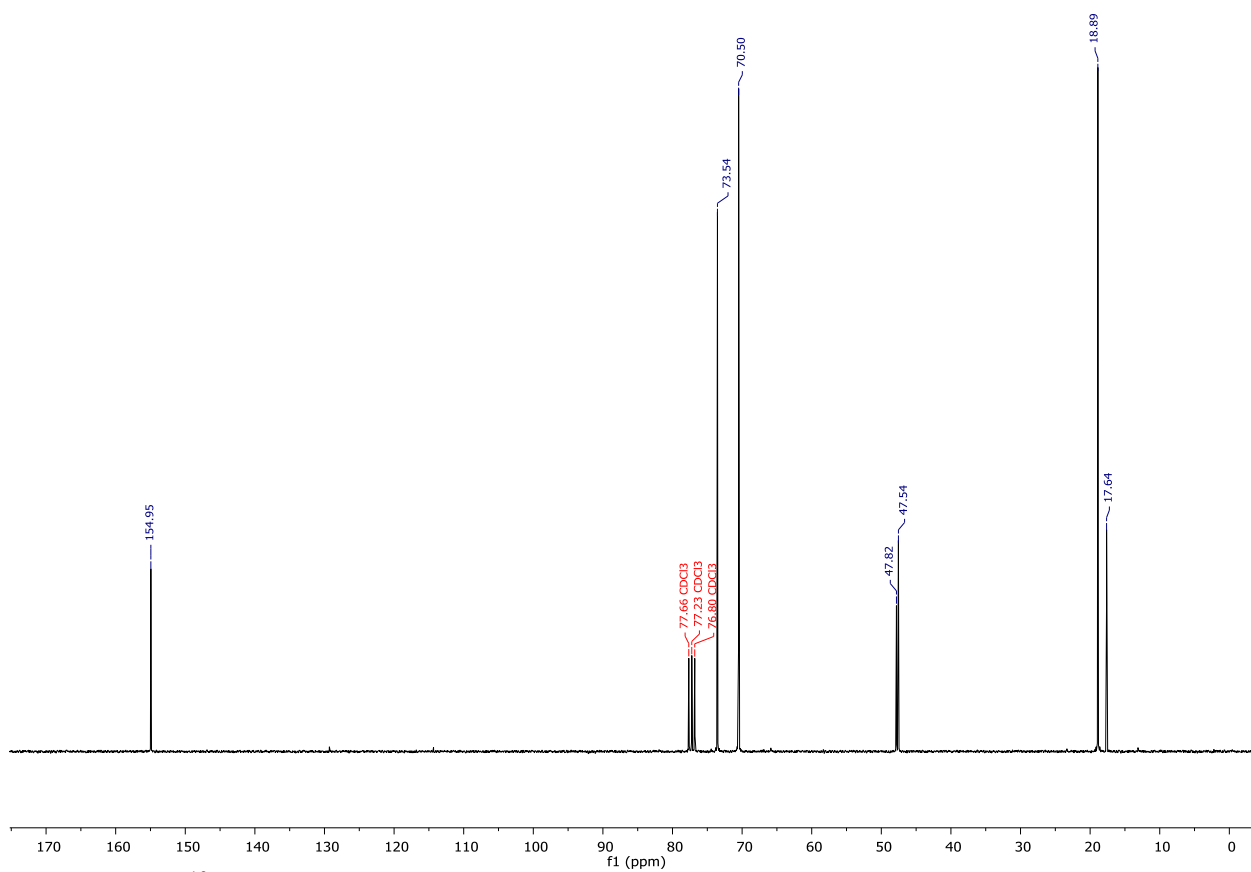


Figure A. 22. ^{13}C NMR spectrum (75.4 MHz, 298 K, CDCl_3) of 4-methyl-1,3-dioxolan-2-one (Table 3.4, entry 1).

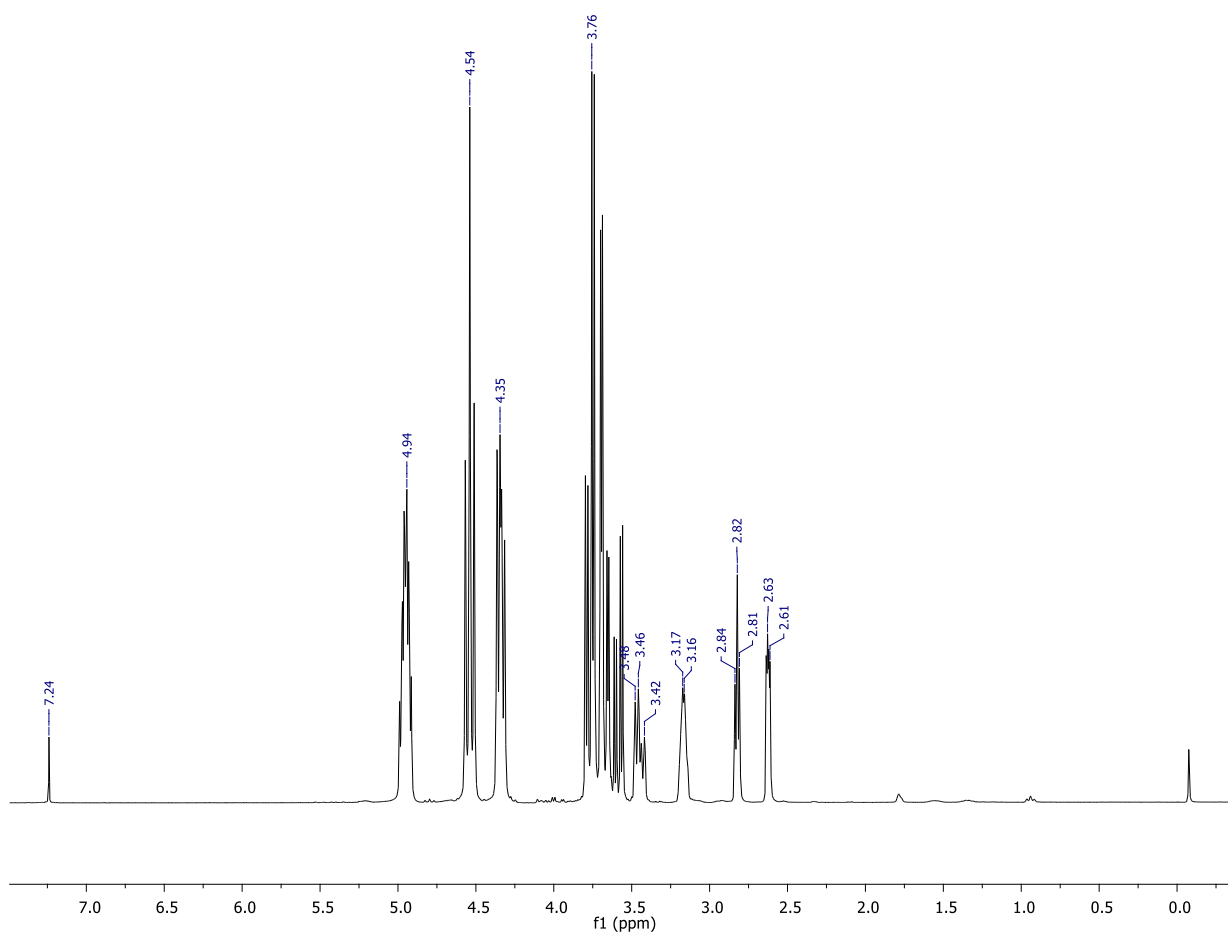


Figure A. 23. ¹H NMR spectrum (300 MHz, 298 K, CDCl₃) of 4-chloromethyl-1,3-dioxolan-2-one (Table 3.4, entry 2).

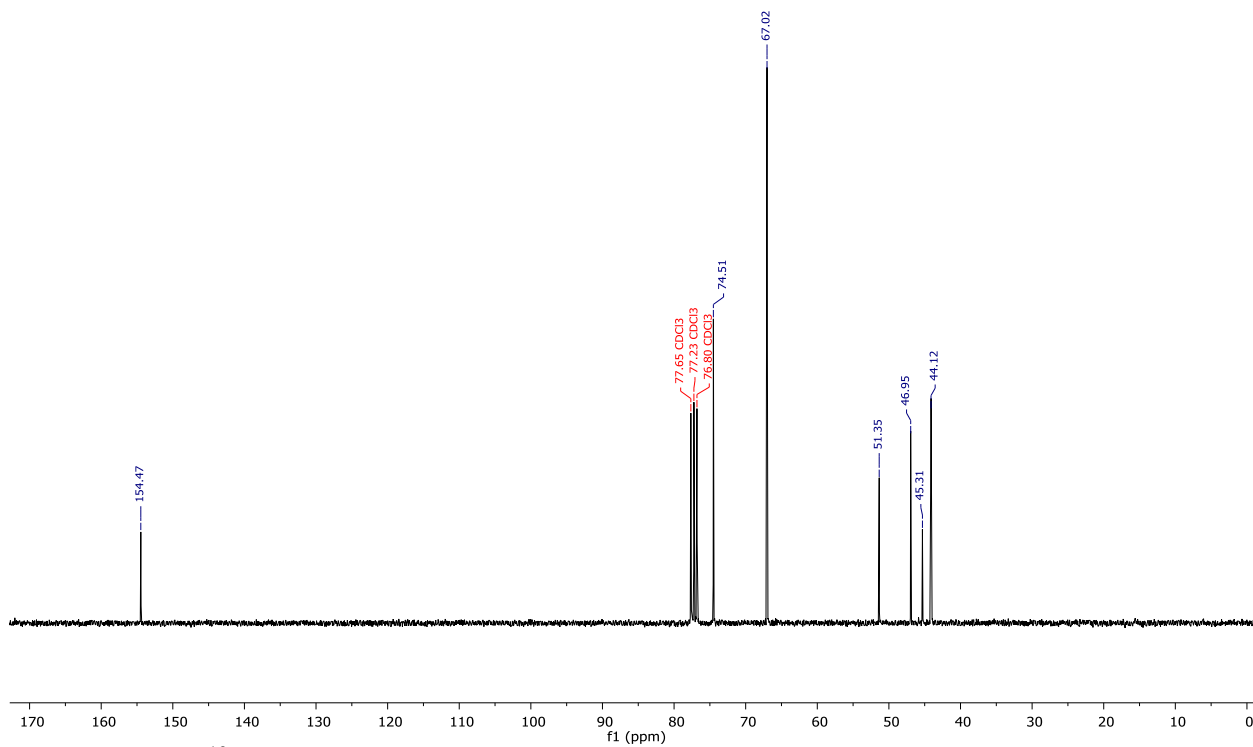


Figure A. 24. ^{13}C NMR spectrum (75.4 MHz, 298 K, CDCl_3) of 4-chloromethyl-1,3-dioxolan-2-one (Table 3.4, entry 2).

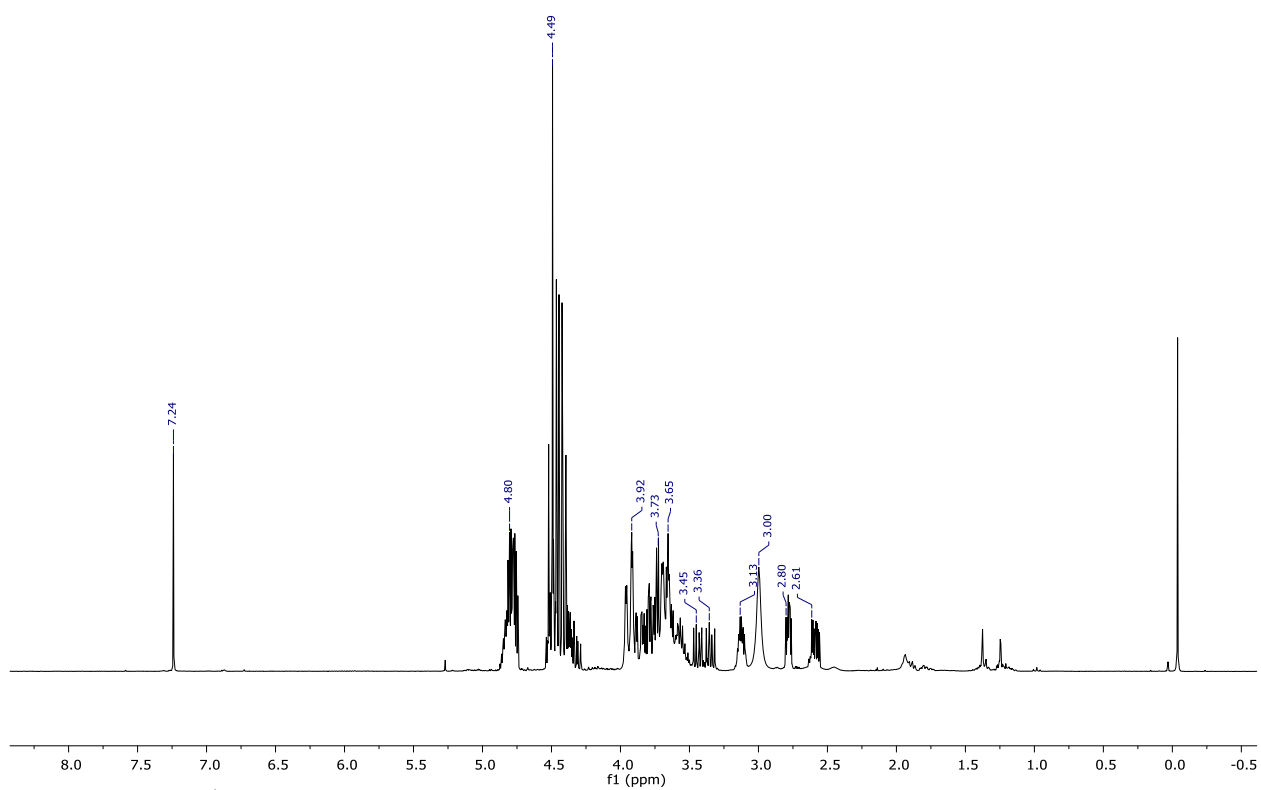


Figure A. 25. ^1H NMR spectrum (300 MHz, 298 K, CDCl_3) of 4-hydroxymethyl-1,3-dioxolan-2-one (Table 3.4, entry 3).

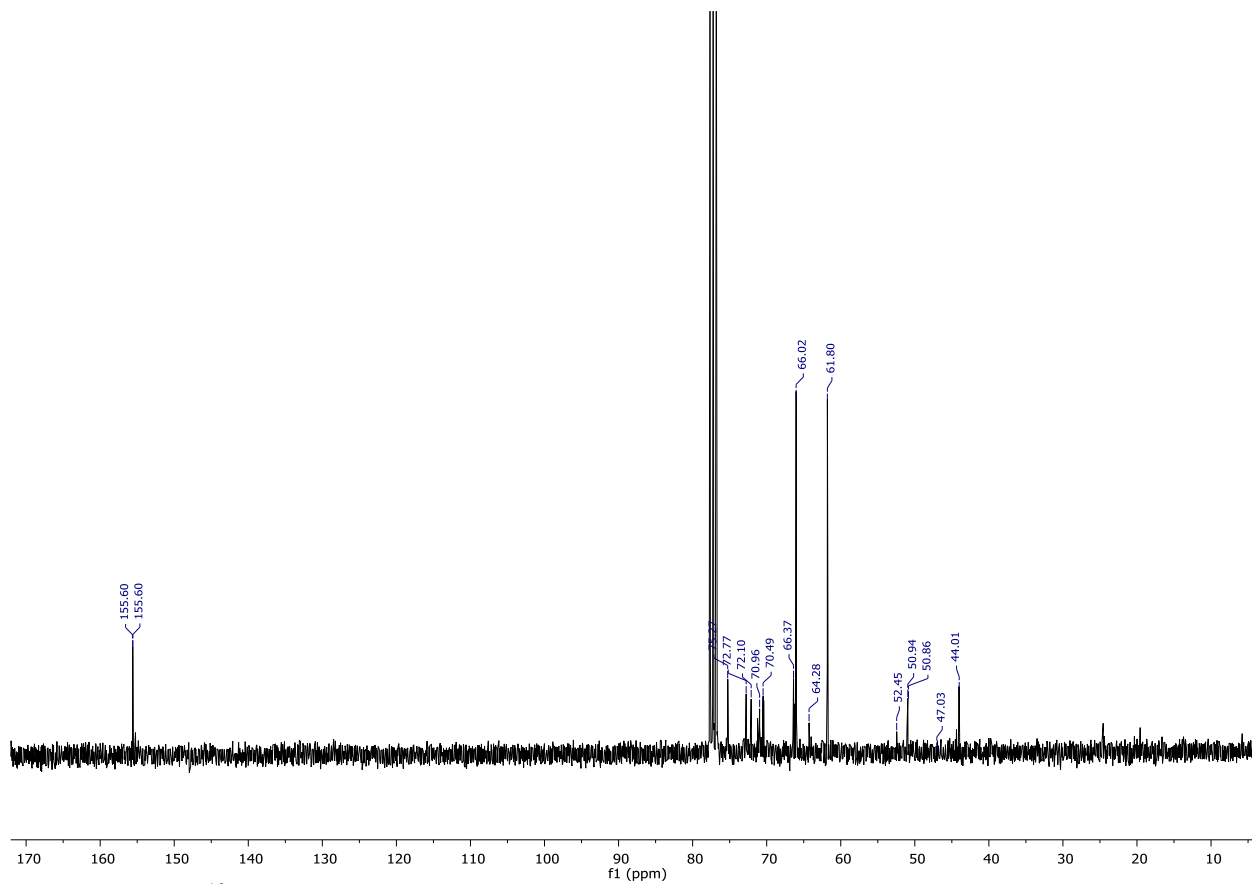


Figure A. 26. ^{13}C NMR spectrum (75.4 MHz, 298 K, CDCl_3) of 4-hydroxymethyl-1,3-dioxolan-2-one (Table 3.4, entry 3).

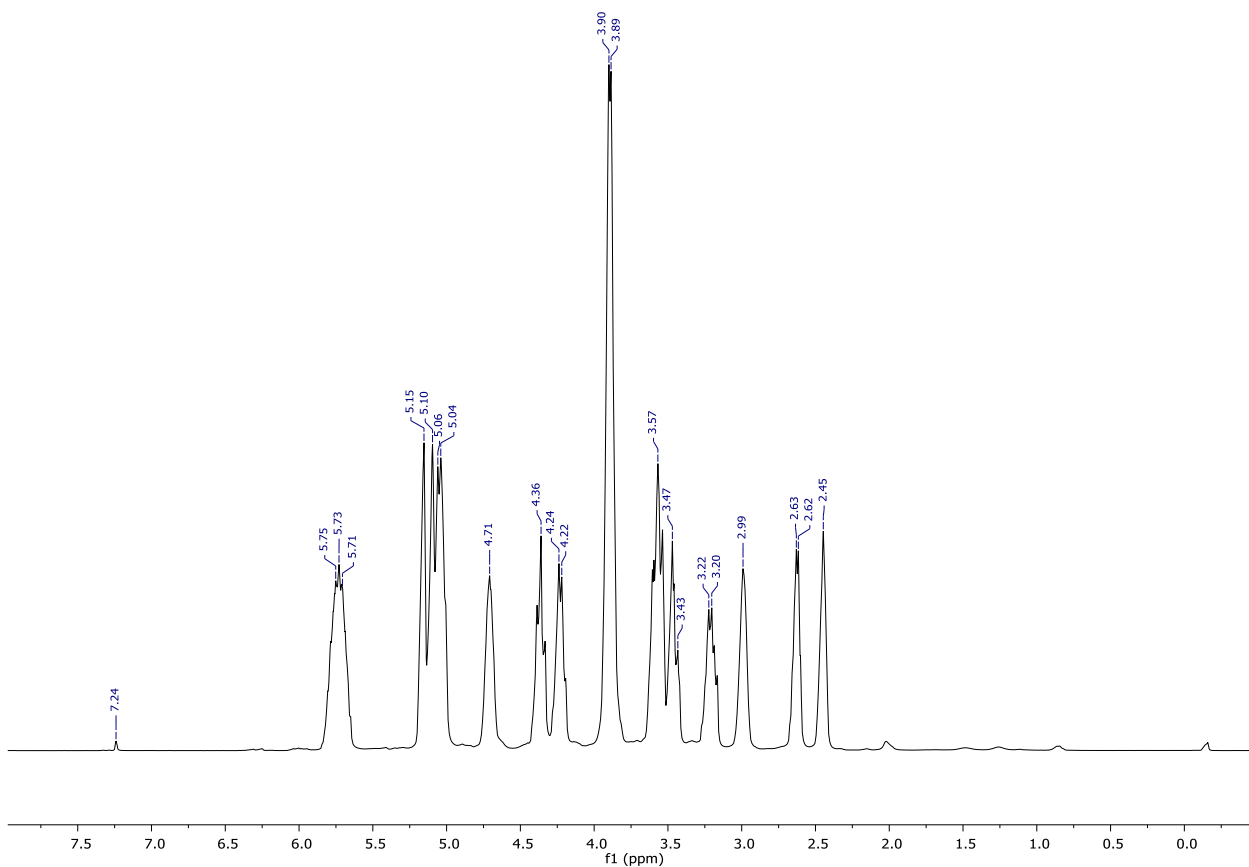


Figure A. 27. ¹H NMR spectrum (300 MHz, 298 K, CDCl₃) of 4-allyloxymethyl-1,3-dioxolan-2-one (Table 3.4, entry 4).

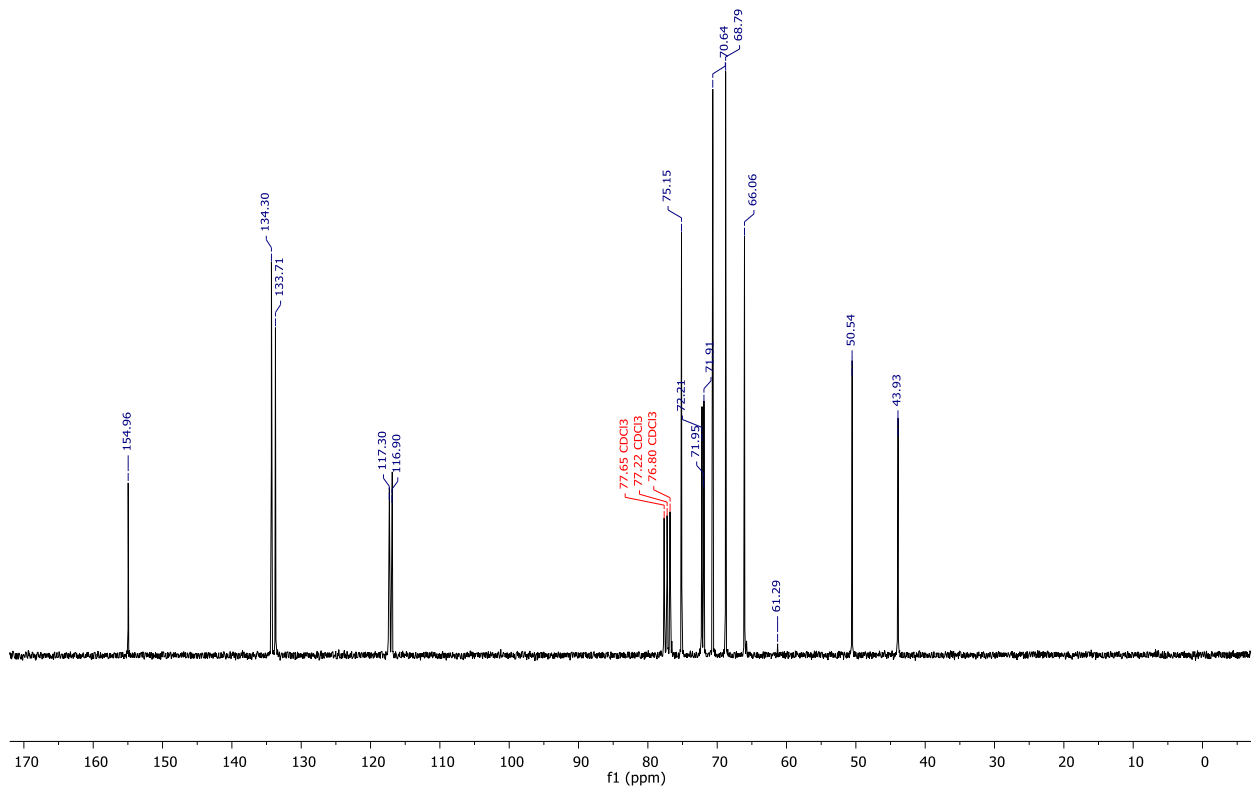


Figure A. 28. ^{13}C NMR spectrum (75.4 MHz, 298 K, CDCl_3) of 4-allyloxymethyl -1,3-dioxolan-2-one (Table 3.4, entry 4).

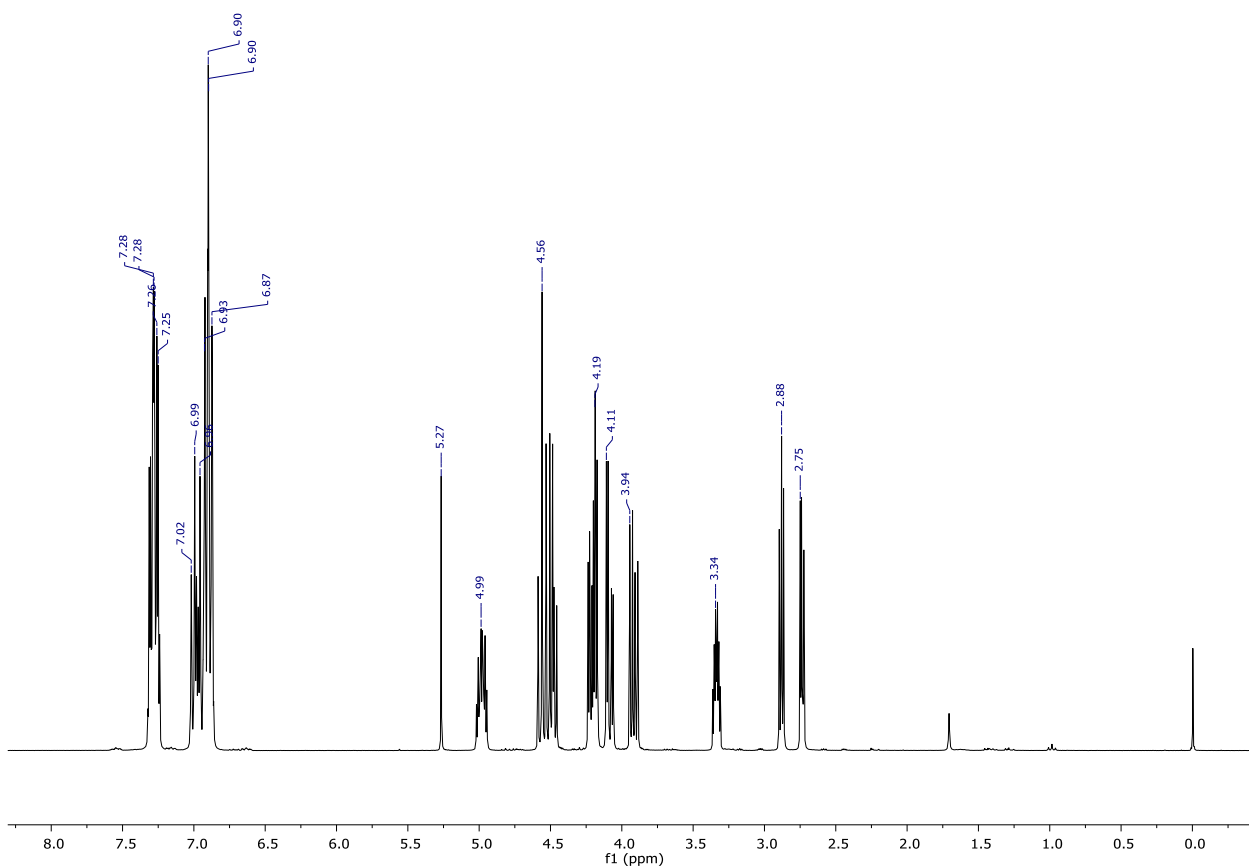


Figure A. 29. ^1H NMR spectrum (300 MHz, 298 K, CDCl_3) of 4-phenoxyethyl-1,3-dioxolan-2-one (Table 3.4, entry 5).

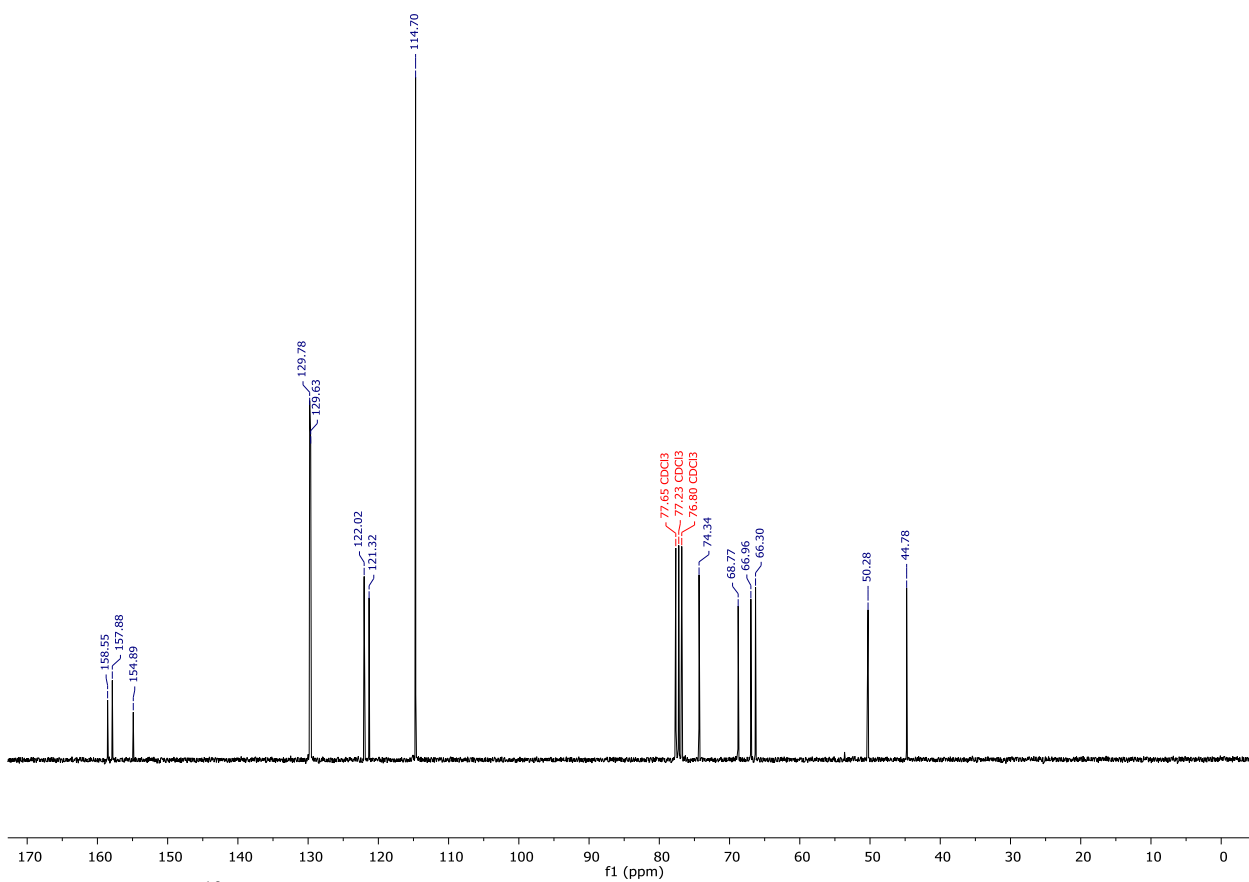


Figure A. 30. ^{13}C NMR spectrum (75.4 MHz, 298 K, CDCl_3) of 4-phenoxyethyl-1,3-dioxolan-2-one (Table 3.4, entry 5).

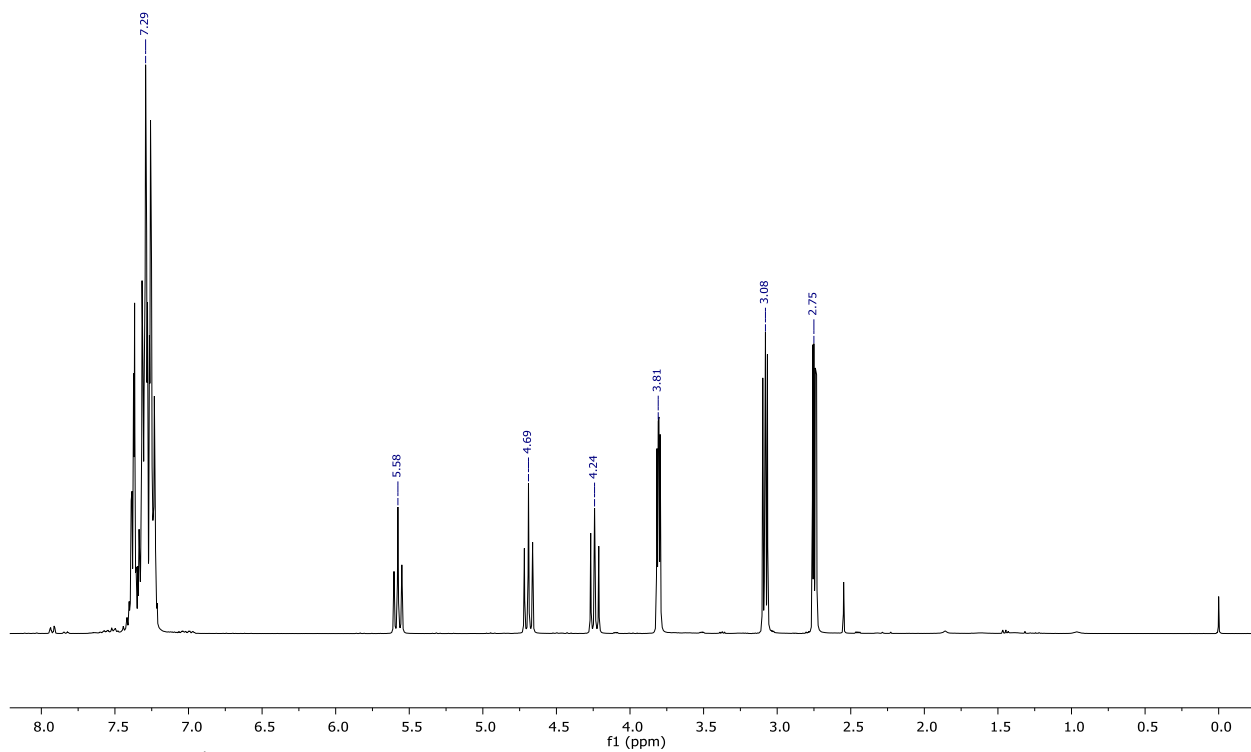


Figure A. 31. ^1H NMR spectrum (300 MHz, 298 K, CDCl_3) of 4-phenyl-1,3-dioxolan-2-one (Table 3.4, entry 6).

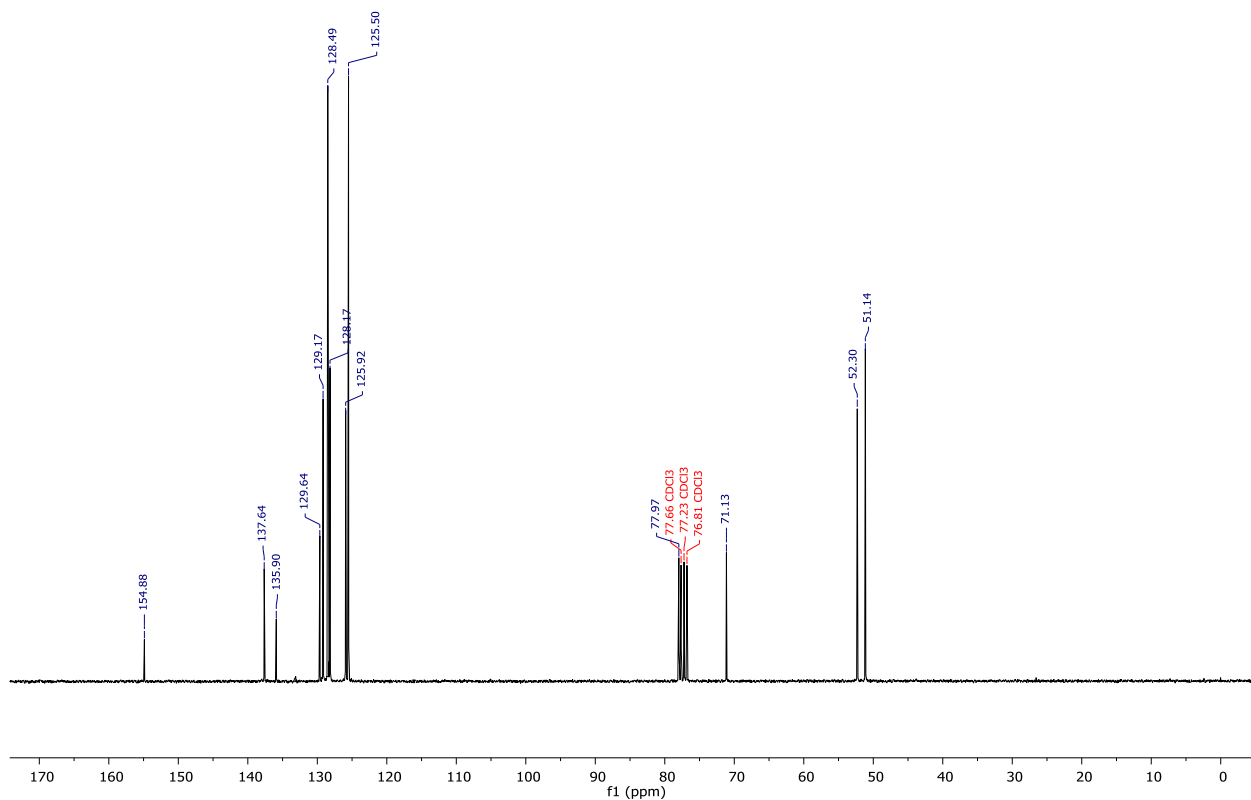


Figure A. 32. ^{13}C NMR spectrum (75.4 MHz, 298 K, CDCl_3) of 4-phenyl-1,3-dioxolan-2-one (Table 3.4, entry 6).

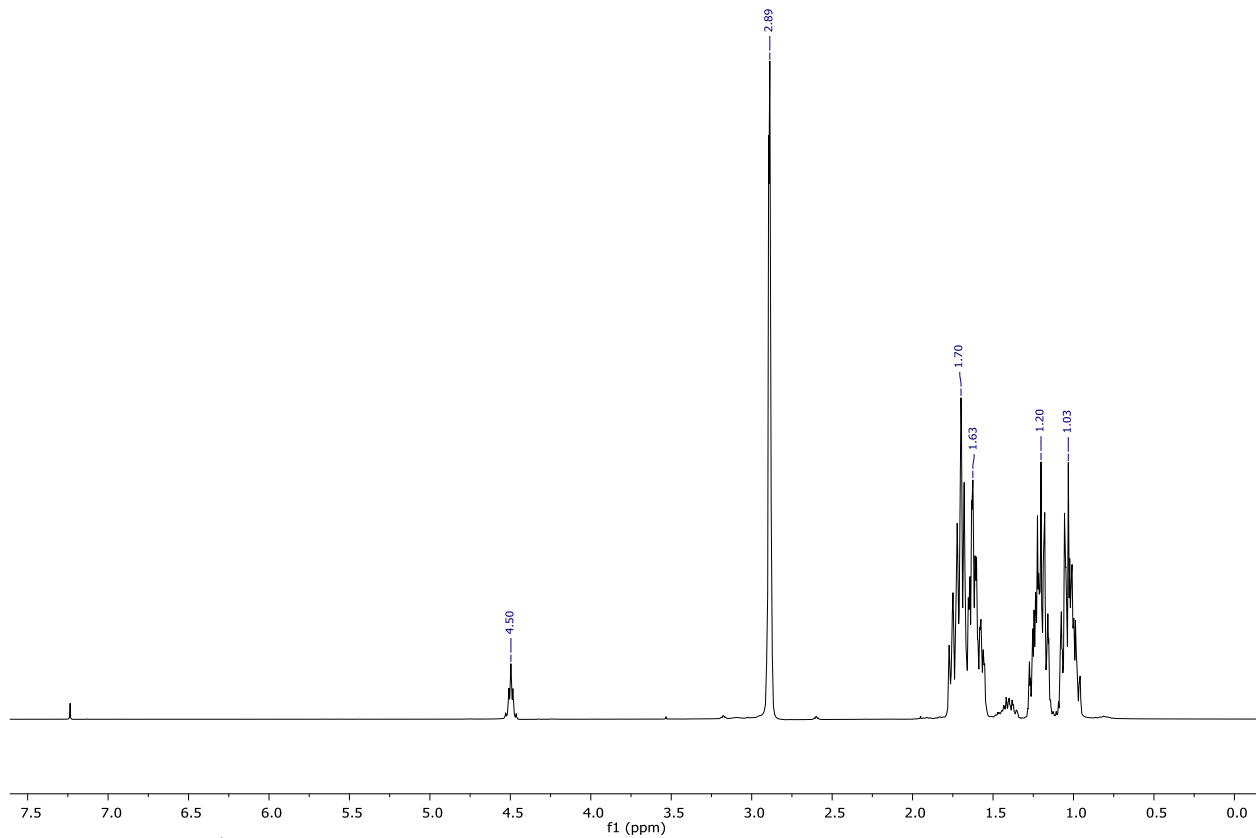


Figure A. 33. ^1H NMR spectrum (300 MHz, 298 K, CDCl_3) of *cis*-1,2-cyclohexene carbonate (Table 3.4, entry 7).

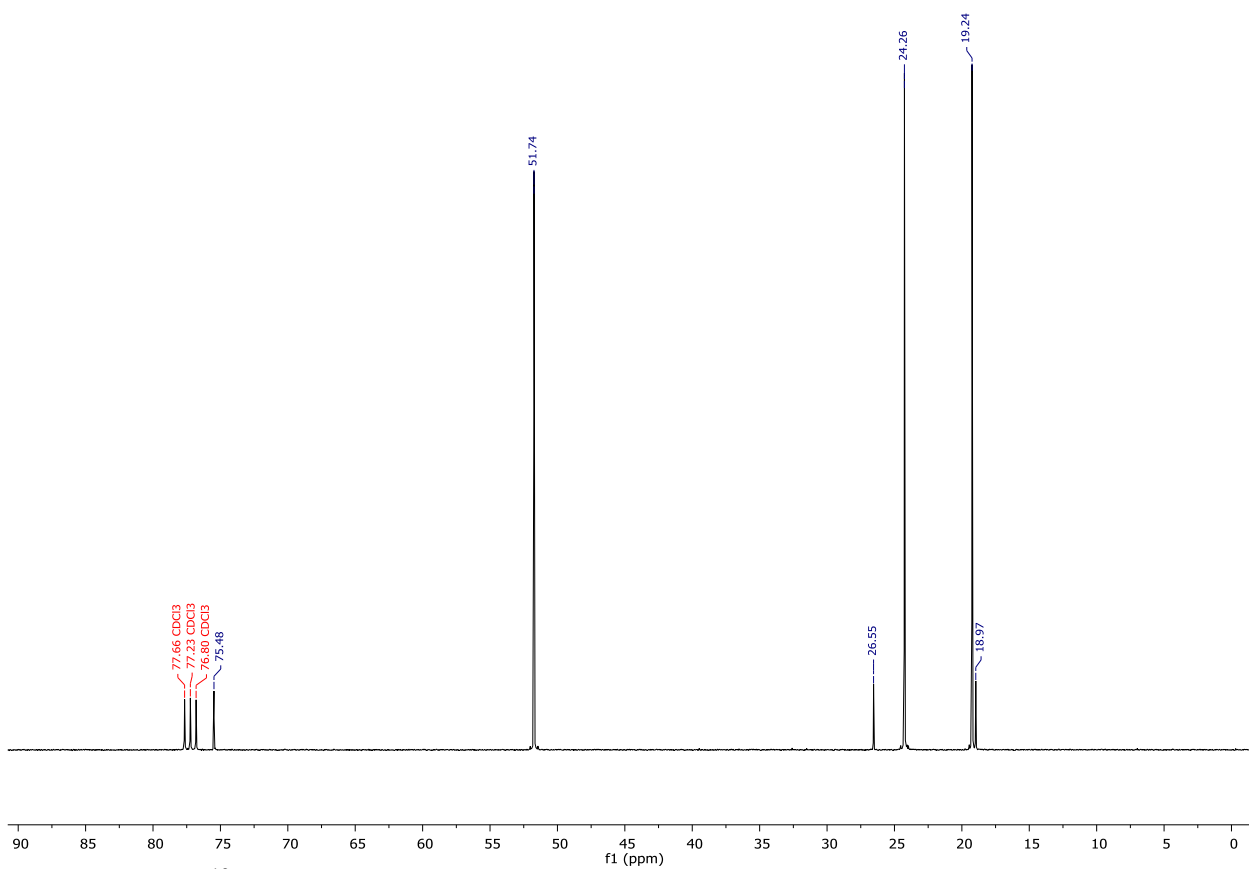


Figure A. 34. ^{13}C NMR spectrum (75.4 MHz, 298 K, CDCl_3) of *cis*-1,2-cyclohexene carbonate (Table 3.4, entry 7).

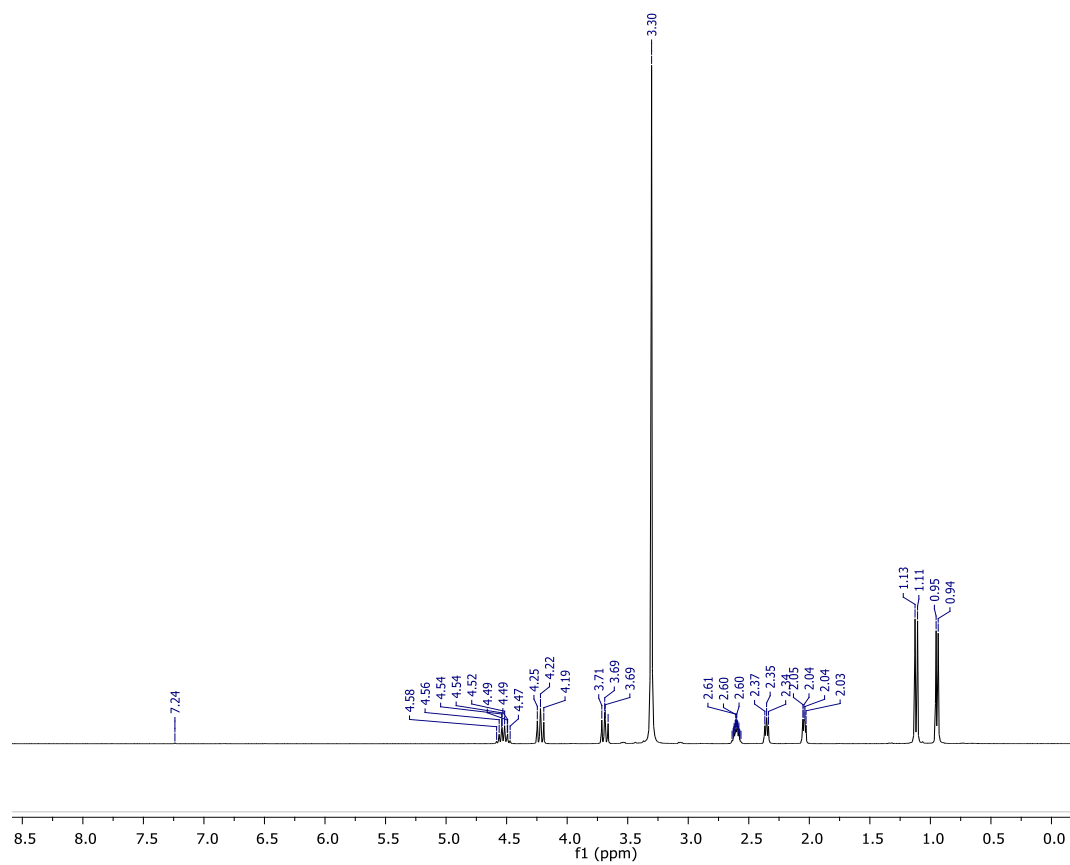


Figure A. 35. ^1H NMR spectrum (300 MHz, 298 K, CDCl_3) of 4-methyl-1,3-dioxolan-2-one (Table 4.1, entry 5).

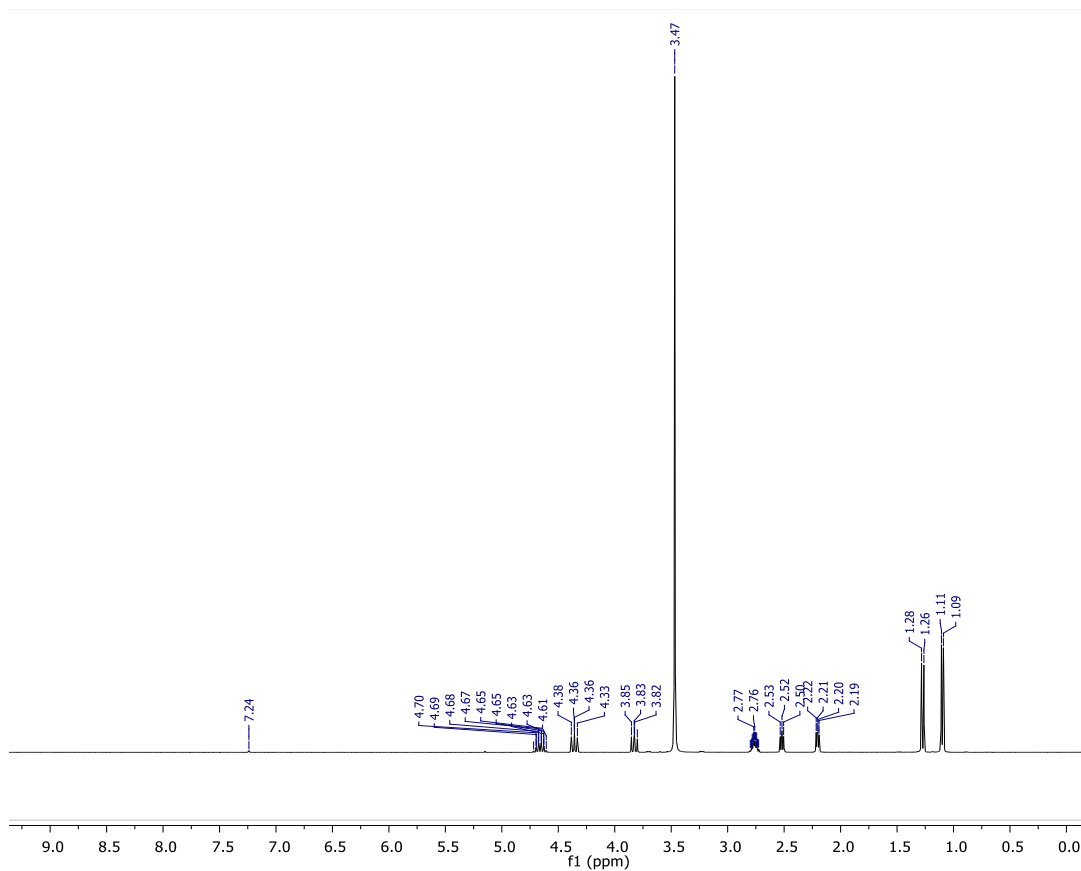


Figure A. 36. ^1H NMR spectrum (300 MHz, 298 K, CDCl_3) of 4-methyl-1,3-dioxolan-2-one (Table 4.1, entry 6).

Appendix B: MALDI-TOF mass spectra

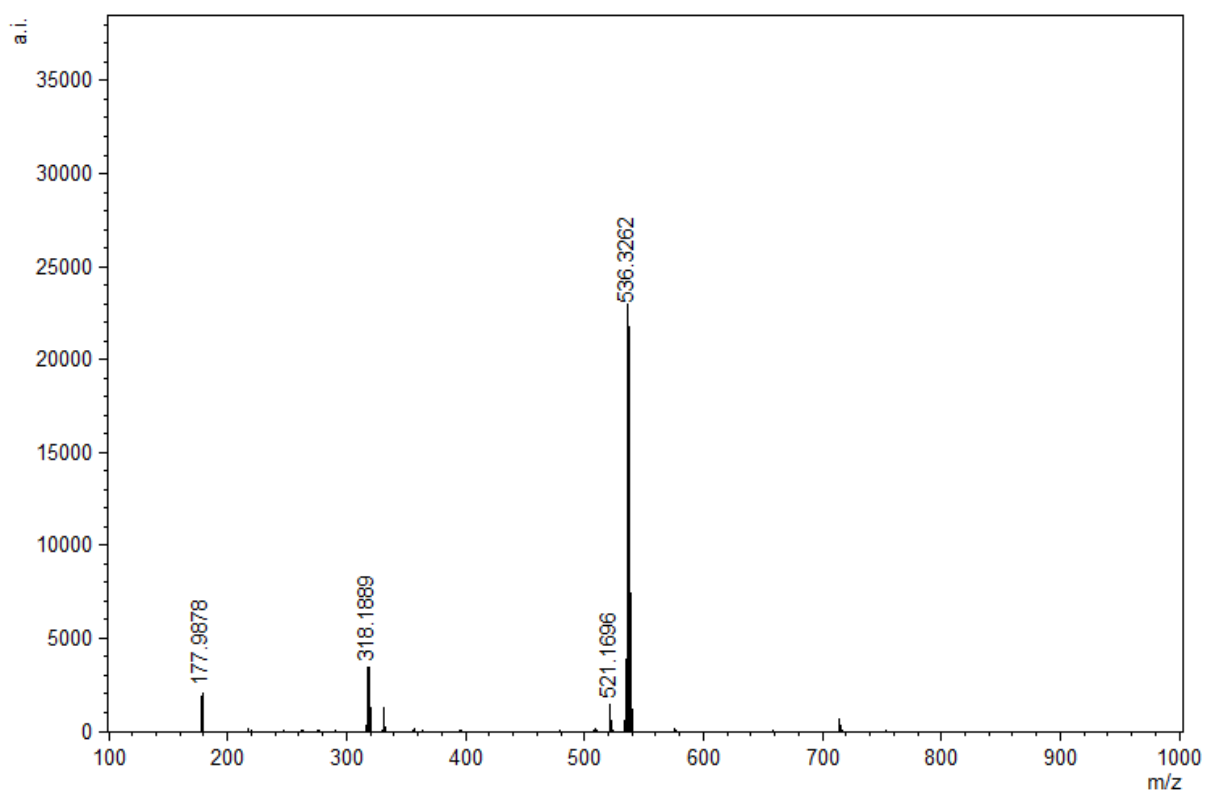


Figure B. 1. MALDI-TOF mass spectrum of $[L1]H_2$.

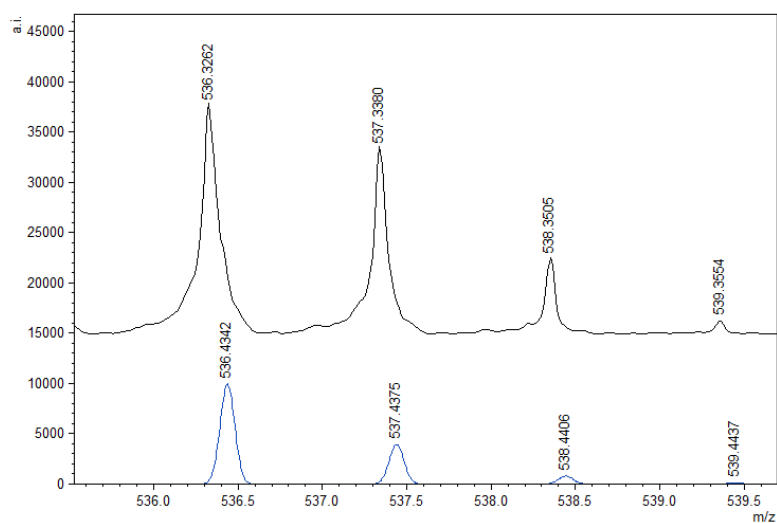


Figure B. 2. Experimental (top) and calculated (bottom) isotopic distribution pattern for $[L1]H_2$.

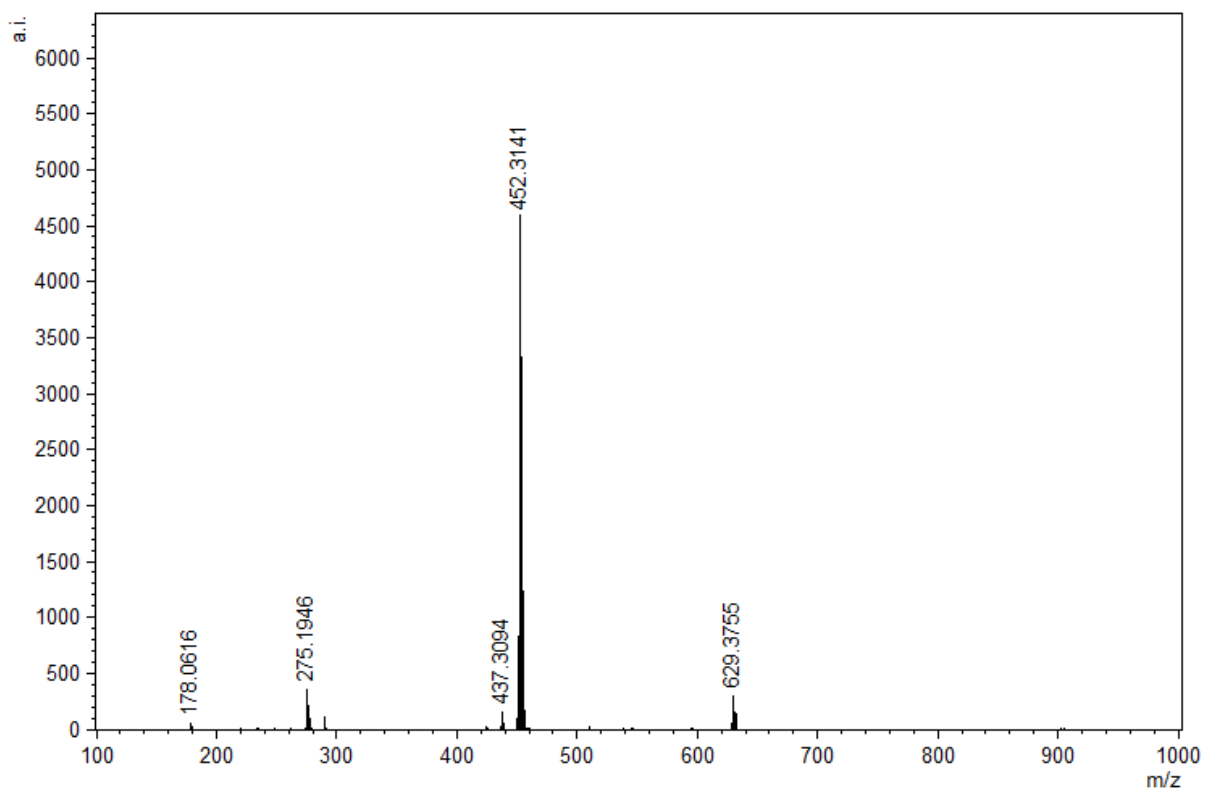


Figure B. 3. MALDI-TOF mass spectrum of $[L2]H_2$.

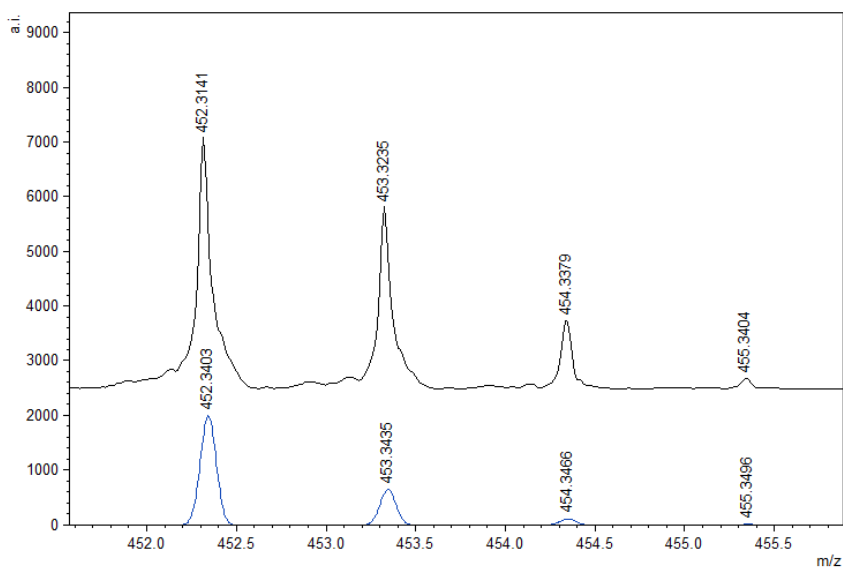


Figure B. 4. Experimental (top) and calculated (bottom) isotopic distribution pattern for $[L2]H_2$.

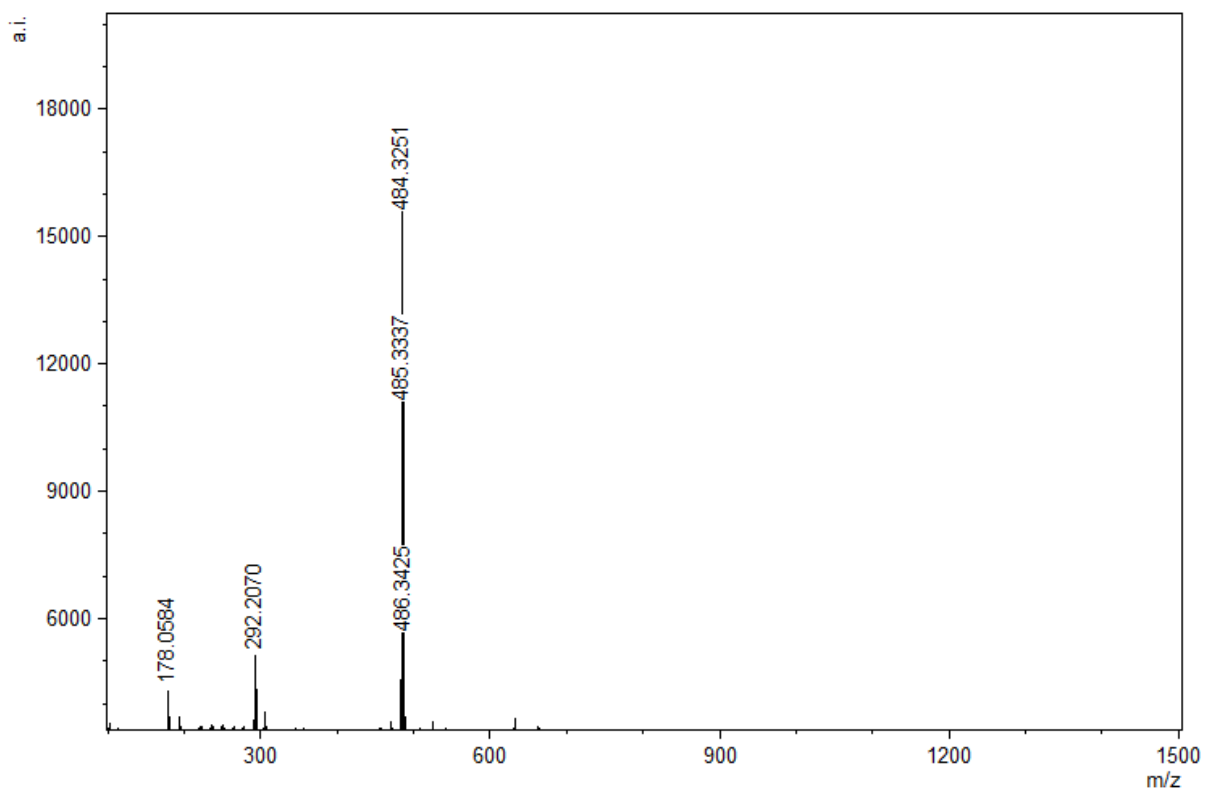


Figure B. 5. MALDI-TOF mass spectrum of [L3]H₂.

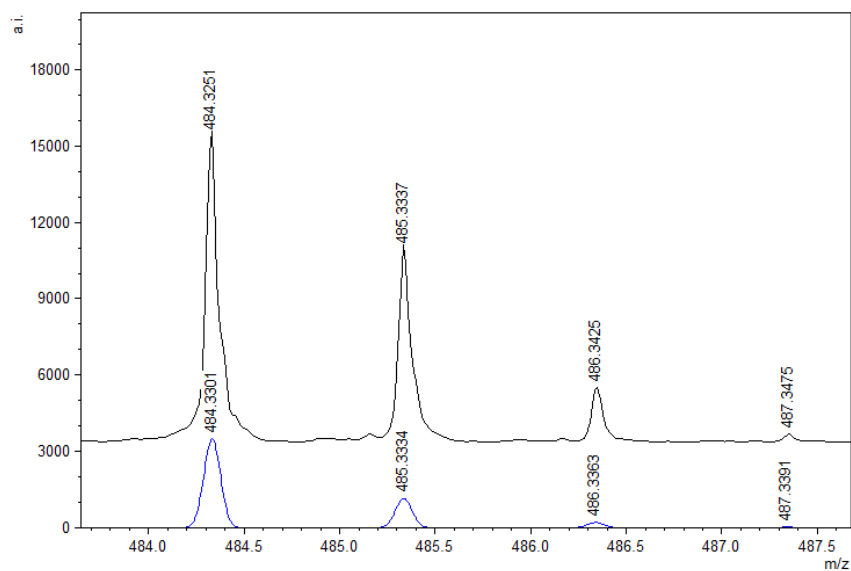


Figure B. 6. Experimental (top) and calculated (bottom) isotopic distribution pattern for [L3]H₂.

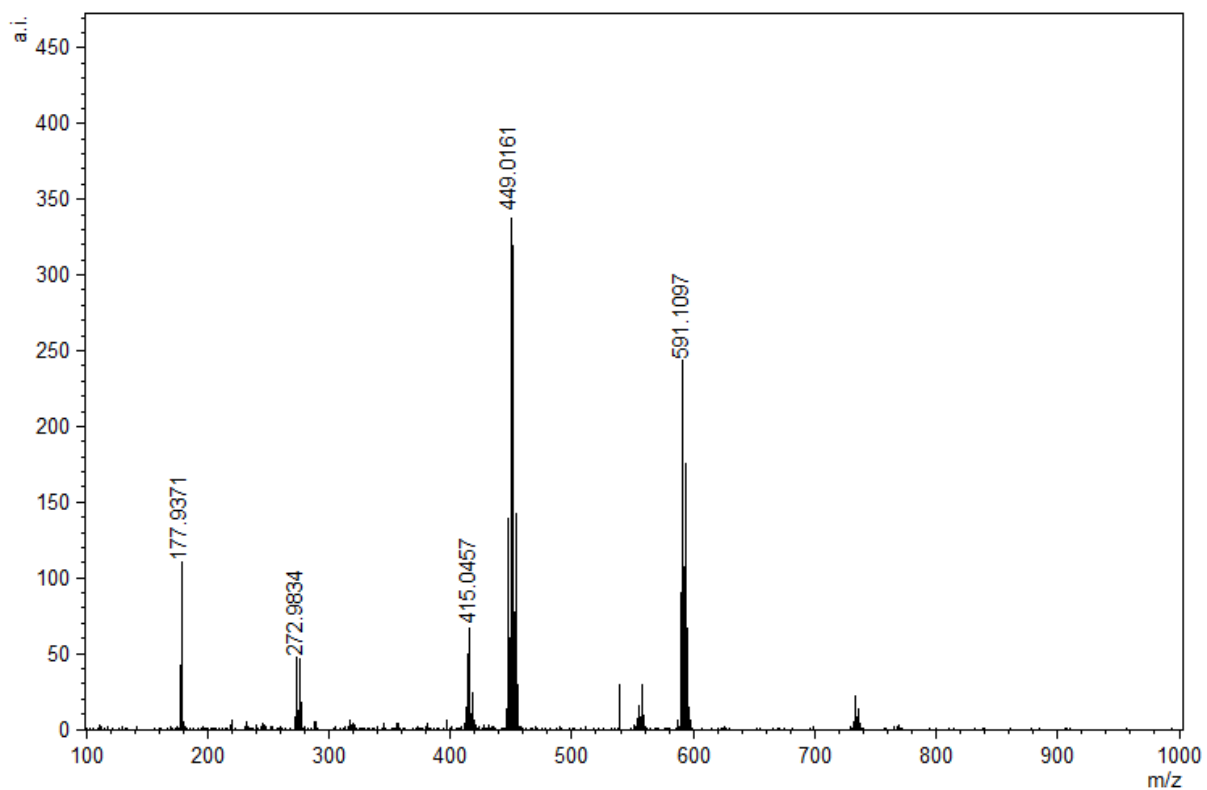


Figure B. 7. MALDI-TOF mass spectrum of [L4]H₂.

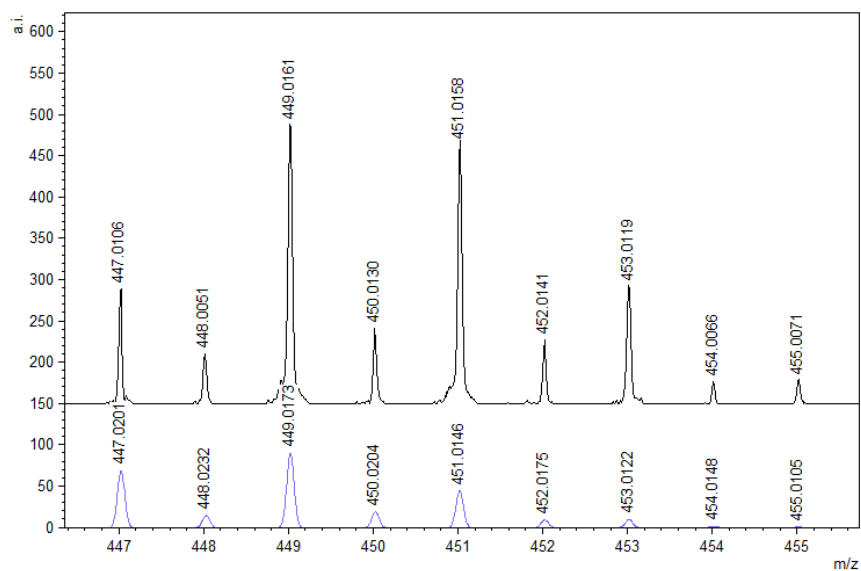


Figure B. 8. Experimental (top) and calculated (bottom) isotopic distribution pattern for [L4]H₂.

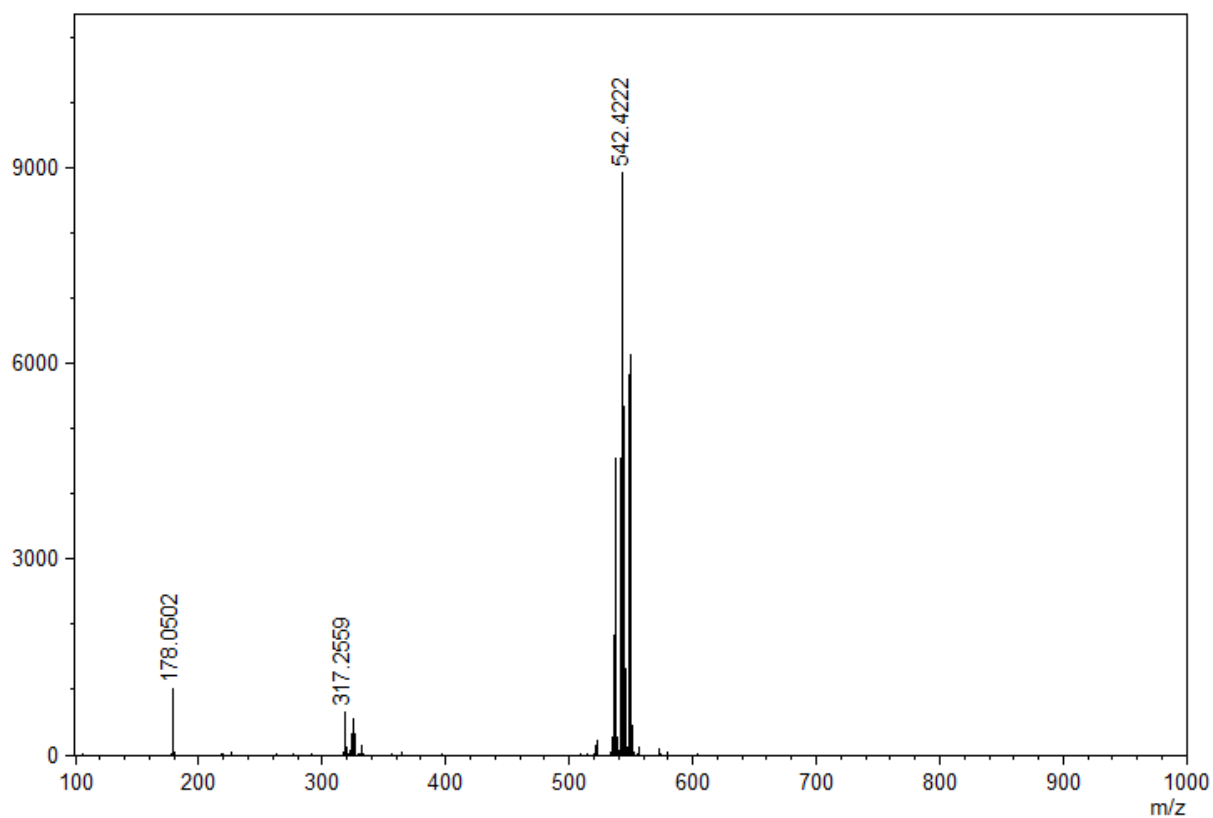


Figure B. 9. MALDI-TOF mass spectrum of 2.4.

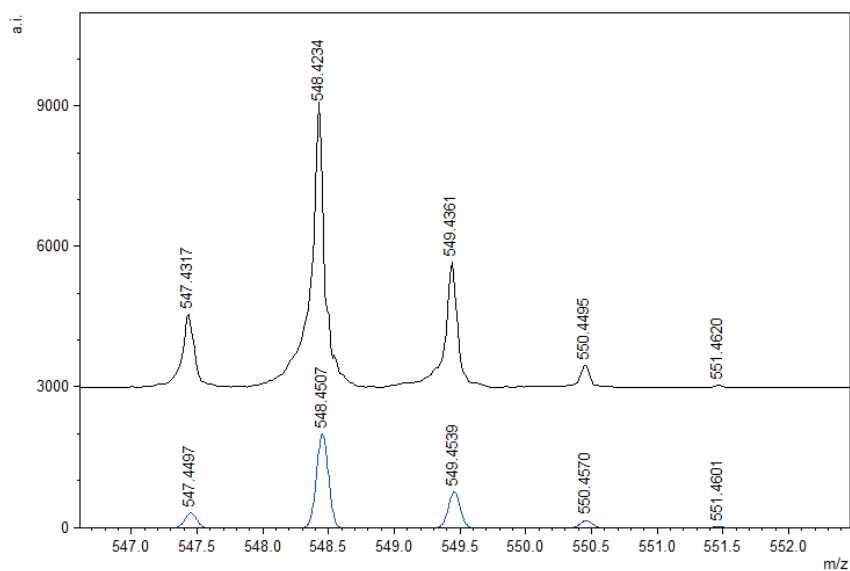


Figure B. 10. Experimental (top) and calculated (bottom) isotopic distribution pattern for 2.4.

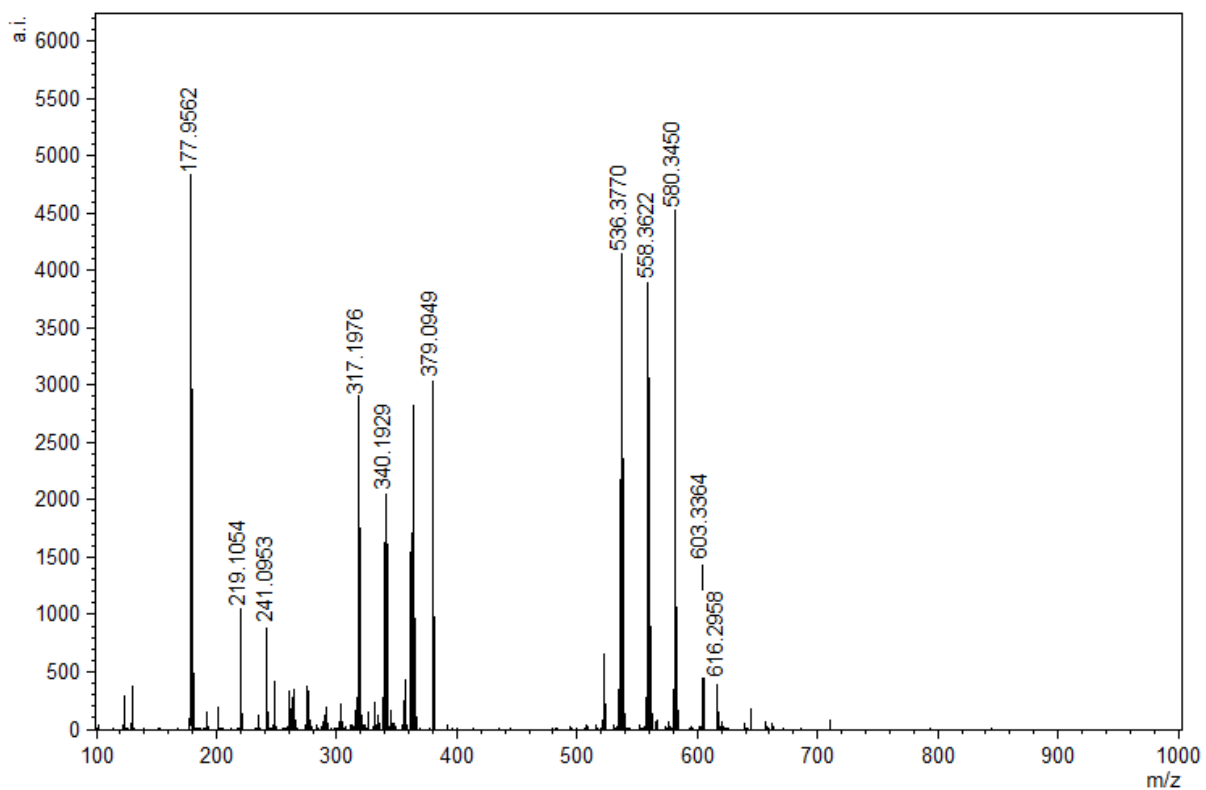


Figure B. 11. MALDI-TOF mass spectrum of **2.5**.

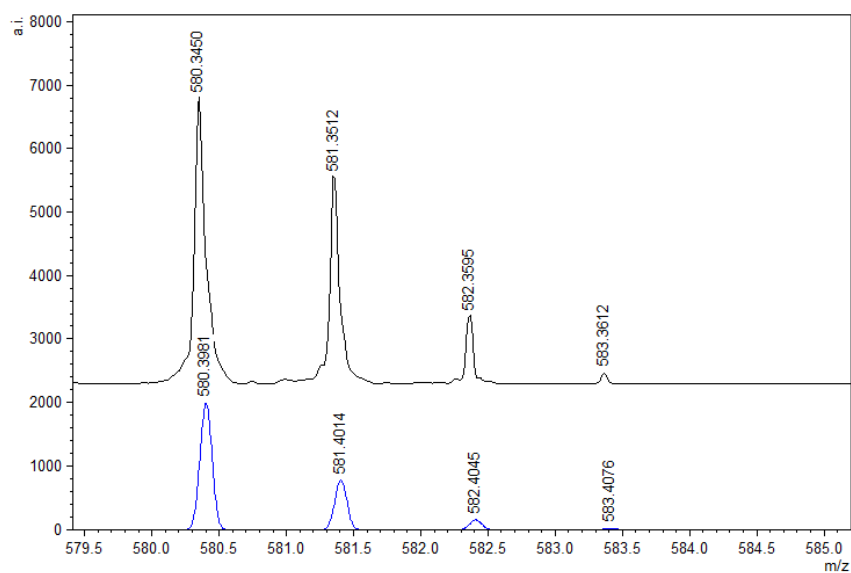


Figure B. 12. Experimental (top) and calculated (bottom) isotopic distribution pattern for **2.5**.

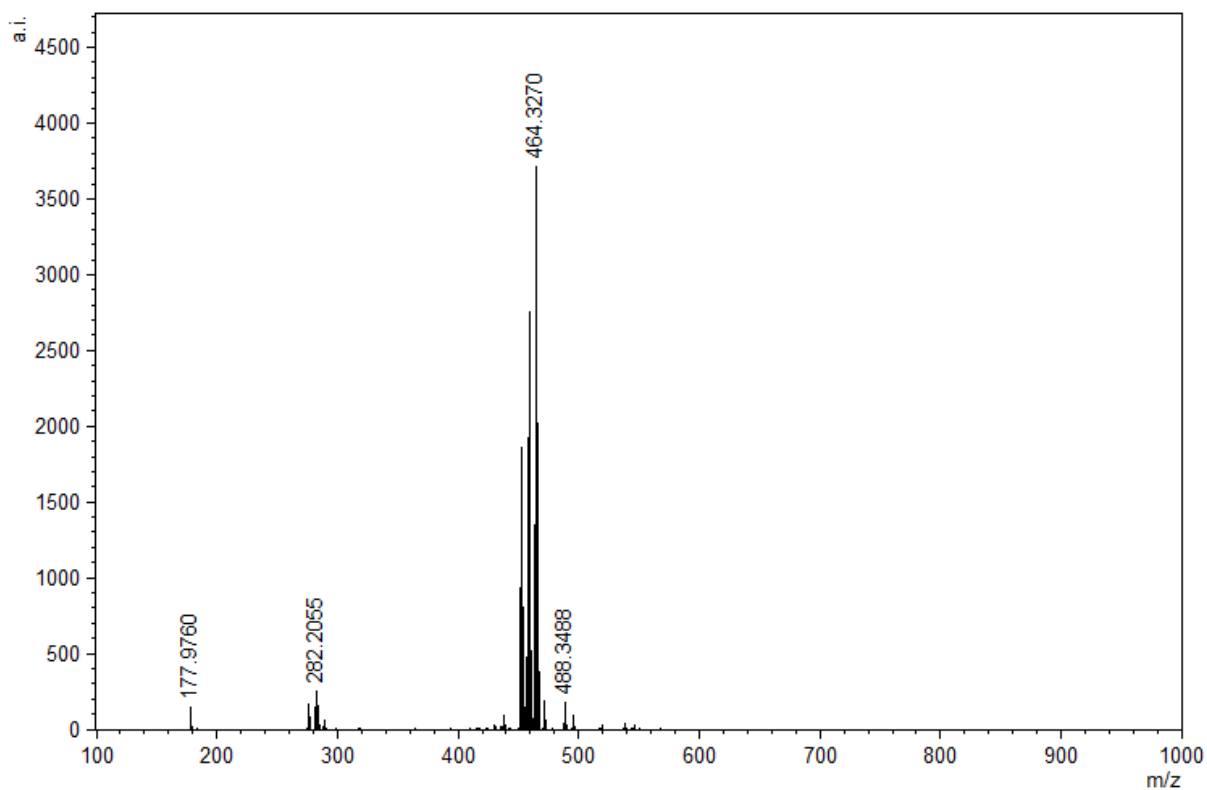


Figure B. 13. MALDI-TOF mass spectrum of **2.6**.

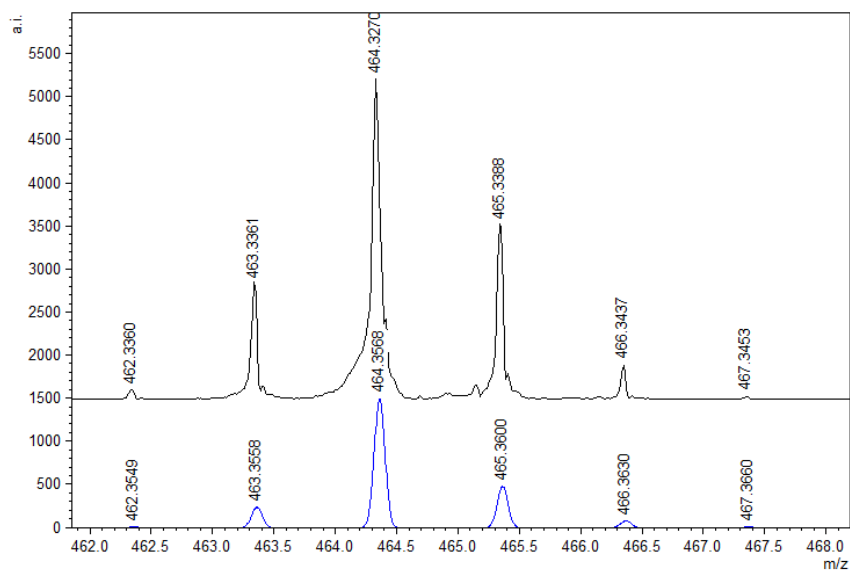


Figure B. 14. Experimental (top) and calculated (bottom) isotopic distribution pattern for **2.6**.

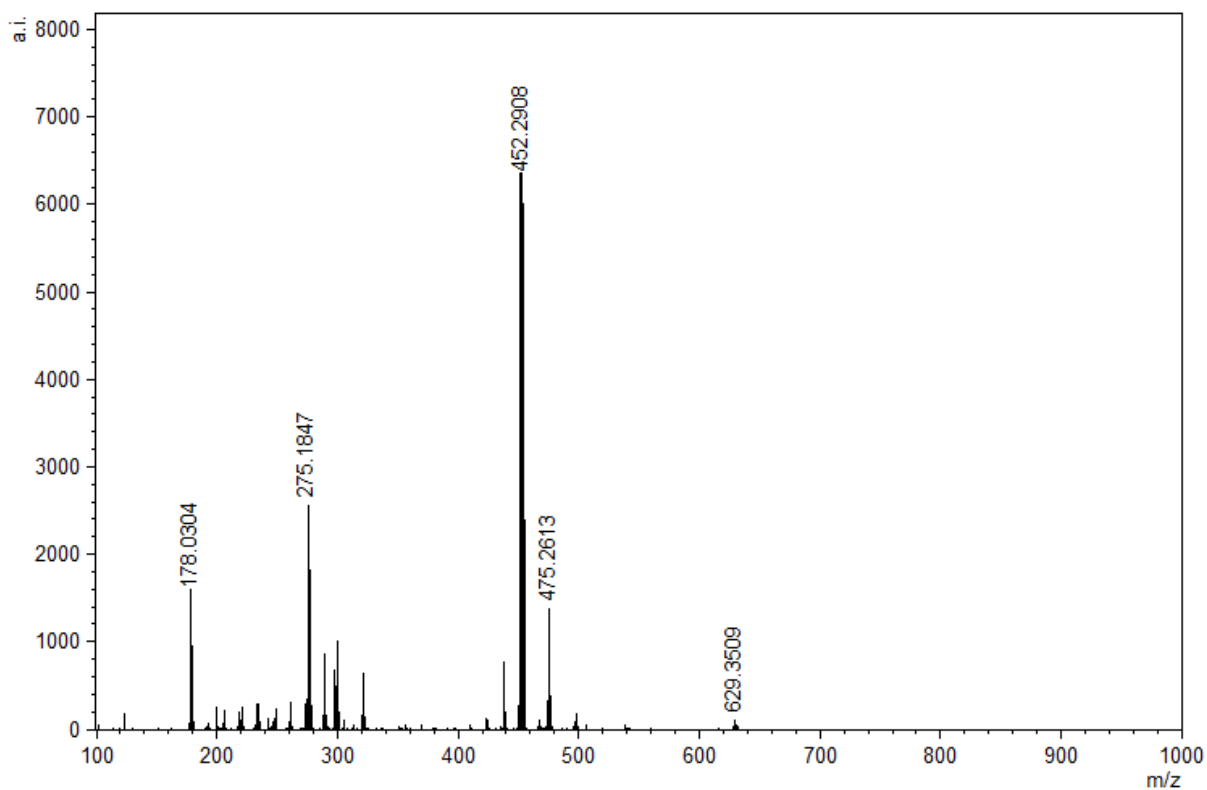


Figure B. 15. MALDI-TOF mass spectrum of **2.7**.

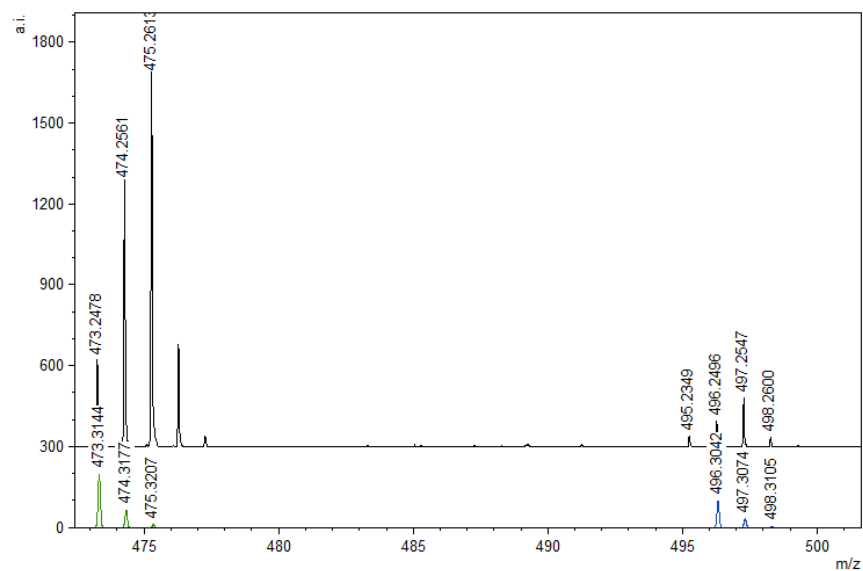


Figure B. 16. Experimental (top) and calculated (bottom) isotopic distribution pattern for **2.7**. Na[L2] (left) and Na₂[L2] (Right).

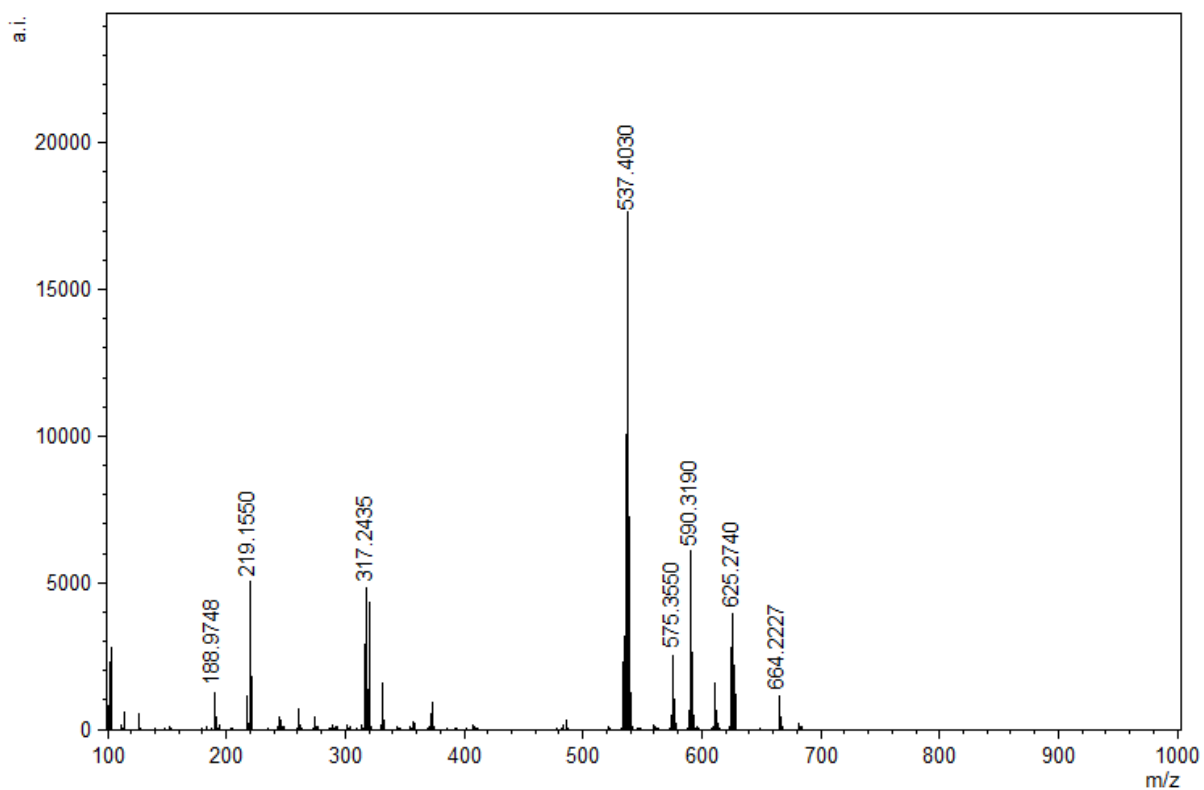


Figure B. 17. MALDI-TOF mass spectrum of 3.1.

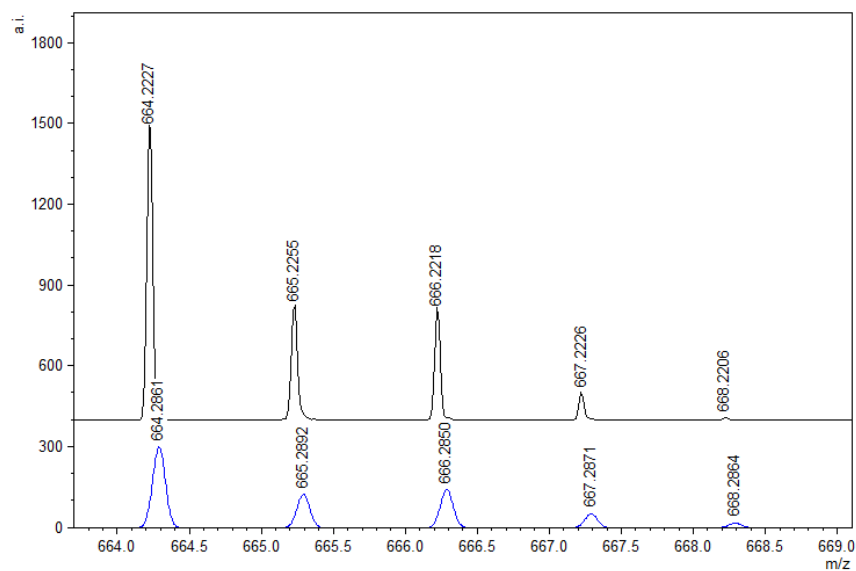


Figure B. 18. Experimental (top) and calculated (bottom) isotopic distribution pattern for 3.1 with K.

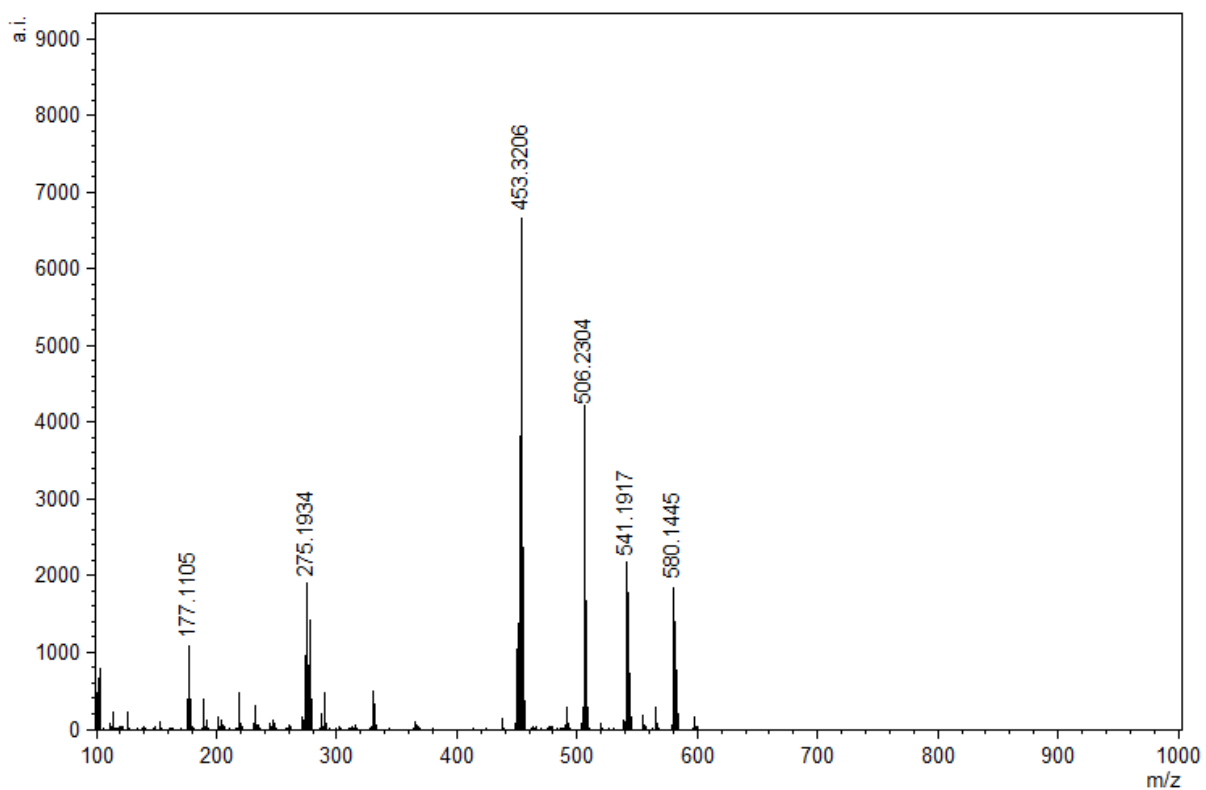


Figure B. 19. MALDI-TOF mass spectrum of 3.2.

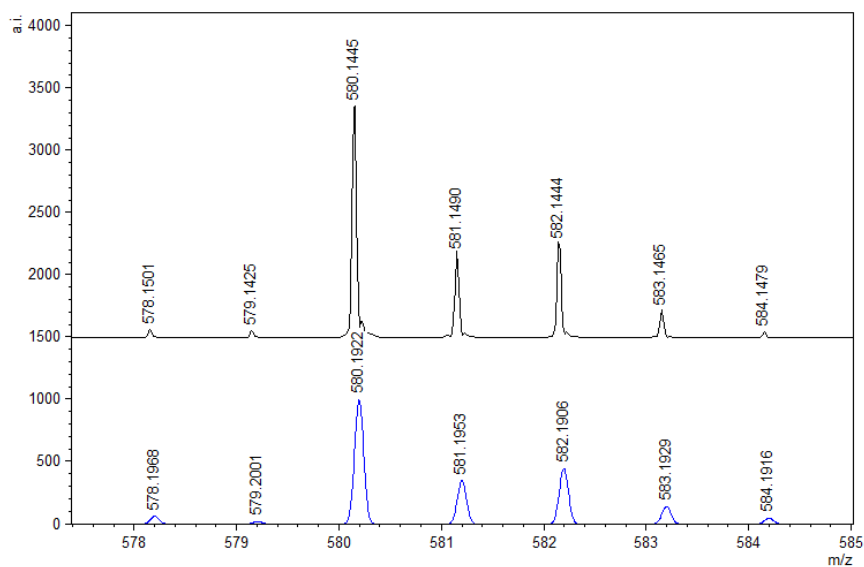


Figure B. 20. Experimental (top) and calculated (bottom) isotopic distribution pattern for 3.2 with K.

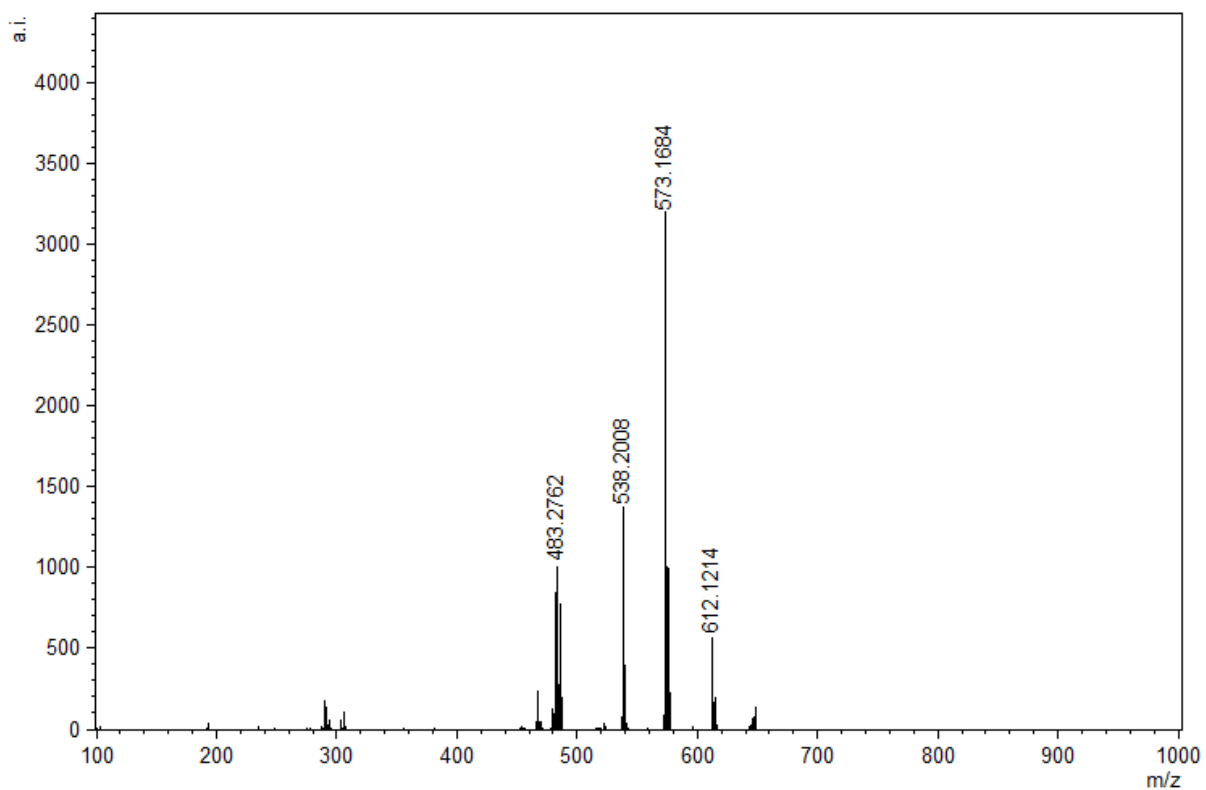


Figure B. 21. MALDI-TOF mass spectrum of **3.3**.

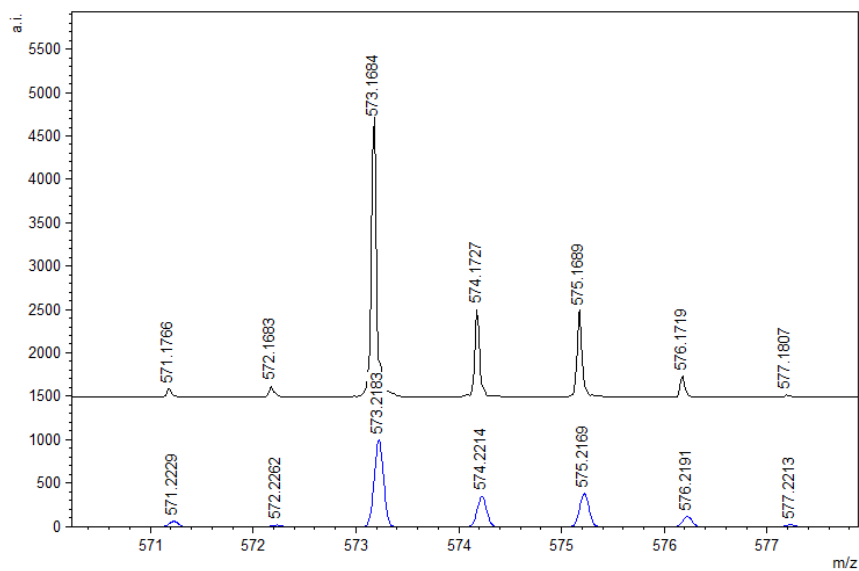


Figure B. 22. Experimental (top) and calculated (bottom) isotopic distribution pattern for **3.3**.

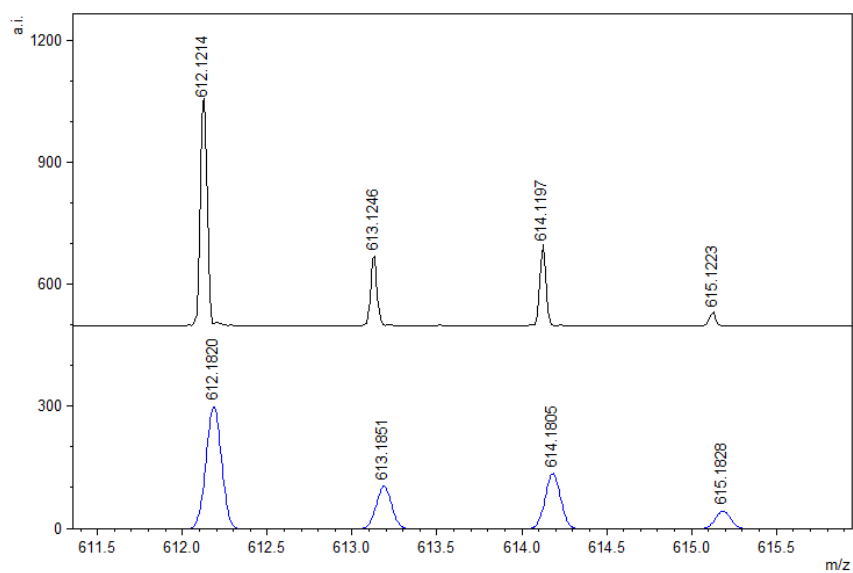


Figure B. 23. Experimental (top) and calculated (bottom) isotopic distribution pattern for **3.3** with K

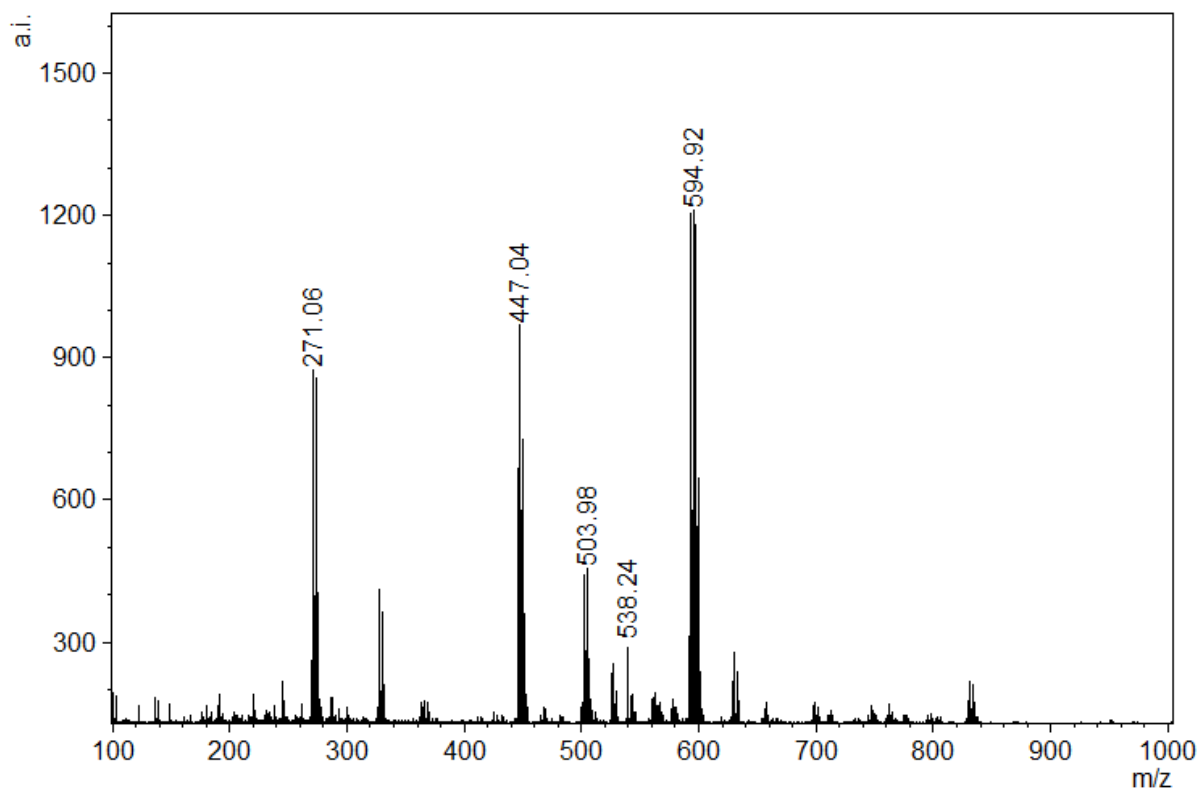


Figure B. 24. MALDI-TOF mass spectrum of 3.4.

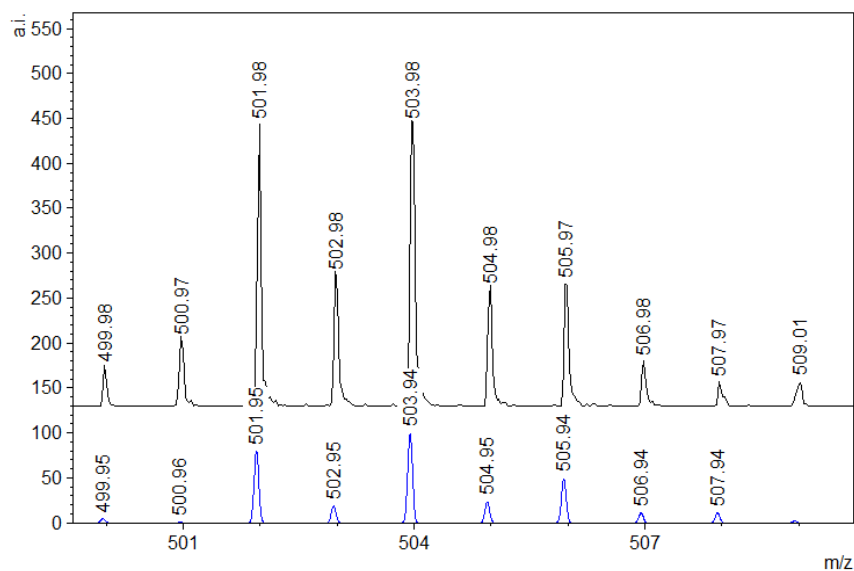


Figure B. 25. Experimental (top) and calculated (bottom) isotopic distribution pattern for 3.4.

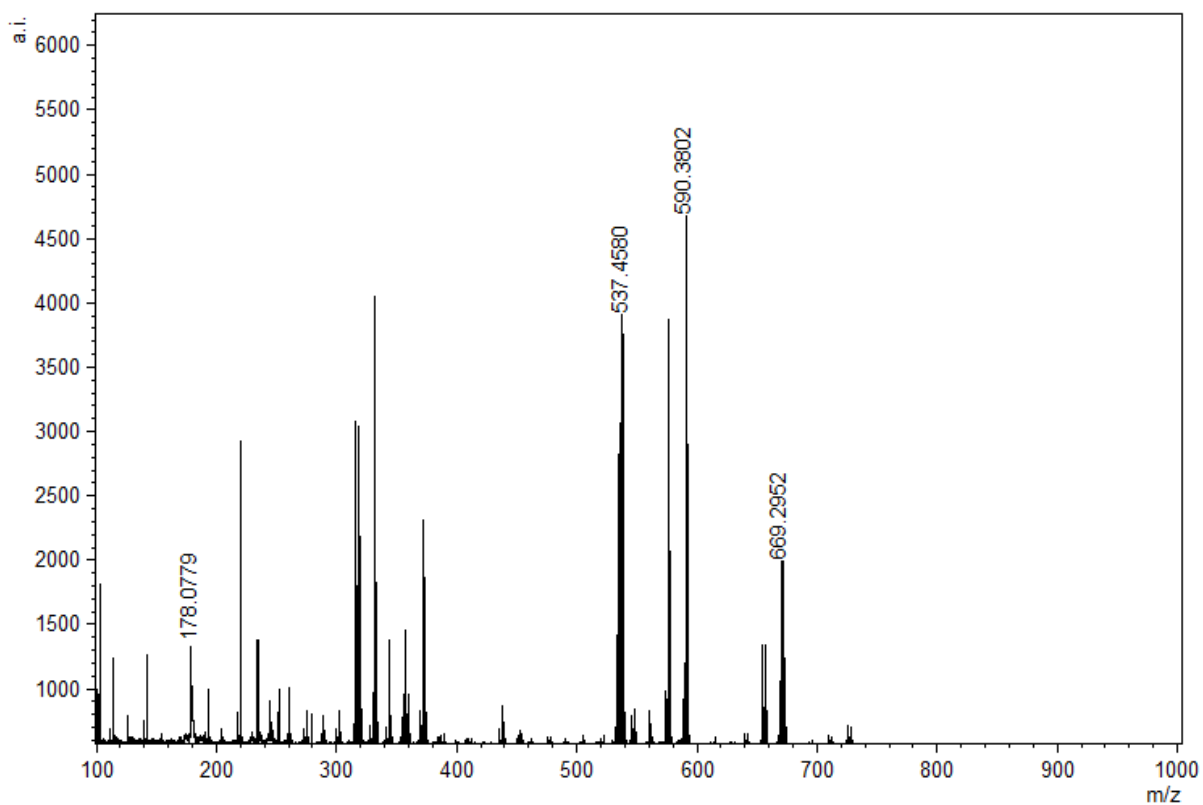


Figure B. 26. MALDI-TOF mass spectrum of 3.5.

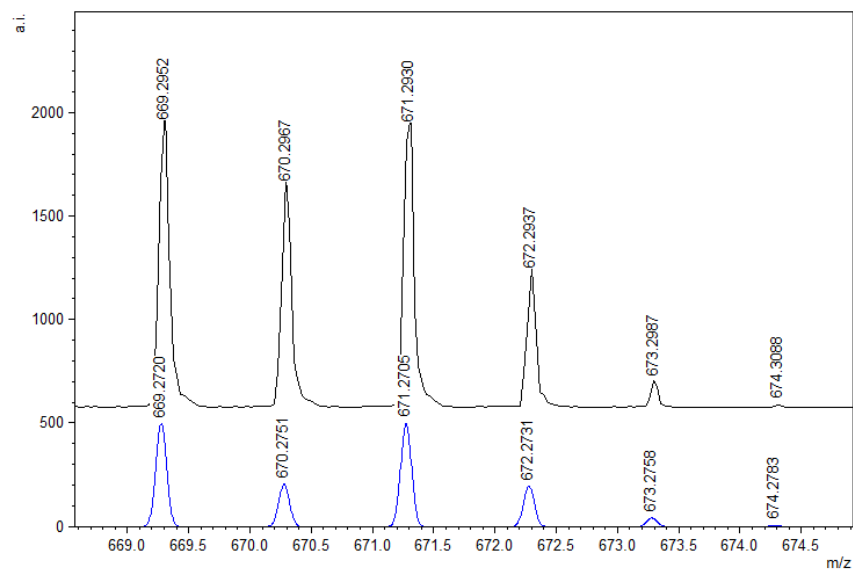


Figure B. 27. Experimental (top) and calculated (bottom) isotopic distribution pattern for 3.5.